STUDY OF PERISTALTIC MOTION OF NON–NEWTONIAN FLUIDS THROUGH POROUS MEDIUM

A THESIS

SUBMITTED TO THE

VISVESVARAYA TECHNOLOGICAL UNIVERSITY, BELAGAVI.

FOR THE AWARD OF THE DEGREE OF

DOCTOR OF PHILOSOPHY

IN

MATHEMATICS

BY

ASHA B. PATIL.

Research centre

(Affiliated to Visvesvaraya Technological University, Belagavi)

Department of Mathematics

BLDEA'S, V.P. Dr. P.G Halakatti College of Engineering and Technology,

Vijayapur – 586 103, Karnataka, India.

May – 2017

CERTIFICATE

This is to certify that the thesis entitled STUDY OF PERISTALTIC MOTION OF NON-NEWTONIAN FLUIDS THROUGH POROUS MEDIUM *submitted to Visvesvaraya Technological University, Belagavi, is the bonafide research work done by* ASHA B. PATIL *under my supervision. The contents of the thesis have not been submitted elsewhere for the award of any degree.*

GURUNATH C. SANKAD

Supervisor

Department of Mathematics

(Affiliated to Visvesvaraya Technological University, Belagavi)

BLDEA'S, V.P. Dr. P.G Halakatti

College of Engineering and Technology,

Vijayapur – 586 103.

Karnataka, India.

Date: 22-05-2017

Place: Vijayapur.

Dedicated to

My Mother

Visvesvaraya Technological University

Jnana Sangama,Belgaum – 590 018.

Prof.SatishAnnigeri Ph.D
Registrar (Evaluation)

Phone: (0831) 2498136
Fax: (0831) 2405461

Ref.No / VTU / Exam / 2016-17/ 1406

Date: 22 APR 2017

Acceptance Letter

Sir/Madam,

The soft copy of Ph.D./M.Sc. (Engineering by research) thesis of **Mr./Mrs. Asha Basanagouda Patil** .bearing **USN 2BL11PGM02** has been submitted for Anti-plagiarism check at the office of the undersigned through "Turn-it-in" package. The scan has been carried out and the scanned output reveals a match percentage of **12%,which is within the acceptable limit of 25%.**

To obtain the comprehensive report of the plagiarism test, research scholar can send a mail to **apc@vtu.ac.in**along with the USN, Name, Name of the Guide/Co-guide, Research centre and title of the thesis.

Registrar (Evaluation)

To,

Mr./Mrs. Asha Basanagouda Patil

Research Scholar

Department of Mathematics

BLDEA's V.P.Dr P.G.H College Of Engg & Tech

Bijapur

Copy to: Dr Gurunath.C.Sankad, Assistant Professor, Dept. of Mathematics., BLDEA's V.P.Dr P.G.H College Of Engg & Tech Bijapur

Abstract

The word peristaltic comes from a Greek word "Peristaltikos" which means clasping and compressing. Thus ‘Peristalsis’ is the rhythmic sequence of smooth muscle contractions that progressively squeeze one small section of the tract and then the next, to push the content along the tract. It induces propulsion and mixing movements and pumps the content against pressure rise, thus finding enormous physiological, biomedical and industrial applications. This is an important mechanism for the mixing and transporting of fluids. This kind of fluid transport appears in many biological systems which have smooth muscle tubes such as, the swallowing of food through the esophagus, movement of chyme in the lower intestinal and gastrointestinal tract, transport of urine from kidney to the bladder, cervical canal and fallopian tube in females, lymphatic vessels and small blood vessels, etc. are some of the physiological applications. Mechanical devices like finger pumps, roller pumps are also based on the peristaltic mechanism. Nuclear industries also use peristaltic transport to curb the flow of toxic liquid to reduce the contamination of the environment. Biomedical instrument such as heart lung machine works on this principle. Even worms like earthworms use peristalsis for their movement. It is also speculated that tall trees may depend on peristalsis for the translocation of water. The translocation of water involves its motion through the porous matrix of the trees.

Though peristalsis is a well known mechanism in biological system, it is only four decades ago that it was given its theoretical and experimental analysis of its fluid dynamic aspects and has recently become the object of scientific research for both mechanical and physiological situations.

A porous medium is a material containing pores or spaces between solid material through which liquid or gas can pass. Examples of natural porous media are beach sand, sandstone, limestone, the human lung, bile duct, gall bladder with stones in small blood vessels.

Flow through a porous medium has several practical applications especially in geophysical fluid dynamics. Also, as most of the tissues in the body are deformable porous media Peristaltic transport of a bio fluid through a channel with permeable walls is of considerable importance in biology and medicine. Flow through porous media has been of significant interest in the recent years, to understand the complexity of disease like intestinal cystitis, bladder stones, bacterial stones, bacterial infections of kidneys, the various medical conditions (viz., tumor growth) and treatments (injections) and so on.

Though Newtonian and several non-Newtonian models have been used to study the motion of blood, it is realized that Herschel-Bulkley model describes the behavior of blood very closely. Herschel-Bulkley fluids are a class of non-Newtonian fluids that require a finite stress, known as yield stress, in order to deform. Therefore, these materials behave like rigid solids when the local shear is below the yield stress. Once the yield stress is exceeded, the material flows with a non-linear stress-strain relationship either as a shear-thickening fluid, or a shear-thinning one. Few examples of fluids behaving in this manner include paints, food products, plastics, slurries, pharmaceutical products etc. Further, in small diameter tubes blood behaves like Herschel-Bulkley fluid rather than power law and Bingham fluids. Herschel-Bulkley fluid is considered to be the more general non-Newtonian fluid as it contains two parameters, the yield stress and the power law index. In addition Herschel-Bulkley fluid’s constitutive equation can be reduced to the constitutive equations of Newtonian, Power law, and Bingham fluid models, by suitable choice of the parameters. The

same model can be used for larger arteries where the effect of yield stress can be ignored. Hence it is appropriate to model blood as a Herschel–Bulkley fluid rather than Casson fluid.

In view of all the studies mentioned above, the study of peristaltic motion of a non-Newtonian fluid, in particular the Herschel Bulkley fluid has been considered to analyze the flow of blood in small vessels. The flow analysis is worked out to explore the impacts of various parameters of concern under uniform, non-uniform, inclined, heat transfer and magnetic effects in the thesis. MATHEMATICA software is used to analyze the results graphically.

The plots of both the pressure difference and the frictional force against flow rate show that the flow rate is more in convergent channel when compared to divergent channel. The frictional force behaves reversely in comparison with the pressure rise in accordance with the results of many prior research establishments. The porous lining of the wall increases the Mechanical efficiency. The absolute value of the Nusselt number increases with rise in Brinkmann number, and the yield stress. The trapped bolus shrinks with rise in the magnetic field.

Acknowledgement

Above all, I praise God for providing me this opportunity and granting me the capability in successively completing my PhD thesis.

The thesis has come out in the current form only with the help of several people for whom I am most obliged.

Thanks to my esteemed promoter Prof. G C Sankad, for accepting me as his PhD student. I am grateful for his thoughtful guidance, assistance, encouragement, useful comments and corrections.

I am deeply indebted to Sri. M B Patil, President, BLDE association, Vijayapur, for his support and encouragement in pursuing my PhD. My earnest thanks to our beloved Principal Dr. V. P. Huggi, for his incessant support during my PhD work.

I am grateful to our HOD, Prof. P K Gonnagar for his continuous support and encouragement and also for providing the necessary facilities. Thanks to all my colleagues of Department of Mathematics of BLDEA's V. P. Dr. P. G. Halakatti College of Engineering and Technology, Vijayapur, for their cooperation, useful discussion and advices.

I thank and appreciate my mother for her encouragement and support in carrying out my PhD studies, without whom I couldn't have been what I'm today. Her emotional and spiritual support has given me strength and courage in achieving my undertaking. I express gratitude and deepest appreciation to my loving husband, Aravind whose support and encouragement has helped me to elicit my ability. I thank my brother and sister in law for their cooperation. I heartily appreciate the patience and endurance of my kids Anusha, Anchal and Anmol and will be always grateful to them.

Contents

CHAPTER -1

Introduction

1.1 Fluid Dynamics:

Fluid dynamics is fundamentally a study of the physical behavior of fluids and fluid system, and the laws governing this behavior. It also deals with the action of forces on fluids and the resulting flow pattern. The fluid flow analysis is generally made by considering certain fundamental principles, concepts and laws, viz, the law of conservation of energy, mass and momentum; the first and the second law of thermodynamics; Newton's law of viscosity; the corresponding peripheral conditions; Euler's, Navier-Stokes and Reynolds equations of motion.

The study of fluid mechanics enables to know the basic principles of fluid behavior and their application to flow problems arising in engineering and physical problems. Owing to the wide applications of fluid dynamics as in biofluid dynamics, geophysical dynamics, aerodynamics, etc, fluid dynamics has raised curiosity of many researchers in the recent years.

1.2 Biofluid:

Mathematical modeling is the representation of a system using mathematical perception and language. In biomechanics mathematical modeling is applied to study problems of medical science. Biofluid mechanics is that branch of biomechanics that deals with the kinematics and dynamics of the fluids present in human beings, animals and plants. The recent study of biofluid mechanics measures and analysis the flow of physiological fluids, applicable for the clinical studies as in: artificial organs, cancer treatment and many more. It is a well known fact that experimentation on physiological fluids is a difficult task to undertake and further the non-invasive experiments do not always give accurate results. Hence the perceptive of biofluid dynamics in the flow of physiological fluids in a human body is rather a difficult task in comparison with the engineering applications. In addition, this necessitates the familiarity of both theoretical and computational biofluid dynamics to understand the bio fluid dynamics in human body. Peristalsis is one among the many mechanisms of fluid transport in the human body.

1.3 Peristalsis:

"Peristaltikos" is a Greek word which implies, clasping and compressing, from which arise the word ‘Peristaltic’. Peristalsis is a coordinated reaction wherein a wave of contraction preceded by a wave of relaxation passes down a hollow viscus. Thus ‘Peristalsis’ is the rhythmic sequence of smooth muscle contractions that progressively squeeze one small section of the tract and then the next, to push the content along the tract. As they are propelled along, would always enter a segment which had actively relaxed and enlarged to receive them. It excites propulsion and amalgamation and pumps the content against pressure rise, thus finding enormous physiological, biomedical and industrial applications. From the perspective of fluid dynamics, peristalsis is typified by the dynamical interface of the fluid flow and movement of the flexible boundaries of the conduit.

Peristalsis is an intrinsic property of any syncytial smooth muscle, like the gastro intestinal tract, bile ducts, ureter, glandular ducts, etc. The physiological applications of peristalsis is observed when the swallowed food moves into the esophagus, urine flows from kidney to the bladder, spermatozoa move in the male and female reproductive organs, lump move in the lymphatic vessels, bile juice flow in the bile duct, blood circulates in small blood vessels like arteries, venules and capillaries. Peristalsis has brought revolutionary developments in industrial appliances as well: transportation of sanitary fluid, caustic fluids, toxic liquid in nuclear industry and also in the finger pump, roller pump and in biomedical instruments, for instance, heart lung and blood pump machinery. Some worms like earth worms use peristalsis for their locomotion. Even the translocation of water in large trees is speculated to occur through peristalsis, through its porous matrix.

1.3.1 Peristalsis in Esophagus:

The usual stimulus of esophagus is swallowing, which at any level results in the development of peristalsis. Thus after reaching the esophagus, food is propelled into the stomach by peristalsis (Fig. 1.1 and Fig. 1.2). It consists of lumen obliterating contractions, 4–8cms in

length, which move down at a speed of 2–4cm/sec. The strength of the peristaltic contractions is proportional to the size of the bolus entering the esophagus.

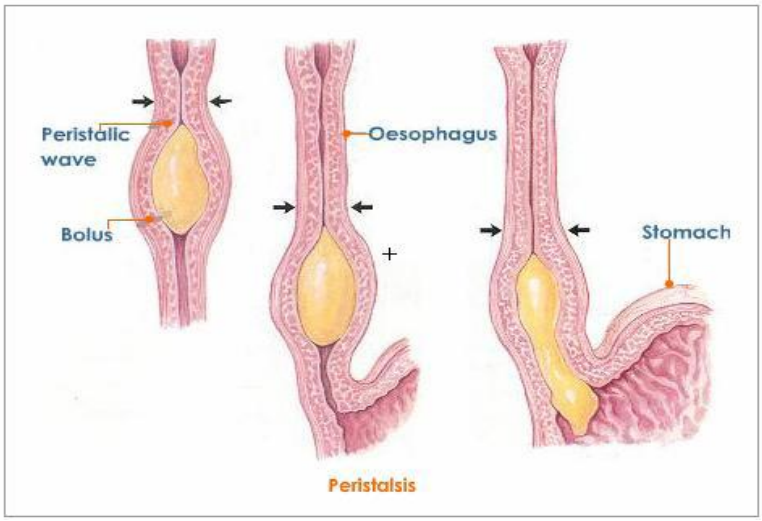

Fig. 1.1

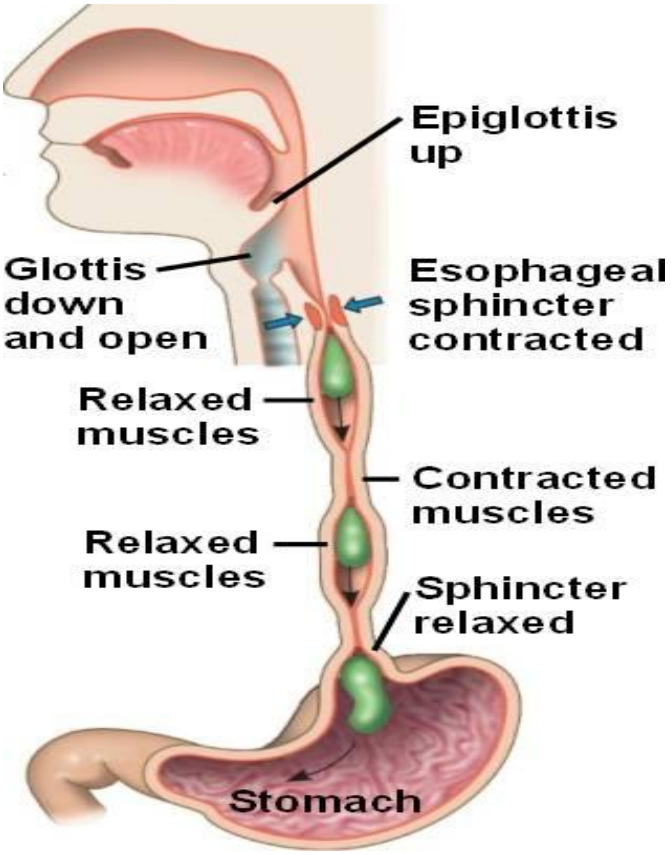

Fig. 1.2

1.3.2 Peristalsis in Kidneys:

Bergman [1] affirmed that urine flow from the kidney to the bladder within the ducts called ureters is due to peristalsis in the ureteral wall (Fig 1.3). The only function of the ureter is to drive the urine to the bladder from the kidneys, beginning right from the kidney and forwarding towards the bladder, through peristaltic action. The ureter wall is made up of

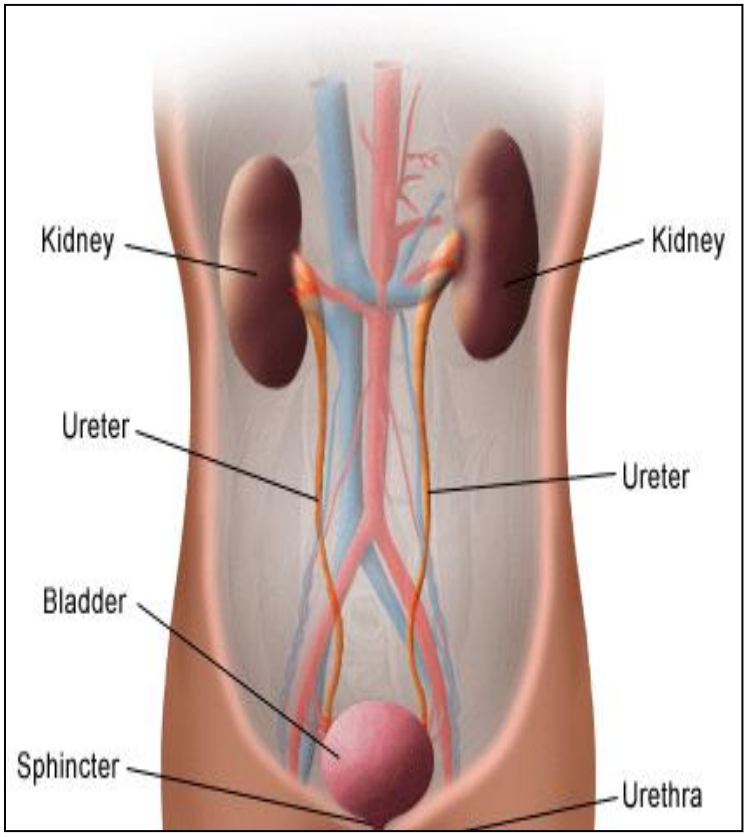

Fig. 1.3

a number of layers (Krstic [2]). The luminal surface of the ureteral wall consists of a transitional epithelium and a lamina propia, comprising of a thick layer of finely vascularized and innervated connective tissue. The remaining portion of the wall is included of smooth muscle along with connective tissue called Tunica Muscularis (TMu). The TMu consists of smooth muscle bundles isolated by abundant loosely-fitted connective tissue. Though not always clearly bordered, the three layers can be distinguished: an interior longitudinal, a central circular layer, and an external longitudinal layer. The peristaltic contractions are simplified by these muscle fibers.

1.3.3 Peristalsis in Intestine:

When the **intestinal** wall is stretched or distended by food (chyme), a circular constriction forms above it due to contraction of longitudinal muscle layer. Therefore the intestinal contents move towards the dilated part; then contraction of circular muscles spread to this part which in turn is constricted, while the segment below it is dilated by contraction of longitudinal muscle layer. Several of these wave like contractions occur simultaneously along the length of the intestine, so that its movement is vermiform and is hence called vermicular or peristaltic movements. Each peristaltic wave lasts for 1-2 seconds and propels the chyme a few centimeters.

1.3.4 Peristalsis in Heart-Lung Machine:

Fig. 1.4

The Heart-Lung machine (Fig 1.4) is used during the surgical procedure which works like both: the heart and the lung, when the heart needs to be stopped. Usually referred to as 'pump', this machine consists of a chamber which does the work of the right atrium of the heart of receiving the blood from the body. This blood is then forced through an oxygenator that endeavors the working of lung: exchange of carbon-di-oxide and oxygen. The oxygenated blood is then pumped back to the body which is the responsibility of the left heart.

1.3.5 Peristaltic Pump:

The peristaltic pump (Fig 1.5) was first popularized by the heart surgeon Dr. Michael. DeBakey, in 1932. The peristaltic pump is used to drive different types of fluids. An elastic tube is fixed inside the spherical pump case which contains the fluid to be pumped. When the rotor attached by means of a numerous rollers, shoes, wipers on the external surface rotates, it constricts the flexible tube. As, part of the compressed tube is pinched the fluid is pushed forward and then again the tube regains its original form allowing the fluid to move inside. Thus the peristaltic action takes place and the fluid is transported.

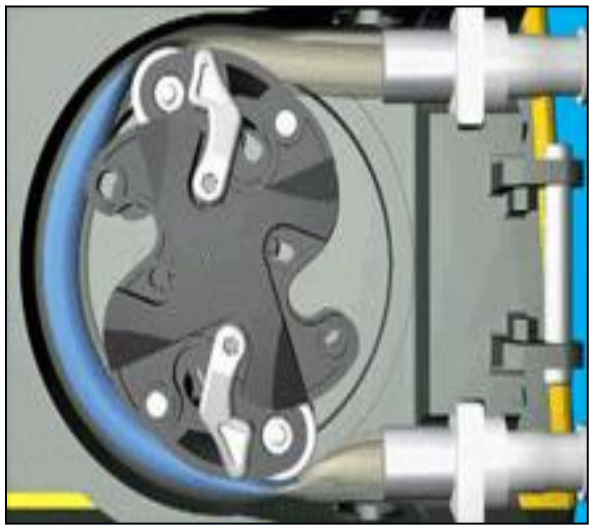

Fig.1.5

1.4 Newtonian / non-Newtonian Fluids:

Depending on the variation of strain rate with the stress within a matter, the viscosity can be classified as linear or non-linear. The matter exhibiting a relationship wherein stress is linearly comparative to the strain rate is termed Newtonian. In contrast, a material exhibiting a non-linear relationship between the stress and the strain rate is termed non-Newtonian.

Biofluids are the fluids present in the ducts of the living body, which are treated either as Newtonian or non-Newtonian fluids depending on the physiological situation. Extensive research work has been carried out on the physiological fluid flow, during the last few

decades, assuming the fluid under peristaltic motion to behave as a Newtonian fluid with constant viscosity. But this consideration of Newtonian fluid fall short in giving sufficient perceptive of peristalsis, the mechanism involved, in the intestine, small blood vessels and ductus efferentes of the male reproductive organ, where the viscosity of the fluid varies along the thickness of the duct. Since chyme is undoubtedly a non Newtonian fluid, its supposition to be a Newtonian material of variable viscosity in the small intestine, is not adequate in reality. The chief characteristic of peristaltic flow: trapping and volume flow rate have been studied widely for Newtonian fluids. In reality the rheological properties of the fluid influence these characteristics appreciably as several of the fluids behave like non-Newtonian fluids.

Moving away from the Newtonian fluids the non-Newtonian fluids cannot be explained with a single constitutive equation between stress and strain rate but their constitutive equations lead to complicated mathematical problems. Thus the physicists, mathematicians, researchers are challenged in modeling, analyzing and solving the non-Newtonian fluid flows.

Through the investigations it is accepted that blood in tiny arteries and liquids in the lymphatic vessels and in the digestive system, urine under certain pathological conditions, etc behave like non-Newtonian fluids. Also, though the solution of non-Newtonian fluids is complex due to the appearance of the non-linear term, blood flow in human body, alloys and metals in industries, mercury amalgams and lubrication with heavy oils and greases in machines, are a few examples of flow of non-Newtonian fluids that show us how important is the study of non-Newtonian fluids.

1.5 Porous Media:

A permeable medium is a material containing pores or spaces in between the solid matter through which gas or liquid can pass. The human lung, bile duct, gall bladder with stones in small blood vessels, beach sand, limestone, sandstone, are some of the examples of natural porous media (Fig. 1.6). Further, movement of underground water, fluid filtration and water discharge in river beds are a few examples of flow through permeable medium.

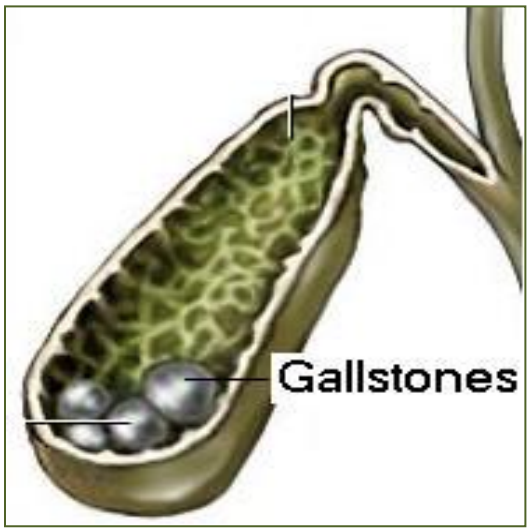
Gallstones

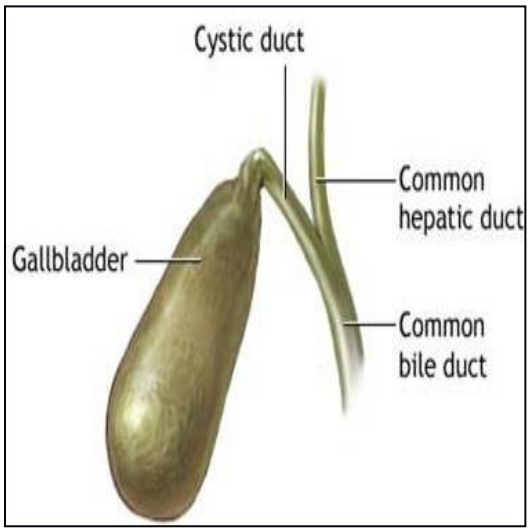
Cystic duct
Common hepatic duct
Gallbladder
Common bile duct

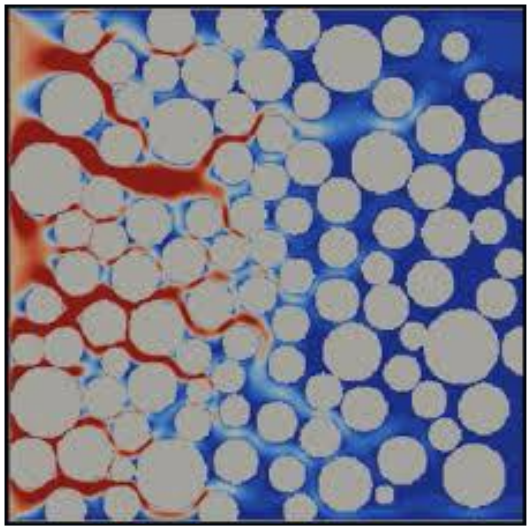

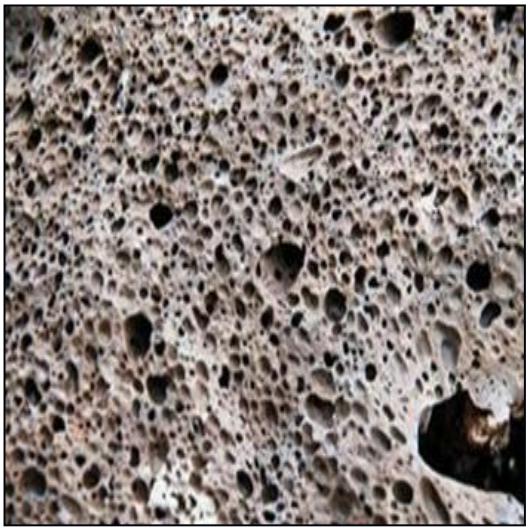

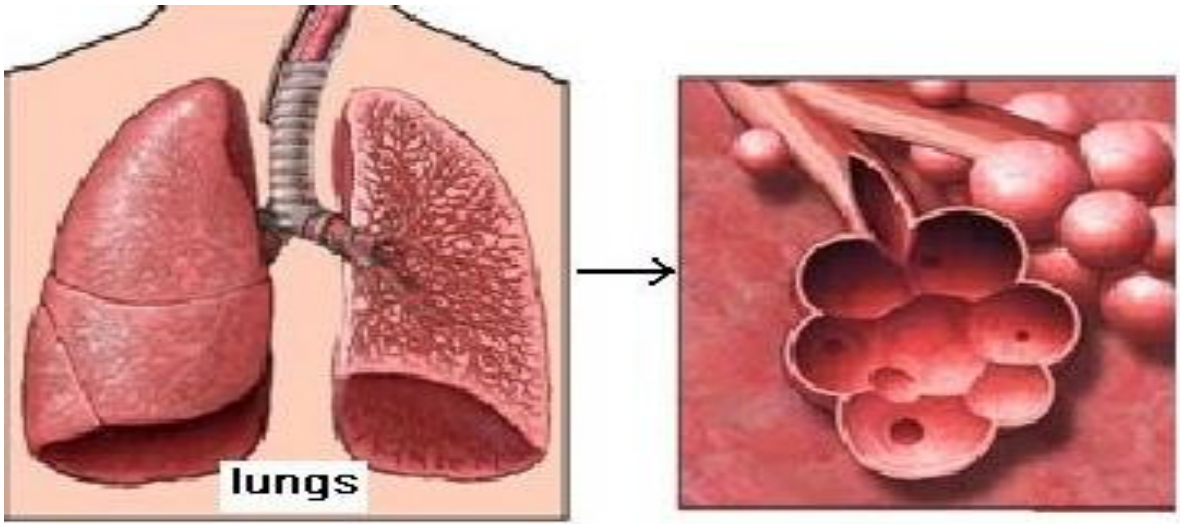
lungs

Fig. 1.6

Peristaltic flow with a porous intermediate has attained significance in the current decade because of its practical applications chiefly in biomechanics and geophysical fluid dynamics. Even in some pathological situations like, transportation of fluids in lungs, in kidneys, gallbladder with stones, movement of small blood vessels and tissues, cartilage and bones and allocation of fatty cholesterol can be well thought-out as a porous medium. The proper functioning of these depends crucially on the flow of blood, nutrients, etc., through them. A number of innervated smooth muscle layers consisting of many folds surround the gastro intestinal tract, with numerous pores in these tight junctions. Even the oil reservoirs are mainly composed of limestone and sandstone wherein the oil is trapped. With the knowledge of flow through porous media, oil extraction from the oil refinery can be enhanced; various medical conditions like tumor growth and their treatment can be well understood.

1.6 Heat Transfer:

The thermodynamic feature of blood becomes more significant once blood is taken out of the body than when it is inside. The studies involving generation of heat are vital for diagnosing the blood distribution disease, in the non invasive measurement of blood glucose, for the quantitative prediction of blood flow rate, etc. With profuse realistic significances: heamodialysis (a method adopted in cases of renal failure of kidney to eliminate the waste materials from blood), oxygenation, separation procedure in chemical engineering, polymer engineering, perfusion of arterial-venous blood, petroleum production, etc the researchers are concentrating on the analysis of peristaltic motion of non-Newtonian fluids under heat transfer. The study of heat transfer is applicable to exploit harmful tissues in cancer cure treatment. Bioheat transfer is being paid attention by biomedical experts recently, for its consideration in heat transfer analysis in the human body, thermotherapy wherein heat is applied to the body for treatment as in pain relief and for increase in the blood flow, human thermoregulation system to maintain the body temperature within certain limits with respect to the variations in the surrounding temperature.

Convecture flow in porous media has been an area of interest recently because of its vivid applications in engineering: heat removal in nuclear reactors past an accident, drying processes, heat exchangers and solar collectors.

1.7 Magneto Hydrodynamics:

Magneto hydrodynamics is the study of dynamics of electrically conducting fluids. One of the vital aspects of the physical situation in the study of MHD fluid flows is the shared interaction amid the motion of the fluid and the magnetic field. This field has widespread appliances in bioengineering and medical science: transport of medicine to the target using magnetic particles as drug transporter, building up of magnetic devices for cell separation, diminution of blood loss during surgical procedure, development of magnetic tracers. The principle of MHD is also applied in designing the heat exchangers, pumps, flow meters, power generation, radar organization, etc.

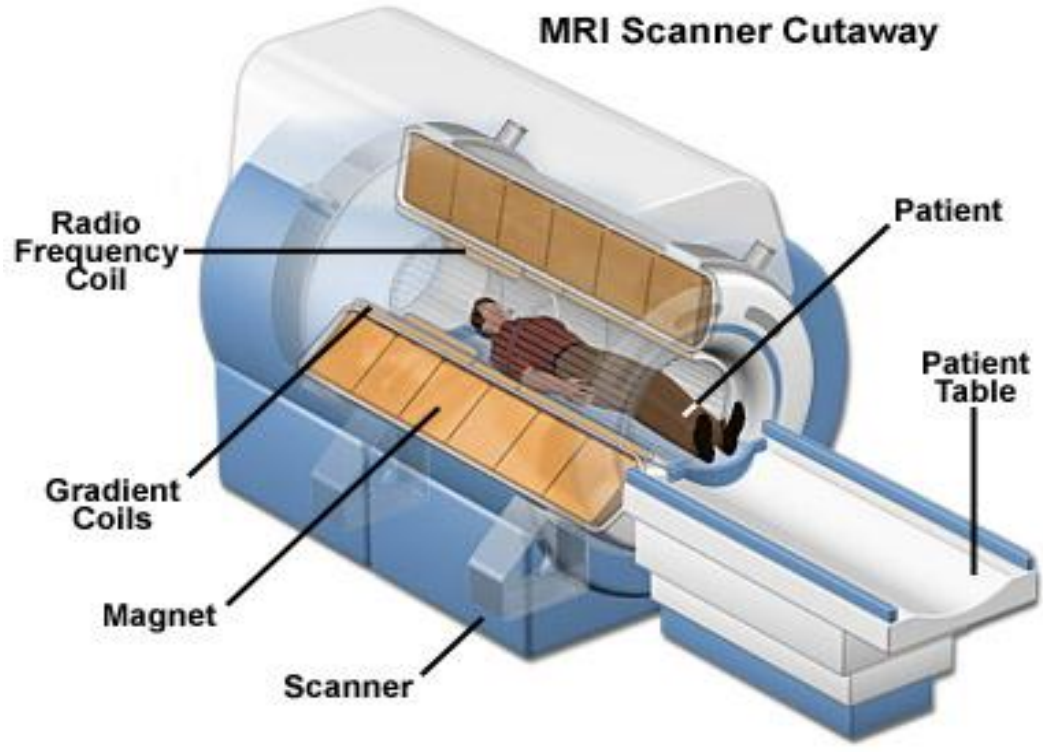

Fig. 1.7

Today, Magnetic Resonance Imaging (MRI) (Fig. 1.7) is the most popular technique used far and wide in the medical field for the diagnosis of not only the brain and vascular diseases but also the whole body. This Magnetic Resonance Imaging is based on the principle of magnetic field.

1.8 Literature Survey:

According to Ayukawa and Takabatake [3], as a consequence of area contraction and expansion of the flexible channel / tube, a progressive wave travels along its length causing the fluid to transmit. Bayliss and Starling [4] described this movement as consisting of area contraction and relaxation.

Peristaltic phenomenon has been observed in the human physiological system centuries ago, but it was only after the first investigation of Latham [5] that peristalsis has become a subject of scientific research for many scholars. The experimental investigations of Latham [5] fully comply with the theoretical investigations of Shapiro [6]. Fung and Yih [7] and Shapiro et al.[8] have explained the medically and biologically important volume flow rate phenomenon, by visualizing peristalsis as an infinitely traversing sinusoidal wave in a two dimensional channel. Fung and Yih [7] modeled the peristaltic transport in the fixed frame of reference further Shapiro et al. [8] in the moving frame of reference.

The peristaltic motion considering the sinusoidal variations at the walls of the pipe and channel, for the flow of viscous fluid has been discussed by Burns and Parkes [9]. This assumption of peristaltic pumping model as a sinusoidal train of waves was applied chiefly to characterize the basic process of fluid mechanics into two classes: i) the peristaltic model restricted to small wave amplitude (at the same time) but with no constraints on the Reynolds number, developed by Fung and Yih [7]; ii) The lubrication theory model wherein the model is considered to be inertia free and the wall curvature is negligible, as suggested by Jaffrin and Shapiro [10]. This model also assumed the wave to be moving with constant wave velocity, simplifying the study to stationary wavy walls. They also explained the importance of various parameters governing the flow after exploring the basic principles. Peristaltic

transport was analyzed assuming long wavelength for the power law fluid by Radhakrishnamacharya [11].

According to Yih and Fung [12], the vasomotion of small blood vessels is due to peristalsis. Experimental and numerical analysis to study the peristaltic mechanism in the male reproductive system has been carried by Batra [13], Guha et al. [14] and Srivastava et al. [15]. The applications of peristaltic mechanism are also seen in industry for transportation of the sanitary fluids, corrosive fluids and toxic liquids in nuclear industry and also in the heart lung and blood pump machinery, thus attracting researchers towards the study of peristalsis.

Modeling the chyme as power law fluid, Lew et al. [16] analyzed the peristaltic transport in small intestine and esophagus. Peristaltic motion of blood in small blood vessels considering visco elastic fluid was inspected by Bohme and Friedrich [17]. To examine the peristaltic flow of blood in small capillaries and in blood vessels, Srivastava and Srivastava [18] modeled blood as Casson fluid. DeVries et al. [19] reported the physiologists' belief that the fluid flow inside the uterine is due to myometrical contraction and may take place in both symmetric and asymmetric conditions.

Eytan and Elad [20] developed a model for examining the effect of peristaltic flow in the transport of embryo within the uterine. They considered the peristaltic motion in a channel with the sinusoidal waves travelling autonomously on the upper and lower walls having a phase difference, causing the intra uterine fluid flow in the uterus and gave a detailed discussion of trapping and impedetion of the embryo implantation at the fundus due to the particle volume flow rate. Further, Eytan et al. [21] applied lubrication theory to get a time dependent solution of the flow in a laboratory frame to analyze the embryo transport inside the uterine cavity.

Misra and Ghosh [22] considered the small blood vessels in lungs to be porous channels and proposed a model mathematically for the flow of blood in a conduit having porous walls and analyzed the pressure and velocity distribution numerically, while Misra and Pandey [23] obtained a model intended for the motion of food bolus in the esophagus. Krishnakumari et al. [24] examined the peristaltic pumping of blood, treating it as a Jeffery fluid.

To study the physiological parameters Tang and Fung [25] assumed the physiological fluids to act as a Newtonian fluid. This advancement failed to explain the peristaltic method in tiny blood vessels and intestine, though it well explained peristalsis in ureter. Misery et al. [26] explored the generalized Newtonian fluid motion in a channel, under peristaltic movement. The peristaltic flow of a generalized Newtonian fluid past a permeable medium was studied by Shehawey et al. [27]. Many authors Hakeem et al. [28], Mishra and Rao [29], Ebaid [30] have considered Newtonian fluid model for their study.

The experimental study of Bruce [31] and Joseph [32] reveals that not only a number of physiological but even the industrial fluids behave as non-Newtonian fluid. Also, Majhi and Nair [33] suggest that the behavior of blood is more likely to be non-Newtonian

It was only after the exploration of Raju and Devanathan [34] that quantitative research on the non Newtonian fluids has been attempted. They considered the power law fluid as the non Newtonian fluid to analyze the stream function. Kapur [35] not only suggested the mathematical models for physiological flows by considering them as Newtonian as well as non-Newtonian fluids but also investigated blood theoretically considering it as both Newtonian and non-Newtonian fluid.

Srivastava and Srivastava [18], Subba Reddy et al. [36] have also examined the motion of non-Newtonian fluids under peristalsis. Taking into account the different wave forms, the impact of partial slip in the flow of a non-Newtonian fluid under peristalsis is studied by Akram and Nadeem [37].

Considering the various amplitudes and periods of the wall deformation, Pozrikidis [38] has examined the mean flow rate and the stream lines. Nagarani [39] has analyzed the flow rate and flow resistance, pressure rise, velocity and stream lines for the transport of a Casson fluid in an inclined peristaltic conduit. Her results concluded that frictional force and pressure rise behave conversely for all the parameters.

Beavers and Joseph [40] experimentally studied the behavior at the interface of the permeable medium and the liquid layer and came out with a slip condition at the interface, useful for the study of flow through the pipes where chemical effects crop up at the walls during the 2 phase flow in permeable medium. Saffman [41] gave a better boundary

condition at the interface, after justifying theoretically with the help of statistical data of the boundary conditions of Beavers and Joseph [40]. Flows in permeable medium analyzed by a number of researchers employing Darcy's law are given by Scheideggar [42].

In regard with the modeling of the flow of synovial fluid in the joint, Reese and Rath [43] considered the flow of Newtonian fluid in a channel coated with an absorbent layer at the walls. Gopalan [44], Chaturani and Ranganathan [45] have reported in their investigations that 'various ducts in living bodies are permeable'. The initial study of flow past a permeable medium under peristaltic action is presented by Shehawey et al. [46]. The effects of porous boundaries over the peristaltic motion have been analyzed by Shehawey and Husseny [47] in a channel and by Shehawey and Sebai [48] in a tube. Shahawey et al. [49] inspected the peristaltic motion through a porous asymmetric channel. Many investigations have been done on the peristaltic transport past a permeable media. Vasudev et al. [50] have considered the peristaltic motion of a Newtonian fluid in a permeable medium under the effect of magnetic field. Ravi Kumar et al. [51] analyzed the flow of a Power law fluid through an asymmetric channel surrounded by permeable walls. The flow past a permeable medium under peristalsis for a Conducting fluid in an asymmetric vertical conduit is discussed by Rami Reddy and Venkataramana [52]. Applying perturbation method Raghunatha Rao and Prasada Rao [53] obtained the solution for the axial and transverse velocities for the couple stress fluid flow in a porous peristaltic conduit. They reported that there is drop in pressure as the couple stress constraint and the permeability constraint increase. Their study concluded that the frictional force and the pressure rise behave oppositely.

The slip effects on the peristaltic flow through porous media is studied by Jyothi and Koteswara Rao [54] for a Williamson fluid in a symmetric channel and Navaneeswara Reddy and Vishwanatha Reddy [55] for a Jeffery fluid in an inclined asymmetric conduit. Wall effects of the peristaltic transport of a hyperbolic tangential fluid are studied by Nagachandrakala et al. [56] through a porous non-uniform channel. Analyzing the flow of couple stress through porous channel, Alsaedi et al. [57] concluded that mechanical efficiency decreases with the permeability parameter. Studying the trapping phenomenon, they said that the magnitude of the bolus enhances as the permeability parameter increases. Several authors (Ellahi et al. [58], Ali et al. [59]) have considered the application of peristaltic flow, in porous media and in non-uniform channel. Ramesh and Devakar [60] have

analyzed the peristaltic motion considering the MHD Williamson fluid through an inclined asymmetric conduit under heat transfer in a porous medium.

With the vision of a more pragmatic model for flow of non-Newtonian fluid flow through a non-uniform tube, Srivastava and Srivastava [61] modeled the fluid flow in the vas deferns supposing it to be non-uniform and the fluid to be a power law fluid.

Various authors (Mekheimer [62], Sankad et al. [63], Sankad and Radhakrishnamacharya [64]) have put forth their investigations on the flow involving peristalsis, considering non-uniform and uniform channels for different fluids and their corresponding parameters. Recently, applying the homotopy perturbation method, Ali et al. [65] have inspected the flow under peristalsis for a hyperbolic tangent fluid inside a three dimensional non-uniform conduit with flexible walls. They concluded that the velocity is utmost at the center of the conduit and minimum at walls.

The magnetic effect on the flow of blood under peristalsis has been reported by Mekheimer [66]. His results reveal that the rise in pressure is more when a couple stress fluid is considered than in the Newtonian fluid. Further he observed that pressure rise is more in a non uniform channel than in a non-uniform one. Sankad and Radhakrishnamacharya [67] considered the effects of wall on the flow of micro polar fluid influenced by magnetic field under peristalsis. Ramanakumari and Radhakrishnamacharya [68] analyzed the consequences of various parameters on the motion of Newtonian fluid past a channel assuming the fluid to be electrically conducting and transverse magnetic field acting across the channel uniformly. Modeling the flow of a couple stress fluid applied with a Hydro magnetic effect, Shit and Roy [69] examined the pressure gradient, pressure rise, axial velocity as well the stream function. Their results exposed that the trapping bolus can be considerably eliminated through application of magnetic field. Bhatti and Ali [70] have considered the peristaltic flow of blood modeled as a Jeffery fluid, in a permeable medium, analyzing the simultaneous effect of slip and MHD. This study revealed that the increase in slip and the porosity parameter diminishes the pressure rise whereas increment in the Hartmann number increases the pressure rise.

1.9 Problem Statement:

With the report of Scott Blair [71] that Herschel Bulkley fluid model is a better fluid to study the flow behavior of blood, many researchers have contributed in this regard. But, the flow of Herschel Bulkley fluid through porous media has not been much considered though many pathological situations are considered to be porous. Even the extraction of oil from the oil refineries and treatment of cancer needs the study of flow through porous media.

This necessity has led to the following research issues:

What is the effect of the porous lining of the wall on the peristaltic flow of a Herschel Bulkley fluid through a channel? What if the channel is considered to be a non-uniform channel? Further what might be the influence of inclination in a non-uniform channel? What are the effects of influencing heat transfer through the flow on the temperature profile and Mechanical efficiency? What effect does an applied magnetic field has on the pumping and trapping phenomenon?

1.10 Objective of the Research:

The thesis aims to study the peristaltic flow of Herschel Bulkley fluid through a channel lined with non- erodible porous material at the walls. The flow is modeled mathematically and analytical solutions are obtained. Graphs are put forth to analyze the effects of various parameters. The major objectives of the study are:

1. To investigate the effects of porous lining, yield stress and other parameters of interest on the flow of a Herschel Bulkley fluid through a peristaltic channel. And also to analyze the stream line patterns.
2. To analyze the influence of the pertinent parameters on the peristaltic flow in a non-uniform channel and on the formation of the trapped bolus.
3. To examine the effects of different parameters when the channel is inclined to the horizontal.
4. To investigate the influence of various parameters on the temperature profile, rate of heat measure, mechanical efficiency on the flow influenced by transfer of heat.

1.11 Herschel Bulkley Fluid:

Herschel Bulkley fluid is a form of non-Newtonian fluid that requires a fixed stress called yield stress for deformation. Hence it behaves as a rigid solid whenever the local sheer is less than the yield stress and the movement yield stress exceeds the local sheer, the substance starts moving with a non-linear stress-strain coordination, as a shear thickening or as a shear thinning fluid. Examples are: paints, food products, plastics, slurries, polymeric suspensions, semi solid materials, pharmaceutical products and paper pulp.

Shear thickening or shear thinning fluids take in a significant role in biomedical science. As known, flows having a non linear strain stress connection, either with shear thinning or shear thickening fluids, is well elucidated by the Herschel Bulkley fluid model which has applications in Biomedical engineering. The study of Herschel Bulkley fluid is more emphasized since the behavior of blood is more similar to Herschel Bulkley fluid in comparison with Bingham and power law fluids, thus making it applicable during the analysis of blood and other physiological fluid flows stimulated by peristalsis.

Herschel Bulkley fluid model is considered to be a better model for flow of blood in arterioles and therefore it might also help in the clinical procedure of blood transportation using the heart lung machine and roller pumps. In the microcirculatory system, the Reynolds number and the ratio of half width of the channel to the wavelength are small and lubrication theory can be applied for the theoretical analysis. To study blood, preferably the Herschel Bulkley fluid model is suggested for its close behavior to blood and its flexibility to reduce into Bingham, Newtonian and Power law model.

1.11.1 Basic Equations:

The governing equations of Herschel-Bulkley fluid flow as given by Tu and Deville [72] are:

The momentum equation is:

$$\nabla \cdot \sigma + \rho F = \nabla \mathrm{p} + \rho \frac{dV}{dt},$$

and the divergence free condition due to the incompressibility strain on the velocity V

$$\nabla \cdot V = 0,$$

where ρ denotes the density, V the velocity and σ denotes the stress.

The more generalized Newtonian fluid is the Herschel-Bulkley fluid where the stress σ is linearly dependent with the pace of deformation tensor D. Further the viscosity η is a function of the shear rate $\dot{\gamma}$. We have

$$\sigma = 2\eta(\dot{\gamma})D$$

where the symmetric part of the velocity denoted by D, is given by:

$$D = \tfrac{1}{2}(L + L^T) \; and \; L = \nabla V.$$

$$\eta = \frac{\tau_0 + k\left(\dot{\gamma}^n - \frac{\tau_0}{\mu_0}\right)^n}{\dot{\gamma}}$$

where n, τ_0 and k respectively represent the flow behavior index, the yield stress and the consistency factor.

The constitutive equation of the Herschel-Bulkley fluid model is commonly given by $\tau = \tau_0 + k\dot{\gamma}^n$, where τ is the shear stress. If $\tau < \tau_0$ the Herschel-Bulkley fluid behaves as a solid, otherwise it behaves as a fluid. For n < 1 the fluid is shear thinning whereas for n > 1 the fluid is shear thickening.

In the Cartesian geometry the momentum equations governing the flow

$$\rho\left(u\frac{\partial u}{\partial x} + v\frac{\partial u}{\partial y}\right) = -\frac{\partial p}{\partial x} + \frac{\partial(\tau_{xx})}{\partial x} + \frac{\partial(\tau_{xy})}{\partial y}. \tag{1.1}$$

$$\rho\left(u\frac{\partial v}{\partial x} + v\frac{\partial v}{\partial y}\right) = -\frac{\partial p}{\partial y} + \frac{\partial(\tau_{yx})}{\partial x} + \frac{\partial(\tau_{yy})}{\partial y}. \tag{1.2}$$

Non- dimensionalising the equations (1.1) and (1.2) the following equations are obtained in the simplified form (Lubrication approach),

$$Re\,\delta\left(u\frac{\partial u}{\partial x} + v\frac{\partial u}{\partial y}\right) = -\frac{\partial p}{\partial x} + \delta\frac{\partial(\tau_{xx})}{\partial x} + \frac{\partial(\tau_{xy})}{\partial y}. \tag{1.3}$$

$$Re\,\delta^3\left(u\frac{\partial u}{\partial x}+v\frac{\partial u}{\partial y}\right)=-\frac{\partial p}{\partial y}+\delta^2\frac{\partial(\tau_{yx})}{\partial x}+\delta\frac{\partial(\tau_{yy})}{\partial y}. \quad (1.4)$$

Herschel-Bulkley fluid model is one of the most used models as the viscous behavior of Newtonian fluids, Bingham plastics, pseudoplastic and dilatant materials can all be described as its special cases as given in the table. The graph below shows the nature of these fluids.

FLUID	K	n	τ_0	EXAMPLES
Herschel-Bulkley	> 0	0 < n < ∞	> 0	Fish paste, raisin paste
Newtonian	> 0	1	0	Water, fruit juice, milk
Pseudoplastic (shear thinning)	> 0	0 < n < 1	0	Apple sauce, banana puree
Dilatent (shear thickening)	> 0	1 < n < ∞	0	40% raw corn starch, some honey
Bingham Plastic	> 0	1	> 0	Tomato paste, some yogurts

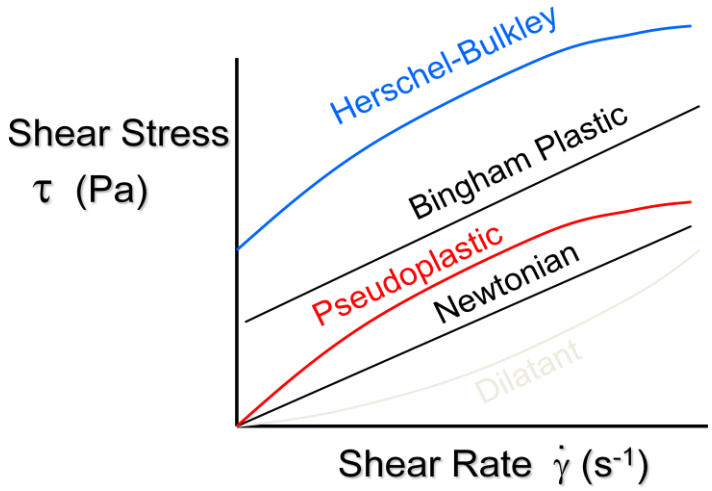

After the report of Scott Blair [71] that, though blood comply with the Casson's model but it is the Herschel Bulkley fluid model that agrees more with the blood flow, a number of scholars have concentrated on the study of Herschel Bulkley fluid. Blair and Spanner's [73] investigations revealed the fact that Herschel-Bulkley fluid model elucidates the phenomenon for cow's blood very closely.

Vajravelu et al. ([74] and [75]) have studied the peristaltic flow through an inclined tube as well in a channel considering the Herschel- Bulkley fluid. Maruthi Prasad and Radhakrishnamacharya [76] studied the transportation of Herschel Bulkley fluid under peristalsis when a low intensity Magnetic field is applied across the channel. Medhavi's [77] study exposed that, the association between the pressure and the flow rates are linear in Bingham and Newtonian fluid models and are non-linear in Herschel-Bulkley and power-law models. Considering an inclined channel coated with permeable material, Sreenadh et al. [78] studied the Herschel Bulkley fluid flow, applicable to analyze the flow of blood considering erythrocytes region as plug flow and plasma region as non plug flow region.

Vajravelu et al. [79] have given a comparative study of Herschel Bulkley, Bingham, Newtonian and Power law fluids through their study. They also have concluded that in comparison to a power law fluid pumping against the pressure rise is more for a Herschel Bulkley fluid. Maiti and Misra [80] have analyzed the non-Newtonian properties of blood flow under peristalsis in micro-vessels, considering blood to be Herschel Bulkley fluid. Hummady and Abdulhadi [81] studied peristaltic motion under MHD analyzing the effects of heat transfer as well as slip on the flow of non-Newtonian fluid through a permeable medium. Recently, Akbar and Butt [82] examined the Herschel Bulkley fluid flow through a non-uniform conduit under peristalsis to study the temperature profile, velocity field, pressure gradient and stream function. They concluded that yield stress increases the temperature profile.

In view of all the studies mentioned above, the study of peristaltic motion of a non-Newtonian fluid, in particular the Herschel Bulkley fluid has been considered to analyze the flow of blood in small vessels. The flow analysis is worked out to explore the impacts of various parameters of concern under uniform, non-uniform, inclined, heat transfer and magnetic effects in the thesis. MATHEMATICA software is used to analyze the results graphically.

1.12 Outline of the Thesis

The first chapter is introductory, dealing the different characteristics of the fluid and the relevant literature survey, thus explaining the reason for consideration of the problems involved in the following chapters of the thesis and the basic equations of the fluid model.

Chapters 2-6 deal with the Peristaltic flow of Herschel-Bulkley fluid under different situations of the flow.

In Chapter 2 the peristaltic flow of the non-Newtonian, Herschel-Bulkley fluid in a flexible channel is considered for analysis. The channel wall is assumed to be coated with porous material. Exact solutions are obtained under the assumptions of long wavelength and low Reynolds number. The physical quantities of importance in peristaltic transport like pressure difference, frictional force and stream line patterns are discussed for various parameters of interest like yield stress, Darcy number, etc. through graphs. It is observed that with increase in porosity, the pressure difference decreases in the pumping region while there is a rise in the pressure difference in the co-pumping region. The behavior of the time averaged volume flow rate is similar for both the pressure difference and frictional force, for the variation of all the parameters. The results are applicable in physiological flows in small blood vessels. The trapped bolus is observed to increase in size with increase in the Darcy number, yield stress, porous thickening, as well the amplitude ratio.

Chapter 3 is concerned with flow in the non-uniform channel. The mathematical model is constructed for the flow of Herschel-Bulkley fluid, induced by the peristaltic motion in a non-uniform channel with porous walls. The solution is obtained under long wave length and low Reynolds number assumptions. The analytical solutions obtained are observed graphically to study the effects of various parameters. Through the analysis it is seen that pressure difference decreases with increase in Darcy number and increases with increase in the yield stress and the porous wall thickening, where as exactly the reverse behavior is observed for the frictional force for the same parameters. Stream line patterns drawn for the problem reveals that bolus enhances with the Darcy number, yield stress, porous thickening and also for the amplitude ratio. Further the bolus is larger in a convergent channel than in the divergent channel.

The study of flow through non-uniform inclined channel is put forth in Chapter 4. The peristaltic motion is modeled for the Herschel Bulkley fluid, considered to flow in a non-uniform inclined channel. The channel wall is supposed to be lined with a non-erodible porous material. The flow is considered to be moving in a wave frame of reference moving with the same velocity as of the sinusoidal wave. Low Reynolds number and long wave length assumptions are made to solve the model analytically. Solutions are obtained for the pressure difference, frictional force and also for the stream function. Graphs are plotted for both the results of pressure difference and frictional force against time average velocity. We observe that increasing the porous thickening, increases the pressure difference while, it decreases the frictional force. It is seen that the behavior of the pressure difference is opposite to the behavior of the frictional force for all the parameters considered. Stream lines are plotted for analyzing the trapped bolus. Rise in the values of Darcy number, yield stress, porous thickening and also for the amplitude ratio leads to enlargement of the trapped bolus.

Chapter 5 deals with the heat transfer effect on the flow of Herschel Bulkley fluid moving in a non-uniform channel under peristalsis. The channel wall is being considered to be coated with a porous lining. Mathematical analysis is done for the temperature profile, rate of temperature, heat transfer coefficient mechanical efficiency and stream lines, under lubrication approach. Graphs are plotted for all the above mentioned analytical solutions. The effects of the pertinent parameters are analyzed through the graphical illustrations. The results show that there is decrease in the temperature profile, heat transfer coefficient and the rate of temperature with increase in the Darcy number. Also as the porous coating of the channel wall is thickened there is rise in the temperature profile and the rate measure of temperature. The mechanical efficiency is seen to be more in a convergent channel than in uniform and divergent channels.

In Chapter 6 the magneto hydrodynamic effect on the Herschel Bulkley fluid moving in a uniform peristaltic channel is analyzed. The elastic channel walls are supposed to have a porous coating of non corrosive material. Closed form solutions are obtained for the pressure rise and frictional force and also for the axial velocity under perturbation method. Graphical illustrations are plotted for the obtained analytical solutions to explore the effects of the relevant parameters. Observations reveal that the behavior of pressure difference is exactly the opposite to that of frictional force, when plotted against the time averaged volume flow

rate. The velocity profile plot explains that strengthening the magnetic intensity descends the velocity. The trapped bolus shrinks by intensifying the magnetic field whereas it grows by enhancing the Darcy number, yield stress, porous thickening and the amplitude ratio.

Chapter 7 encloses the prominent outcomes of the present study and opens up the scope for future research work.

CHAPTER -2

Effect of Porosity on the Peristaltic Pumping of a Non-Newtonian Fluid in a Channel

2.1 Introduction:

'Peristalsis' is the rhythmic sequence of contractions of smooth muscle that progressively squeeze one small section of the tract and then the next, to push the content along the tract. It stimulates propulsion and amalgamation movements and drives the content in opposition to pressure rise, thus finding enormous physiological, biomedical and industrial applications as seen in esophagus, gastrointestinal tract, mechanical devices like finger pumps, roller pumps, etc. and even in translocation of water in tall trees, through its porous matrix.

Probably Latham [5] was the first to study the peristaltic mechanism which has attracted a large number of researchers towards the study of peristalsis.

For physiological peristalsis blood and other biofluids are believed to behave as Newtonian fluid. Though the Newtonian approach of blood gives satisfactory results for the ureter mechanism, it fails to do so in small blood vessels and intestine. Through the investigations [17, 22, 49] it is accepted that blood and most of the biofluids in tiny arteries and liquids in the lymphatic vessels and in the digestive system, the mercury amalgams, lubrication with heavy oils and greases, liquid metals etc which have industrial applications, behave non-Newtonianly. Hence, the study of non-Newtonian fluids has gained significance in the recent years. The peristaltic flow of a non-Newtonian fluid was first discussed by Raju and Devanathan [34].

A permeable medium is a material containing pores or spaces between solid matter wherein gas and liquid can pass through. As most of the tissues in the body are deformable porous media, in the recent years, studies involving flow past a porous media has gained significant interest, to understand various medical conditions (viz., tumor growth) and treatments (injections).

The study of peristaltic motion past a permeable medium was first presented by Shehawey et al. [46]. Since then many investigations have been done on the peristaltic transport in porous media. Vasudev et al. [50] have studied the peristaltic motion of a Newtonian fluid in a permeable medium in a vertical tube beneath the impact of magnetic field. The transport of a conducting fluid in a permeable medium under peristalsis in an asymmetric vertical channel

is discussed by Rami Reddy and Venkataramana [52]. Srinivas et al. [83] have considered the peristaltic transport of a Casson fluid in a conduit having permeable walls.

Herschel-Bulkley fluid is considered to be the more general non-Newtonian fluid as it has two parameters namely the power law index and yield stress. The constitutive equations of Power law, Newtonian and Bingham fluid models can be obtained from the constitutive equation of Herschel-Bulkley fluid. Santhosh Nallapu and Radhakrishnamacharya [84] have considered the motion of Herschel-Bulkley fluid along narrow tubes. Sankad and Radhakrishnamacharya [85] have examined the wall effects on the transport of a Herschel-Bulkley fluid in a non-uniform channel under peristalsis.

As mentioned above, many authors have worked on different non-Newtonian fluids without porosity. Therefore in this chapter the peristaltic flow of a Herschel-Bulkley fluid in a channel with porous lining has been considered. The flow is modeled for the non-Newtonian fluid flow in a uniform conduit with porous lining of the flexible walls. This helps in the better insight of the peristaltic flow of blood in small vessels. Pressure rise and frictional force are obtained under lubrication approach. The impacts of Darcy number, thickness of the porous lining, yield stress, amplitude ratio and index on the pressure rise and the frictional force are discussed and depicted through graphs. Stream lines are drawn to understand the trapping phenomenon.

2.2 Mathematical formulation:

The flow in a channel for a non-Newtonian fluid, obeying Herschel–Bulkley model, with half width 'a' and lined with non erodible porous material is considered. The flexible wall of the channel is subjected to a progressive sinusoidal wave with amplitude 'b', wave length 'λ' and wave speed 'c'. The discussion is restricted to half width of the channel and is depicted in Fig. 2.1. The section in between $y = 0$ and $y = y_0$ is known as the plug flow region where $|\tau_{xy}| \leq \tau_0$ and in the section between $y = y_0$ and $y = H$, $|\tau_{xy}| \geq \tau_0$.

The equation of the wall is given by,

$$Y = H(X, t) = a + b\, sin\frac{2\pi}{\lambda}(X - ct). \tag{2.1}$$

Also, assuming the pressure difference across the boundaries of the channel to be constant and length of the channel to be an integral multiple of the λ, the wavelength, the flow becomes steady in the wave frame (x, y), moving away from the laboratory frame (X, Y) with the velocity c.

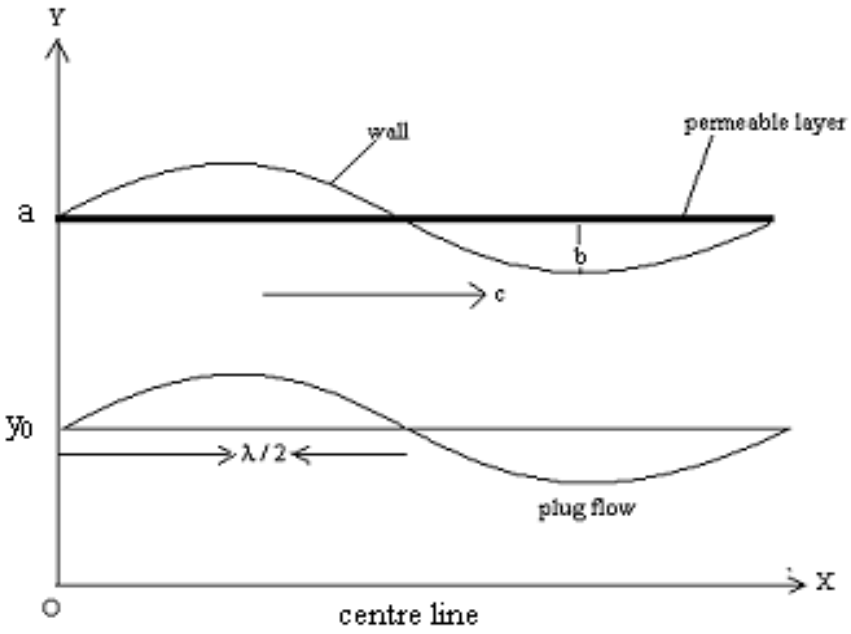

Fig. 2.1: Geometry of the flow

The transformation from laboratory frame to wave frame is given by

$$x = X - ct;\ \ y = Y;\ \ u(x,y) = U(X - ct, Y) - c\ ;\ \ v(x,y) = V(X - ct, Y);\ p(x) = P(X,t)$$

where (U, V) and (u, v) are the velocity components in the laboratory frame and wave frame respectively. As proved experimentally, the Reynolds number of the flow is very small in many physiological situations. The flow is assumed to be inertia free and the wavelength to be infinite. The non-dimensional quantities used to formulate the basic equations and the peripheral conditions to be dimensionless are,

$$x' = \frac{x}{\lambda}\ ; \qquad y' = \frac{y}{a}; \qquad h' = \frac{h}{a}; \qquad t' = \frac{ct}{\lambda}; \qquad \epsilon' = \frac{\epsilon}{a}; \qquad {\tau_0}' = \frac{\tau_0}{\mu\left(\frac{c}{a}\right)^n};$$

$$\psi' = \frac{\psi}{ac}; \qquad q' = \frac{q}{ac}; \qquad u' = \frac{u}{c}; \qquad F' = \frac{fa}{\mu\lambda c}; \qquad \phi = \frac{b}{a}; \qquad Da = \frac{s}{a^2}$$

Assuming low Reynolds number and long wavelength, the governing equations of motion (1.3) and (2.1) after sinking the primes are as follows,

$$h(x) = 1 + \phi \sin 2\pi x \tag{2.2}$$

$$\frac{\partial}{\partial y}(\tau_{yx}) = -\frac{\partial p}{\partial x}, \tag{2.3}$$

$$\text{where } \tau_{yx} = \left(-\frac{\partial u}{\partial y}\right)^n + \tau_0, \tag{2.4}$$

and the peripheral conditions are,

$$\psi = 0 \quad at \quad y = 0. \tag{2.5}$$

$$\psi_{yy} = 0 \quad at \quad y = 0. \tag{2.6}$$

$$\tau_{yx} = 0 \quad at \quad y = 0. \tag{2.7}$$

$$u = -\frac{\sqrt{Da}}{\alpha}\frac{\partial u}{\partial y} - 1 \quad at \quad y = h(x) - \epsilon. \tag{2.8}$$

where, u is the velocity, α denotes the slip parameter, Da the Darcy number, τ represents the yield stress and ϵ the porous thickening of the channel wall. Also ψ denotes the stream function with $u = \frac{\partial \psi}{\partial y}$ and $v = -\frac{\partial \psi}{\partial x}$.

2.3 Solution of the problem:

On solving equations (2.3) and (2.4) along with $u = \frac{\partial \psi}{\partial y}$, $v = -\frac{\partial \psi}{\partial x}$ and the boundary conditions (2.5) − (2.8), we obtain the velocity field as:

$$u = P^m \left[\frac{1}{m+1}\{(h - \epsilon - y_o)^{m+1} - (y - y_o)^{m+1}\} + \frac{\sqrt{Da}}{\alpha}(h - \epsilon - y_o)^m\right] - 1, \tag{2.9}$$

where

$$P = -\frac{\partial p}{\partial x} \ and \ m = \frac{1}{n}. \tag{2.10}$$

The upper limit of the plug flow region is obtained using the boundary condition

$\psi_{yy} = 0, \ at \ y = y_0$, which gives, $y_0 = \frac{\tau_0}{P}$.

Also by using the condition $\tau_{xy} = \tau_{h-\epsilon}$ at $y = h - \epsilon$, we get $P = \frac{\tau_{h-\epsilon}}{h-\epsilon}$.

Therefore $\frac{y_0}{h-\epsilon} = \frac{\tau_0}{h-\epsilon} = \tau$; for $0 < \tau < 1$.

Velocity in the plug flow region is obtained taking $y = y_o$ in (2.9) as,

$$u_p = P^m(h - \epsilon - y_o)^m \left(\frac{h - \epsilon - y_o}{1+m} + \frac{\sqrt{Da}}{\alpha}\right) - 1. \tag{2.11}$$

Integrating equations (2.9) and (2.11) and with the use of conditions $\psi_p = 0$ and $\psi = \psi_p$ at $y = y_o$, the stream function is given as,

$$\psi = P^m \left[\frac{1}{m+1}\left\{(h - \epsilon - y_o)^{m+1} y - \frac{(y-y_o)^{m+2}}{m+2}\right\} + \frac{\sqrt{Da}}{\alpha}(h - \epsilon - y_0)^m \, y\right] - y. \tag{2.12}$$

$$\psi_p = \int u_p dy = P^m(h - \epsilon - y_0)^m \left(\frac{h-\epsilon-y_0}{m+1} - \frac{\sqrt{Da}}{\alpha}\right) y - y. \tag{2.13}$$

The volume flow rate 'q' in the wave frame, through every cross section, is given by,

$$q = \int_0^{y_0} u_p dy + \int_{y_0}^{h-\epsilon} u \, dy.$$

$$q = P^m \left[\frac{(h-\epsilon-y_0)^{m+1}}{m+1}\left\{h - \epsilon - \frac{(h-\epsilon-y_0)}{m+2}\right\} + (h - \epsilon - y_0)^m \frac{\sqrt{Da}}{\alpha}(h - \epsilon)\right] - (h - \epsilon). \tag{2.14}$$

From equation (2.14) we get,

$$P = -\frac{\partial p}{\partial x} = \left[\frac{(q+h-\epsilon)(m+1)(m+2)\alpha}{(h-\epsilon)^{m+1}(1-\tau)^m\{\alpha(h-\epsilon)(1-\tau)\{(m+2)-(1-\tau)\} + \sqrt{Da}(m+1)(m+2)\}}\right]^{\frac{1}{m}}. \tag{2.15}$$

The instantaneous volume flow rate $Q(X, t)$ in between the central line and the boundary of the channel, in the laboratory frame is,

$$Q(X,t) = \int_0^H U(X,Y,t)dY. \tag{2.16}$$

Averaging equation (2.16) over a single period yield the (time mean flow) time-averaged volume flow rate $\bar{Q}$ as,

$$\bar{Q} = \frac{1}{T}\int_0^T Q dt = q + 1. \tag{2.17}$$

The pressure rise over one cycle of the wave is obtained by integrating equation (2.15) w.r.t 'x' over one wavelength as,

$$\Delta P = \int_0^1 \frac{\partial p}{\partial x}\, dx = -\int_0^1 P\, dx. \tag{2.18}$$

The frictional force F across one wavelength is given by

$$F = \int_0^1 h\left(-\frac{\partial p}{\partial x}\right) dx. \tag{2.19}$$

2.4 Results and discussion:

The idea of pumping characteristic was first introduced by Shapiro et al. [8], signifying that pumping is determined through the variation in time averaged flux with difference in pressure across one wavelength. To analyze the pumping characteristics the pressure difference ΔP is obtained as function of the time averaged volume flow rate $\bar{Q}$, as in equation (2.18), considering Herschel Bulkley fluid. The effects of various parameters, the Darcy number Da, the yield stress τ, the porous thickening of the channel wall ϵ and the index number n, are observed with the help of graphs that are obtained using Mathematica software.

Figure 2.2 shows the pressure difference ΔP as a function of the time averaged volume flow rate $\bar{Q}$ for various values of Darcy number and for fixed values of τ, n, α and ϵ. Observation in the pumping region ($\Delta P > 0$), for a given time averaged volume flow rate $\bar{Q}$ reveals that the pressure difference decreases as the Darcy number increases and for a fixed

pressure difference ΔP, it is seen that the time averaged volume flow rate $\bar{Q}$ reduces with enhancement in the values Darcy number. In the free pumping region ($\Delta P = 0$), the variation of Darcy number has no effect on $\bar{Q}$. In the co-pumping region ($\Delta P < 0$), for a given time averaged volume flow rate $\bar{Q}$ the pressure difference enhances with rise in the Darcy number and for a fixed pressure difference ΔP, as the Darcy number increases, the time averaged volume flow rate $\bar{Q}$ also increases.

Figure 2.3 shows the impact of τ on the pressure difference ΔP plotted as a function of the time averaged volume flow rate $\bar{Q}$, for fixed values of other parameters. It is observed that in the pumping region, for a fixed time averaged volume flow rate $\bar{Q}$ the pressure difference raises with the yield stress τ, because as the yield stress threshold increases then more deformation will occur and molecules are put together that increases the pressure difference. This result agrees with that of Akbar and Butt [82]. Further it is seen that for a fixed pressure difference ΔP, the time averaged volume flow rate $\bar{Q}$ also enhances as the yield stress increases. In the free pumping region there is no effect of τ on $\bar{Q}$. In the co-pumping region, for a given time averaged volume flow rate $\bar{Q}$, the pressure difference decreases as the yield stress increases and for a fixed pressure difference ΔP, the time averaged volume flow rate $\bar{Q}$ decreases as the yield stress increases.

The effect of porous thickening ϵ, for fixed $Da,\ n,\ \alpha$ and τ is shown in Fig. 2.4. In the pumping region it is seen that, for a fixed time averaged volume flow rate $\bar{Q}$ the pressure difference enhances with rise in the value of ϵ and for a fixed pressure difference ΔP, the time averaged volume flow rate $\bar{Q}$ also rises with rise in ϵ. In the free pumping region also, time averaged volume flow rate $\bar{Q}$ increases with rise in ϵ. In the co-pumping region, for $0.4 < \bar{Q} < 0.85$ there is no effect of ϵ on ΔP as well on $\bar{Q}$ and for $0.85 < \bar{Q} < 1$, for fixed time averaged volume flow rate $\bar{Q}$, ΔP decreases as ϵ increases and for fixed ΔP, $\bar{Q}$ decreases slightly for increase in the values of ϵ.

The effect of the index n for fixed values of other parameters $\alpha,\ \epsilon,\ \tau$ and Da is shown in Fig. 2.5. It is seen that in the pumping region, when the time averaged volume flow rate $\bar{Q}$ is fixed, the pressure difference decreases with rise in the index n and for a fixed pressure difference ΔP, observations show that the time averaged volume flow rate $\bar{Q}$ also reduces

with rise in the index number. For free pumping region, time averaged volume flow rate $\bar{Q}$ reduces when n is increased. In the co-pumping region, when the time averaged volume flow rate $\bar{Q}$ is held constant the pressure difference rises with n and for a fixed pressure difference ΔP, as the index increases, the time averaged volume flow rate $\bar{Q}$ also increases.

From equation (2.19), the Frictional force F is obtained as a function of $\bar{Q}$, and the consequences of the parameters under consideration are depicted in Fig. 2.6 to Fig. 2.9.

Figure 2.6 depicts the effect of Darcy number variation, for fixed values of τ, n, α and ϵ. It is seen that for fixed averaged volume flow rate $\bar{Q}$, the Frictional force first increases and then reduces with gain in the values of Darcy number. For a fixed Frictional force F, the time averaged volume flow rate $\bar{Q}$ first reduces and then increase with rise in the Darcy number. The variation of Darcy number has no effect on $\bar{Q}$ for $F = 0$.

In Fig. 2.7 the Frictional force F is obtained as a function of the time averaged volume flow rate $\bar{Q}$, for various values of τ and for fixed Da, n, α and ϵ. For fixed time averaged volume flow rate $\bar{Q}$ the Frictional force decreases first and later increases for increase in the yield stress τ. For a fixed Frictional force, it is seen that the time averaged volume flow rate, increase and then decrease, as the yield stress increases. There is no effect of τ on $\bar{Q}$ between $0.3 < \bar{Q} < 0.6$ for $F = 0$.

The effect of porous thickening ϵ, with fixed values of the other parameters is shown in Fig. 2.8. For $0 < \bar{Q} < 0.4$, the Frictional force F decreases as ϵ increases and for $\bar{Q} > 0.85$, the Frictional force increases with an increase in the value of ϵ. For a fixed Frictional force F, the time averaged volume flow rate $\bar{Q}$ increases in $0 < \bar{Q} < 0.4$ and for $\bar{Q} > 0.85$, the time averaged volume flow rate decreases as ε is increased and for $0.4 < \bar{Q} < 0.85$, there is no effect of variation in ϵ.

For fixed values of Da, α, ϵ and τ, the effect of the index n is depicted in Fig. 2.9. Observations say that, for fixed time averaged volume flow rate $\bar{Q}$, the Frictional force F enhances and then decreases with rise in the index n. And for a fixed Frictional force, the graph discloses that the time averaged volume flow rate $\bar{Q}$ decreases and then rises with rise

in the index number. For $F = 0$, time averaged volume flow rate $\bar{Q}$ lessens with an enhancement in n.

The frictional force F behaves reversely in comparison with the pressure rise, thus obeying the results of Vajravelu [75]

The stream line patterns from Figs. 2.10 - 2.15 reveal the trapping characteristics. Increase in the values of Darcy number Da (Fig. 2.10), yield stress τ (Fig. 2.11), porous thickening ϵ (Fig. 2.12), as well the amplitude ratio ϕ (Fig. 2.13) increases the magnitude of the trapped bolus. But with increase in the values of n and $\bar{Q}$, the size of the trapped bolus decreases, as seen from Fig. 2.14 and Fig. 2.15 respectively.

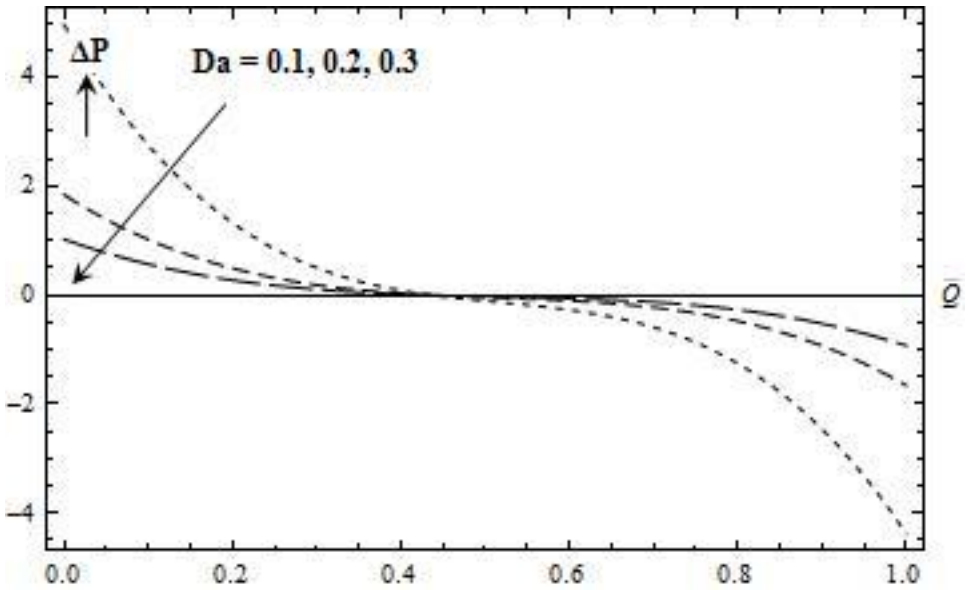

Fig. 2.2: Effect of Da on ΔP against $\bar{Q}$ with:

$n = 3;\ \alpha = 0.1;\ \tau = 0.1;\ \epsilon = 0.3;\ \phi = 0.3$

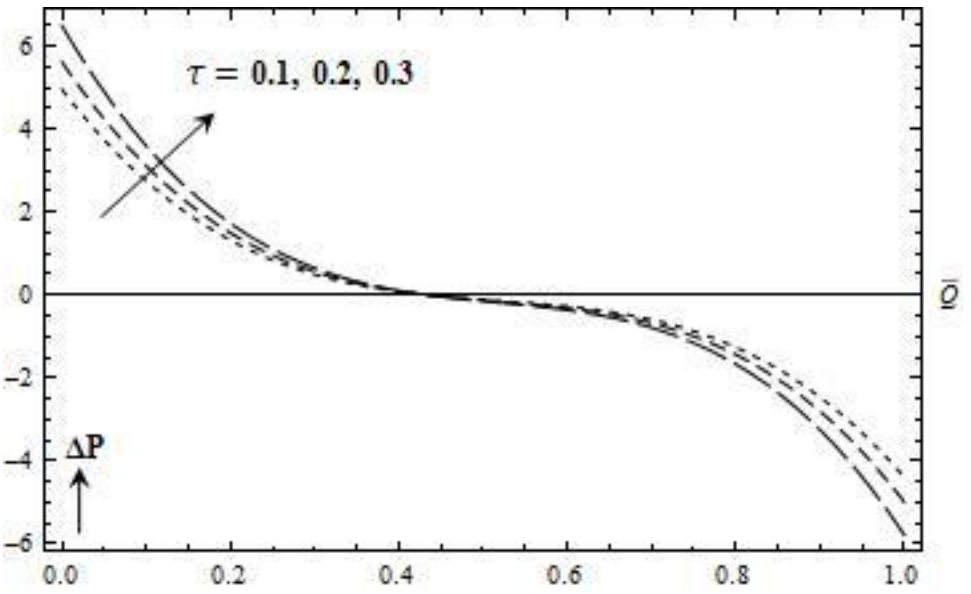

Fig. 2.3: Effect of τ on ΔP against $\bar{Q}$ with:

$n = 3;\ \alpha = 0.1;\ Da = 0.1;\ \epsilon = 0.3;\ \phi = 0.3$

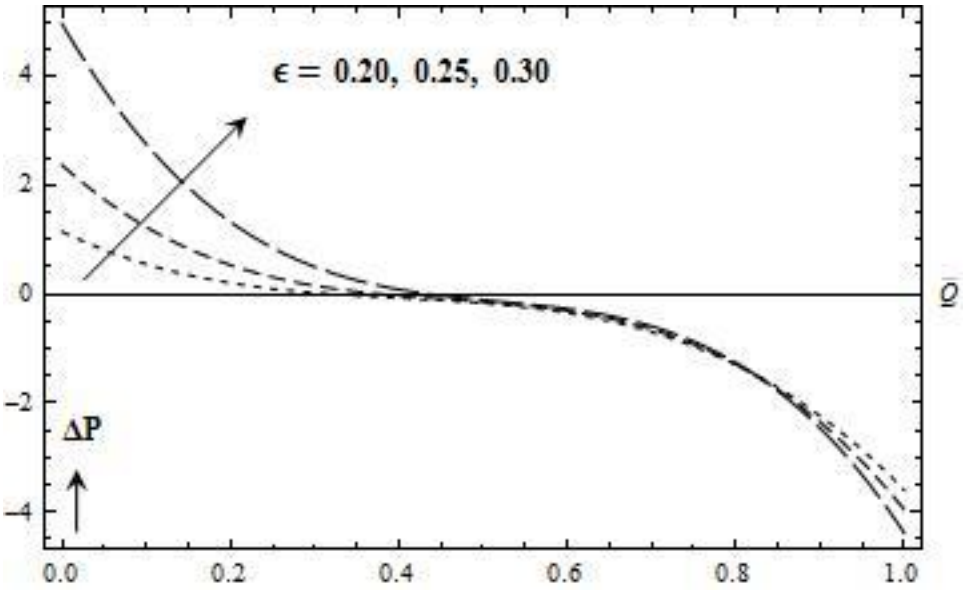

Fig. 2.4: Effect of ϵ on ΔP against $\bar{Q}$ with:
$n = 3;\ \alpha = 0.1;\ Da = 0.1;\ \tau = 0.1;\ \phi = 0.3$

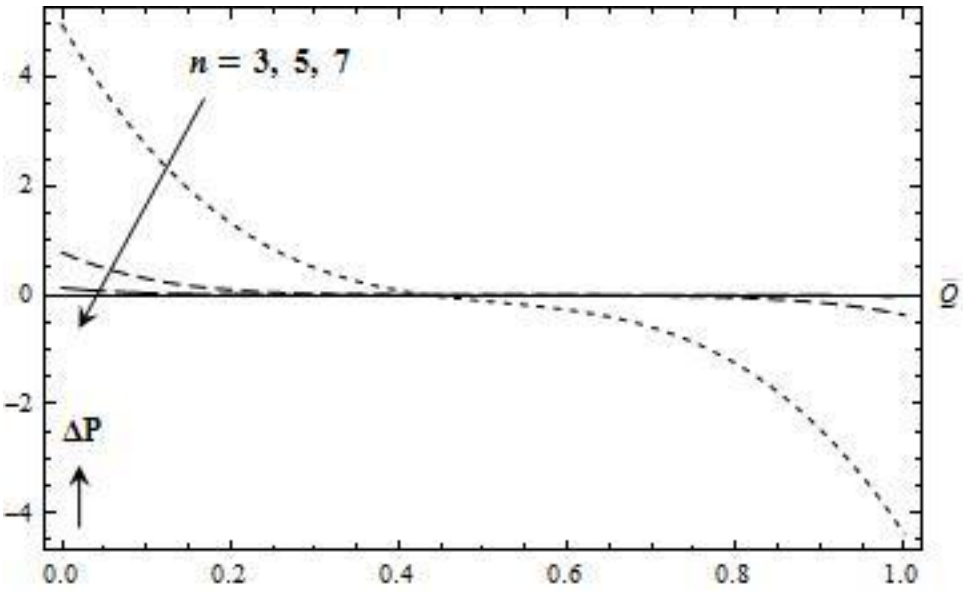

Fig. 2.5: Effect of n on ΔP against $\bar{Q}$ with:
$\alpha = 0.1;\ Da = 0.1;\ \tau = 0.1;\ \epsilon = 0.3;\ \phi = 0.3$

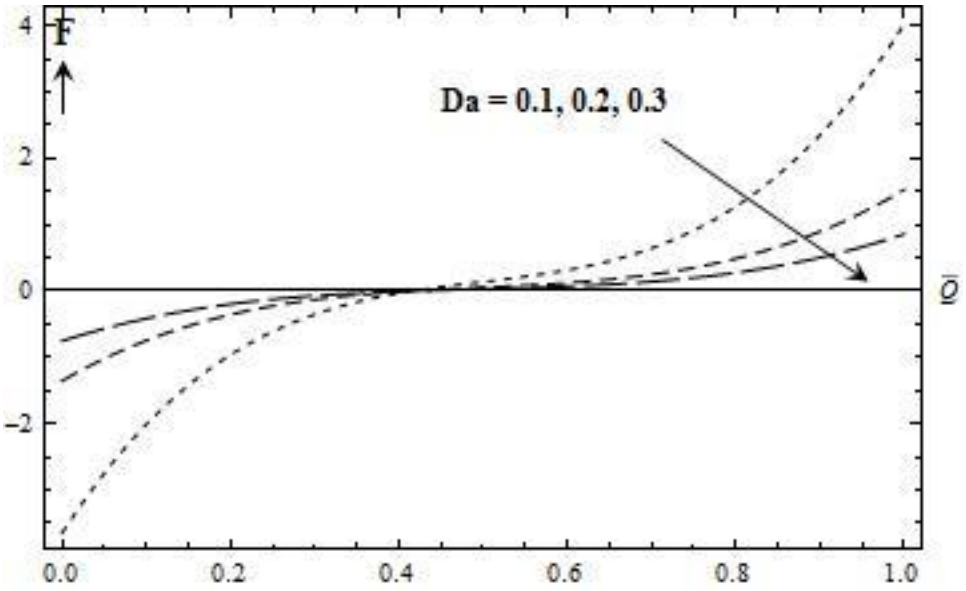

Fig. 2.6: Effect of Da on F against $\bar{Q}$ with:

$n = 3$; $\alpha = 0.1$; $\tau = 0.1$; $\epsilon = 0.3$; $\phi = 0.3$

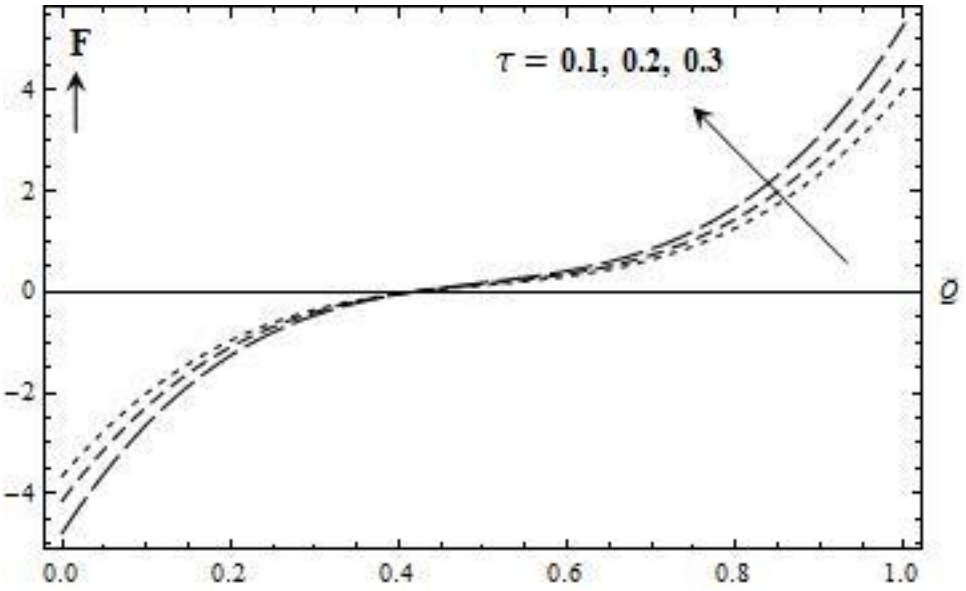

Fig. 2.7: Effect of τ on F against $\bar{Q}$ with:

$n = 3$; $\alpha = 0.1$; $Da = 0.1$; $\epsilon = 0.3$; $\phi = 0.3$

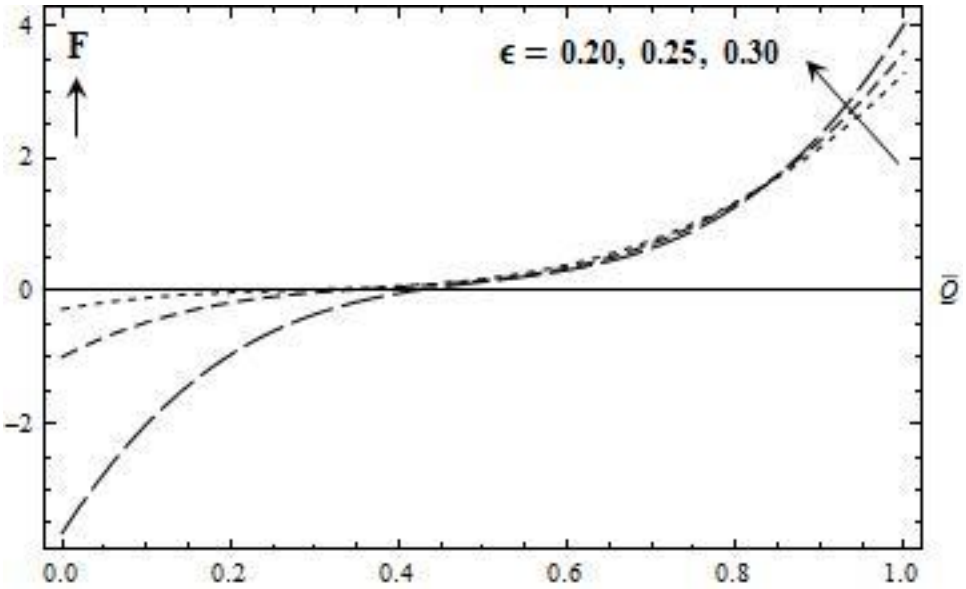

Fig. 2.8: Effect of ϵ on F against $\bar{Q}$ with:

$n = 3;\ \alpha = 0.1;\ Da = 0.1;\ \tau = 0.1;\ \phi = 0.3$

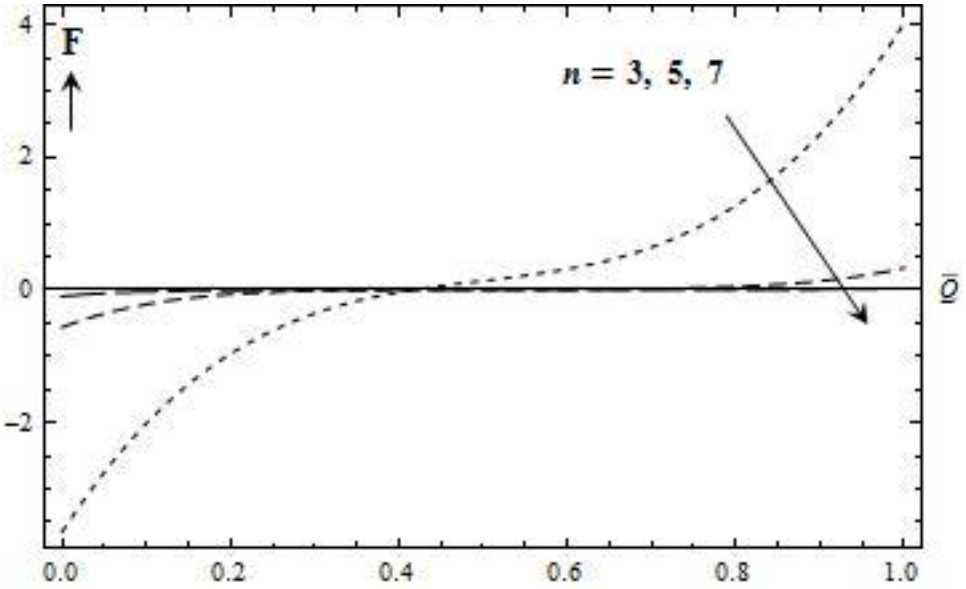

Fig. 2.9: Effect of n on F against $\bar{Q}$ with:

$\alpha = 0.1;\ Da = 0.1;\ \tau = 0.1;\ \epsilon = 0.3; \phi = 0.3$

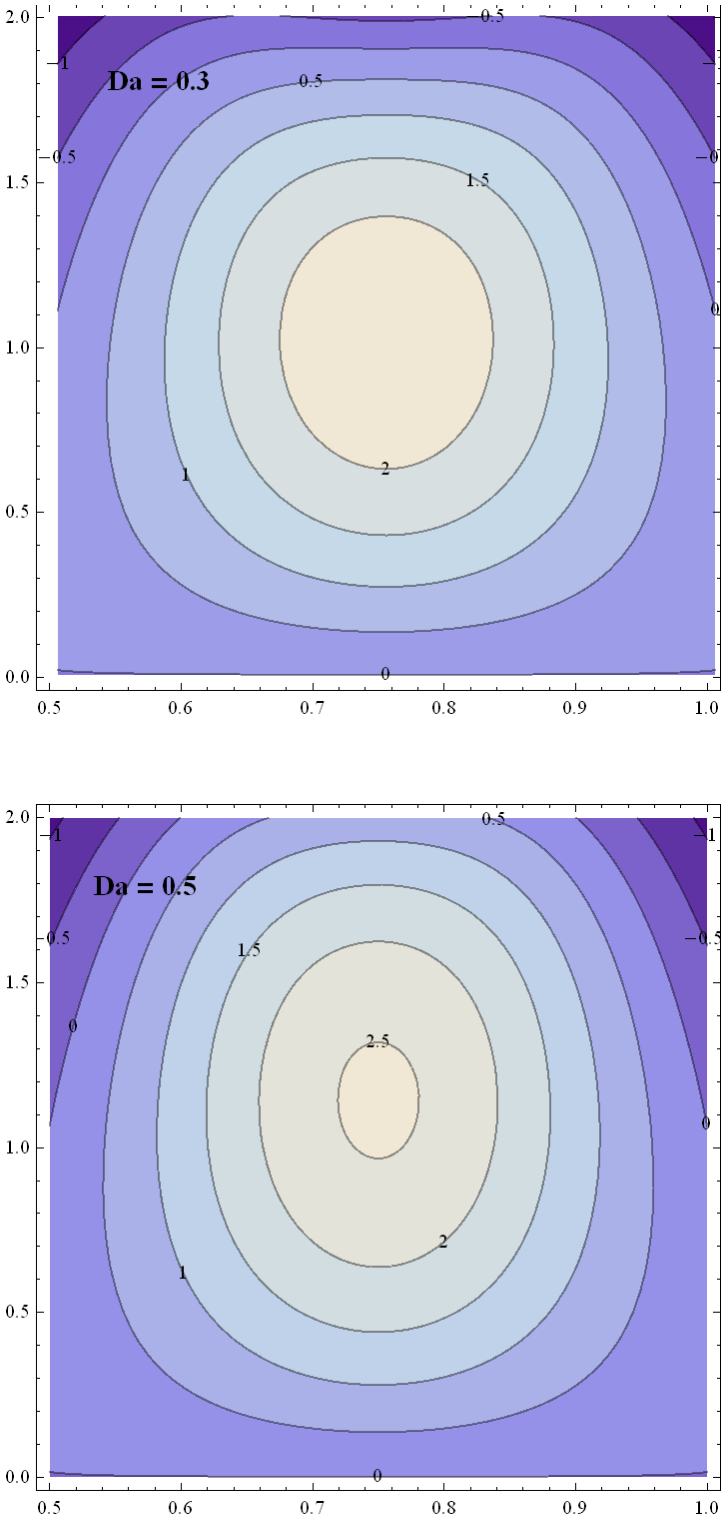

Fig. 2.10: Stream line plots for variation in Da with:

$n = 3$; $\alpha = 1$; $\tau = 0.5$; $\epsilon = 0.3$; $\bar{Q} = 0.1$; $\phi = 0.3$

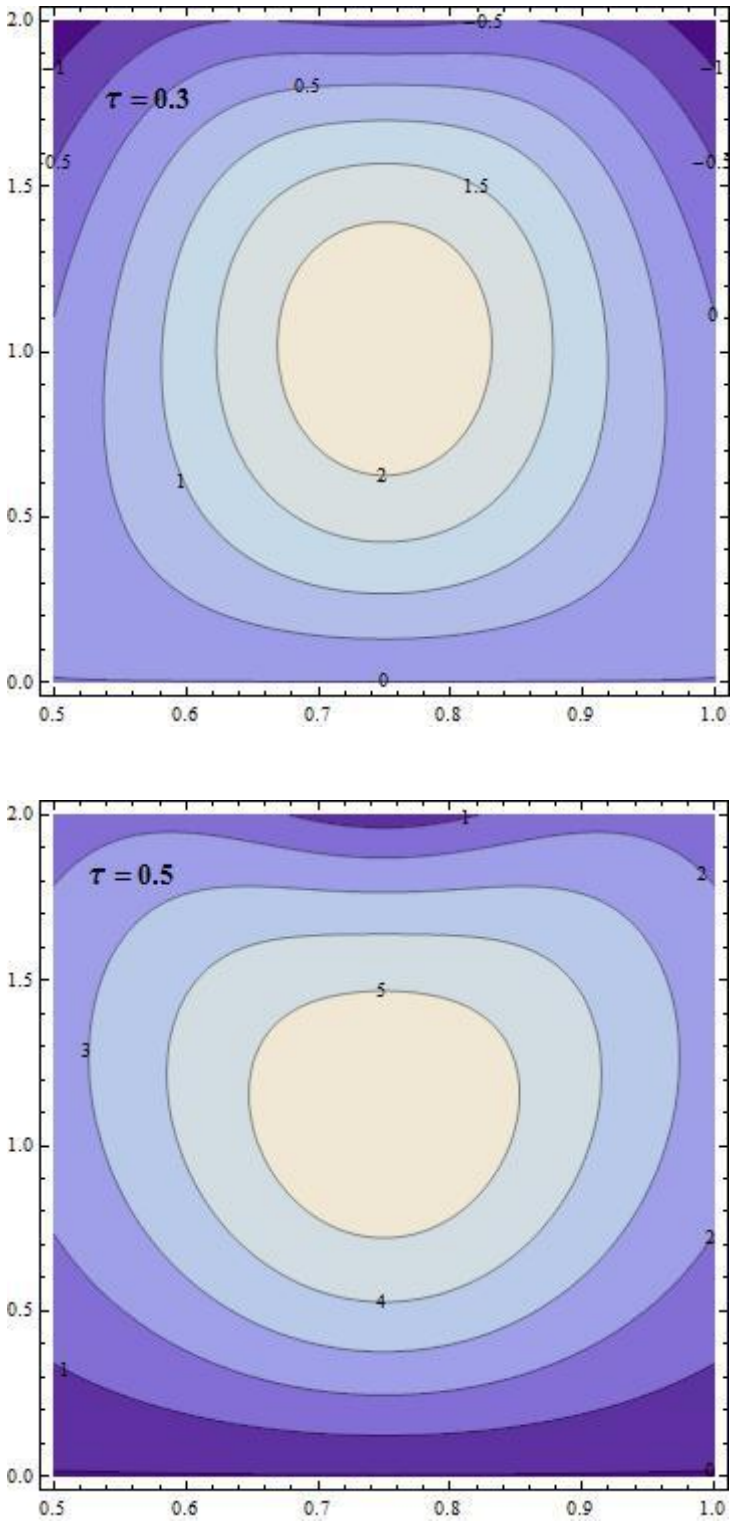

Fig. 2.11: Stream line plots for variation in τ with:

$$n = 3;\ \alpha = 1;\ Da = 0.3;\ \epsilon = 0.3;\ \bar{Q} = 0.1;\ \phi = 0.3$$

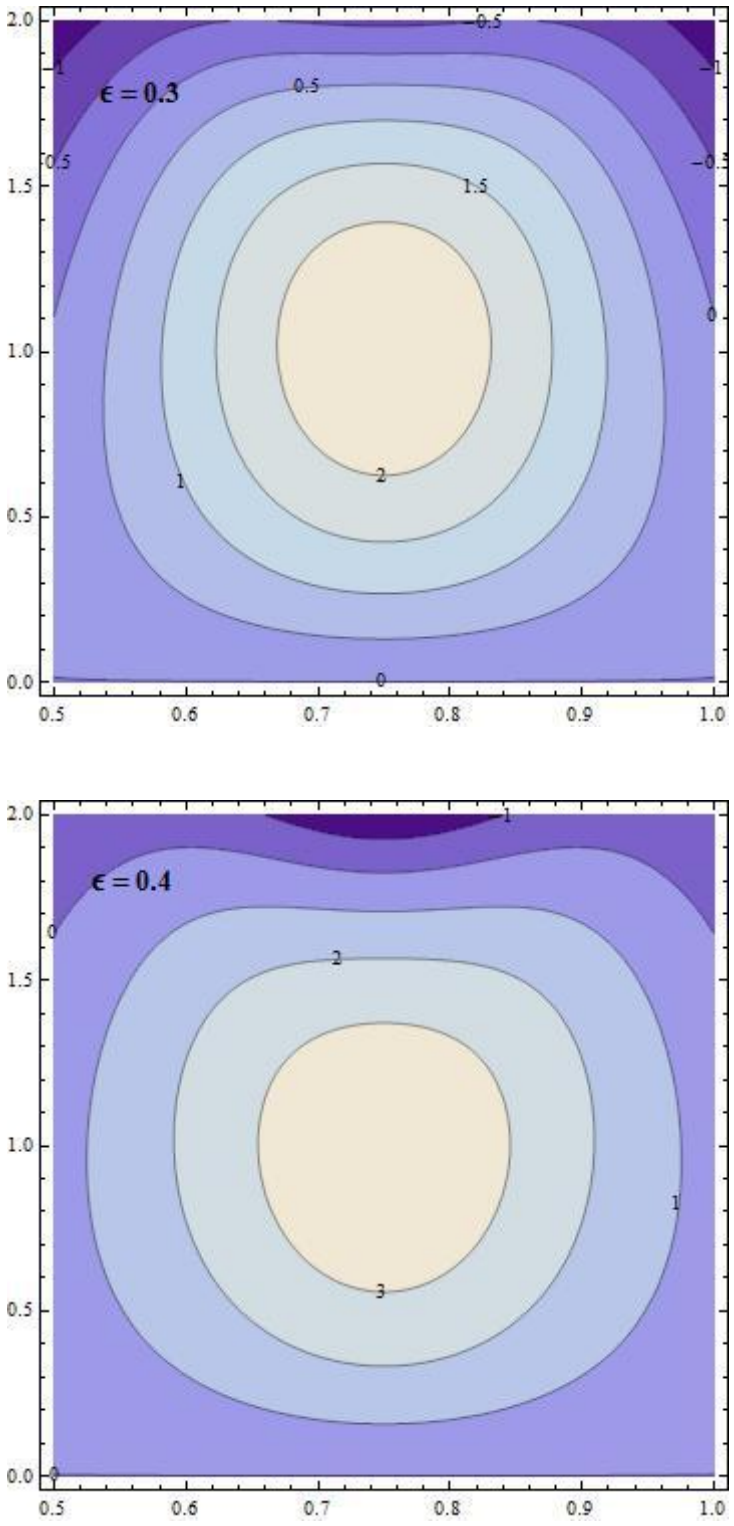

Fig. 2.12: Stream line plots for variation in ϵ with:

$$n = 3;\ \alpha = 1;\ Da = 0.3;\ \tau = 0.5;\ \bar{Q} = 0.1;\ \phi = 0.3$$

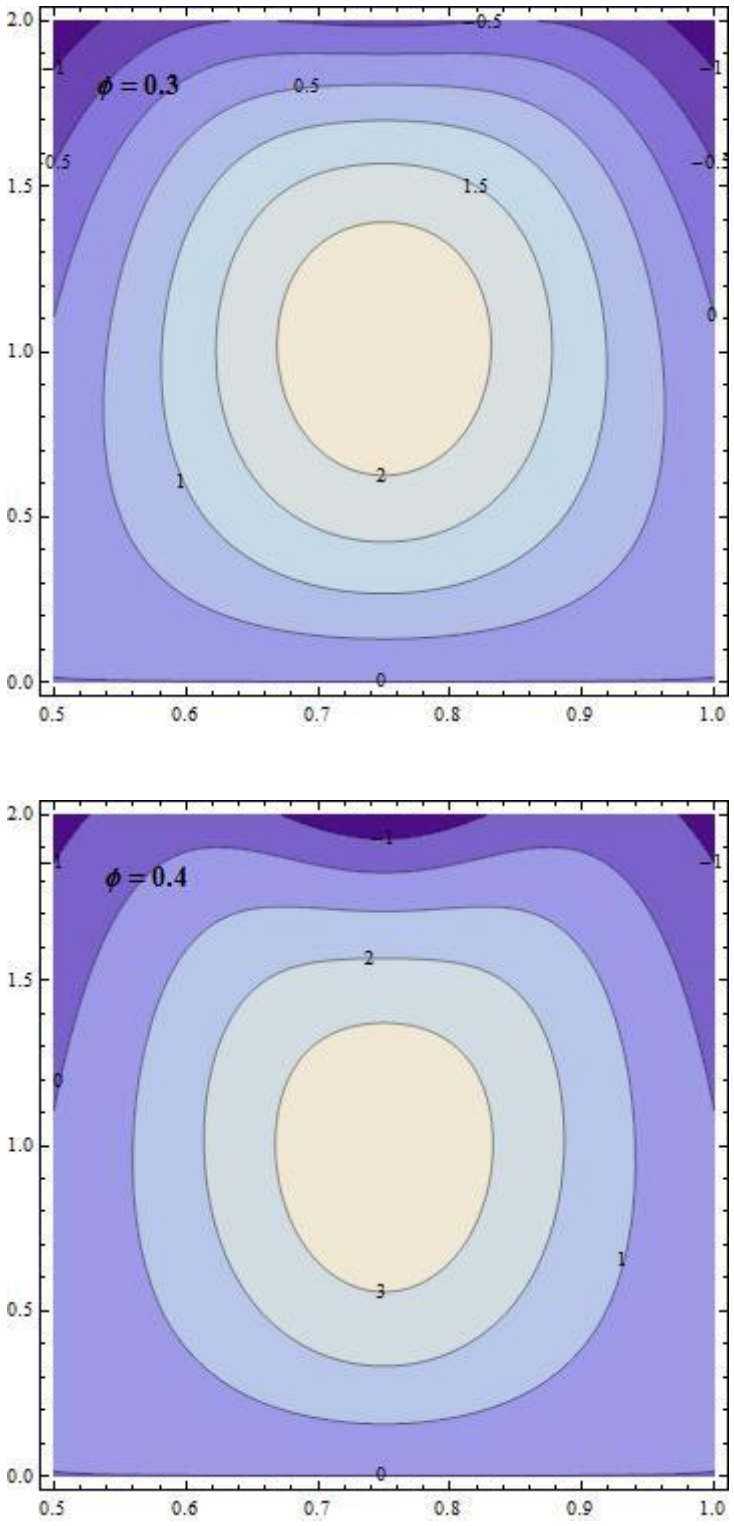

Fig. 2.13: Stream line plots for variation in ϕ with:

$n = 3;\ \alpha = 1;\ Da = 0.3;\ \tau = 0.3;\ \bar{Q} = 0.1;\ \epsilon = 0.3$

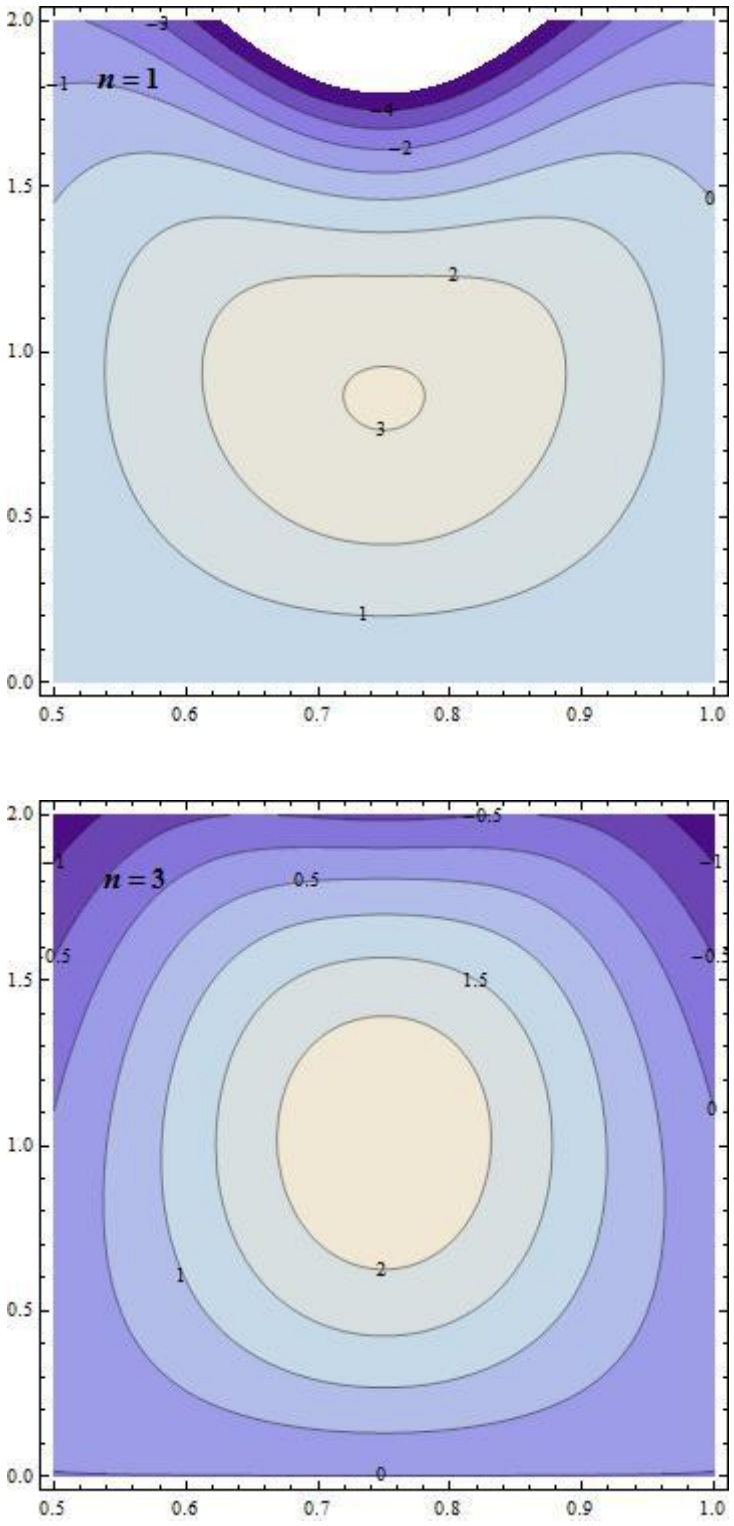

Fig. 2.14: Stream line plots for variation in n with:

$$Da = 0.3; \alpha = 1; \tau = 0.5; \epsilon = 0.3; \bar{Q} = 0.1; \phi = 0.3$$

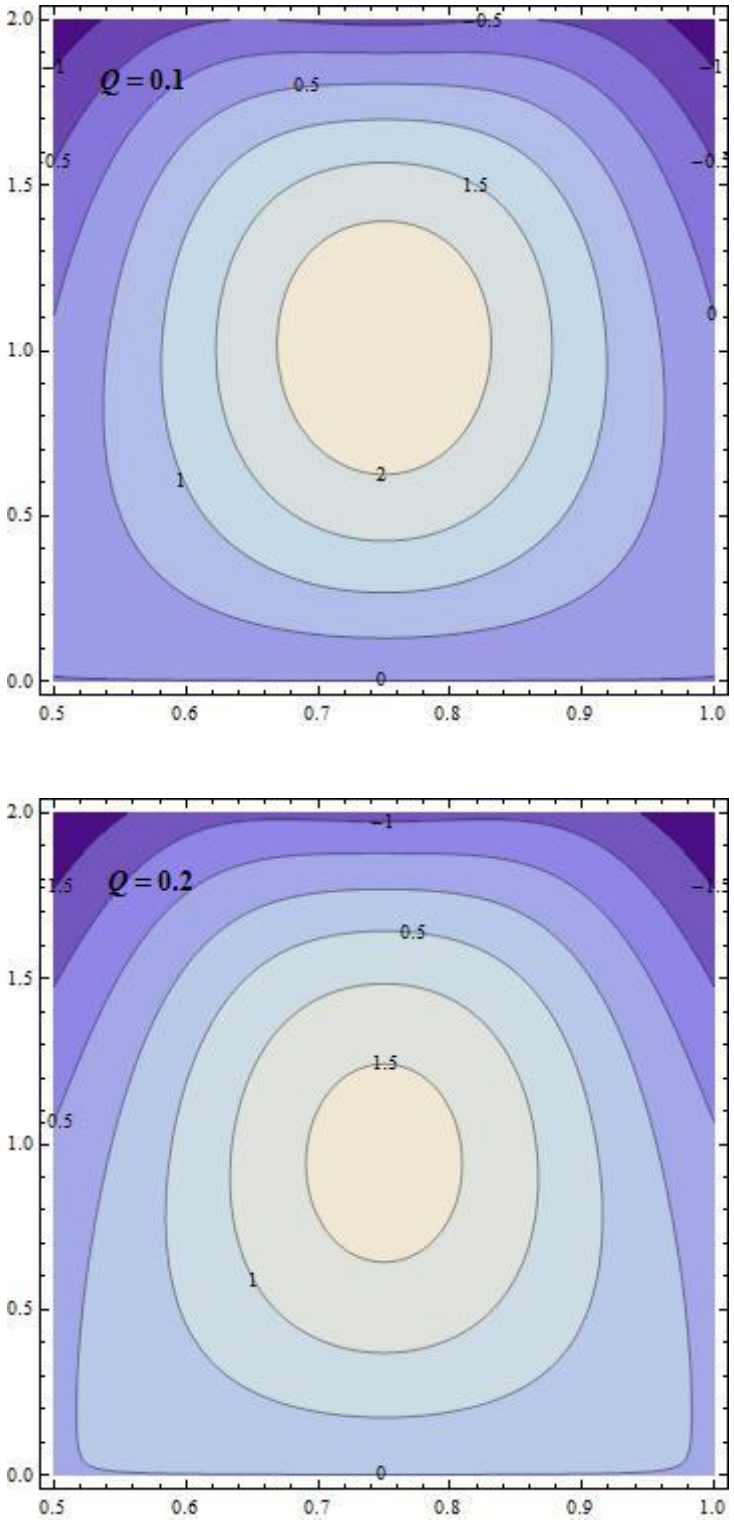

Fig. 2.15: Stream line plots for variation in $\overline{Q}$ with:
$n = 3;\ Da = 0.3;\ \alpha = 1;\ \tau = 0.5;\ \epsilon = 0.3;\ \phi = 0.3$

CHAPTER-3

Peristaltic Flow of Herschel Bulkley Fluid in a Non-Uniform Channel with Porous Lining

3.1. Introduction:

The peristaltic flow through pipes and channels is widely studied due to its vivid applications in Mechanics and Biophysics. Mechanical device like roller pump and biomechanical device like heart lung machine are based on the pumping of fluid through flexible tubes through a sinusoidal wave of area contraction and relaxation called 'Peristalsis'.

In the second chapter we have considered the peristaltic motion of the non Newtonian Herschel-Bulkley fluid in a uniform conduit. But it is observed in many physiological structures that the ducts are not always uniform. Therefore the peristaltic transport of a non Newtonian Herschel-Bulkley fluid past a non uniform channel having porous lining of the walls has been studied in this chapter.

In view of this Gupta and Sheshadri [86] considered a non-uniform duct in their study, but without elasticity. Also it is seen that the human body is made up of several non-uniform ducts, viz., intestine, lymphatic vessels, ductus efferentus of the reproductive tract, etc. (Haynes [87], Lee and Fung [88], Srivastava.et.al [15]).

The magnetic effect on the peristaltic blood transport in a non uniform channel is examined by Mekheimer [66]. The slip flow and couple stress interaction in uniform as well as non-uniform channels has been analyzed by Sobh [89]. Sobh and Mady [90] have investigated the consequences of the pertinent parameters in their study on peristaltic flow of an incompressible Newtonian fluid through a non uniform conduit with porosity. Nagachandrakala.et.al. [56] analyzed the impact of slip conditions in the motion of a hyperbolic tangential fluid with MHD peristaltic motion through a non-uniform conduit with porosity.

Herschel Bulkley fluid is a non-Newtonian fluid which needs yield stress to deform. With the increment and decrement of the yield stress, the fluid behaves as shear thickening or shear thinning fluid. Illustration of this are paints, plastics, food products, polymeric solutions etc which have applications in real life and biomedical engineering. Also since Herschel Bulkley fluid model is considered to be better than the Casson's model (Blair and Spanner [73]), we have carried on our studies with Herschel-Bulkley fluid as the non Newtonian fluid. The motion has been considered through a non uniform channel with porous lining. Obtaining the

solution with long wavelength as well as small Reynolds number presumptions, the impacts of distinct parameters are studied for the rise in pressure and frictional force. The stream line patterns are also sketched for analysis.

3.2 Mathematical formulation:

The peristaltic transport of a non-Newtonian fluid in a non-uniform channel is considered for analysis. The walls of the channel are lined with the porous material. A train of progressive infinite sinusoidal wave is assumed to travel in a channel with two dimensions having width $2a$ and velocity c. x-axis is taken along the direction of propagation of wave through the centre line and y-axis perpendicular to the x-axis as shown in Fig.3.1.

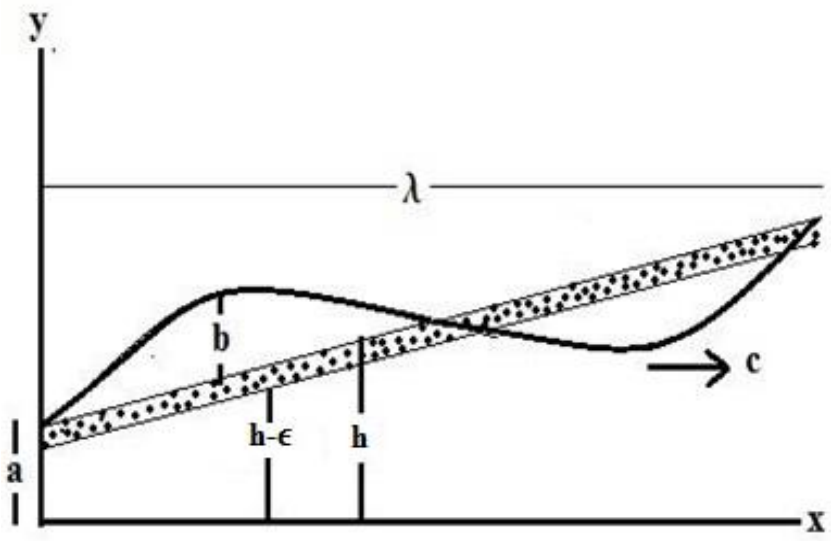

Fig. 3.1: Geometry of the flow

The channel wall is governed by the equation

$$Y = H(X,t) = a + b\,sin\frac{2\pi}{\lambda}(X - ct), \tag{3.1}$$

where $a = a_0 + kx$ and λ being taken as the wavelength, b as amplitude of the wave, and a as half the width of the channel from the inlet at any axial distance and a_0 being the channel half width at the inlet, k represents the non-uniformity of the channel.

The equations governing the flow after dropping primes are as follows,

$$\frac{\partial}{\partial y}(\tau_{yx}) = -\frac{\partial p}{\partial x}, \tag{3.2}$$

where $\tau_{yx} = \left(-\frac{\partial u}{\partial y}\right)^n + \tau_0$. (3.3)

and the dimensionless conditions at the boundary are,

$$\psi = 0 \ \ at \ \ y = 0. \tag{3.4}$$

$$\psi_{yy} = 0 \ \ at \ \ y = 0. \tag{3.5}$$

$$\tau_{yx} = 0 \ \ at \ \ y = 0. \tag{3.6}$$

$$u = -\frac{\sqrt{Da}}{\alpha}\frac{\partial u}{\partial y} - 1 \ \ at\ y = h(x) - \epsilon, \tag{3.7}$$

where $u, \alpha, Da, \epsilon, \tau, \psi$ are the parameters with their usual meanings as already discussed in Chapter-2.

3.3 Solution of the problem:

On working out with the equations (3.2) and (3.3) together with $u = \frac{\partial \psi}{\partial y}$ and $v = -\frac{\partial \psi}{\partial x}$ and the constraints (3.4) – (3.7), the velocity field is obtained as,

$$u = P^m\left[\frac{1}{m+1}\{(h-\epsilon-y_o)^{m+1} - (y-y_o)^{m+1}\} + \frac{\sqrt{Da}}{\alpha}(h-\epsilon-y_o)^m\right] - 1, \tag{3.8}$$

where,

$$P = -\frac{\partial p}{\partial x} \ and \ m = \frac{1}{n}. \tag{3.9}$$

The upper bound of the plug region is found with the help of peripheral conditions,

$\psi_{yy} = 0, \ when \ y = y_0$, thus, $y_0 = \frac{\tau_0}{P}$.

Furthermore, $\tau_{xy} = \tau_{h-\epsilon}$ at $y = h - \epsilon$, gives $P = \frac{\tau_{h-\epsilon}}{h-\epsilon}$.

Therefore, $\frac{y_0}{h-\epsilon} = \frac{\tau_o}{h-\epsilon} = \tau\ ;\ 0 < \tau < 1.$

Using $y = y_o$ in (3.8), gives the plug flow velocity as,

$$u_p = P^m(h - \epsilon - y_o)^m \left(\frac{h - \epsilon - y_o}{1+m} + \frac{\sqrt{Da}}{\alpha}\right) - 1. \tag{3.10}$$

Integrating both the equations (3.9) and (3.10) and employing the conditions $\psi = \psi_p$ and $\psi_p = 0$ at $y = y_o$, the stream function is obtained as,

$$\psi = P^m \left[\frac{1}{m+1}\left\{(h - \epsilon - y_o)^{m+1} y - \frac{(y-y_o)^{m+2}}{m+2}\right\} + \frac{\sqrt{Da}}{\alpha}(h - \epsilon - y_0)^m\, y\right] - y. \tag{3.11}$$

$$\psi_p = \int u_p dy = P^m(h - \epsilon - y_0)^m \left(\frac{h-\epsilon-y_0}{m+1} - \frac{\sqrt{Da}}{\alpha}\right) y - y. \tag{3.12}$$

At each cross section the volume flow rate 'q' is

$$q = \int_0^{y_0} u_p dy + \int_{y_0}^{h-\epsilon} u\, dy.$$

$$q = P^m \left[\frac{(h-\epsilon-y_0)^{m+1}}{m+1}\left\{h - \epsilon - \frac{(h-\epsilon-y_0)}{m+2}\right\} + (h - \epsilon - y_0)^m \frac{\sqrt{Da}}{\alpha}(h - \epsilon)\right] - (h - \epsilon). \tag{3.13}$$

From equation 3.13 we get,

$$P = -\frac{\partial p}{\partial x} = \left[\frac{(q+h-\epsilon)(m+1)(m+2)\alpha}{(h-\epsilon)^{m+1}(1-\tau)^m\{\alpha(h-\epsilon)(1-\tau)\{(m+2)-(1-\tau)\} + \sqrt{Da}(m+1)(m+2)\}}\right]^{\frac{1}{m}}. \tag{3.14}$$

The volume flow rate $Q(X,t)$ and the time-averaged volume flow rate $\bar{Q}$ are calculated using the formulas mentioned in previous chapter, given in equation (2.16) and (2.17) respectively.

Equation 3.14 is integrated over one wavelength w. r. t. 'x' to obtain the pressure rise over a wave cycle as,

$$\Delta P = \int_0^1 \frac{\partial p}{\partial x}\, dx = -\int_0^1 P\, dx. \tag{3.15}$$

The Frictional force F across a single wavelength of the wall is given by

$$F = \int_0^1 h\left(-\frac{\partial p}{\partial x}\right) dx. \tag{3.16}$$

3.4 Results and discussion:

The pumping characteristic of the non-uniform channel is observed by the graphs of flow rate against pressure difference. Using Mathematica software the graphs are plotted for equation 3.15.

From Figs. 3.2 and 3.3, we observe decrease in the pressure difference ΔP with increasing Darcy number Da in the pump region and in the region of co-pump as Darcy number Da increases the pressure difference also increases, for both converging and diverging channels. Between $\bar{Q} = 0.5$ and $\bar{Q} = 0.7$ in the convergent channel and between $\bar{Q} = 0.3$ and $\bar{Q} = 0.5$ in the divergent channel variation of Darcy number shows hardly any effect on the pressure difference. For fixed pressure difference, as Da increases $\bar{Q}$ decreases in the region of pumping while in the region of co-pumping, increase in Da increases $\bar{Q}$ in both convergent and divergent channels.

Figure 3.4 and Fig. 3.5 depict that increase in the yield stress in the pumping region, for both converging and diverging channels the pressure difference also increases. There is no effect of the variation of yield stress in the convergent channel from $\bar{Q} = 0.3$ to $\bar{Q} = 0.8$ and from $\bar{Q} = 0.3$ to $\bar{Q} = 0.5$ in the divergent channel. Further as τ increases ΔP reduces in the co-pumping expanse for both channels. For fixed pressure difference, increase in τ increases $\bar{Q}$ in the region of pumping and decreases in the region of co-pumping.

It is observed from Fig. 3.6 and 3.7 that, as the porous wall thickening ϵ increases the pressure difference ΔP also increases in the region of pumping where as it reduces in the region of co-pumping, for both convergent and divergent channels. For $\bar{Q}$ between 0.5 and 0.9 in a convergent channel and for $\bar{Q} = 0.3$ and $\bar{Q} = 0.9$ in the divergent channel, the pressure difference decreases irrespective of the variation in the values of the porous wall

thickening ϵ. For fixed pressure difference as the porous wall thickening ϵ increases, the time-averaged volume flow rate $\bar{Q}$ also increases in the region of pumping, where as $\bar{Q}$ decreases in the region of co-pumping.

Enhancing the values of the amplitude ratio ϕ, the pressure difference ΔP also enhances in the pump region whereas in the co-pump region there is no effect of variation in the values of amplitude ratio in both convergent and divergent channels as noticeable from Fig. 3.8 and Fig. 3.9. The point of convergence for a convergent channel is at $\bar{Q} = 0.5$ and $\bar{Q} = 0.4$ for a divergent channel. For fixed ΔP, $\bar{Q}$ increases with ϕ in the pumping region.

As can be seen from Figs. 3.10 and 3.11, with rise in the value of the index number n, the pressure difference ΔP reduces in both regions of pumping and co-pumping, of the convergent as well divergent channels.

Also we note from the graphs that the effect of various parameters is alike for both convergent channels (Figs. 3.2, 3.4, 3.8, 3.10) and divergent channels (Figs. 3.3, 3.5, 3.7, 3.9, 3.11), but the variation is more significant in a divergent channel when compared to a convergent channel in the region of pumping where as the variation in pressure difference is exactly the same in the co-pumping region for both convergent and divergent channels.

The graphs of Frictional force against the volume flow rate are plotted from equation 3.16. From Figs. 3.12 and 3.13 that is, for both converging and diverging channels, as the flow rate $\bar{Q}$ increases, we observe rise in the Frictional force F with gain in the Darcy number Da in the region of co-pumping and further in the region of pumping as Da increases, F decreases. At fixed pressure difference, as the Darcy number increases volume flow rate $\bar{Q}$ also enhances in the region of pumping and in the region of co-pumping as Darcy number increases flow rate $\bar{Q}$ decreases.

The graphs in Fig. 3.14 and Fig. 3.15 depict that with increase in the volume flow rate $\bar{Q}$, as the yield stress τ increases, the Frictional force decreases in the region of co-pumping and increases in the region of pumping. For fixed Frictional force F, as τ enhances $\bar{Q}$ reduces in the region of pumping and in the region of co-pumping as τ increases $\bar{Q}$ also increases for both converging and diverging channels.

From the graphs of variation in the porous wall thickening ϵ, Figs. 3.16 and 3.17, we observe that as $\bar{Q}$ increases the Frictional force F decreases with increasing ϵ in the region of co-pumping up to $\bar{Q} = 0.5$ in the convergent channel and up to $\bar{Q} = 0.3$ in the divergent channel. In the convergent channel for $\bar{Q} > 0.5$ up to $\bar{Q} > 0.9$ and in the divergent channel for $\bar{Q} > 0.3$ up to $\bar{Q} = 0.8$ variation of ϵ has no effect on the increasing behavior of F, further the Frictional force F increases with increase in ϵ in the region of pumping. For fixed Frictional force F, as ϵ adds up the values $\bar{Q}$ declines in the region of pumping and in the region of co-pumping as ϵ increases $\bar{Q}$ decreases.

The consequences of variation in the amplitude ratio ϕ are depicted in Fig. 3.18 and Fig. 3.19 for a convergent and divergent channel respectively. In the region of co-pumping the Frictional force reduces with rise in the amplitude ratio ϕ upto $\bar{Q} = 0.5$ in a convergent and $\bar{Q} = 0.4$ in a divergent channel. Furtherance the Frictional force increases irrespective of any variation in the values of ϕ, in the pumping region. Also the graph reveals that for fixed F, $\bar{Q}$ increases.

The Figs. 3.20 and 3.21 show the effect of variation in the values of the index number n. As n increases, Frictional force also increases in the co-pumping region up to $\bar{Q} = 0.5$ in a convergent and $\bar{Q} = 0.3$ in a divergent channel. Henceforth the Frictional force decreases when the value of the index number is raised, in the pumping region.

The impact of the several parameters on the Frictional force F is exactly the same for both the convergent and divergent channels in the pumping region, whereas the effect is more significant in the convergent channel than in the divergent channel in the co-pumping region. Also it is observed that the frictional force and pressure rise behave reversely and are in accordance with the results of Sobh [89].

Trapping phenomenon is observed for all the parameters in both the convergent and the divergent channels. The magnitude of the bolus enhances with rise in the values of Da, τ, ϵ and ϕ, whereas bolus decreases in size for increase in the values of $\bar{Q}$ and n, as described clearly from the stream line patterns shown in Fig. 3.22 to Fig. 3.33.

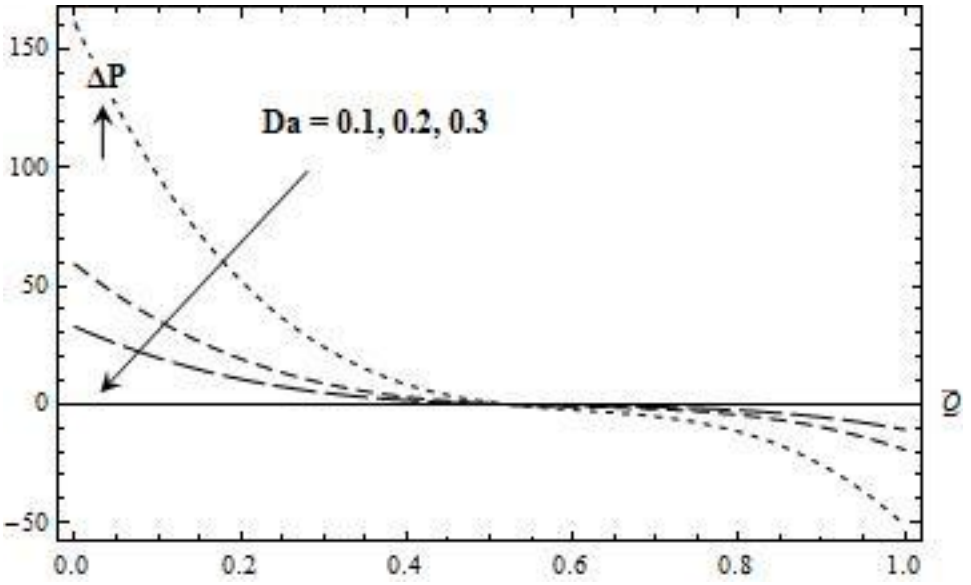

Fig. 3.2: Effect of Da on ΔP against $\bar{Q}$ in a converging channel with:

$n = 3$; $\alpha = 0.1$; $\tau = 0.1$; k = – 0.1; $\epsilon = 0.3$; $\phi = 0.3$

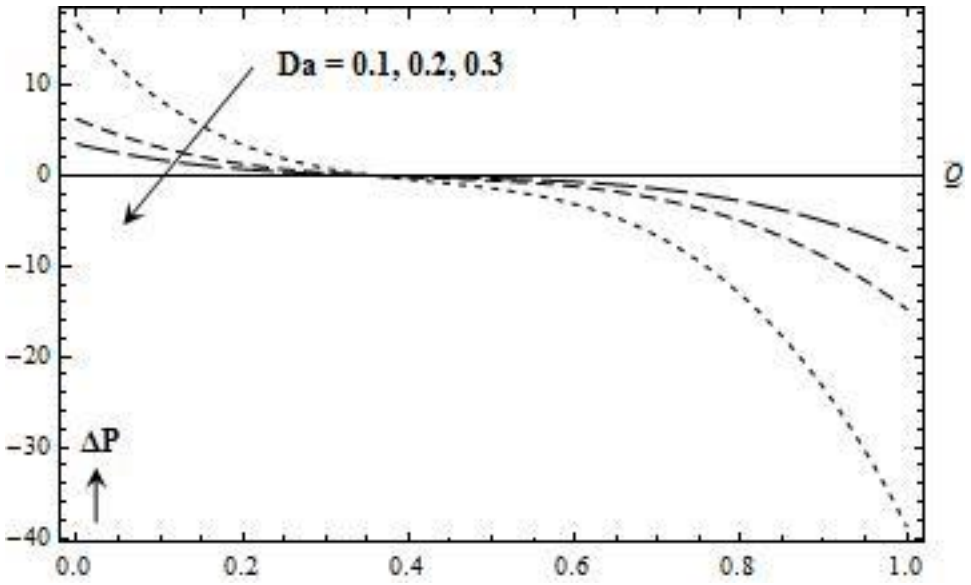

Fig. 3.3: Effect of Da on ΔP against $\bar{Q}$ in a diverging channel with:

$n = 3$; $\alpha = 0.1$; $\tau = 0.1$; k = 0.1; $\epsilon = 0.3$; $\phi = 0.3$

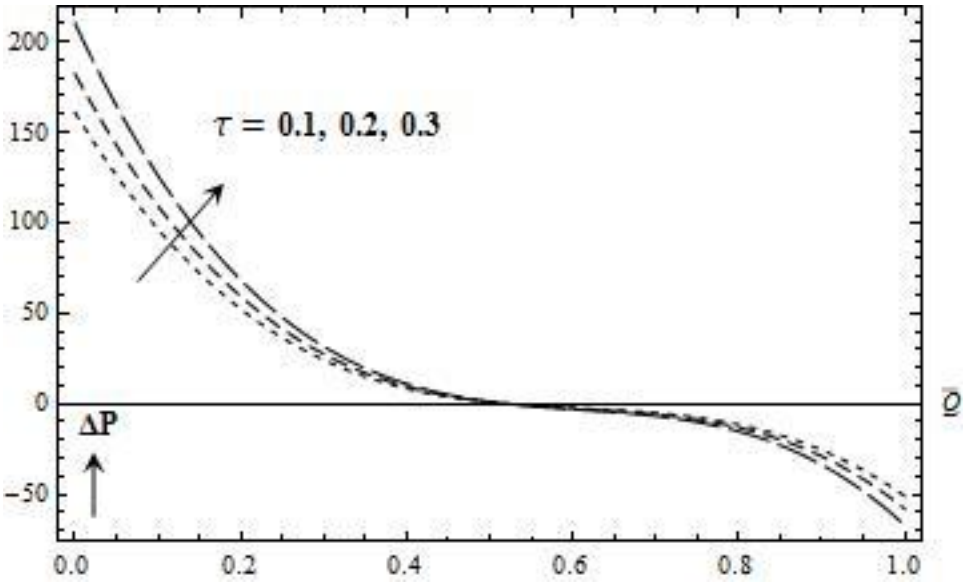

Fig. 3.4: Effect of τ on ΔP against $\bar{Q}$ in a converging channel with:

$n = 3$; Da $= 0.1$; $\alpha = 0.1$; k $= -0.1$; $\epsilon = 0.3$; $\phi = 0.3$

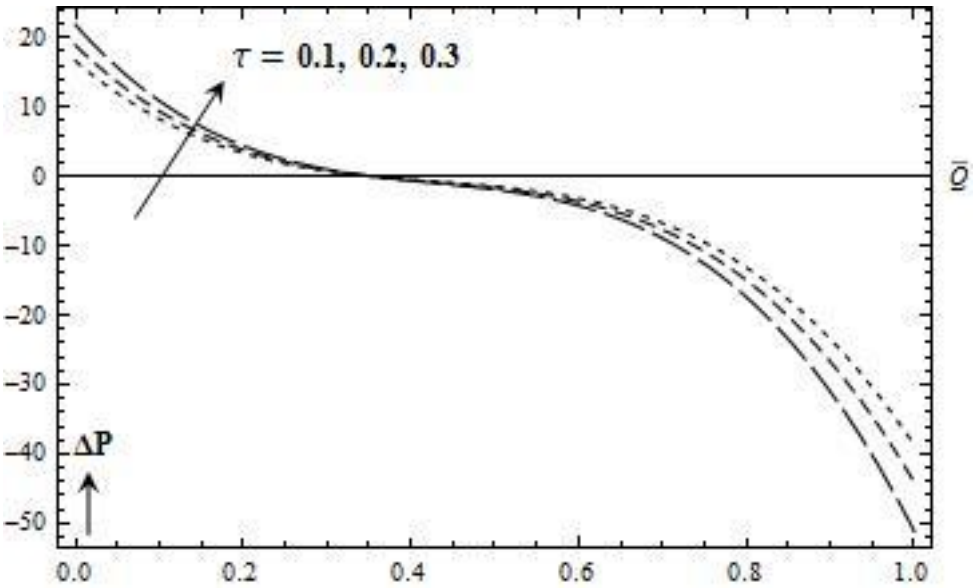

Fig. 3.5: Effect of τ on ΔP against $\bar{Q}$ in a diverging channel with:

$n = 3$; Da $= 0.1$; $\alpha = 0.1$; k $= 0.1$; $\epsilon = 0.3$; $\phi = 0.3$

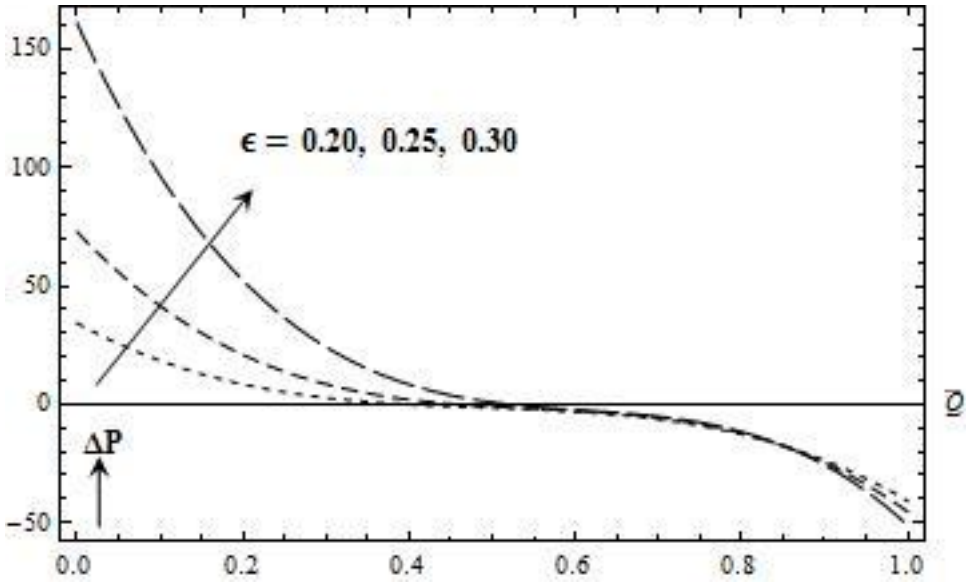

Fig. 3.6: Effect of ϵ on ΔP against $\bar{Q}$ in a converging channel with:

$n = 3$; Da $= 0.1$; $\alpha = 0.1$; $\tau = 0.1$; k $= -0.1$; $\phi = 0.3$

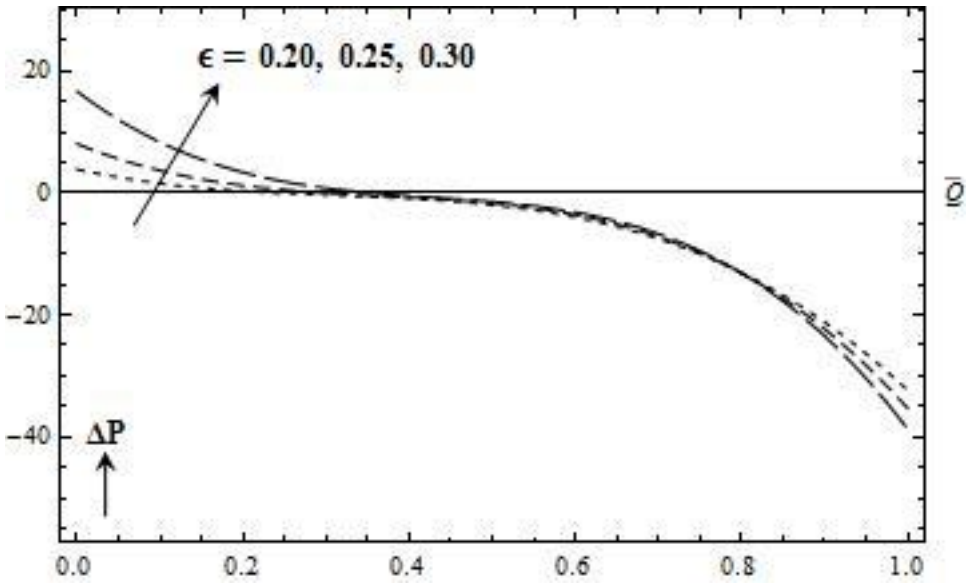

Fig. 3.7: Effect of ϵ on ΔP against $\bar{Q}$ in a diverging channel with:

$n = 3$; Da $= 0.1$; $\alpha = 0.1$; $\tau = 0.1$; k $= 0.1$; $\phi = 0.3$

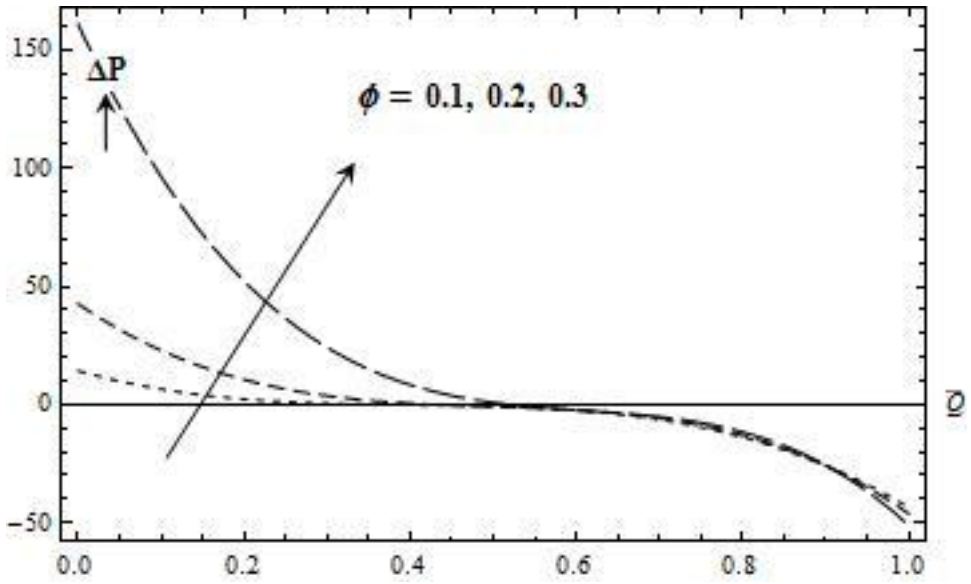

Fig. 3.8: Effect of ϕ on ΔP against $\bar{Q}$ in a converging channel with:

$n = 3$; Da $= 0.1$; $\alpha = 0.1$; $\tau = 0.1$; k $= -0.1$; $\epsilon = 0.3$

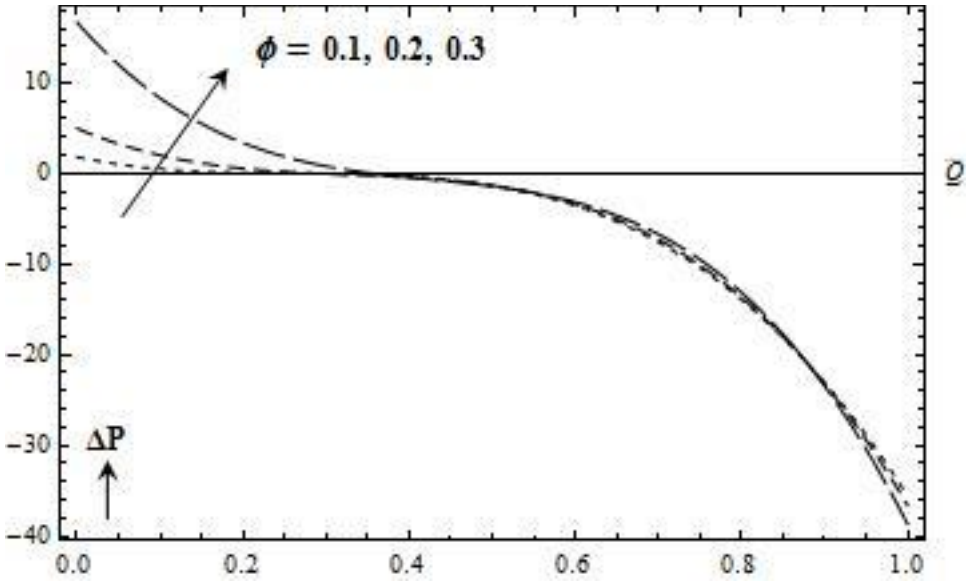

Fig. 3.9: Effect of ϕ on ΔP against $\bar{Q}$ in a diverging channel with:

$n = 3$; Da $= 0.1$; $\alpha = 0.1$; $\tau = 0.1$; k $= 0.1$; $\epsilon = 0.3$

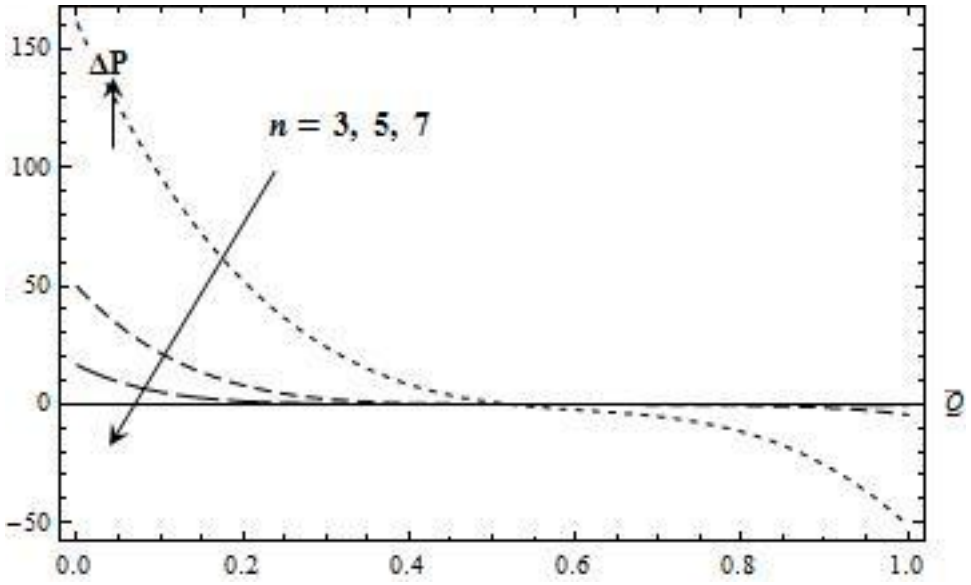

Fig. 3.10: Effect of n on ΔP against $\bar{Q}$ in a converging channel with:

Da = 0.1; $\alpha = 0.1$; $\tau = 0.1$; k = – 0.1; $\epsilon = 0.3$; $\phi = 0.3$

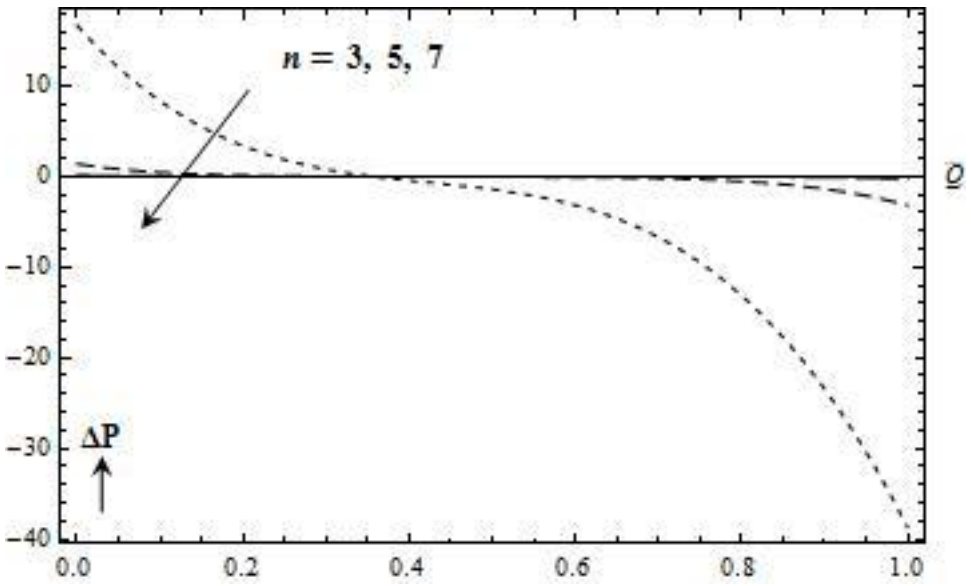

Fig. 3.11: Effect of n on ΔP against $\bar{Q}$in a diverging channel with:

Da = 0.1; $\alpha = 0.1$; $\tau = 0.1$; k = 0.1; $\epsilon = 0.3$; $\phi = 0.3$

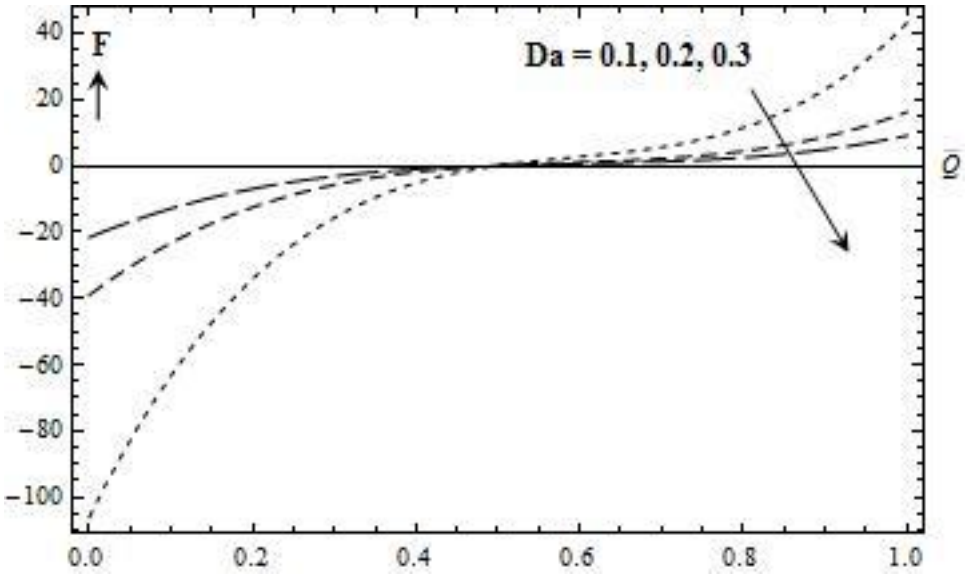

Fig. 3.12: Effect of Da on F against $\bar{Q}$ in a converging channel with:

$n = 3$; $\alpha = 0.1$; $\tau = 0.1$; k = – 0.1; $\epsilon = 0.3$; $\phi = 0.3$

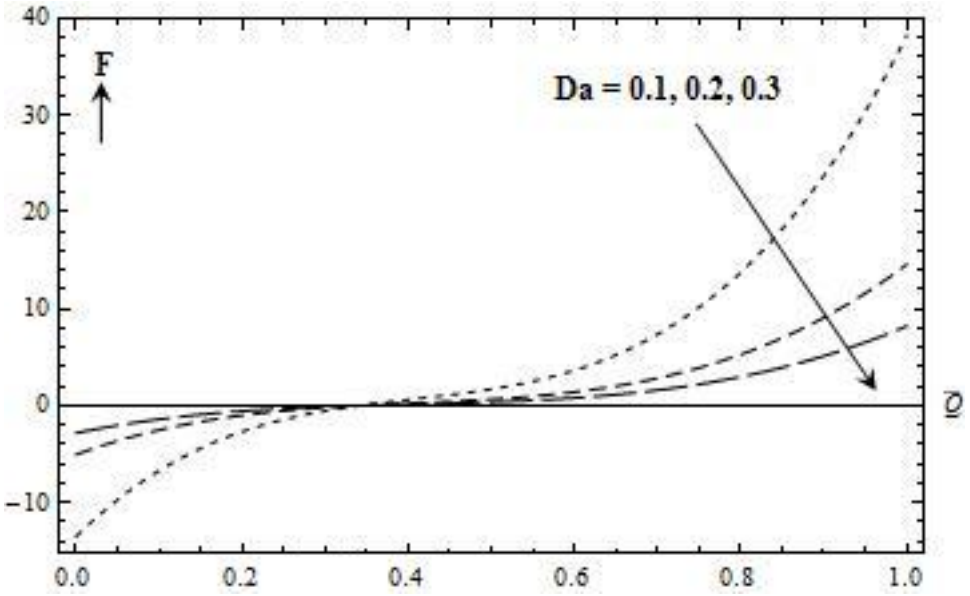

Fig. 3.13: Effect of Da on F against $\bar{Q}$ in a diverging channel with:

$n = 3$; $\alpha = 0.1$; $\tau = 0.1$; k = 0.1; $\epsilon = 0.3$; $\phi = 0.3$

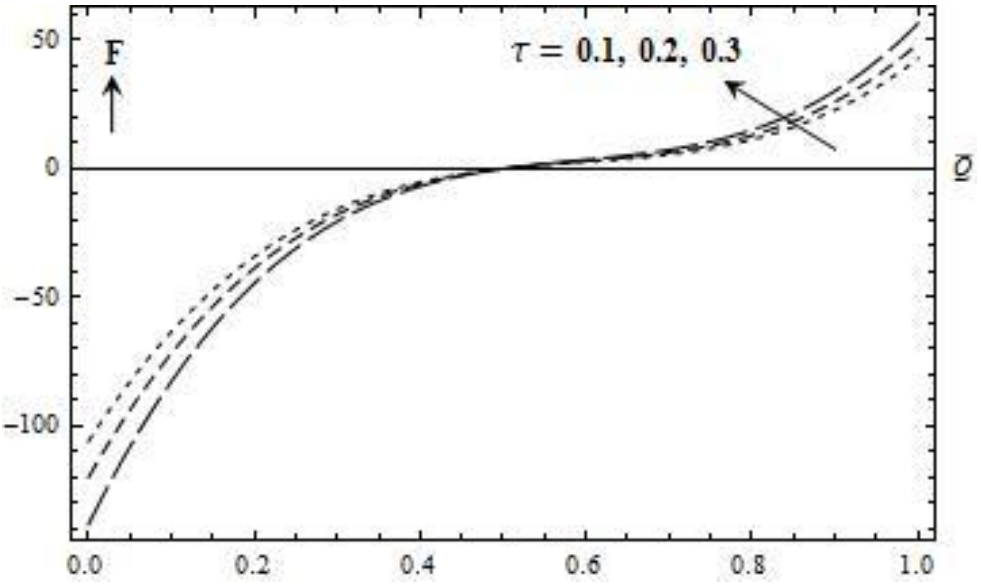

Fig. 3.14: Effect of τ on F against $\bar{Q}$ in a converging channel with:

$n = 3$; $Da = 0.1$; $\alpha = 0.1$; $k = -0.1$; $\epsilon = 0.3$; $\phi = 0.3$

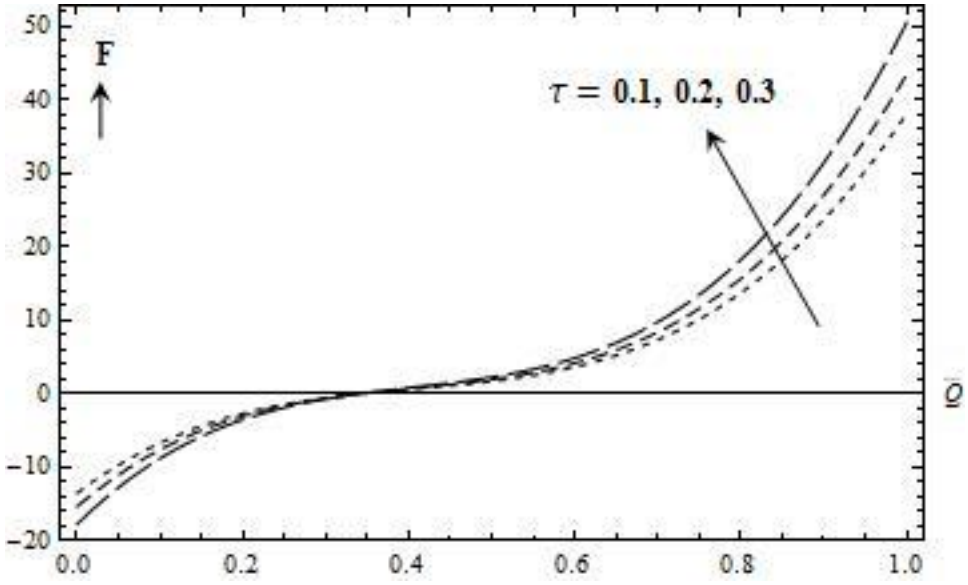

Fig. 3.15: Effect of τ on F against $\bar{Q}$ in a diverging channel with:

$n = 3$; $Da = 0.1$; $\alpha = 0.1$; $k = 0.1$; $\epsilon = 0.3$; $\phi = 0.3$

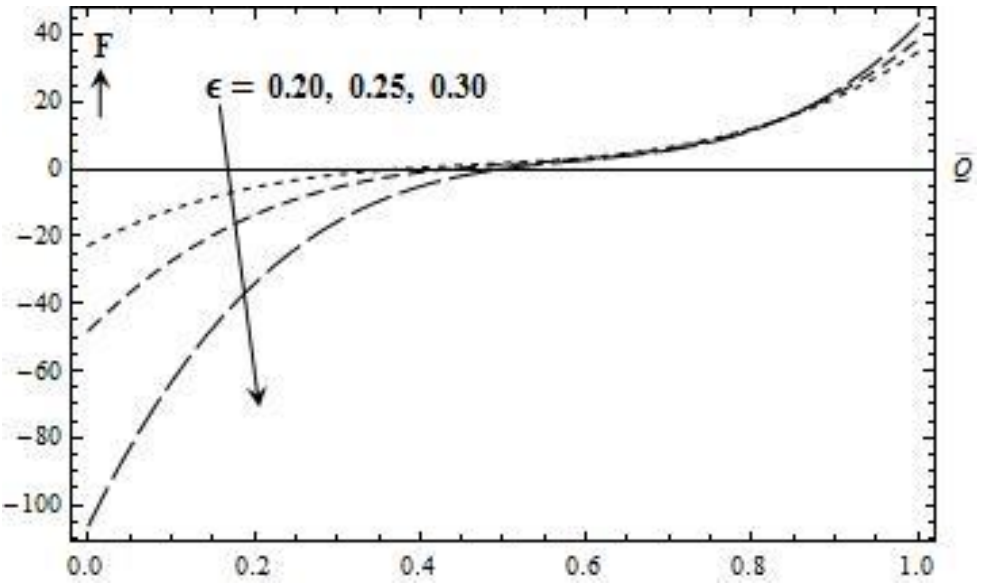

Fig. 3.16: Effect of ϵ on F against $\bar{Q}$ in a converging channel with:

$n = 3$; $Da = 0.1$; $\alpha = 0.1$; $\tau = 0.1$; $k = -0.1$; $\phi = 0.3$

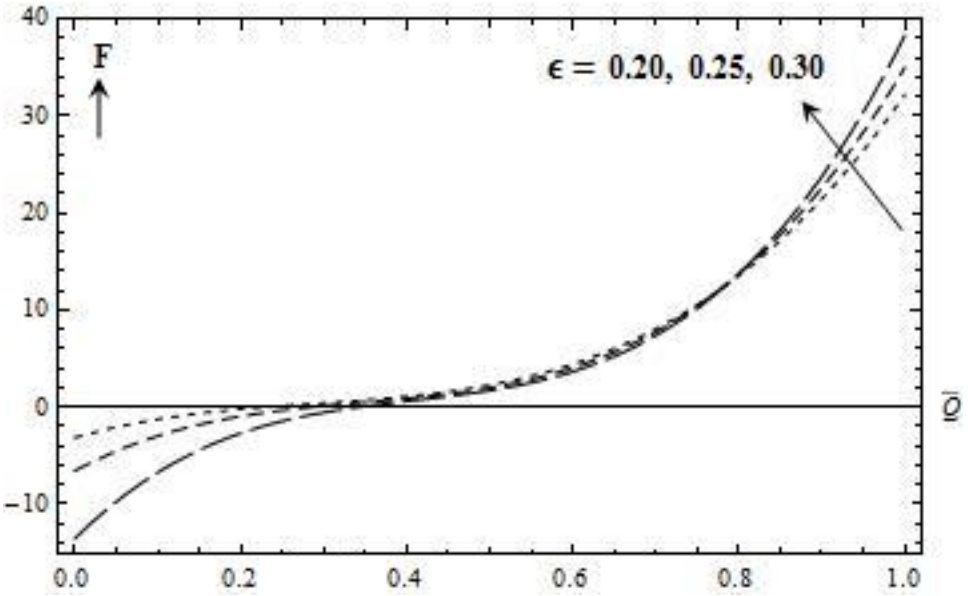

Fig. 3.17: Effect of ϵ on F against $\bar{Q}$ in a diverging channel with:

$n = 3$; $Da = 0.1$; $\alpha = 0.1$; $\tau = 0.1$; $k = 0.1$; $\phi = 0.3$

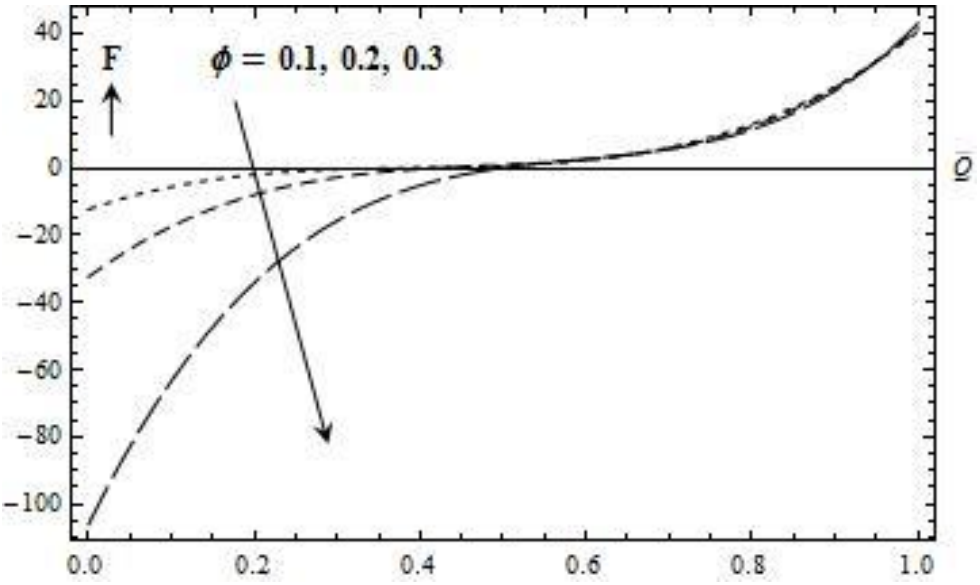

Fig. 3.18: Effect of ϕ on F against $\bar{Q}$ in a converging channel with:

$n = 3$; $Da = 0.1$; $\alpha = 0.1$; $\tau = 0.1$; $k = -0.1$; $\epsilon = 0.3$

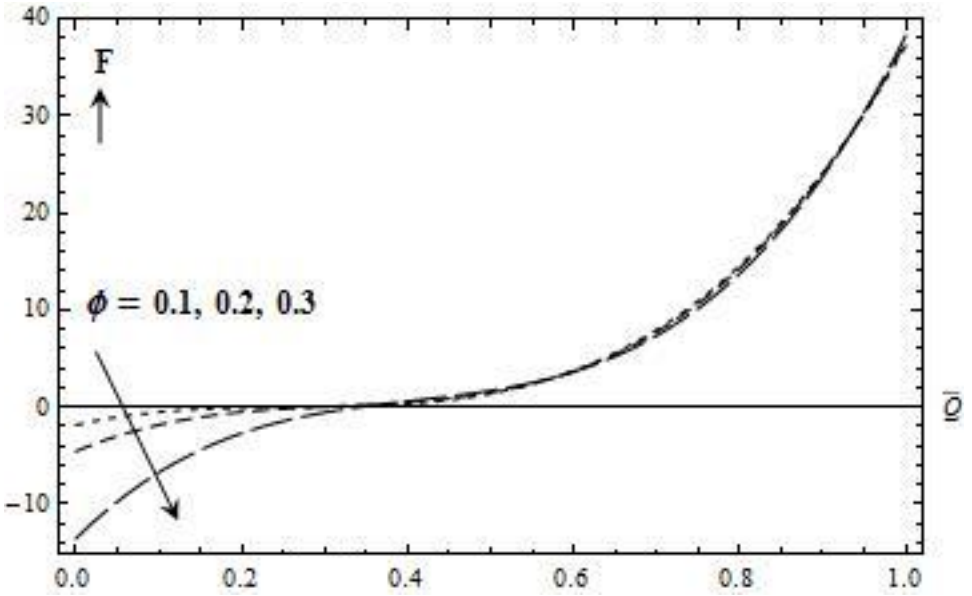

Fig. 3.19: Effect of ϕ on F against $\bar{Q}$ in a diverging channel with:

$n = 3$; $Da = 0.1$; $\alpha = 0.1$; $\tau = 0.1$; $k = 0.1$; $\epsilon = 0.3$

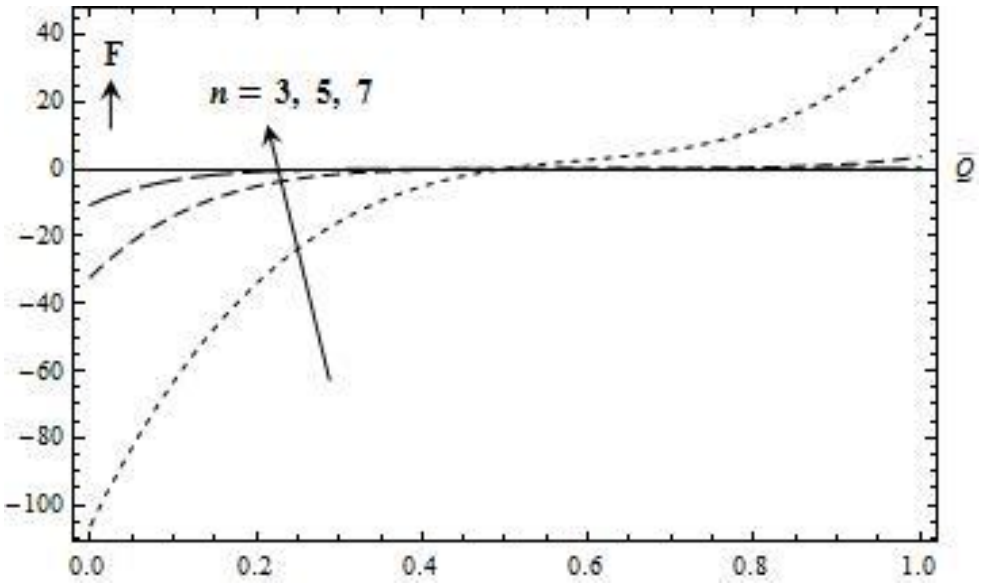

Fig. 3.20: Effect of n on F against $\bar{Q}$ in a converging channel with:

$\mathrm{Da} = 0.1$; $\alpha = 0.1$; $\tau = 0.1$; $\mathrm{k} = -0.1$; $\epsilon = 0.3$; $\phi = 0.3$

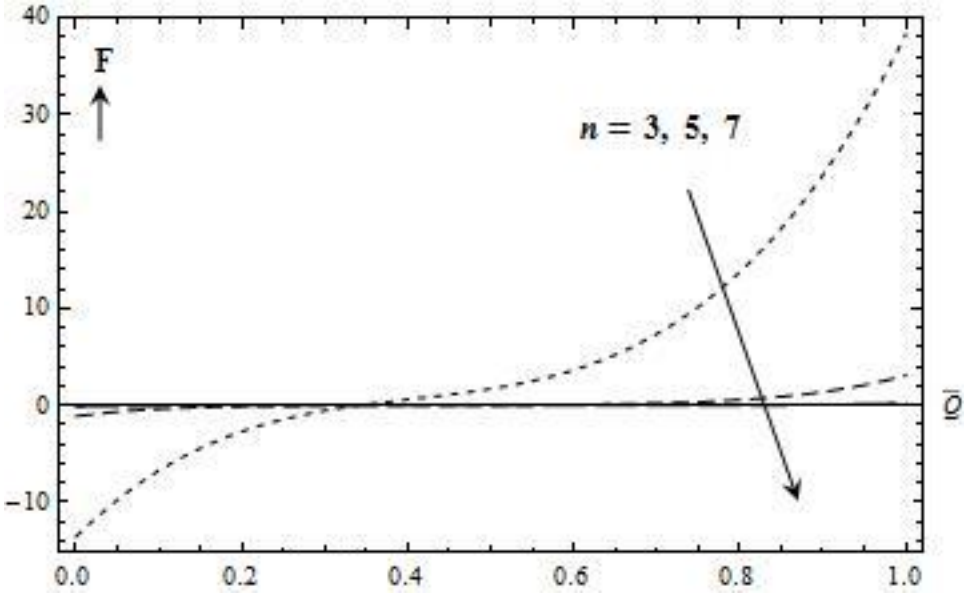

Fig. 3.21: Effect of n on F against $\bar{Q}$ in a diverging channel with:

$Da = 0.1$; $\alpha = 0.1$; $\tau = 0.1$; $k = 0.1$; $\epsilon = 0.3$; $\phi = 0.3$

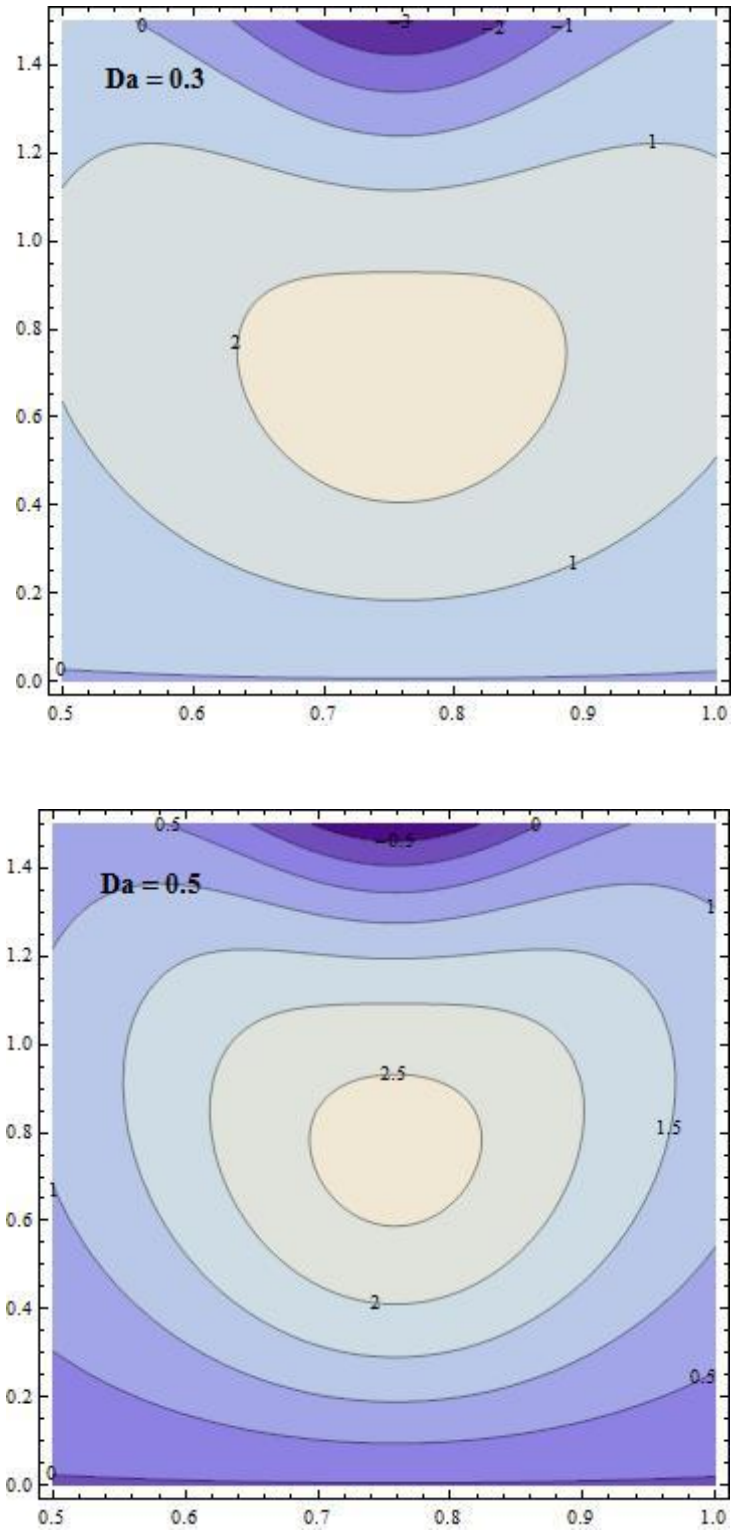

Fig. 3.22: Stream line patterns in a convergent channel for variation in Da with:

$$n = 3;\ \alpha = 1;\ \tau = 0.5;\ \epsilon = 0.3;\ \bar{Q} = 0.1;\ k = -0.1;\ \phi = 0.3$$

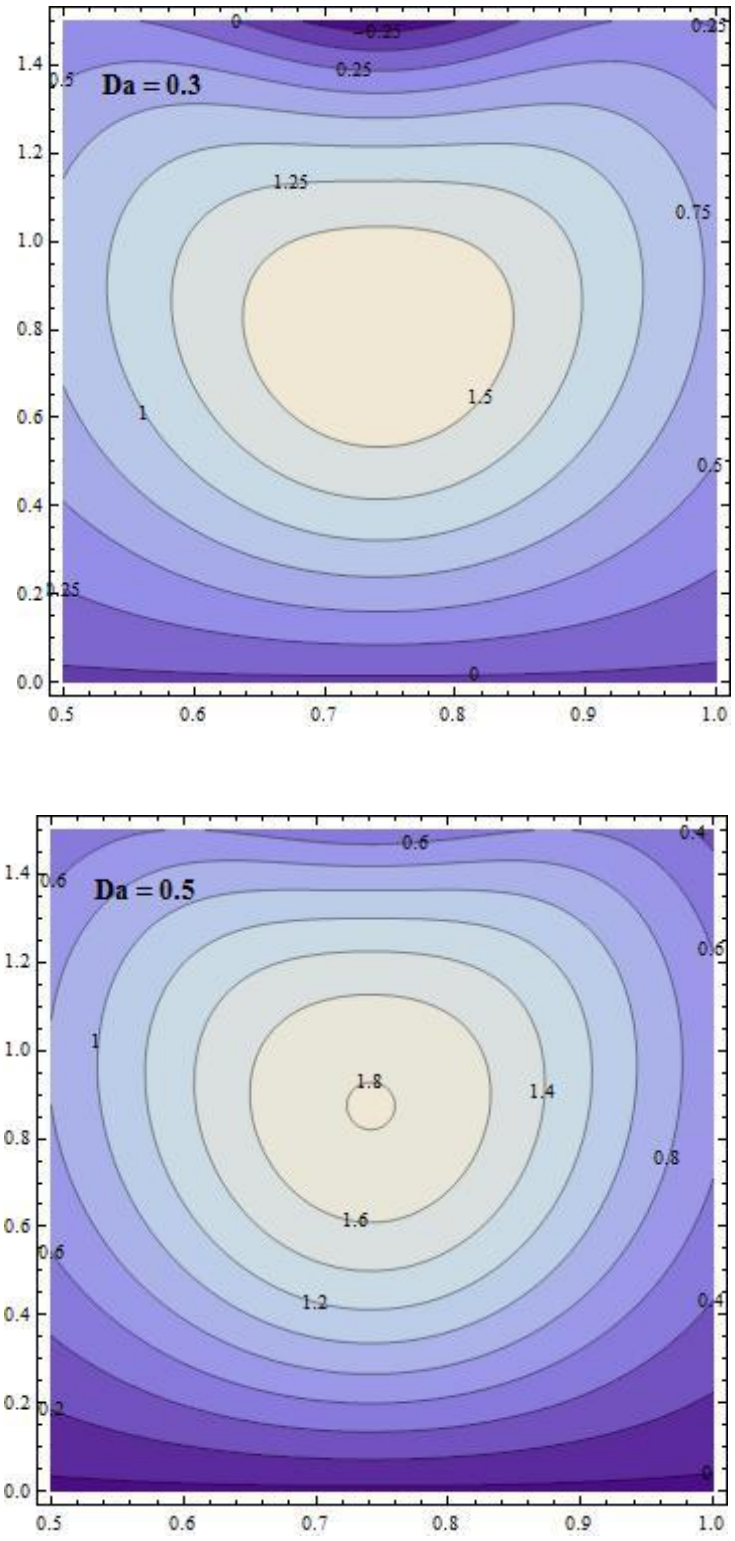

Fig. 3.23: Stream line patterns in a divergent channel for variation in Da with:

$$n = 3; \alpha = 1; \tau = 0.5; \epsilon = 0.3; \bar{Q} = 0.1; k = 0.1; \phi = 0.3$$

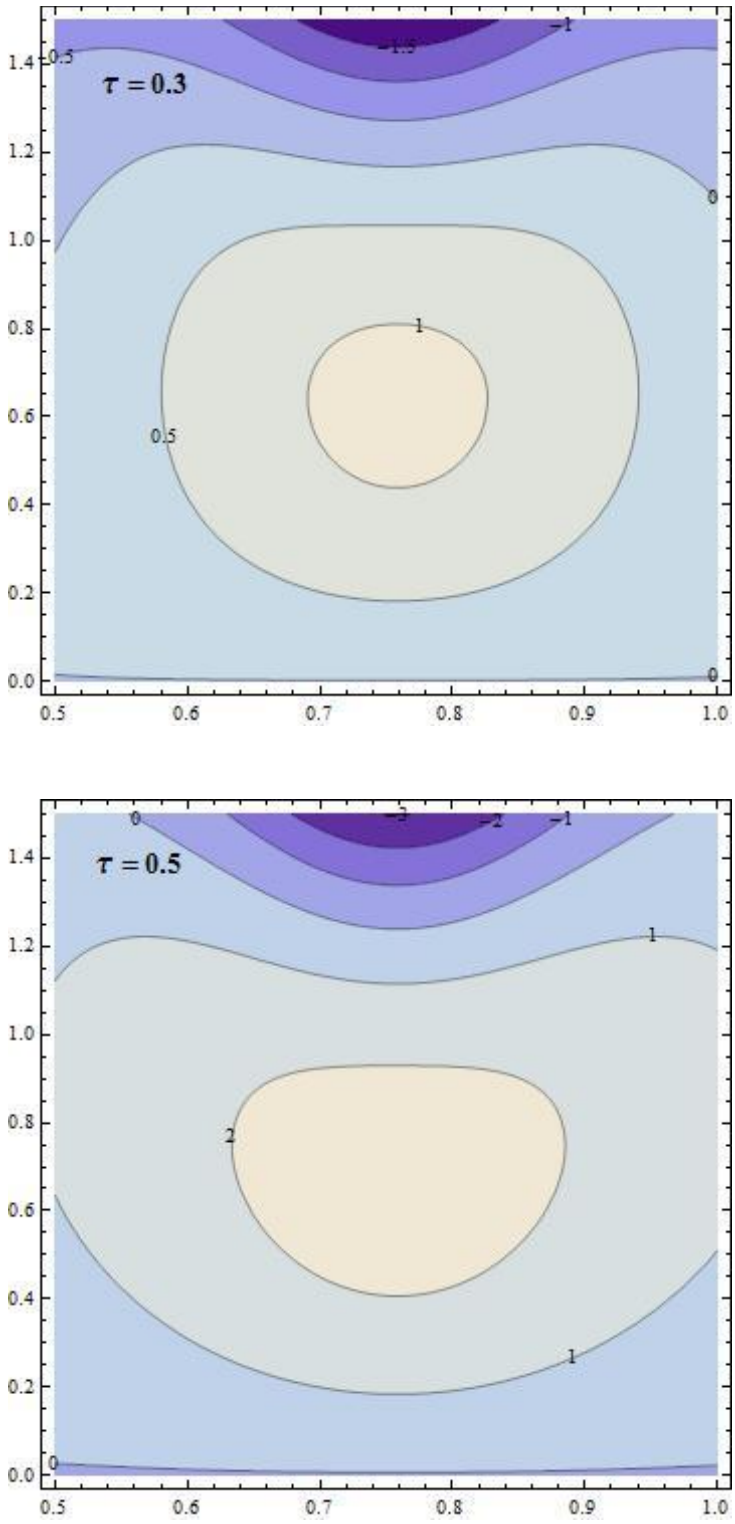

Fig. 3.24: Stream line patterns in a convergent channel for variation in τ with:

$$n = 3; \mathrm{Da} = 0.3; \alpha = 1;\ \epsilon = 0.3;\ \bar{Q} = 0.1;\ k = -0.1;\ \phi = 0.3$$

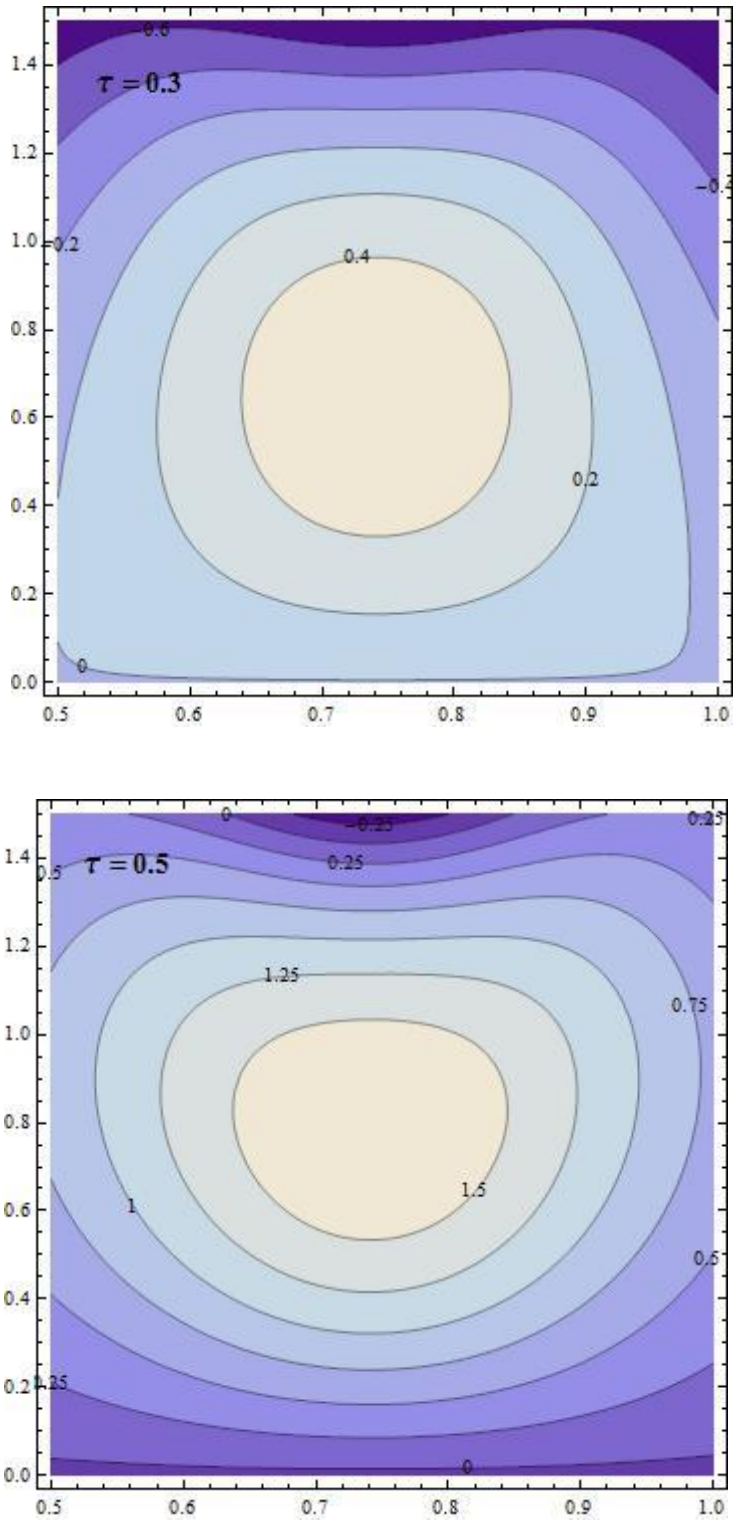

Fig. 3.25: Stream line patterns in a divergent channel for τ with:

$$n = 3; \mathrm{Da} = 0.3; \alpha = 1; \epsilon = 0.3; \bar{Q} = 0.1; k = 0.1; \ \phi = 0.3$$

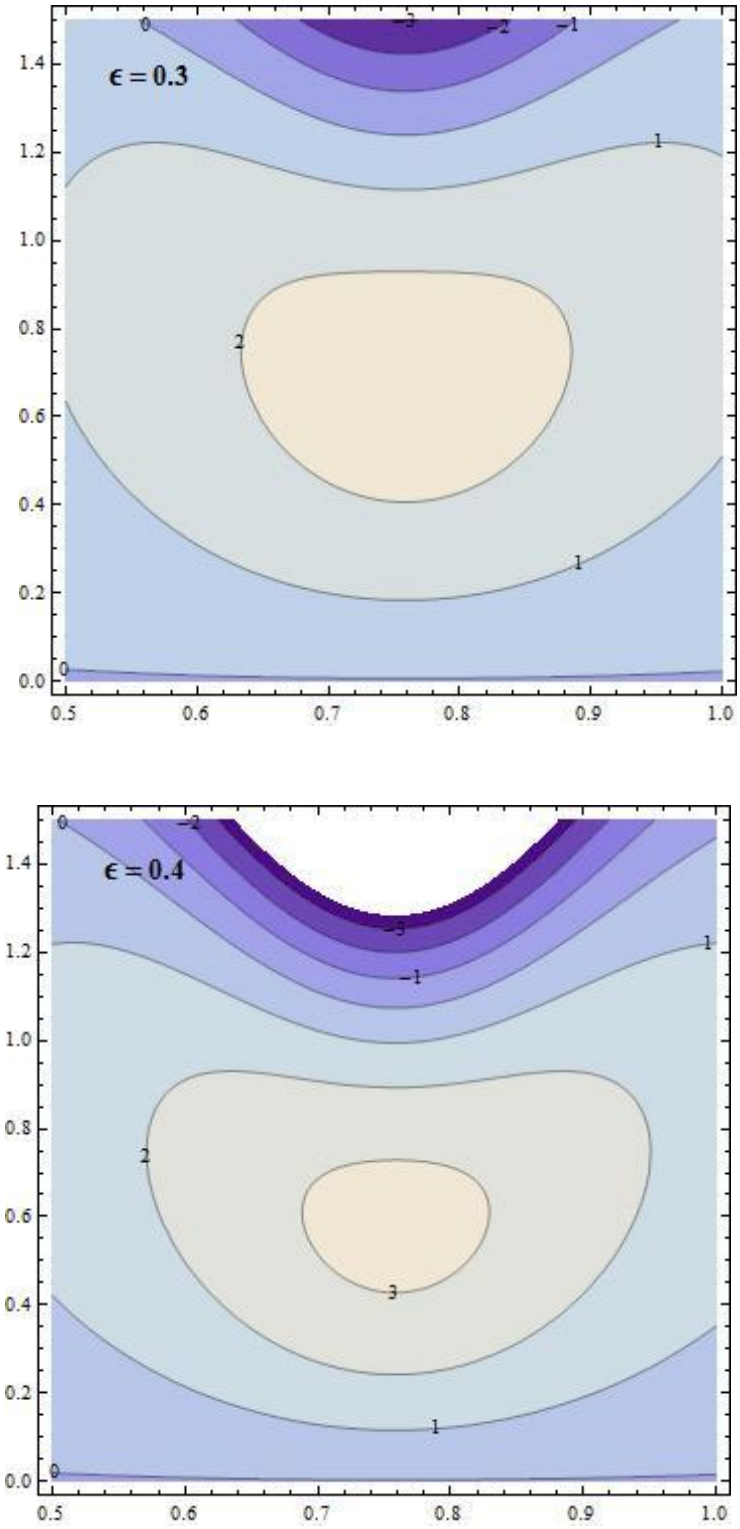

Fig. 3.26: Stream line patterns in a convergent channel for variation in ϵ with:

$$n = 3; \mathrm{Da} = 0.3; \alpha = 1;\ \tau = 0.5;\ \bar{Q} = 0.1;\ k = -0.1;\ \phi = 0.3$$

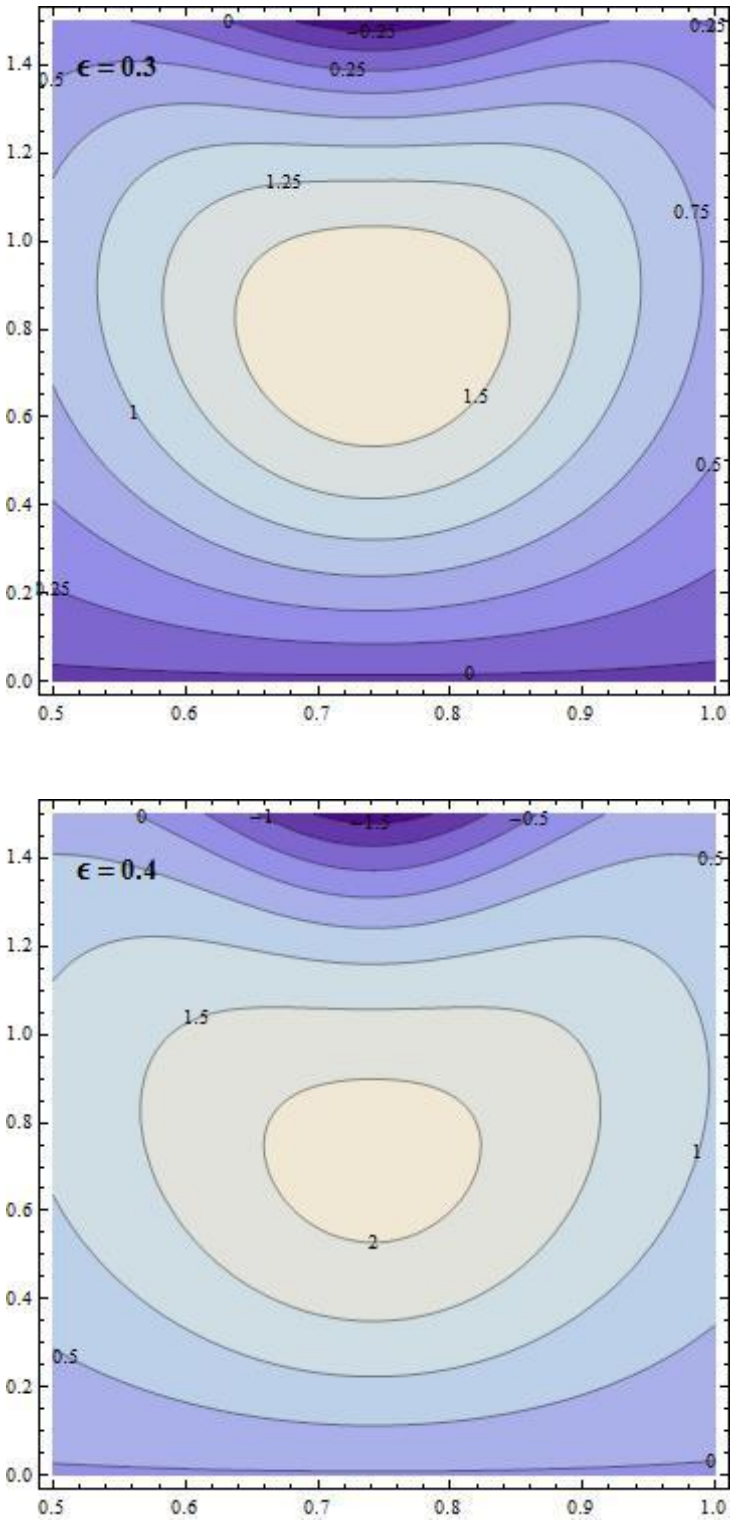

Fig. 3.27: Stream line patterns in a divergent channel for variation in ϵ with:

$$n = 3; \mathrm{Da} = 0.3; \alpha = 1;\ \tau = 0.5;\ \bar{Q} = 0.1;\ k = 0.1;\ \phi = 0.3$$

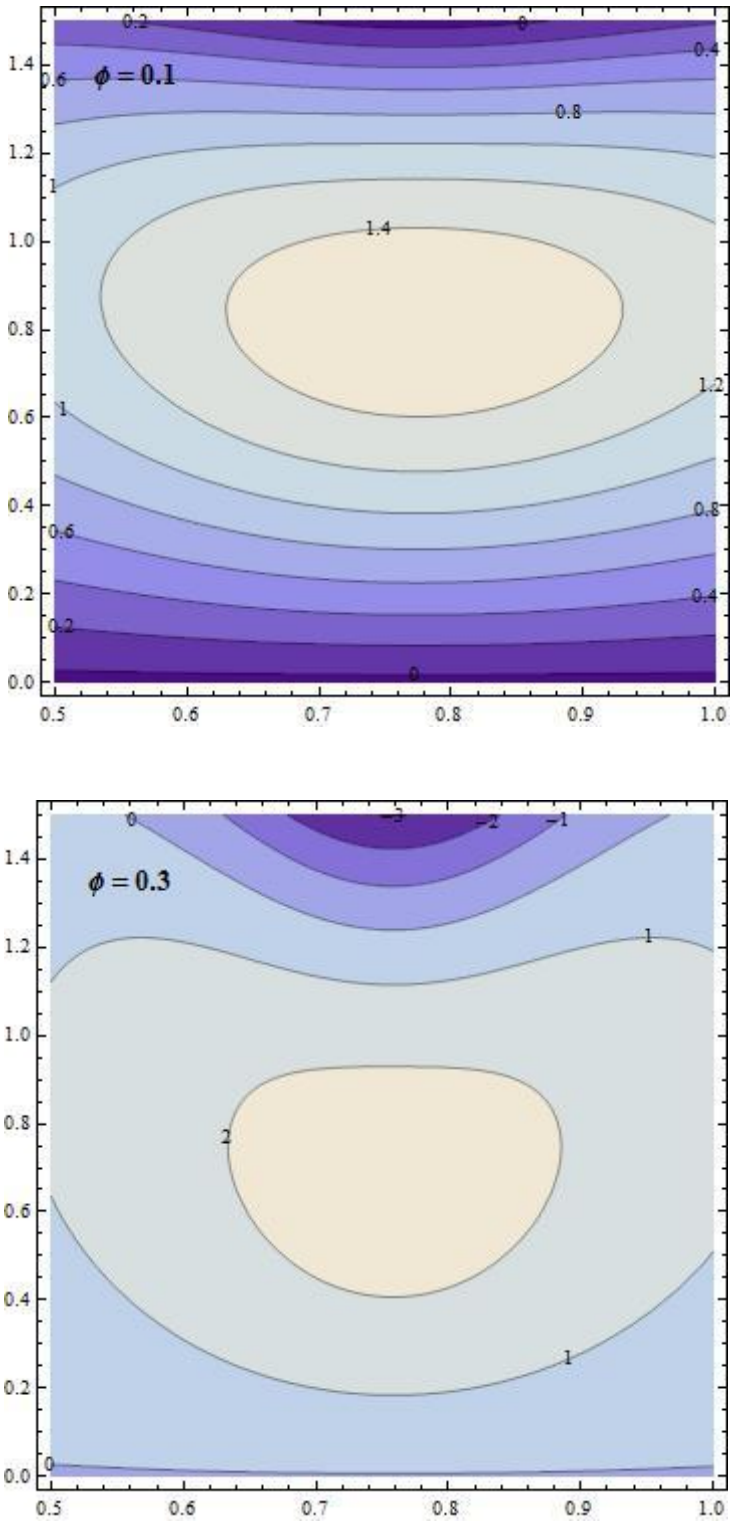

Fig. 3.28: Stream line patterns in a convergent channel for variation in ϕ with:

$$n = 3; \mathrm{Da} = 0.3; \alpha = 1;\ \tau = 0.5;\ \epsilon = 0.3;\ \bar{Q} = 0.1;\ k = -0.1$$

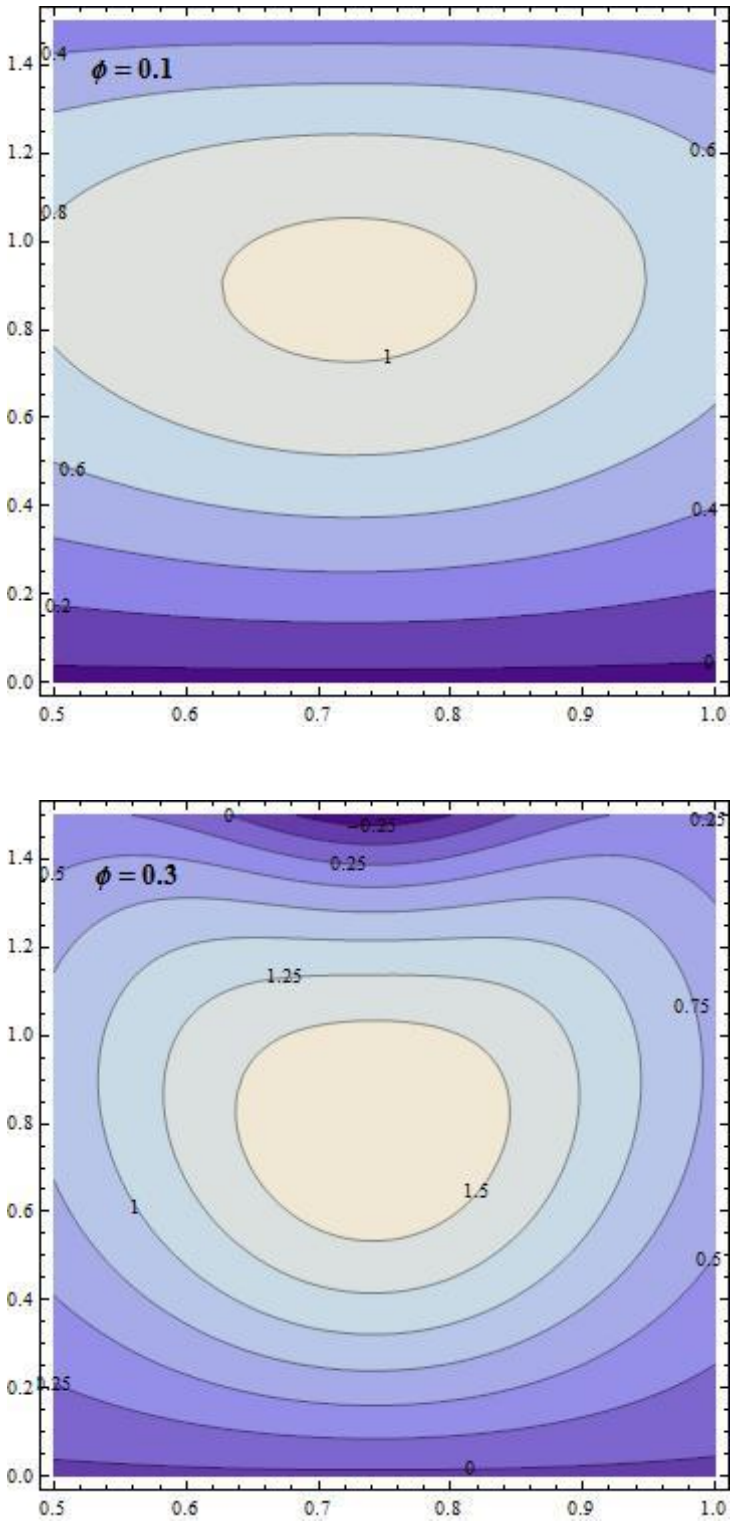

Fig. 3.29: Stream line patterns in a divergent channel for variation in ϕ with:

$$n = 3; \mathrm{Da} = 0.3; \alpha = 1; \tau = 0.5; \epsilon = 0.3; \bar{Q} = 0.1; k = 0.1$$

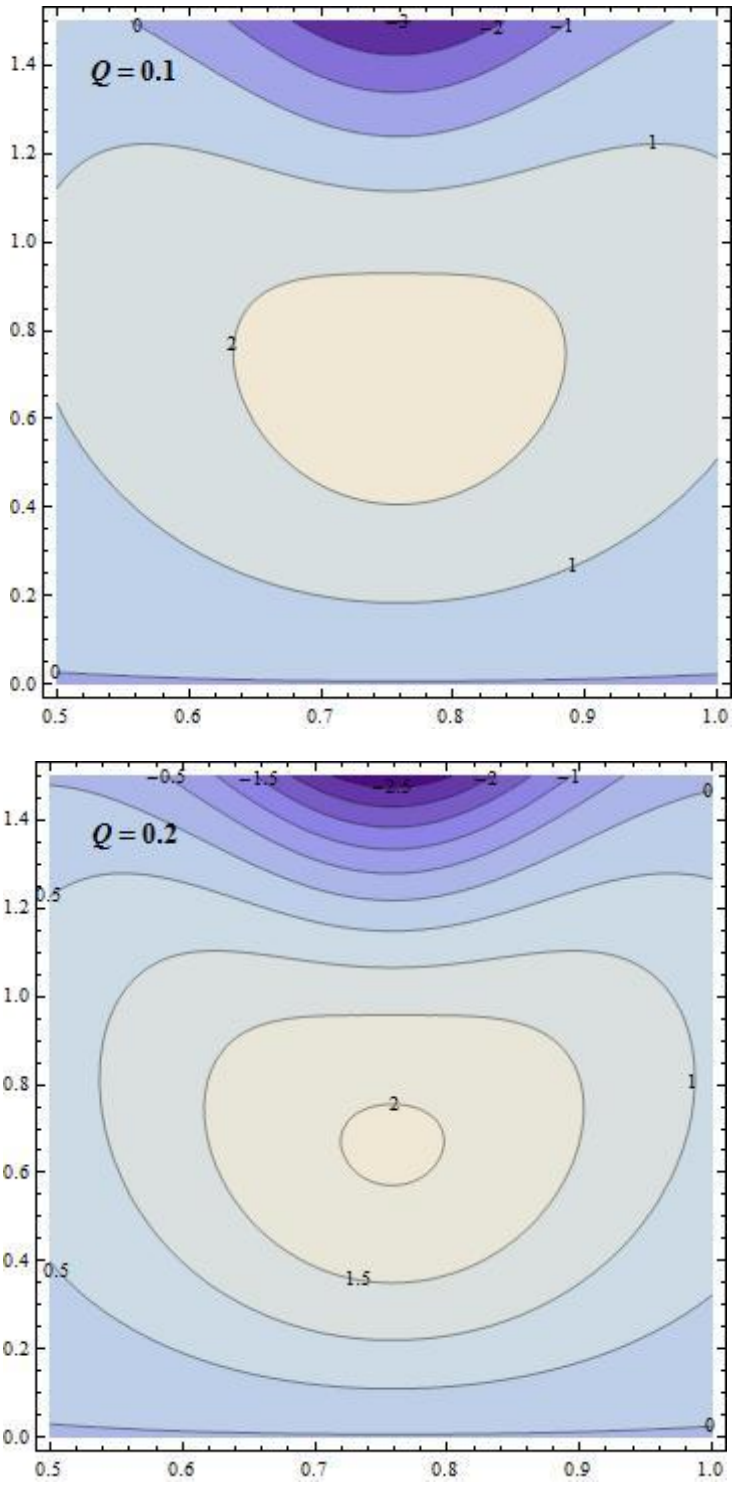

Fig. 3.30: Stream line patterns in a convergent channel for variation in $\bar{Q}$ with:

$$n = 3; \mathrm{Da} = 0.3; \alpha = 1;\ \tau = 0.5;\ \epsilon = 0.3;\ k = -0.1;\ \phi = 0.3$$

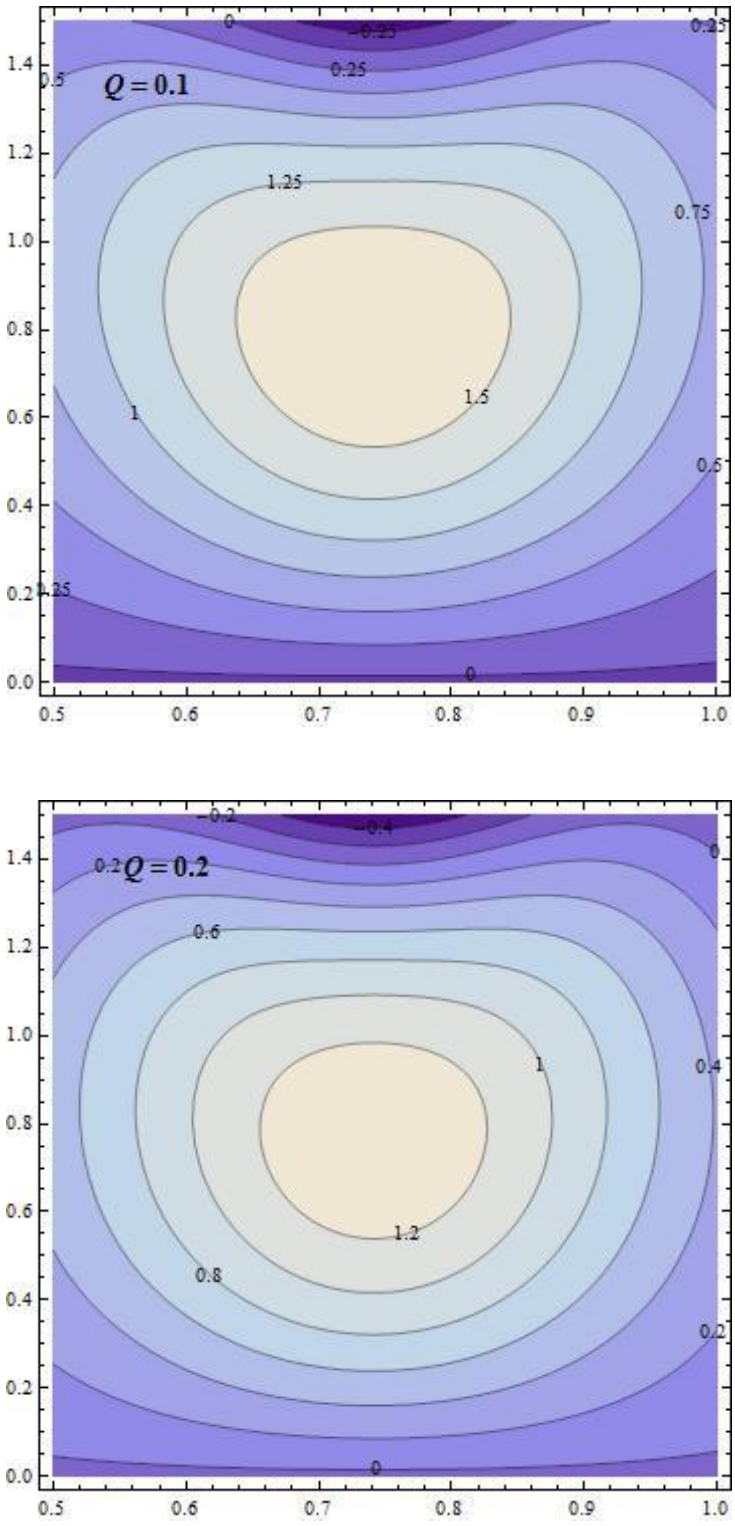

Fig. 3.31: Stream line patterns in a divergent channel for variation in $\bar{Q}$ with:

$$n = 3; \mathrm{Da} = 0.3; \alpha = 1; \tau = 0.5; \epsilon = 0.3;\ k = 0.1; \phi = 0.3$$

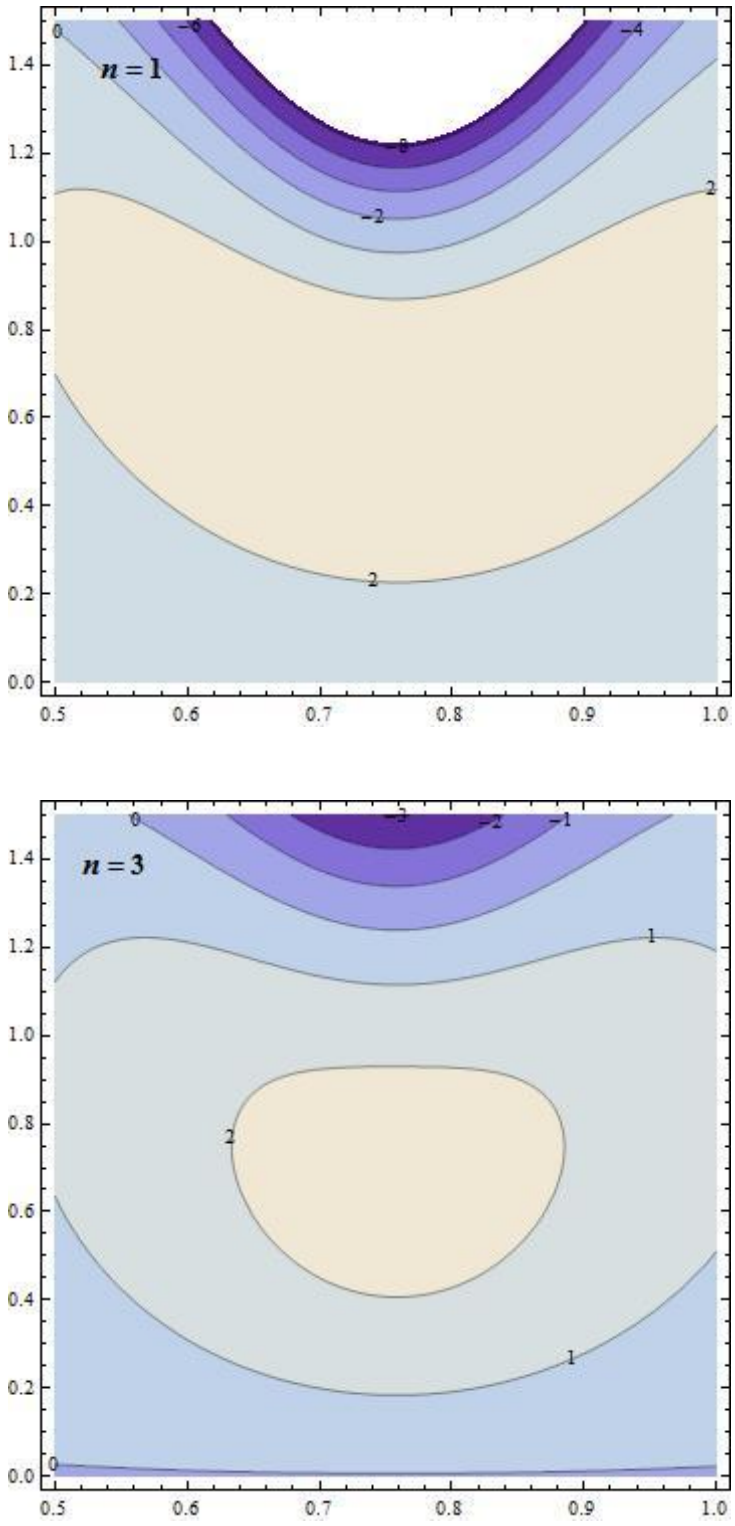

Fig. 3.32: Stream line patterns in a convergent channel for variation in n with:

$$\mathbf{Da} = 0.3; \alpha = 1;\ \tau = 0.5;\ \epsilon = 0.3;\ \bar{Q} = 0.1;\ k = -0.1;\ \phi = 0.3$$

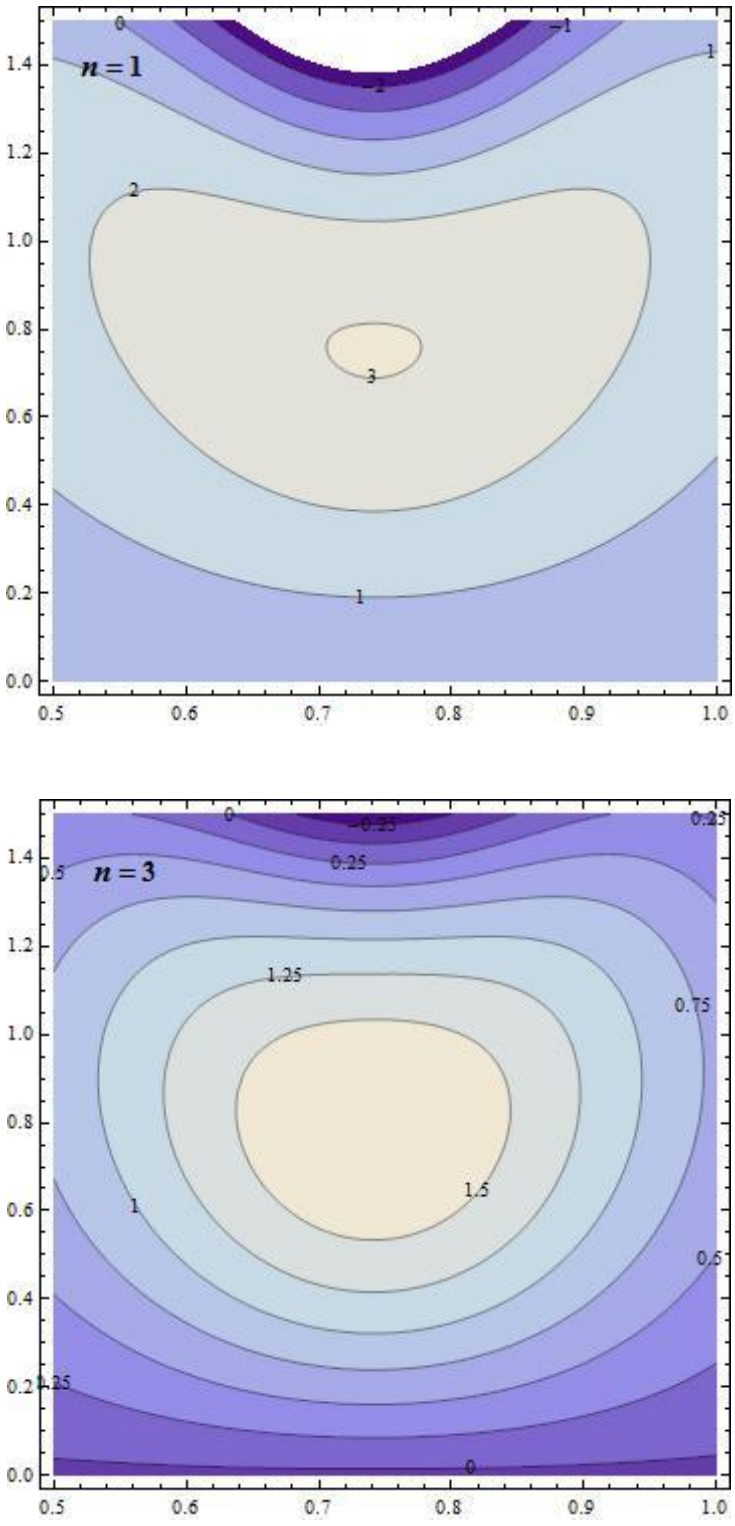

Fig. 3.33: Stream line patterns in a divergent channel for n with:

$\mathrm{Da} = 0.3; \alpha = 1; \tau = 0.5; \epsilon = 0.3; \bar{Q} = 0.1; k = 0.1; \phi = 0.3$

CHAPTER-4

Impact of Permeable Lining of the Wall on the Peristaltic Flow of Herschel Bulkley Fluid

4.1 Introduction:

'Peristalsis', the mechanism of fluid transport through the elastic pipe by means of a sinusoidal wave, is an important action enabling many biological and mechanical processes. Though the solution of non-Newtonian fluids is complex due to the appearance of the non-linear term, the flow of blood in human body, alloys and metals in industries, mercury amalgams and lubrication with heavy oils and greases in machines are a few examples of flow of non-Newtonian fluids that show us how important is the study of non-Newtonian fluids. Many authors have put forth their investigations of peristaltic flow, considering uniform and non-uniform channels amid different fluids and their corresponding parameters.

After studying movement of the Herschel Bulkley fluid in uniform and non-uniform channels under peristalsis in the previous chapters and also noticing that several ducts in physiological structure are inclined to the axis, in the present chapter we have considered an inclined channel for modeling the flow.

The study of peristaltic flow in a deformable inclined tube was taken by Hakeem et al. [91] under the wall slip conditions. Riahi and Roy [92] studied the flow in a tube and in an annulus respectively, representing the flow of chyme in the digestive tract, in the absence and presence of a cylindrical endoscope. Sankad and Radhakrishnamacharya [93] observed the influence of, an inclined channel having wall properties, on the flow of micropolar fluid under peristalsis. Considering the micro polar fluid, Krishna Kumari et al. [94] have analyzed the peristaltic flow under the magnetic effect in an inclined channel. Smita and Anamol Kumar [95] examined the blood flow through arteries under peristalsis. Kothandapani and Prakash [96] put forward the effects of heat source, inclined magnetic field as well as thermal radiation on the peristaltic motion, considering a hyperbolic tangent fluid through an asymmetric conduit. Rathod and Sridhar [97] analyzed the peristaltic motion in an inclined channel and concluded that with increment in the angle of inclination, pressure rise and the Frictional force both increase. Govindaraja et al. [98] analyzed the peristaltic transport of a couple stress fluid in a porous inclined asymmetric channel to study the effects of heat and mass transfer on MHD.

Looking into the above studies, in this chapter we have considered the flow of Herschel

Bulkley fluid in a non uniform inclined conduit and have obtained the solution under lubrication method. The study has been analyzed to look into the nature of pressure gradient and Frictional force for different parameters and to examine the stream lines.

4.2 Mathematical formulation:

Herschel–Bulkley fluid is considered to be moving in a channel of half width 'a' coated with non erodible permeable material. The flexible wall of the channel is influenced by a progressive peristaltic wave with amplitude 'b', wave length 'λ' and wave speed 'c'. The channel under consideration is non-uniform and inclined at an angle 'θ'. The discussion is considered for only the half width of the channel. In the plug flow expanse i.e. in the section between $y = 0$ and $y = y_0$ we have $|\tau_{xy}| \leq \tau_0$ and for the region involving $y = y_0$ and $y = H$, $|\tau_{xy}| \geq \tau_0$.

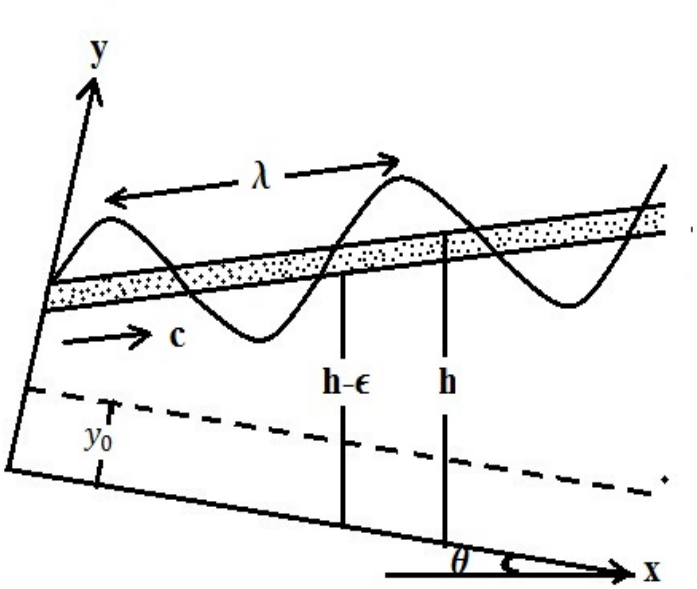

Fig. 4.1: Geometry of the flow

The deformation of the wall is thus described by,

$$Y = H(X,t) = a + b\,sin\frac{2\pi}{\lambda}(X - ct). \tag{4.1}$$

Here $a = a_0 + kx$ and k represents the non-uniformity parameter of the channel.

The flow geometry and the transformation from laboratory frame to wave frame is considered along with the necessary geometric conditions and the non-dimensional parameters, accordingly as mentioned in Chapter-2.

The governing equations of motion after declining the primes are as follows:

$$\frac{\partial}{\partial y}(\tau_{yx}) = -\frac{\partial p}{\partial x} + \eta\, sin\theta, \tag{4.2}$$

where

$$\tau_{yx} = \left(-\frac{\partial u}{\partial y}\right)^n + \tau_0\,, \tag{4.3}$$

and the peripheral conditions are

$$\psi = 0 \;\; at \;\; y = 0. \tag{4.4}$$

$$\psi_{yy} = 0 \;\; at \;\; y = 0. \tag{4.5}$$

$$\tau_{yx} = 0 \;\; at \;\; y = 0. \tag{4.6}$$

$$u = -\frac{\sqrt{Da}}{\alpha}\frac{\partial u}{\partial y} - 1, \;\; at \;\; y = h(x) - \epsilon. \tag{4.7}$$

4.3 Solution of the problem:

Equations (4.2) and (4.3) are solved along with $u = \frac{\partial \psi}{\partial y}\; and \;\; v = -\frac{\partial \psi}{\partial x}$ and the boundary conditions (4.4) - (4.7), to get the velocity field as,

$$u = P^m\left[\frac{1}{m+1}\{(h-\epsilon-y_o)^{m+1} - (y-y_o)^{m+1}\} + \frac{\sqrt{Da}}{\alpha}(h-\epsilon-y_o)^m\right] - 1, \tag{4.8}$$

where

$$P = -\frac{\partial p}{\partial x} + \eta\, sin\theta \;\; and \;\; m = \frac{1}{n}. \tag{4.9}$$

In the plug flow region the upper limit $y_0 = \frac{\tau_0}{P}$, is obtained taking the boundary condition $\psi_{yy} = 0,\ at\ y = y_0$.

The condition $\tau_{xy} = \tau_{h-\epsilon}$ at $y = h - \epsilon$, is applied to get $P = \frac{\tau_{h-\epsilon}}{h-\epsilon}$.

Therefore $\frac{y_0}{h-\epsilon} = \frac{\tau_o}{\tau_{h-\epsilon}} = \tau\ ;\ 0 < \tau < 1.$

To obtain the velocity in the plug flow region, we consider $y = y_o$ in (4.8) and get

$$u_p = P^m(h - \epsilon - y_o)^m \left(\frac{h-\epsilon-y_o}{1+m} + \frac{\sqrt{Da}}{\propto}\right) - 1. \tag{4.10}$$

Equations (4.9) and (4.10) are integrated along with the conditions $\psi_p = 0$ and $\psi = \psi_p$ at $y = y_o$ to obtain the stream functions as:

$$\psi = P^m \left[\frac{1}{m+1}\left\{(h - \epsilon - y_o)^{m+1} y - \frac{(y-y_o)^{m+2}}{m+2}\right\} + \frac{\sqrt{Da}}{\alpha}(h - \epsilon - y_0)^m\, y\right] - y. \tag{4.11}$$

$$\psi_p = \int u_p dy = P^m(h - \epsilon - y_0)^m \left(\frac{h-\epsilon-y_0}{m+1} - \frac{\sqrt{Da}}{\alpha}\right) y - y. \tag{4.12}$$

The volume flow rate across each cross section, denoted by q is given by

$$q = \int_0^{y_0} u_p dy + \int_{y_0}^{h-\epsilon} u\, dy.$$

$$q = P^m \left[\frac{(h-\epsilon-y_0)^{m+1}}{m+1}\left\{h - \epsilon - \frac{(h-\epsilon-y_0)}{m+2}\right\} + (h - \epsilon - y_0)^m\ \frac{\sqrt{Da}}{\alpha}(h - \epsilon)\right] - (h - \epsilon). \tag{4.13}$$

From equations (4.9) and (4.13) we get,

$$\frac{\partial p}{\partial x} = -P + \eta\, sin\theta\ = \left[\frac{-(q+h-\epsilon)(m+1)(m+2)\alpha}{(h-\epsilon)^{m+1}(1-\tau)^m\{\alpha(h-\epsilon)(1-\tau)\{(m+2)-(1-\tau)\} + \sqrt{Da}(m+1)(m+2)\}}\right]^{\frac{1}{m}} +\ \eta\, sin\theta. \tag{4.14}$$

The volume flow rate $Q(X,t)$ and the time-averaged volume flow rate $\bar{Q}$ are calculated using the formulas mentioned in previous chapter, given in equation no (2.16) and (2.17) respectively.

Integrating equation (4.14) over one wavelength, the pressure difference over a cycle of the wave is given as

$$\Delta P = \int_0^1 \frac{\partial p}{\partial x}\, dx = \int_0^1 (-P + \eta\, sin\theta)\; dx \tag{4.15}$$

The frictional force F, at the wall over one wavelength is

$$F = \int_0^1 h\left(-\frac{\partial p}{\partial x}\right) dx = \int_0^1 h\,(P - \eta\, sin\,\theta)\, dx \tag{4.16}$$

4.4 Results and discussion:

Graphs are plotted for equation (4.15), using Mathematica software, for the pressure difference ΔP against time-averaged volume flow rate $\bar{Q}$.

As the Darcy number increases, ΔP decreases up to $\bar{Q} = 0.3$ and reverse behavior is seen for $\bar{Q} > 0.5$. For $0.3 < \bar{Q} < 0.5$, the variation of $\bar{Q}$ hardly has any effect on ΔP for a convergent channel ($k = -0.1$) as shown in Fig. 4.2. A similar effect in the divergent channel ($k = 0.1$) can be seen in Fig. 4.3, except for the region where we observe no effect is $0.5 < \bar{Q} < 0.7$.

The opposite behavior is seen for variation of the yield stress τ. Figure 4.4 depicts that the curves intersect at $\bar{Q} = 0.4$ and it is seen that to the left ΔP increases with τ, where as to the right of intersection point, ΔP reduces with enhancement in τ in a convergent channel. Again a similar effect is observed for a divergent channel, but for the point of convergence being $\bar{Q} = 0.5$ as observed from Fig. 4.5.

Figures 4.6 and 4.7 describe the effect of ϵ. As the porous thickening ϵ increases, pumping increases and the effect of the porous thickening on the wall is negligible on ΔP once the pumping graphs intersect. The graphs of pumping intersect at $\bar{Q} = 0.5$ in a convergent channel and at $\bar{Q} = 0.7$ in a divergent channel.

We also observe from Fig. 4.8 and Fig. 4.9 that the pumping increases, with increase in the angle of intersection θ in the convergent channel as well in the divergent channels respectively. The increased inclination forces the fluid to move rapidly thus enhancing the

pressure difference. We notice that effect is very less in the divergent channel compared to the convergent channel. The result agrees with that of Akbar and Butt [82].

The graphs drawn underneath the variation of ϕ as shown in Fig. 4.10 reveals increase in pumping for an increase in the amplitude ratio only for $0 \leq \bar{Q} \leq 0.3$ and further for $\bar{Q} > 0.3$ the pressure difference drops irrespective of any change in ϕ, for a convergent channel. In a divergent channel the pressure difference increases with ϕ up to $\bar{Q} = 0.5$, and further there is no effect of any changes in the amplitude ratio ϕ as illustrated in Fig.4.11. As the amplitude increases the channel becomes more non-uniform compelling the fluid to move very slowly and consequently there is increase in pressure difference according to Akbar and Butt [82].

Using equation (4.16) graphs of Frictional force F against time-averaged volume flow rate $\bar{Q}$ are plotted. Figure 4.12 shows that the increase in Darcy number, increases the Frictional force up to $\bar{Q} = 0.4$ and further observation reveals that the frictional force reduces with rise in the Darcy number in the convergent channel. The same effect of Darcy number is observed in the divergent channel also as plotted in Fig. 4.13, i.e., the Frictional force increases with Darcy number up to $\bar{Q} = 0.5$ and next it declines with Da.

The graphs drawn for the discrepancy of τ are shown in Fig. 4.14 and Fig. 4.15. We observe that as τ increases the Frictional force decrease up to $\bar{Q} = 0.3$ in a convergent channel and up to $\bar{Q} = 0.5$ in a divergent channel and then onwards it is seen that increase in τ increases the Frictional force F.

As the porous thickening ϵ increases, the Frictional force F decreases up to $\bar{Q} = 0.5$. For $0.5 < \bar{Q} < 0.8$, variation of ϵ has no effect on the increase in F, but further increase in ϵ increases the Frictional force as observed from Fig. 4.16. A similar effect is observed from Fig. 4.17 in a divergent channel, except for the null effect region being $0.7 < \bar{Q} < 0.9$.

With increase in the inclination θ, we observe a drop in the Frictional force for both convergent and divergent channels as plotted in Fig. 4.18 and Fig. 4.19 respectively. What we observe here is variation of angle of inclination has less effect on a divergent channel compared to the convergent channel.

The Frictional force is observed to decrease with increase in the amplitude ratio ϕ in both convergent (Fig. 4.20) as well in divergent (Fig. 4.21) channels. The amplitude ratio ϕ has no effect on the increase of Frictional force F for $\bar{Q} > 0.5$ in a convergent channel and for $\bar{Q} > 0.3$ in a divergent channel.

The consequences of the pertinent parameters observed for the stream line patterns are depicted in Fig. 4.22 to Fig. 4.25. Stream line patterns reveal that trapping phenomenon occurs and the bolus increases in size with rise in the values of $Da,\ \tau,\ \epsilon\ and\ \phi$, whereas bolus decreases in size for increase in the values of $\bar{Q}$ (Fig. 4.26).

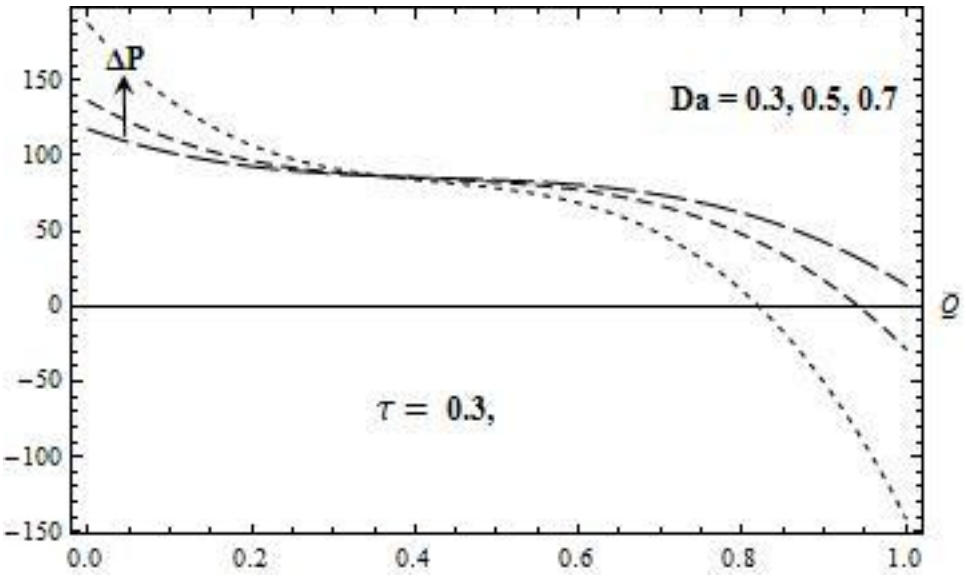

Fig. 4.2: Effect of Da on ΔP against $\bar{Q}$ in a convergent channel with:
$n = 3$; $\alpha = 0.3$; $\tau = 0.1$; $\epsilon = 0.3$; $\phi = 0.3$; $\eta = 0.1$; $\theta = \pi/3$

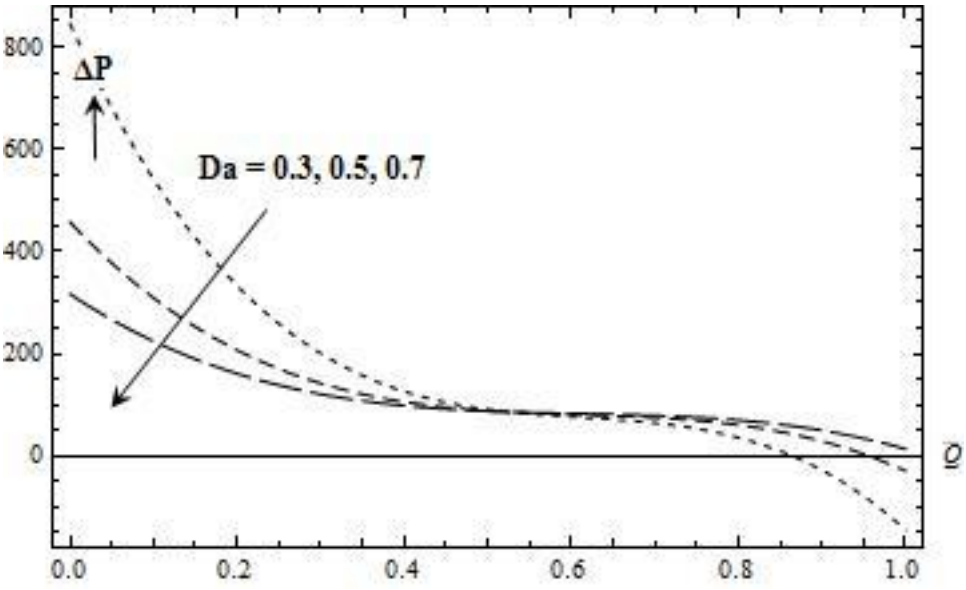

Fig. 4.3: Effect of Da on ΔP against $\bar{Q}$ in a divergent channel with:
$n = 3$; $\alpha = 0.3$; $\tau = 0.1$; $\epsilon = 0.3$; $\phi = 0.3$; $\eta = 0.1$; $\theta = \pi/3$

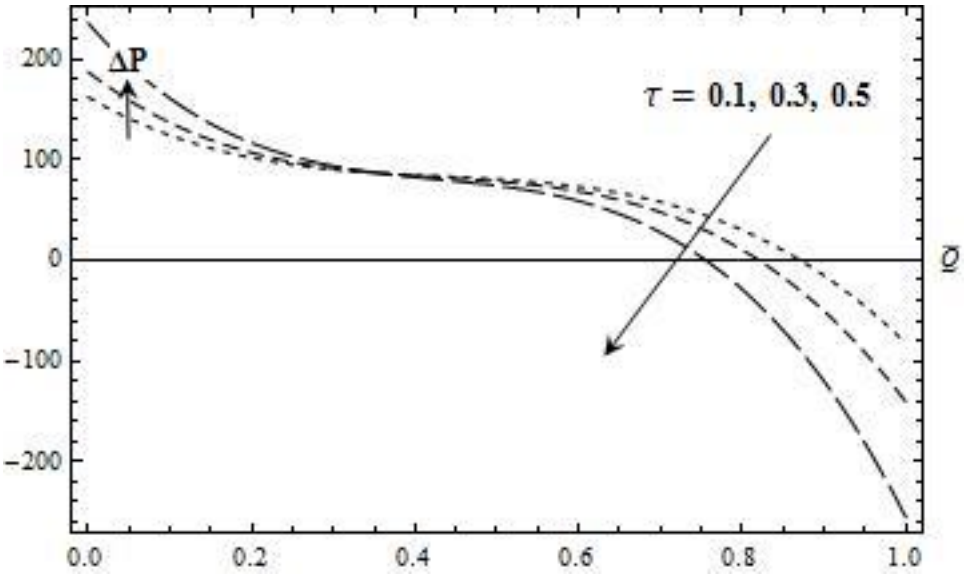

Fig. 4.4: Effect of τ on ΔP against $\bar{Q}$ in a convergent channel with: $n = 3;\ \alpha = 0.3;\ Da = 0.3;\ \epsilon = 0.3;\ \phi = 0.3;\ \eta = 0.1;\ \theta = \pi/3$

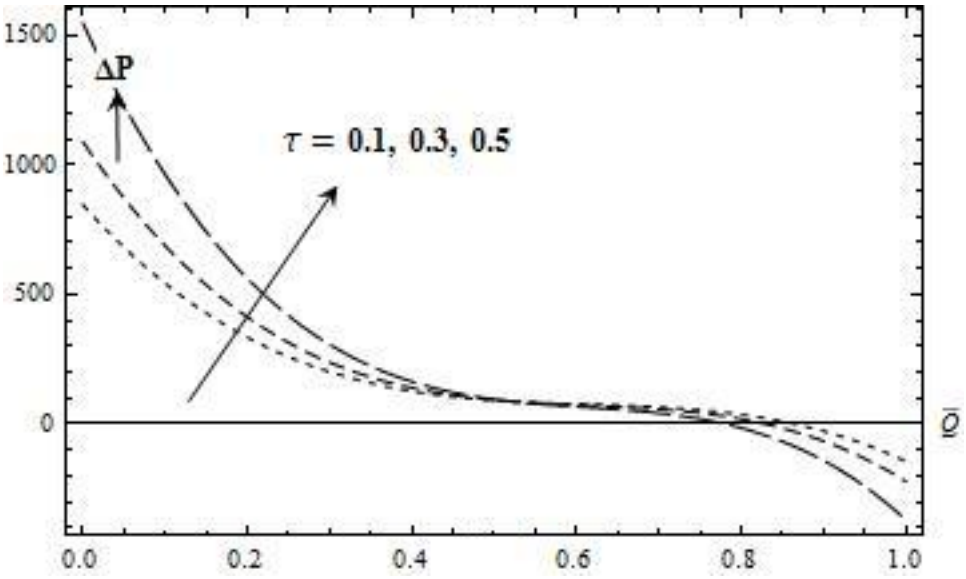

Fig. 4.5: Effect of τ on ΔP against $\bar{Q}$ in a divergent channel with: $n = 3;\ \alpha = 0.3;\ Da = 0.3;\ \epsilon = 0.3;\ \phi = 0.3;\ \eta = 0.1;\ \theta = \pi/3$

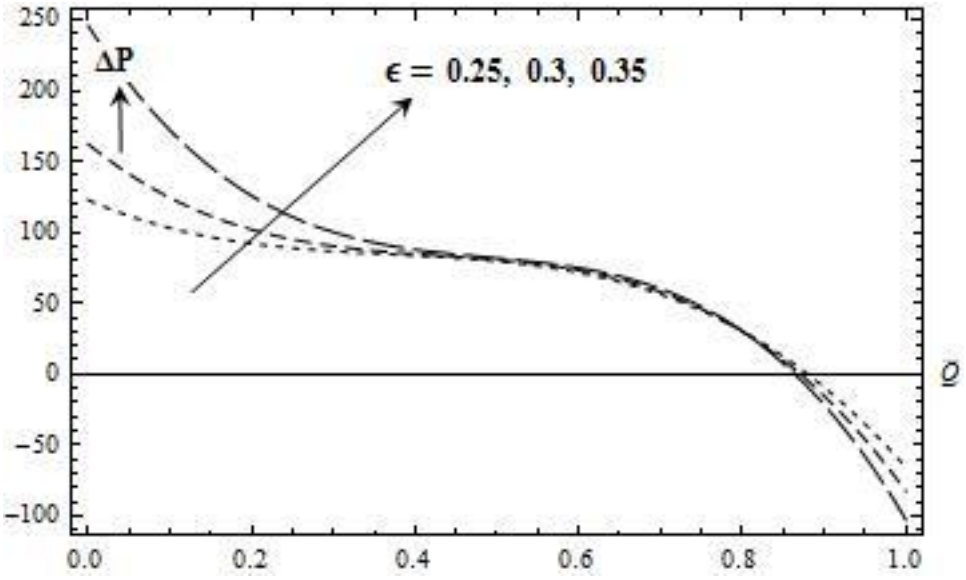

Fig. 4.6: Effect of ϵ on ΔP against $\bar{Q}$ in a convergent channel with: $n = 3;\ \alpha = 0.3;\ Da = 0.3;\ \tau = 0.1;\ \phi = 0.3;\ \eta = 0.1;\ \theta = \pi/3$

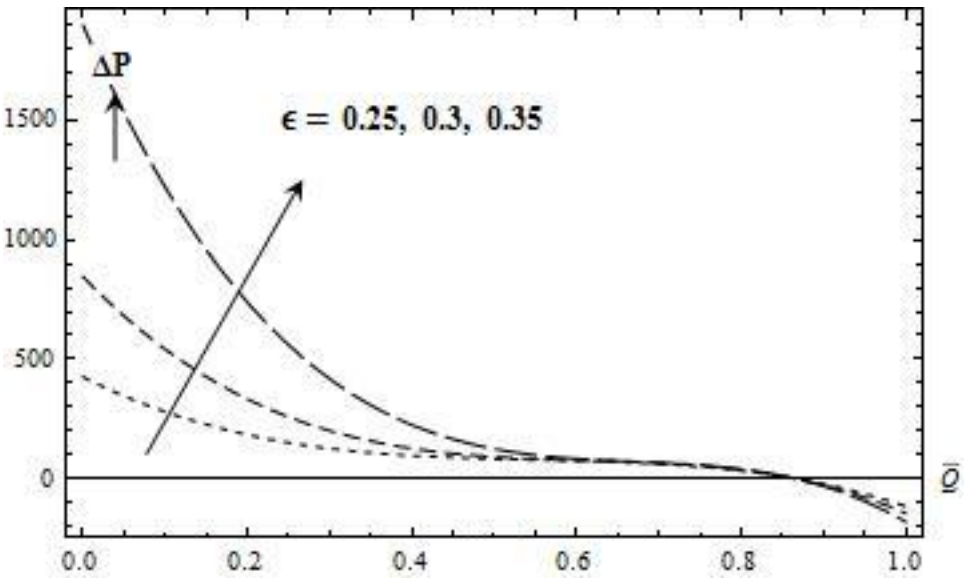

Fig. 4.7: Effect of ϵ on ΔP against $\bar{Q}$ in a divergent channel with: $n = 3;\ \alpha = 0.3;\ Da = 0.3;\ \tau = 0.1;\ \phi = 0.3;\ \eta = 0.1;\ \theta = \pi/3$

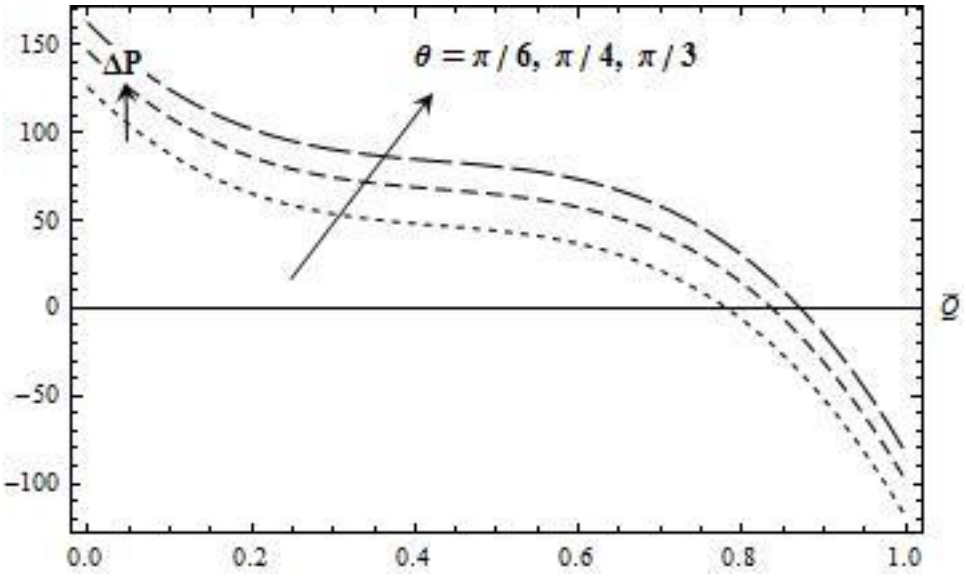

Fig. 4.8: Effect of θ on ΔP against $\bar{Q}$ in a convergent channel with: $n = 3$; $\alpha = 0.3$; $Da = 0.3$; $\epsilon = 0.3$; $\tau = 0.1$; $\phi = 0.3$; $\eta = 0.1$

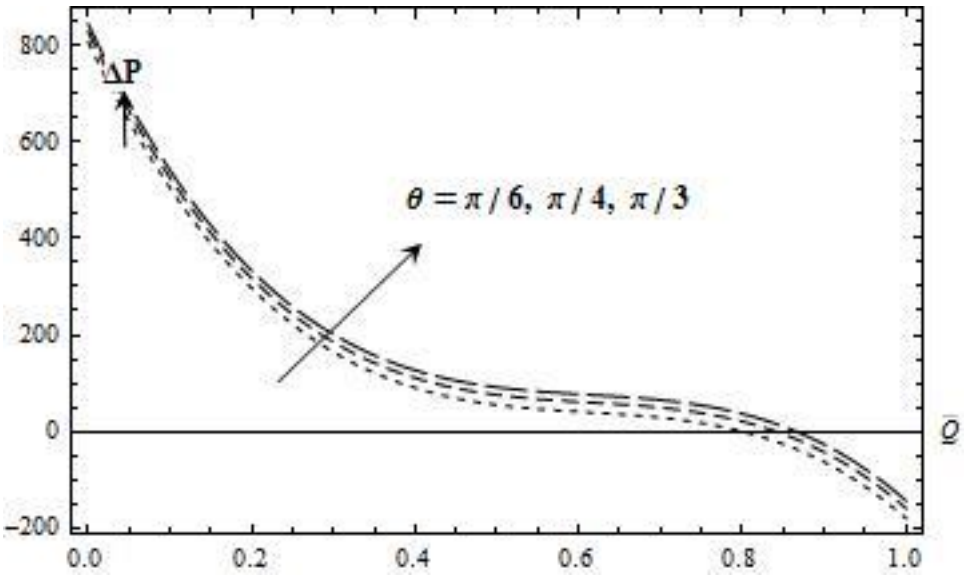

Fig. 4.9: Effect of θ on ΔP against $\bar{Q}$ in a divergent channel with: $n = 3$; $\alpha = 0.3$; $Da = 0.3$; $\epsilon = 0.3$; $\tau = 0.1$; $\phi = 0.3$; $\eta = 0.1$

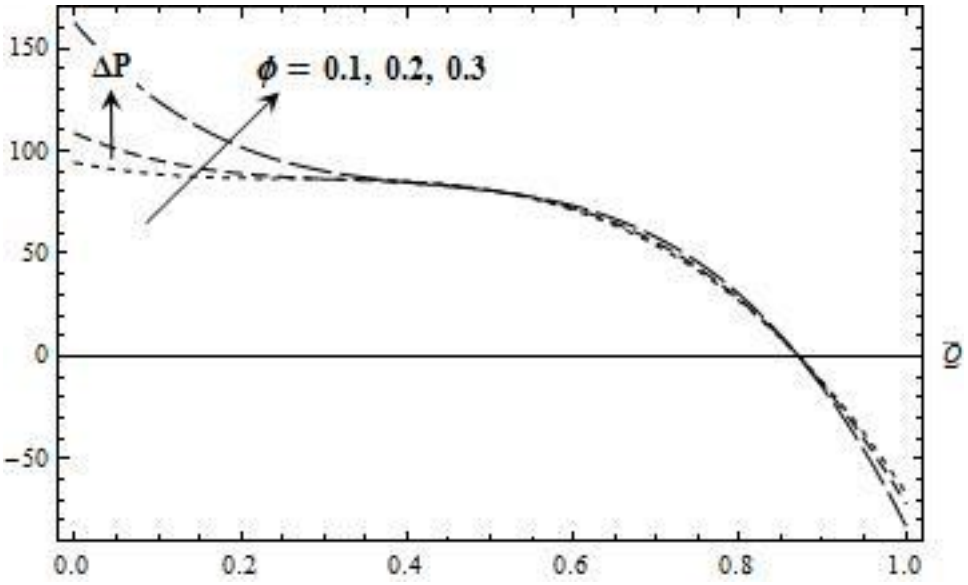

Fig. 4.10: Effect of ϕ on ΔP against $\bar{Q}$ in a convergent channel with:
$n = 3;\ \alpha = 0.3;\ Da = 0.3;\ \tau = 0.1;\ \epsilon = 0.3;\ \eta = 0.1;\ \theta = \pi/3$

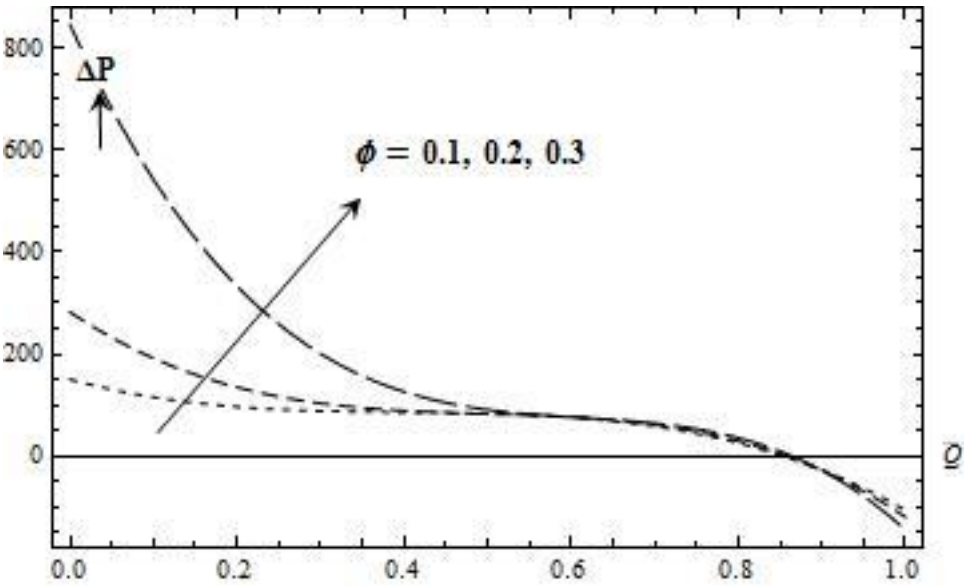

Fig. 4.11: Effect of ϕ on ΔP against $\bar{Q}$ in a divergent channel with:
$n = 3;\ \alpha = 0.3;\ Da = 0.3;\ \tau = 0.1;\ \epsilon = 0.3;\ \eta = 0.1;\ \theta = \pi/3$

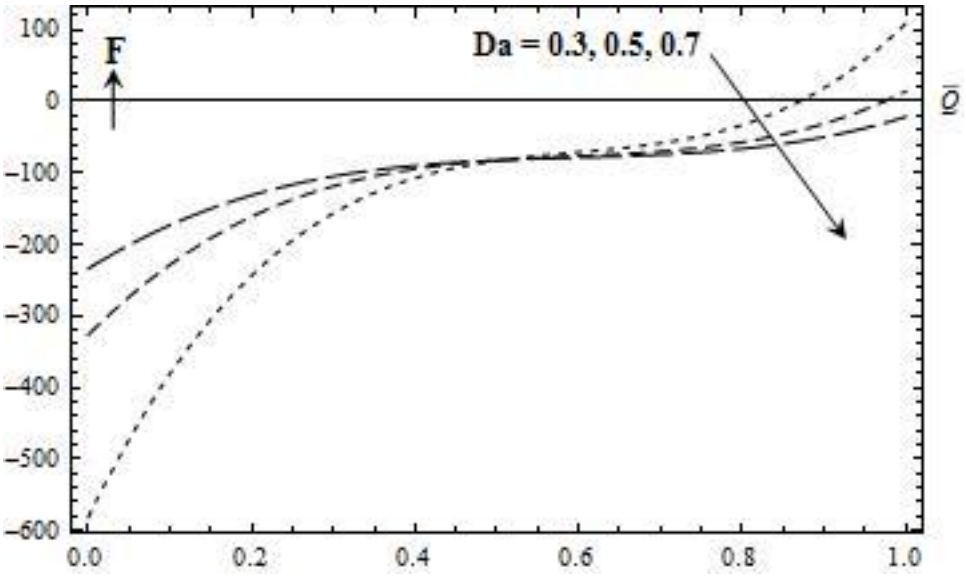

Fig. 4.12: Effect of Da on F against $\bar{Q}$ in a convergent channel with:

$n = 3;\ \alpha = 0.3;\ \tau = 0.1;\ \epsilon = 0.3;\ \eta = 0.1;\ \theta = \pi/3;\ \phi = 0.3$

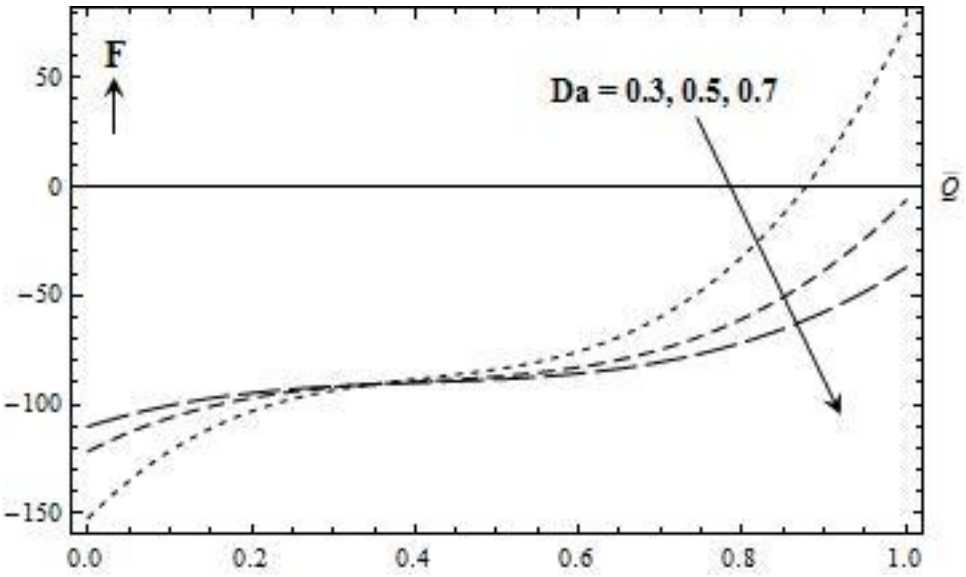

Fig. 4.13: Effect of Da on F against $\bar{Q}$ in a divergent channel with:

$n = 3;\ \alpha = 0.3;\ \tau = 0.1;\ \epsilon = 0.3;\ \eta = 0.1;\ \theta = \pi/3;\ \phi = 0.3$

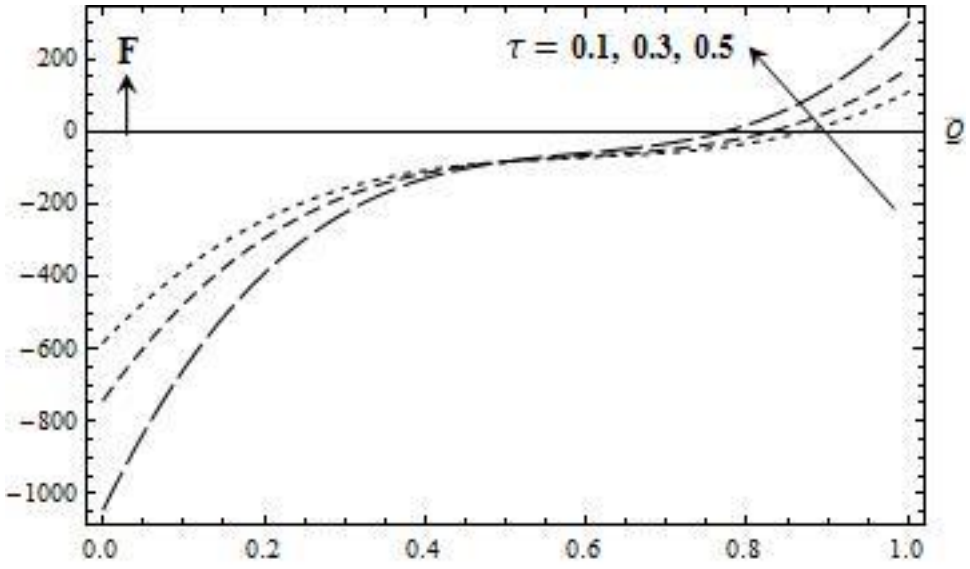

Fig. 4.14: Effect of τ on F against $\bar{Q}$ in a convergent channel with: $n = 3;\ \alpha = 0.3;\ Da = 0.3;\ \epsilon = 0.3;\ \eta = 0.1;\ \theta = \pi/3;\ \phi = 0.3$

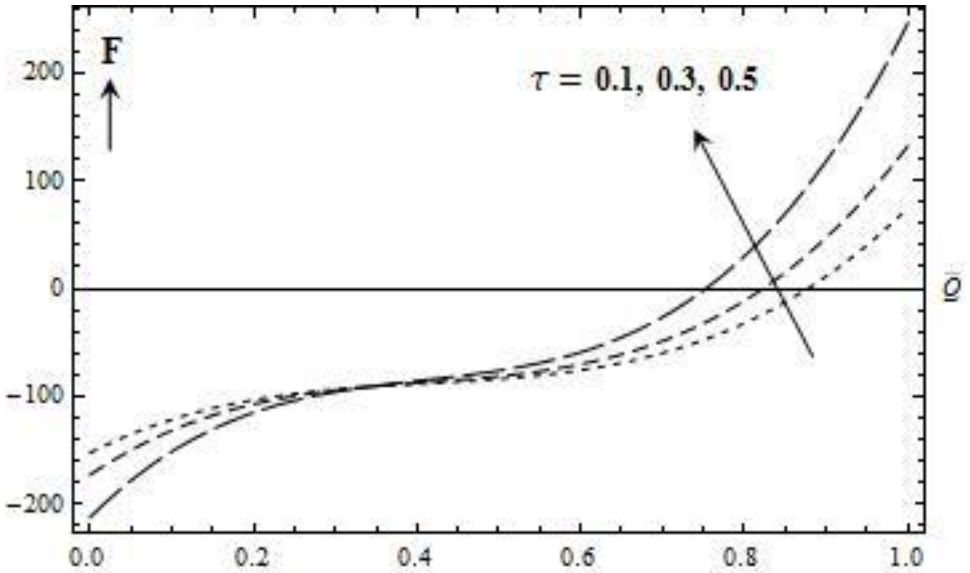

Fig. 4.15: Effect of τ on F against $\bar{Q}$ in a divergent channel with: $n = 3;\ \alpha = 0.3;\ Da = 0.3;\ \epsilon = 0.3;\ \eta = 0.1;\ \theta = \pi/3;\ \phi = 0.3$

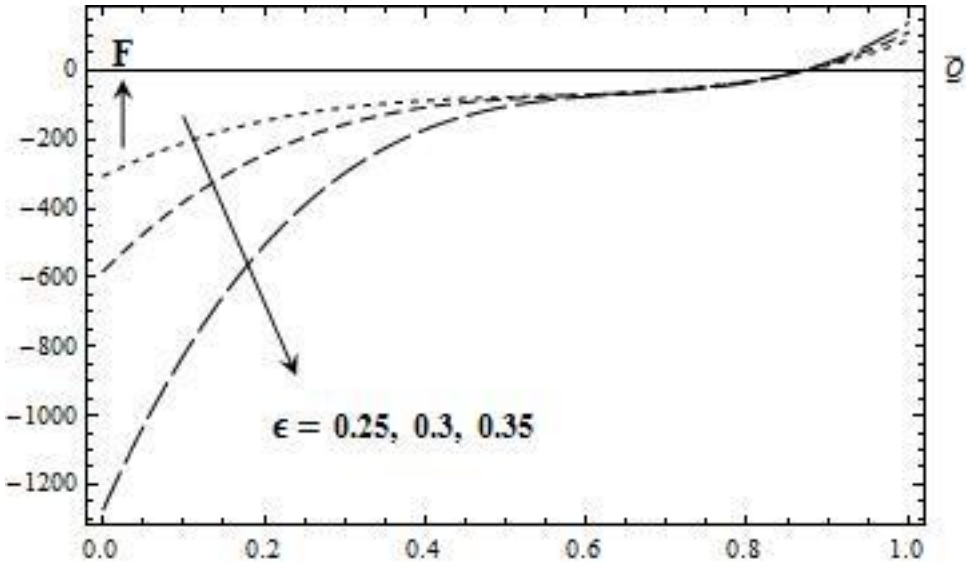

Fig. 4.16: Effect of ϵ on F against $\bar{Q}$ in a convergent channel with: $n = 3;\ \alpha = 0.3;\ Da = 0.3;\ \tau = 0.1;\ \eta = 0.1;\ \theta = \pi/3;\ \phi = 0.3$

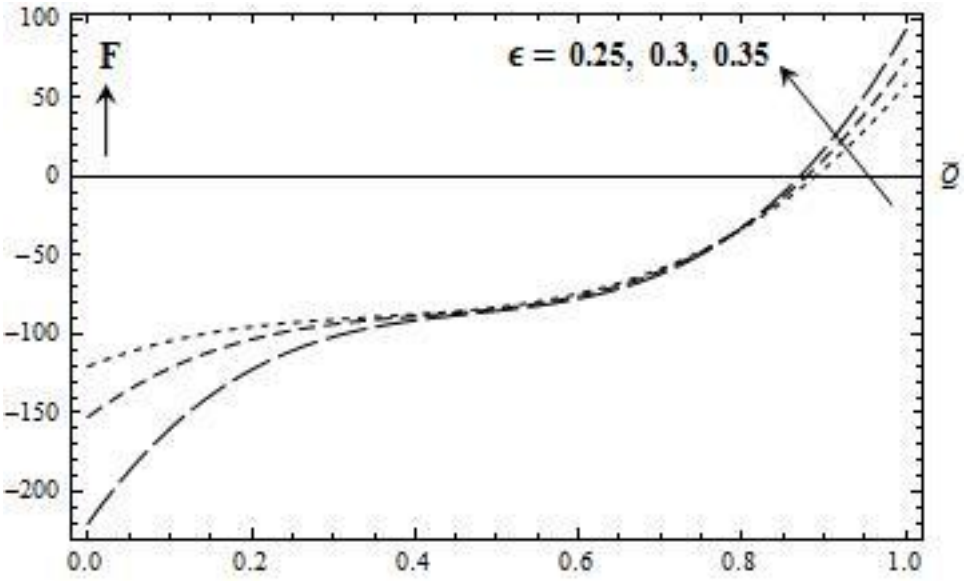

Fig. 4.17: Effect of ϵ on F against $\bar{Q}$ in a divergent channel with: $n = 3;\ \alpha = 0.3;\ Da = 0.3;\ \tau = 0.3;\ \eta = 0.1;\ \theta = \pi/3;\ \phi = 0.3$.

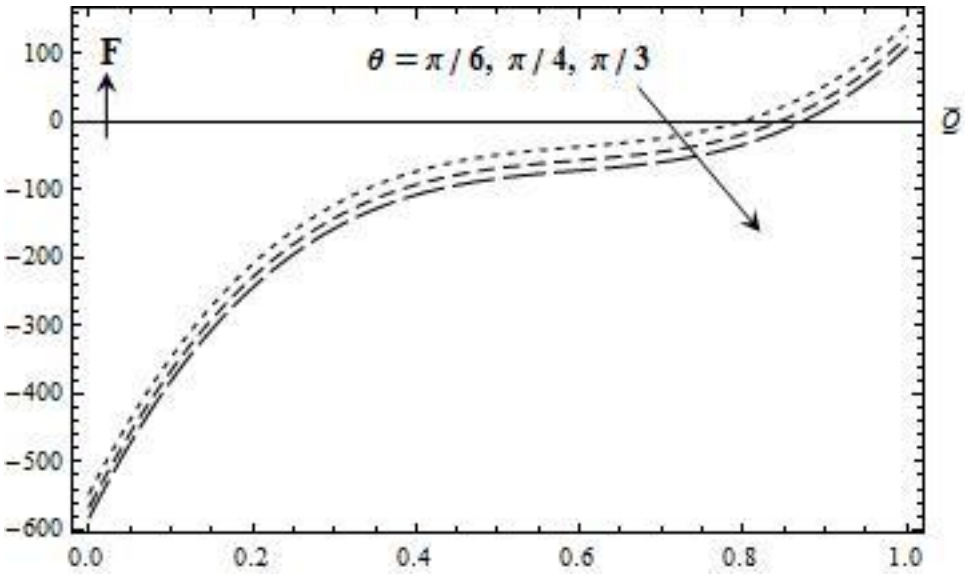

Fig. 4.18: Effect of θ on F against $\bar{Q}$ in a convergent channel with: $n = 3;\ \alpha = 0.3;\ Da = 0.3;\ \epsilon = 0.3;\ \tau = 0.1;\ \eta = 0.1;\ \phi = 0.3$

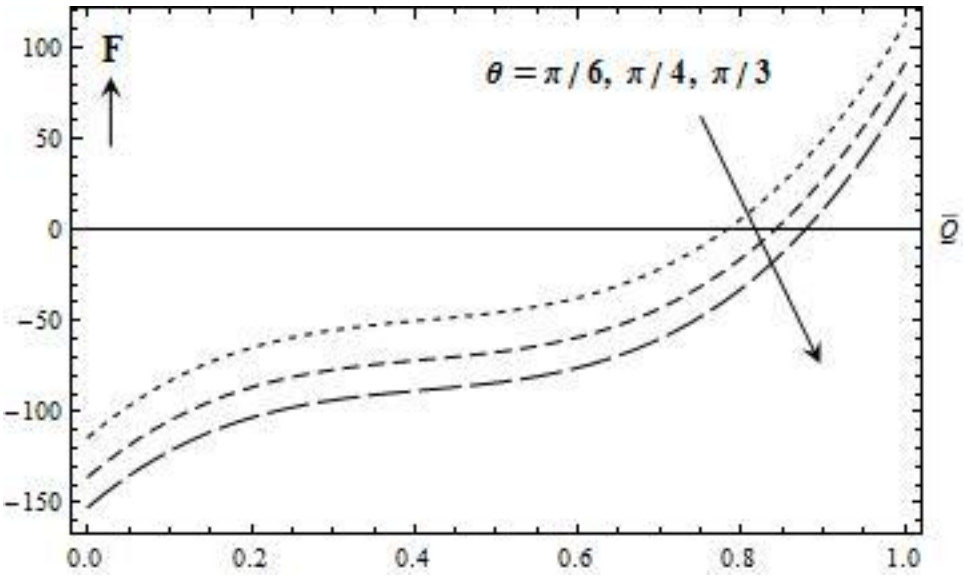

Fig. 4.19: Effect of θ on F against $\bar{Q}$ in a divergent channel with: $n = 3;\ \alpha = 0.3;\ Da = 0.3;\ \epsilon = 0.3;\ \tau = 0.3;\ \eta = 0.1;\ \phi = 0.3$

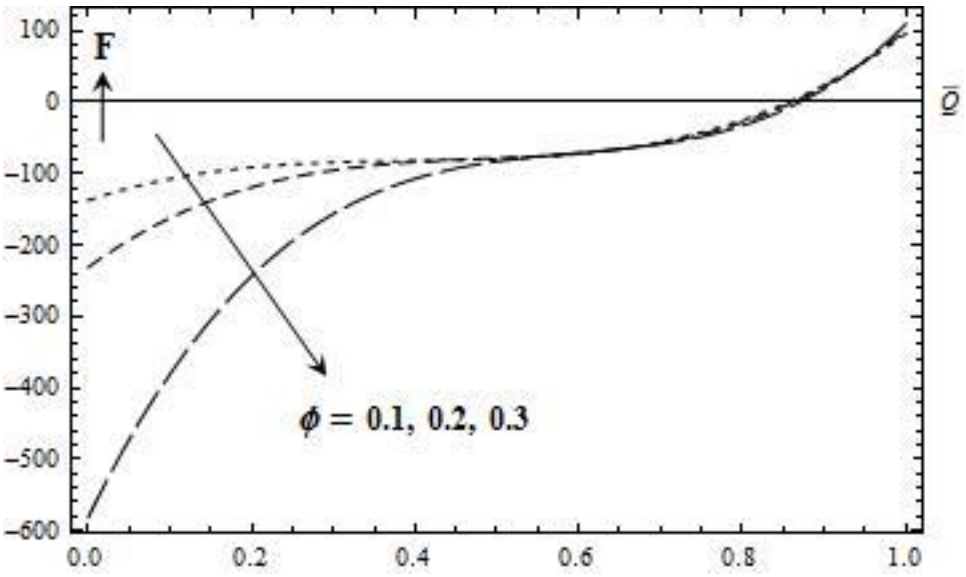

Fig. 4.20: Effect of ϕ on F against $\bar{Q}$ in a convergent channel with $n = 3;\ \alpha = 0.3;\ Da = 0.3;\ \epsilon = 0.3;\ \tau = 0.1;\ \eta = 0.1; \theta = \pi/3$

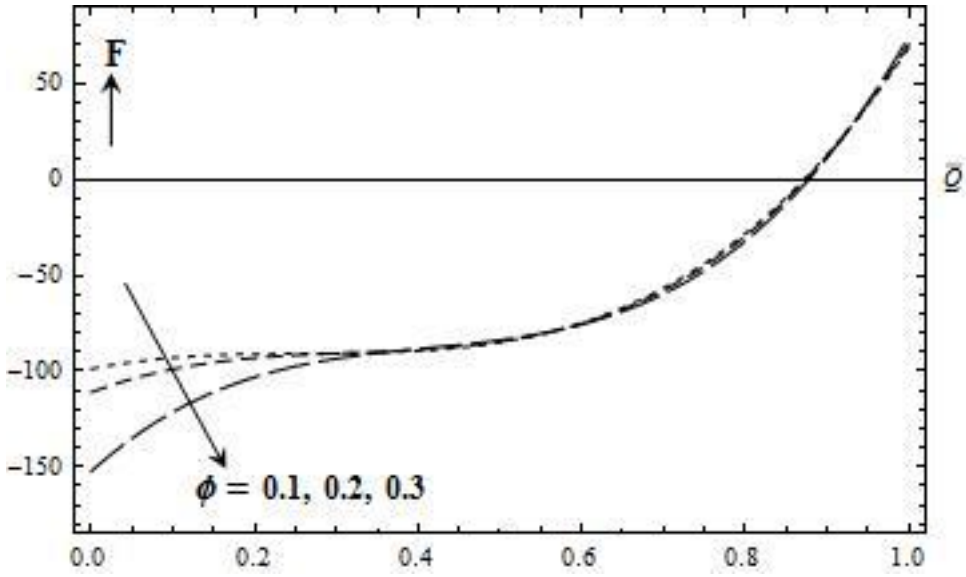

Fig. 4.21: Effect of ϕ on F against $\bar{Q}$ in a divergent channel with: $n = 3;\ \alpha = 0.3;\ Da = 0.3;\ \epsilon = 0.3;\ \tau = 0.3;\ \eta = 0.1; \theta = \pi/3$

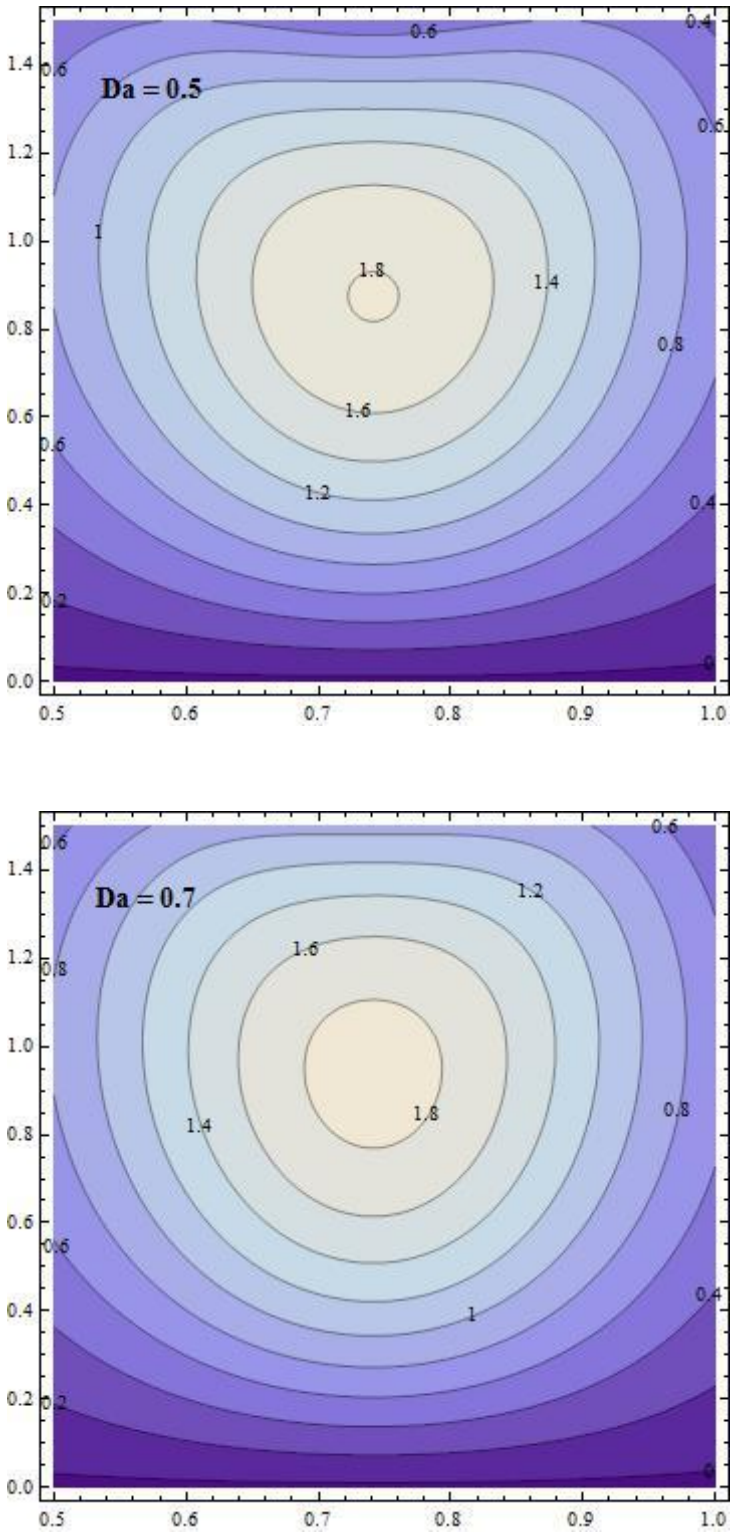

Fig. 4.22: Stream line plots for variation in Darcy number Da with:

$\boldsymbol{n = 3;\ \alpha = 1; \tau = 0.5; \epsilon = 0.3;\ \phi = 0.3;\ \bar{Q} = 0.1; k = 0.1;\ \eta = 0.5;\ \theta = \pi/3}$

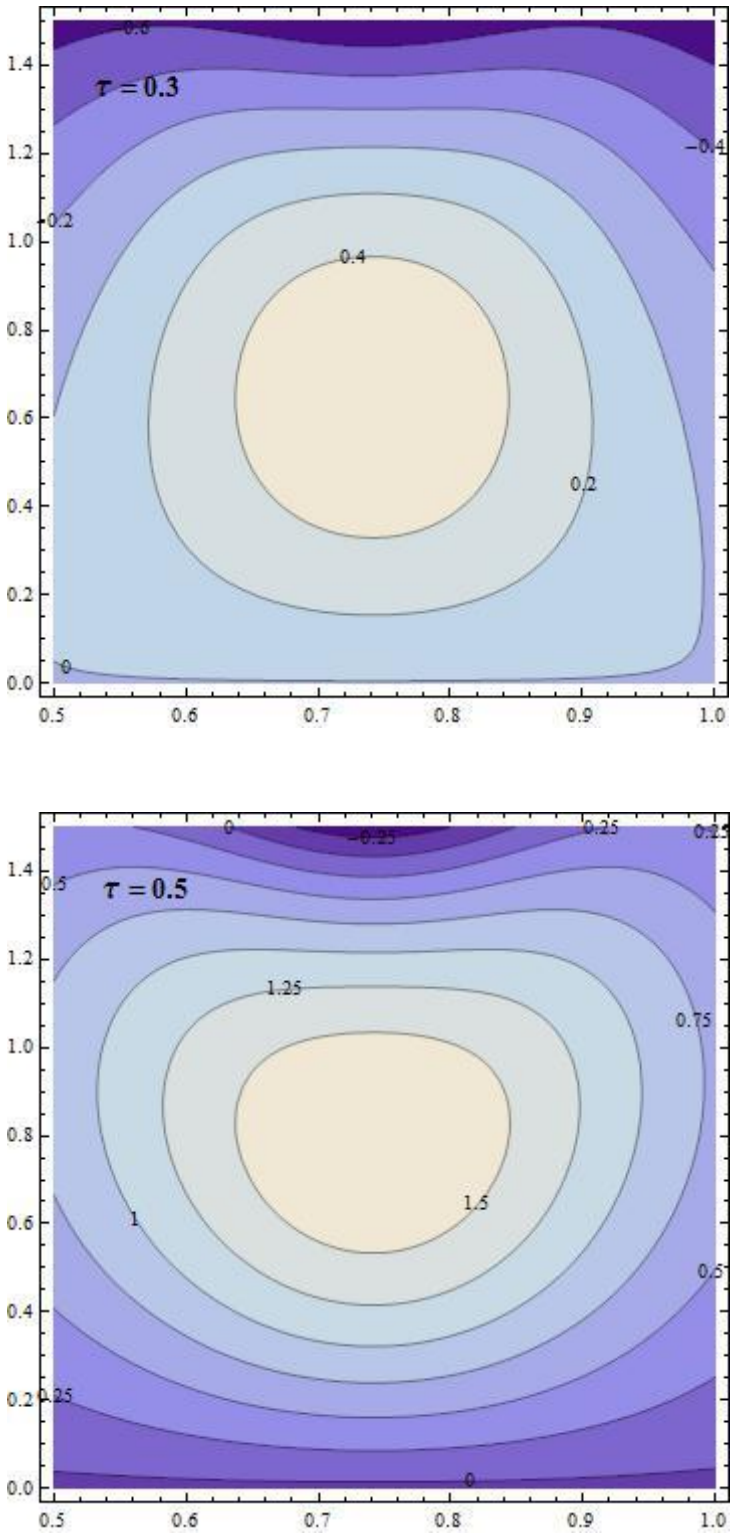

Fig. 4.23: Stream line plots for variation in yield stress τ with:

$n = 3;\ \mathrm{Da} = 0.3;\ \alpha = 1;\ \epsilon = 0.3;\ \phi = 0.3;\ \bar{Q} = 0.1;\ k = 0.1;\ \eta = 0.5;\ \theta = \pi/3$

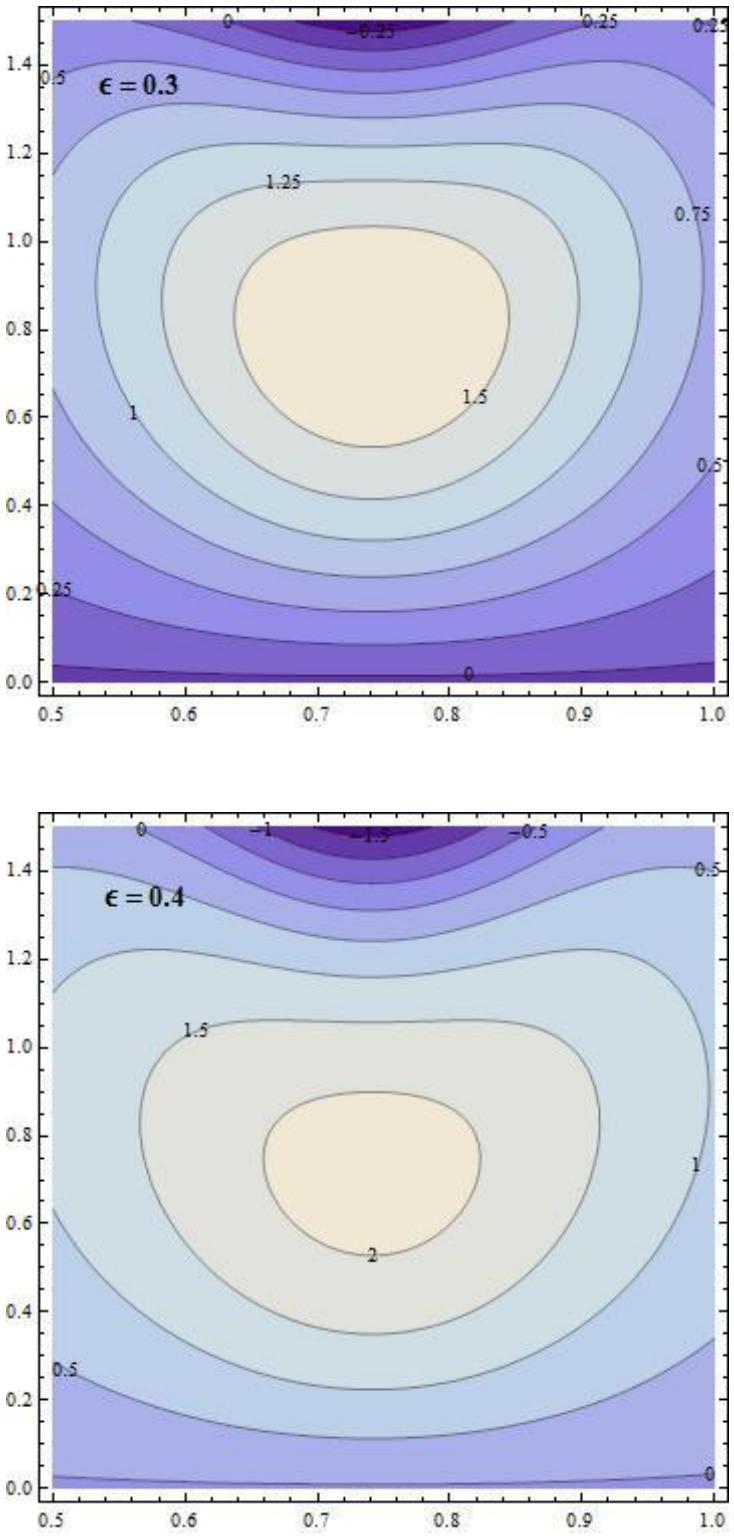

Fig. 4.24: Stream line plots for variation in porous lining ϵ with:

$$n = 3;\ \mathrm{Da} = 0.3;\ \alpha = 1;\ \tau = 0.5;\ \phi = 0.3;\ \bar{Q} = 0.1;\ k = 0.1;\ \eta = 0.5;\ \theta = \pi/3$$

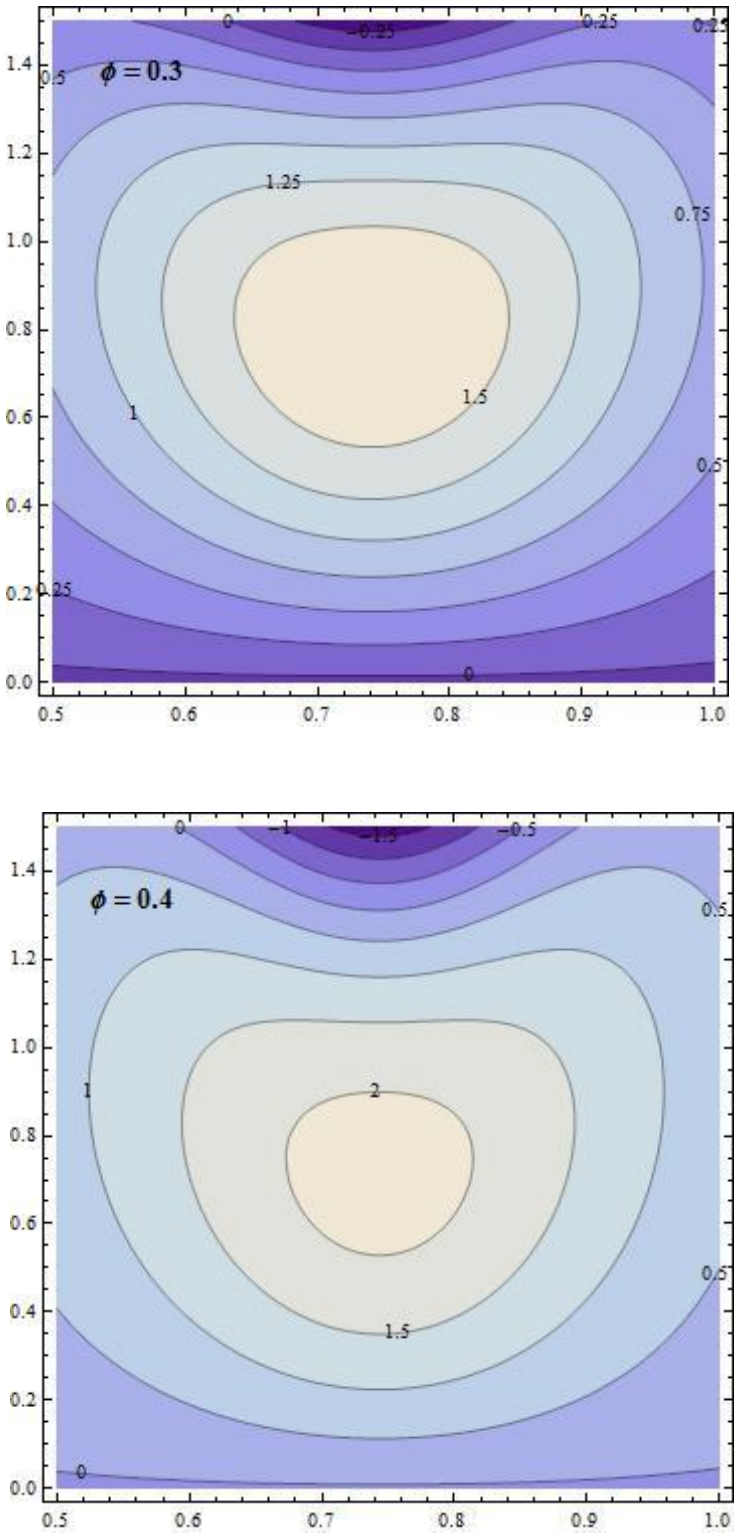

Fig. 4.25: Stream line plots for variation in amplitude ratio ϕ with $n = 3$; $\mathrm{Da} = 0.3$; $\alpha = 1$; $\tau = 0.5$; $\epsilon = 0.3$; $\bar{Q} = 0.1$; $k = 0.1$; $\eta = 0.5$; $\theta = \pi/3$

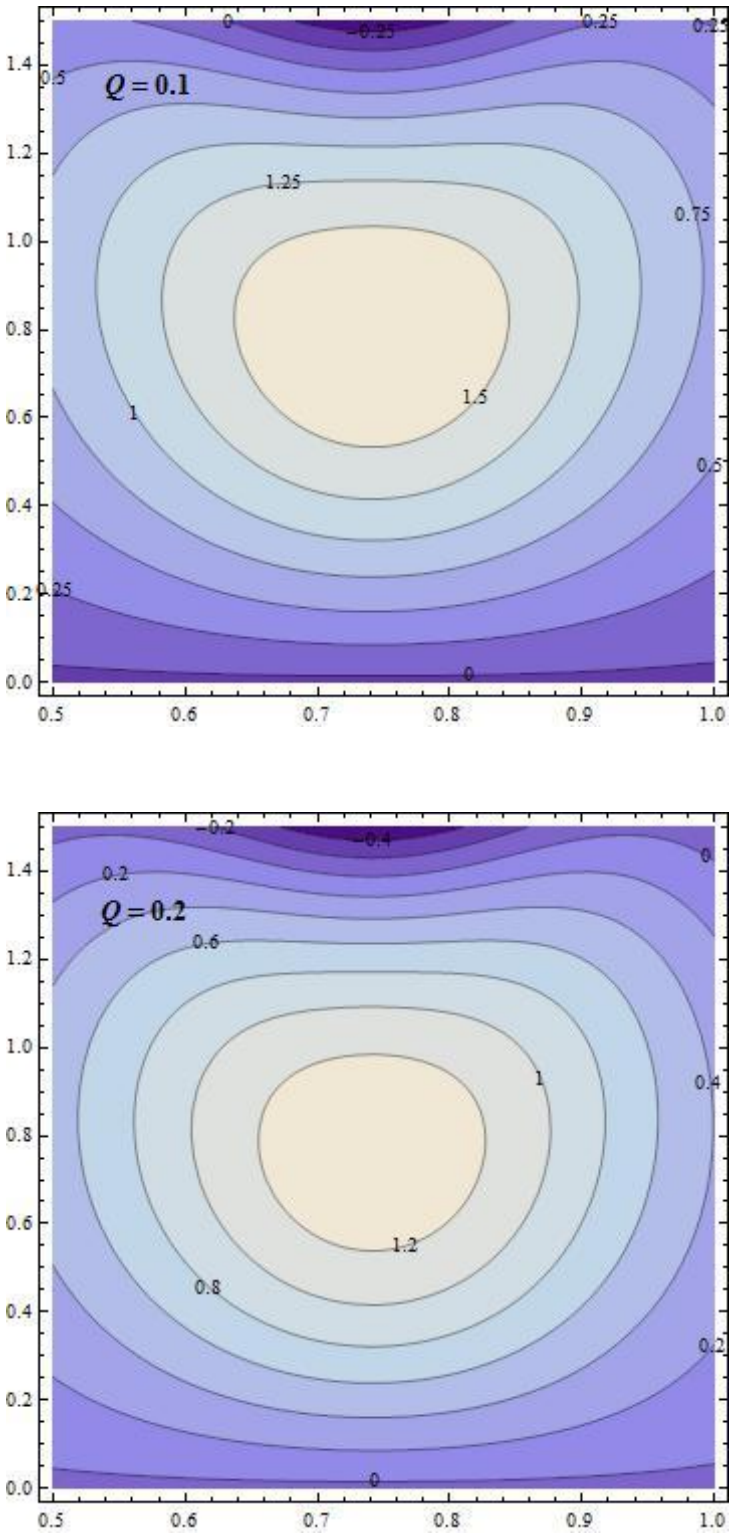

Fig. 4.26: Stream line plots for variation in time-averaged volume flow rate $\bar{Q}$ with: $n = 3$; $\mathrm{Da} = 0.3$; $\alpha = 1$; $\tau = 0.5$; $\epsilon = 0.3$; $\phi = 0.3$; $k = 0.1$; $\eta = 0.5$; $\theta = \pi/3$

CHAPTER-5

Heat Transfer Inferences on the Herschel Bulkley Fluid Flow under Peristalsis

5.1. Introduction:

Peristalsis is a coordinated action wherein a contraction wave followed by a relaxation wave, pass through the channel. As they are propelled along, they would always enter a segment which had actively relaxed and enlarged to receive them. Peristaltic applications can also be found in human physiological system for movement of fluids, mechanical devices in the transportation of corrosive materials, slurries and blood transfusion through the heart lung machine.

After studying the flow of the non Newtonian fluid in uniform, non uniform and inclined channels in the previous chapters, in this chapter the study has been extended to examine the of heat transfer effects. Though it seems that the interaction of peristaltic flow of blood with heat transfer is not vital when we consider blood inside the body, it needs significance once it is drawn out of the body.

Latham's [5] initial investigation on peristalsis paved way for many scholars to study and analyze the peristaltic motion (Shapiro [6], Burns and Parkes [9], Fung and Yin [99]). Many authors including Tang and Fung [25] have presented their study with the view that many physiological fluids as well as blood, flowing under peristalsis behave like a Newtonian fluid. Later on, it was concluded that under peristalsis, physiological fluids behave Newtonianly or non-Newtonianly. Misery et al. [26] explored the generalized Newtonian fluid motion through a channel under peristalsis.

To bring out the importance of heat transfer in blood flow, assuming blood to be Casson fluid, Victor and Shah [100] published their study on thermo dynamical impacts on the transport of blood in a tube. Radhakrishnamacharya and Srinivasalu [101] examined the wall property aspects on the peristaltic flow under heat transfer. Mekheimer and Elmaboud [102] gave a report of the consequences of heat transfer as well as the magnetic field, for the motion of a Newtonian fluid under peristalsis, in an annulus held vertical. Srinivas and Gayathri [103] analyzed the peristaltic motion in a vertical asymmetric porous conduit to analyze the heat transfer effects. Akbar et al. [104] considered the flow through an asymmetric inclined channel with partial slip to analyze the heat transfer effect in the peristaltic transport. Dheia and Abdulhadi [105] inspected the motion of Jeffery fluid through

a porous channel to analyze the heat transfer and wall effects. They concluded that the temperature coefficient increases with the thermal conductivity.

Among the non-Newtonian fluids 'Herschel Bulkley' fluid is considered to be the more general fluid providing more accurate results than other forms of non-Newtonian fluids. To study blood, preferably the Herschel Bulkley fluid model is suggested for its close behavior to blood and its flexibility to reduce into Bingham, Newtonian and Power law model. This chapter deals with the heat transfer effect, studied under small Reynolds number and long wavelength assumptions, for the flow of Herschel Bulkley fluid under peristalsis, through a non uniform channel. The influences of various parameters are compared through the graphs.

5.2. Mathematical formulation:

Herschel Bulkley fluid is considered to move in a non-uniform channel, whose walls are coated with a permeable material, under heat transfer. A sinusoidal wave train is assumed to travel along the elastic walls generating peristaltic motion in the fluid. The problem is discussed for half width of the channel. The plug flow region is the region between $y = 0\ and\ y = y_0$ where $|\tau_{xy}| \leq \tau_0$. In the region above the plug flow, i.e. in the section $y = y_0\ and\ y = H,\ |\tau_{xy}| \geq \tau_0$.

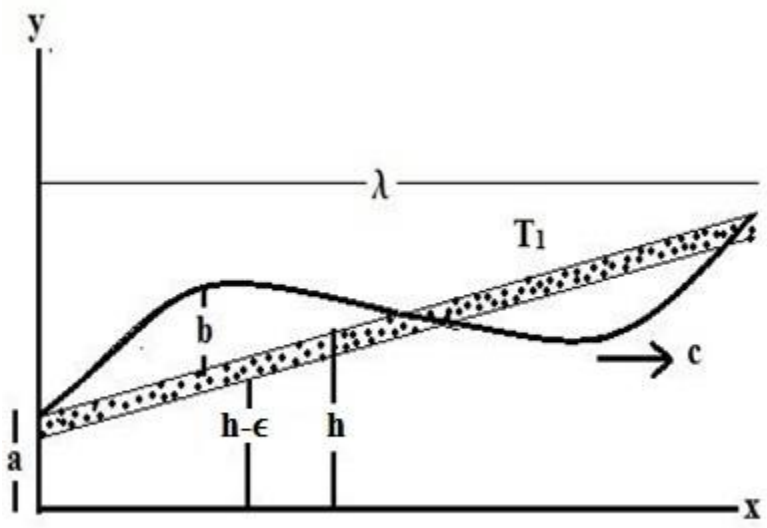

Fig. 5.1: Geometry of the flow.

The channel wall is governed by the equation:

$$Y = H(X,t) = a + bsin\frac{2\pi}{\lambda}(X - ct), \tag{5.1}$$

where $a = a_0 + kx$ and k denotes the dimensional non-uniformity parameter of the channel.

The flow geometry and the transformation from laboratory frame to wave frame is considered along with the necessary geometric conditions and the non-dimensional parameters, accordingly as mentioned in Chapter-2.

Introducing the non dimensional quantities, the governing equations of motion are reduced to:

$$h(x) = 1 + kx + \phi\, sin\, 2\pi x \tag{5.2}$$

$$\frac{\partial}{\partial y}(\tau_{yx}) = -\frac{\partial p}{\partial x}, \tag{5.3}$$

$$where\ \tau_{yx} = \left(-\frac{\partial u}{\partial y}\right)^n + \tau_0. \tag{5.4}$$

$$\frac{\partial^2 \omega}{\partial y^2} = Br\left[\tau_{yx}\left(-\frac{\partial u}{\partial y}\right)\right], \tag{5.5}$$

where, $Br = E_c P_r$, is the Brinkman number.

Further, the boundary conditions are:

$$\psi = 0\ \ when\ \ y = 0. \tag{5.6}$$

$$\psi_{yy} = 0\ \ when\ \ y = 0. \tag{5.7}$$

$$\tau_{yx} = 0\ \ when\ \ y = 0. \tag{5.8}$$

$$u = -\frac{\sqrt{Da}}{\alpha}\frac{\partial u}{\partial y} - 1\ \ \ when\ y = h(x) - \epsilon. \tag{5.9}$$

$$\frac{\partial \omega}{\partial y} = 0\ \ when\ y = 0. \tag{5.10}$$

$$\omega = 0 \ when \ y = h(x) - \epsilon, \tag{5.11}$$

where u, $\alpha, Da, \epsilon, \tau, \psi$ are the parameters with their usual meanings as already discussed in Chapter-2 and ω denotes the temperature profile.

5.3 Solution of the problem:

Resolving equation (5.3) and equation (5.4), together with the conditions (5.6) – (5.9), the velocity u is obtained as,

$$u = P^m \left[\frac{1}{m+1}\{(h-\epsilon-y_o)^{m+1} - (y-y_o)^{m+1}\} + \frac{\sqrt{Da}}{\alpha}(h-\epsilon-y_o)^m\right] - 1, \tag{5.12}$$

where,

$$P = -\frac{\partial p}{\partial x} \ \ and \ \ m = \frac{1}{n}. \tag{5.13}$$

In the plug flow region the velocity u_p is obtained as,

$$u_p = P^m(h-\epsilon-y_o)^m\left(\frac{h-\epsilon-y_o}{1+m} + \frac{\sqrt{Da}}{\alpha}\right) - 1. \tag{5.14}$$

At each cross section the volume flow rate q is,

$q = \int_0^{y_0} u_p dy + \int_{y_0}^{h-\epsilon} u \, dy$, this gives,

$$q = P^m\left[\frac{(h-\epsilon-y_0)^{m+1}}{m+1}\left\{h-\epsilon-\frac{(h-\epsilon-y_0)}{m+2}\right\} + (h-\epsilon-y_0)^m\frac{\sqrt{Da}}{\alpha}(h-\epsilon)\right] - (h-\epsilon). \tag{5.15}$$

From equation (5.16) we get,

$$P = -\frac{\partial p}{\partial x} = \left[\frac{(q+h-\epsilon)(m+1)(m+2)\alpha}{(h-\epsilon)^{m+1}(1-\tau)^m\{\alpha(h-\epsilon)(1-\tau)\{(m+2)-(1-\tau)\} + \sqrt{Da}(m+1)(m+2)\}}\right]^{\frac{1}{m}}. \tag{5.16}$$

The volume flow rate $Q(X,t)$ and the time-averaged volume flow rate $\bar{Q}$ are calculated using the formulas mentioned in the previous chapter, given in equation no (2.16) and (2.17) respectively.

Using equation (5.12),

$$\frac{\partial u}{\partial y} = -(Py - \tau_0)^m . \tag{5.17}$$

Substituting in equation (5.5), we get,

$$\frac{\partial^2 \omega}{\partial y^2} = E_c P_r \left[\left(-\frac{\partial u}{\partial y} \right)^{n+1} + \tau_0 \left(-\frac{\partial u}{\partial y} \right) \right]. \tag{5.18}$$

Solving equation (5.18) along with the conditions (5.10) and (5.11),

$$\omega = \frac{Br\ (Py - \tau_0)^{m+2}}{P(m+1)(m+2)(m+3)} [(Py - \tau_0)(m+1) + \tau_0(m+3)] + c_1 y + c_2, \tag{5.19}$$

where c_1 and c_2 are given by,

$c_1 = \frac{Br(-\tau_0)^{m+2}}{P(m+1)(m+2)}$ and

$$c_2 = \frac{-Br\ [P(h-\epsilon) - \tau_0]^{m+2}}{P(m+1)(m+2)(m+3)} [P(h-\epsilon)(m+1) + 2\tau_0] - c_1(h-\epsilon).$$

The coefficient of heat transfer is given by $z = h_x \omega_y$, which gives z as a function of x,

$$z = \frac{Br(k + 2\pi\phi\ cos\ 2\pi x)}{P(m+1)(m+2)} [(Py - \tau_0)^{m+1}(Py(m+1) + \tau_0) + (-\tau_0)^{m+2}]. \tag{5.20}$$

Also, the Nusselt number Nu which measures the rate of the heat transfer is given by

$$Nu = -\omega_y \ at\ y = h - \epsilon. \tag{5.21}$$

Measure of the effectiveness of a machine in transforming the input energy and power into an output force and movement is called the Mechanical efficiency.

Mathematically, the Mechanical efficiency is obtained by the relation:

$$E = \frac{\bar{Q}\Delta p}{\emptyset I}, \tag{5.22}$$

where, $I = \int_0^1 \frac{\partial p}{\partial x} sin(2\pi x)\, dx$

5.4 Results and discussion:

5.4.1 Temperature profile:

From equation (5.19), the graphs of the temperature profile ω against the radial coordinate y are plotted by means of Mathematica software and are displayed in Figs.5.2–5.6. Effects of the parameters involved, Darcy number Da, amplitude ratio ϕ, porous thickening ϵ, Brinkman number Br and yield stress τ are analyzed for: $n = 3;\ k = 0.02;\ a = 1;\ \phi = 0.1;\ \bar{Q} = 0.3;\ \epsilon = 0.6;\ \tau = 0.1;\ \alpha = 0.3; Da = 0.3; z = 0.5;\ Br = 2.$

Figure 5.2 notices that rise in the Darcy number Da reduce the temperature. As the porous thickening ϵ increases, the temperature ω also increases as shown in Fig. 5.3. Fig. 5.4. reveals that temperature is an increasing function of Brinkman number Br. With rise in the values of Brinkman number, there corresponds a strong viscous dissipation effect resulting in temperature rise. The results of Ramesh and Devakar [60], Hayat et al. [106], Hina et al. [107] and Lakshminarayana et al. [108] are also in accordance with the same result. The effect of variation in τ is revealed from Fig. 5.5. It depicts that enhancing the value of τ, the yield stress threshold causes more deformation, since the molecules are put together and hence the temperature profile increases gradually. This result is in agreement with Akbar and Butt [82] and Lakshminarayana et al. [108]. From Fig. 5.6 it can be inferred that rise in temperature is more in a convergent channel than in a uniform and a divergent channel.

5.4.2 Heat transfer coefficient:

As a result of the peristaltic phenomenon, an oscillatory behavior of the coefficient of heat transfer is observed. Figures 5.7–5.11 elucidate the impact of various parameters on the coefficient of heat transfer *z*, figured out with the help of equation (5.20). The values taken for the parameters are: $n = 3;\ k = 0.02;\ a = 1;\ \phi = 0.1;\ \bar{Q} = 0.3;\ \epsilon = 0.3;\ \tau = 0.1;\ \alpha = 0.3;\ Da = 0.3;\ Br = 2.$

Figure 5.7 shows that, with rise in Darcy number Da, the magnitudinal value of the coefficient of heat transfer z decreases. The effect of ϕ on the heat transfer coefficient is seen in Fig. 5.8. The graph says that the absolute value of z enhances with ϕ. It is clear from Fig. 5.9 that, as the porous thickening ϵ increases the magnitudinal value of heat transfer coefficient decreases up to $x = 0.5$, further it is seen that with rise in the value of ϵ there is rise in the absolute value of z. As the value of Brinkman number increases the magnitudinal value of z also enhances as depicted in Fig. 5.10., in accordance with Hayat et al. [106], Hina et al. [107] and Kalidas [109]. Adding on the values of τ reduces the heat transfer coefficient up to $x = 0.5$ and for values of x greater than 0.5, z is not affected by varying the values of τ as shown in Fig. 5.11.

5.4.3 Rate of heat transfer:

The Nusselt number (Nu) value is to quantify of the heat transfer rate. To observe the influence of the parameters: Da, ϕ, ϵ, Br and τ on the rate of heat transfer, equation (5.21) has been evaluated numerically and the consequences are depicted through the graphs shown in Figs. 5.12–5.17. The values of the parameters under consideration are: $n = 3;\ k = 0.02;\ a = 1;\ \phi = 0.1;\ \bar{Q} = 0.3;\ \epsilon = 0.3;\ \tau = 0.1;\ \alpha = 0.3;\ Da = 0.3;\ y = 0.3;\ Br = 2.$

It is clear from the graph in Fig. 5.12 that as the Darcy number Da is increased there is decrease in the absolute value of the Nusselt number. From Figs. 5.13, 5.14 and 5.16 it is seen that enhancing the values of amplitude ratio ϕ, Brinkmann number Br and the yield stress τ respectively, the absolute value of the rate of heat transfer Nu rises. These results are comparable with Dhananjaya et al. [110]. The results obtained for Brinkmann number and

the yield stress agree exactly with those of Lakshminarayana et al. [108]. From Fig. 5.15 we observe that the heat transfer reduces as the porous lining ϵ gets thicker. It is also inferred that the rate of heat transfer is more in a convergent channel when compared to a uniform and divergent channel from Fig. 5.17.

5.4.4 Mechanical efficiency:

Figures 5.18–5.20, display the behavior of Mechanical efficiency with the variations in the different parameters of interest, after getting the analytical solution of Mechanical efficiency as in equation (5.22), taking: $n = 3;\ k = 0.02;\ a = 1;\ \phi = 0.5;\ \epsilon = 0.3;\ \tau = 0.1;\ \alpha = 0.1;\ Da = 0.3$.

The graphs in Figs. 5.18, 5.19 and 5.20 correspondingly clarify that the Mechanical efficiency rises with the amplitude ratio ϕ and also for the porous thickening ϵ whereas the Mechanical efficiency E decreases with increases in the values of k. Thus, Fig. 5.20 shows that the efficiency is more in a convergent channel than in uniform and divergent channels. Also it is observed that the efficiency declines with the time average velocity $\bar{Q}$ for all the parameters.

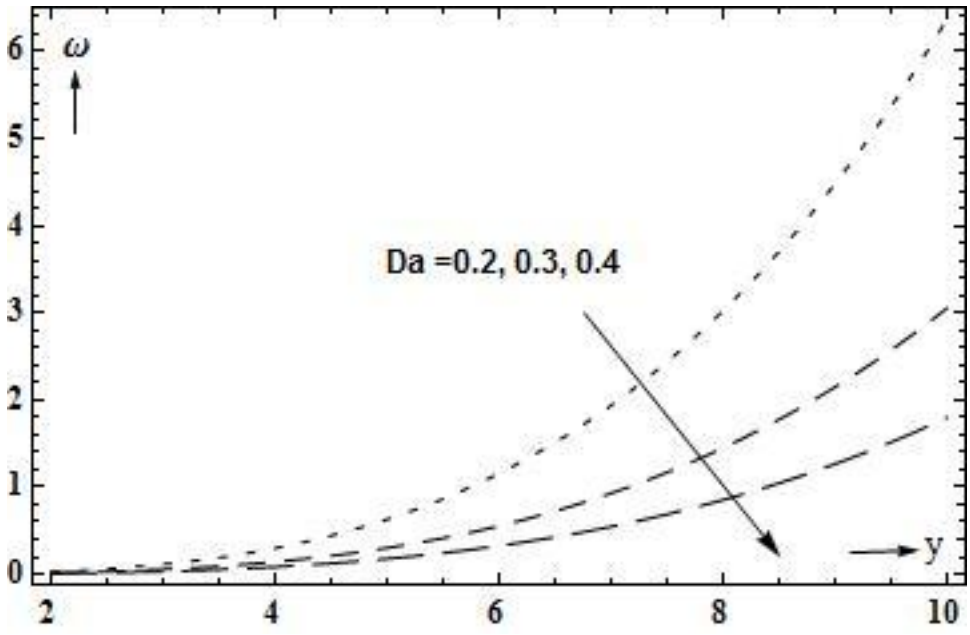

Fig. 5.2: Effect of Da on the temperature profile with:

$n = 3;\ k = 0.02;\ a = 1;\ \phi = 0.1;\ \bar{Q} = 0.3;\ \epsilon = 0.6;\ \tau = 0.1;\ \alpha = 0.3; z = 0.5;\ Br = 2$

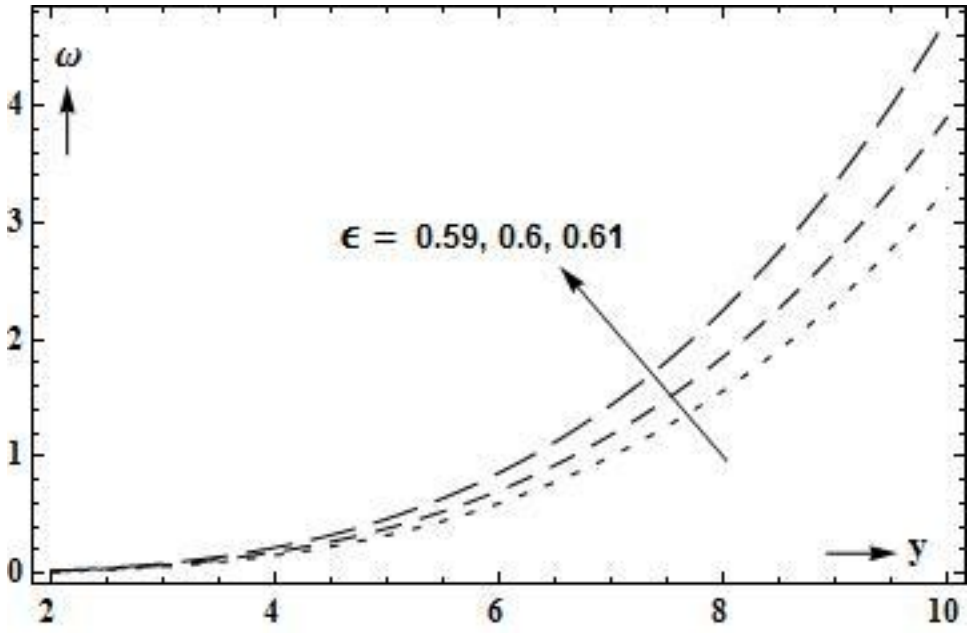

Fig. 5.3: Effect of ϵ on the temperature profile with:

$n = 3;\ k = 0.02;\ a = 1;\ \phi = 0.1;\ \bar{Q} = 0.3;\ \tau = 0.1;\ \alpha = 0.3; Da = 0.3; z = 0.5;\ Br = 2$

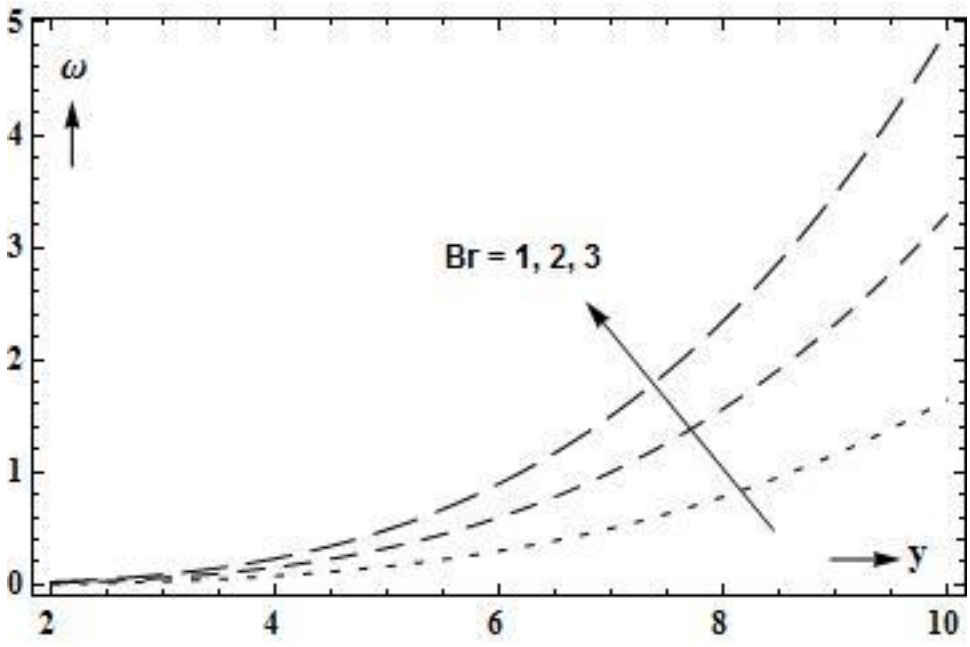

Fig. 5.4: Effect of Br on the temperature profile with:

$n = 3;\ k = 0.02;\ a = 1;\ \phi = 0.1;\ \bar{Q} = 0.3;\ \epsilon = 0.6;\ \tau = 0.1;\ \alpha = 0.3; Da = 0.3; z = 0.5$

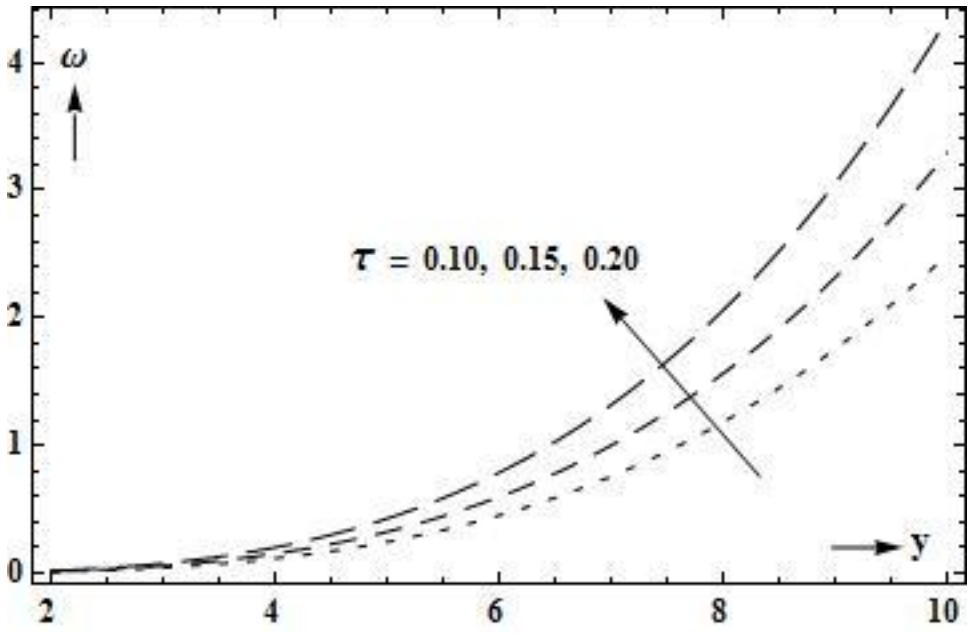

Fig. 5.5: Effect of τ on the temperature profile with:

$n = 3; k = 0.02;\ a = 1;\ \phi = 0.1;\ \bar{Q} = 0.3;\ \epsilon = 0.6;\ \alpha = 0.3; Da = 0.3; z = 0.5;\ Br = 2$

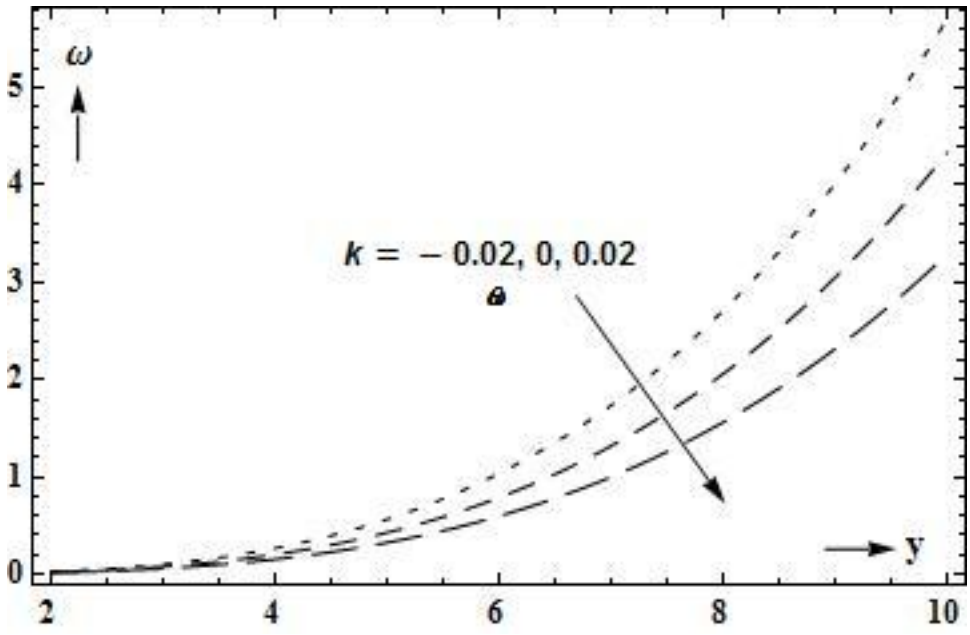

Fig. 5.6: Effect of k on the temperature profile with:

$n = 3;\ a = 1;\ \phi = 0.1;\ \bar{Q} = 0.3;\ \epsilon = 0.6;\ \tau = 0.1;\ \alpha = 0.3; Da = 0.3; z = 0.5;\ Br = 2$

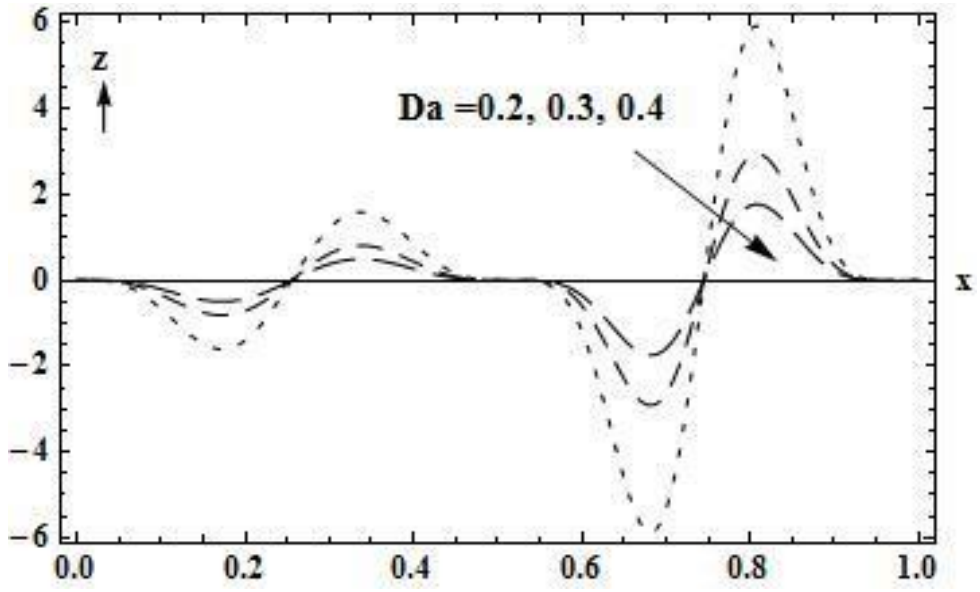

Fig. 5.7: Effect of τ on the heat transfer coefficient with:

$n = 3;\ k = 0.02;\ a = 1;\ \phi = 0.1;\ \bar{Q} = 0.3;\ \epsilon = 0.3;\ \tau = 0.1;\ \alpha = 0.3;\ Br = 2$

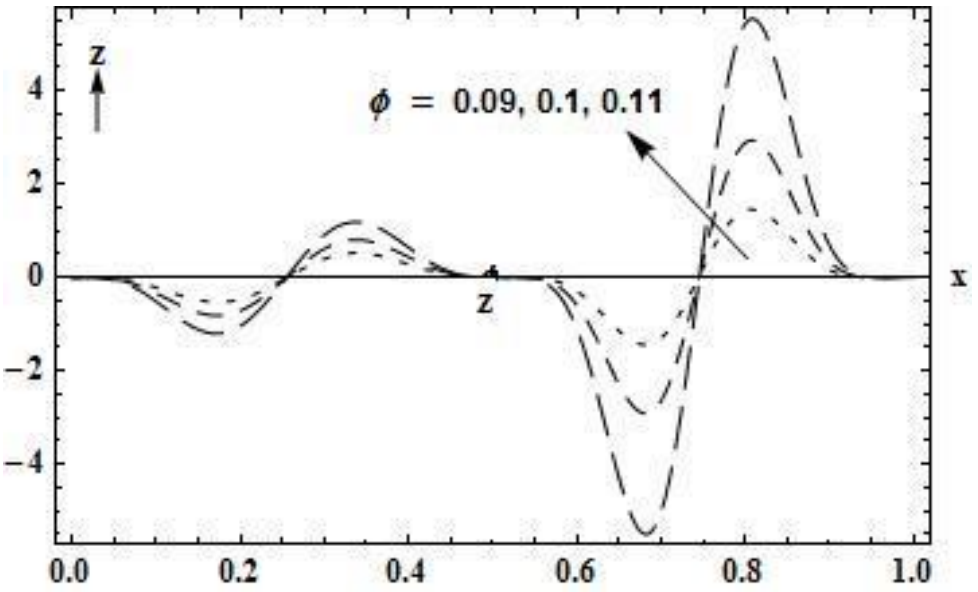

Fig. 5.8: Effect of ϕ on the heat transfer coefficient with:

$n = 3;\ k = 0.02;\ a = 1;\ \overline{Q} = 0.3;\ \epsilon = 0.3;\ \tau = 0.1;\ \alpha = 0.3;\ Da = 0.3;\ Br = 2$

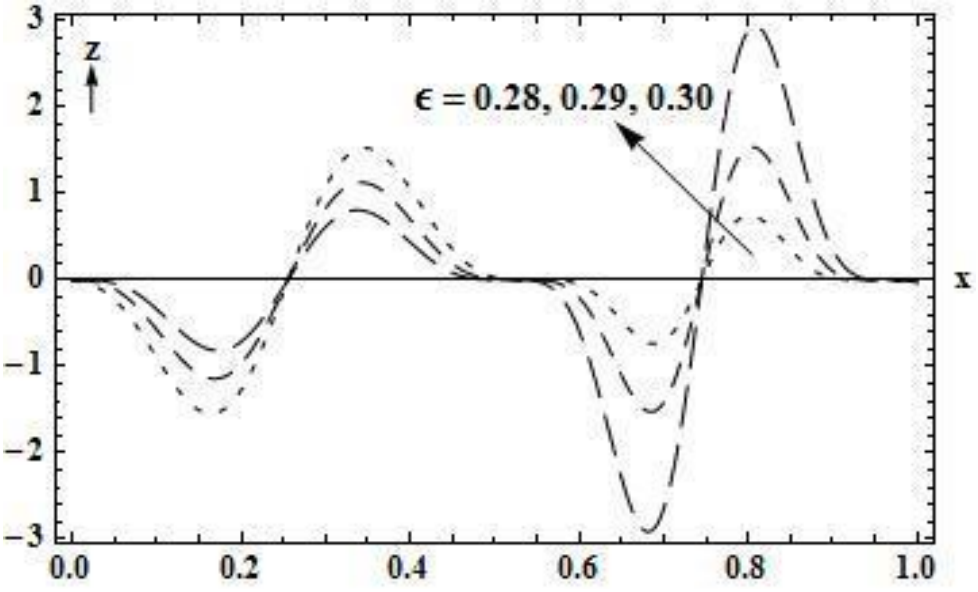

Fig. 5.9: Effect of ϵ on the heat transfer coefficient with:

$n = 3; k = 0.02;\ a = 1;\ \phi = 0.1;\ \overline{Q} = 0.3;\ \tau = 0.1;\ \alpha = 0.3;\ Da = 0.3;\ Br = 2$

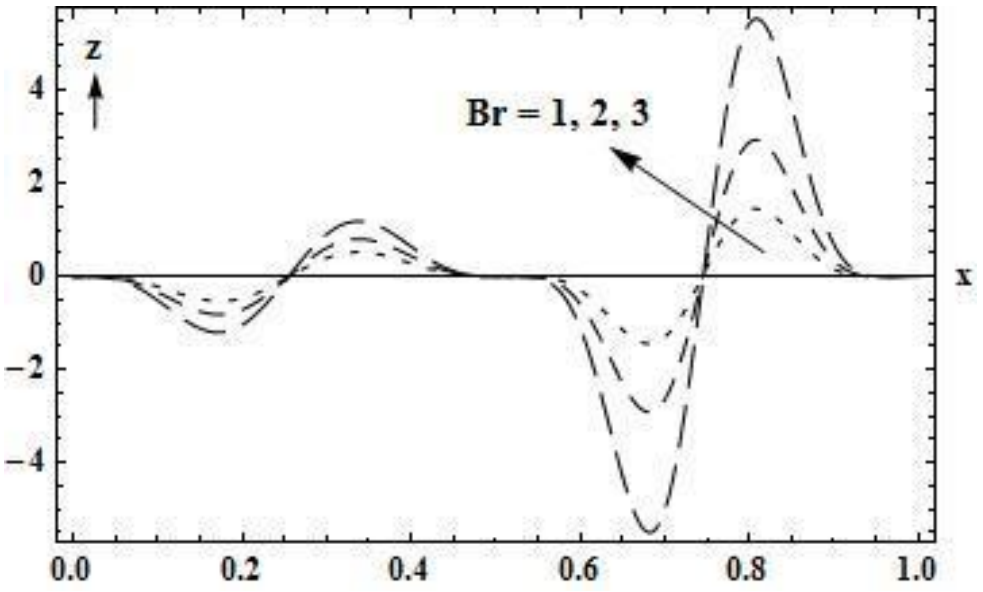

Fig. 5.10: Effect of Br on the heat transfer coefficient with:

$n = 3; k = 0.02;\ a = 1;\ \phi = 0.1;\ \bar{Q} = 0.3;\ \epsilon = 0.3;\ \tau = 0.1;\ \alpha = 0.3;\ Da = 0.3$

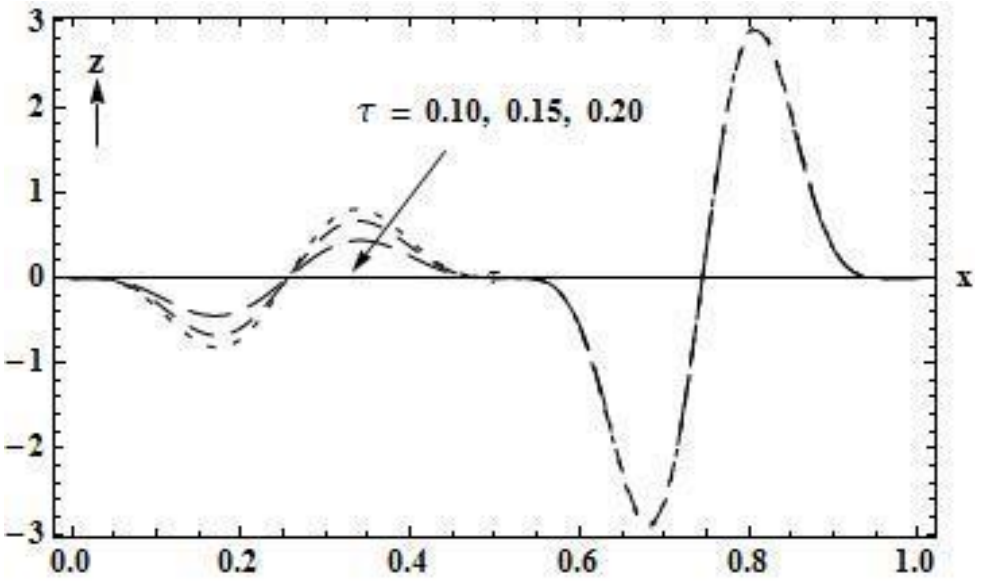

Fig. 5.11: Effect of τ on the heat transfer coefficient with:

$n = 3;\ k = 0.02;\ a = 1;\ \phi = 0.1;\ \bar{Q} = 0.3;\ \epsilon = 0.3;\ \alpha = 0.3;\ Da = 0.3;\ Br = 2$

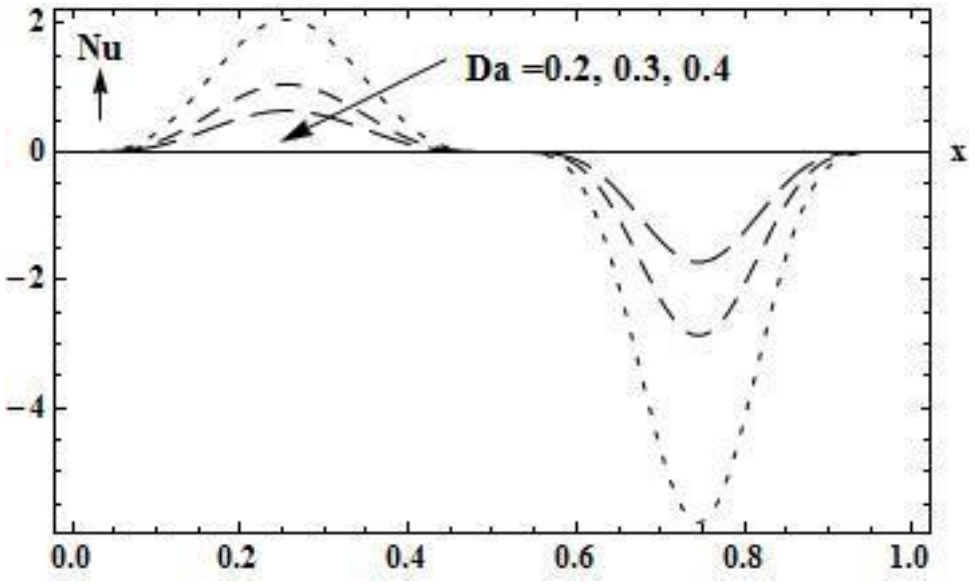

Fig. 5.12: Effect of Da on the Nusselt number with:

$n = 3;\ k = 0.02;\ a = 1;\ \phi = 0.1;\ \bar{Q} = 0.3;\ \epsilon = 0.3;\ \tau = 0.1;\ \alpha = 0.3;\ Br = 2$

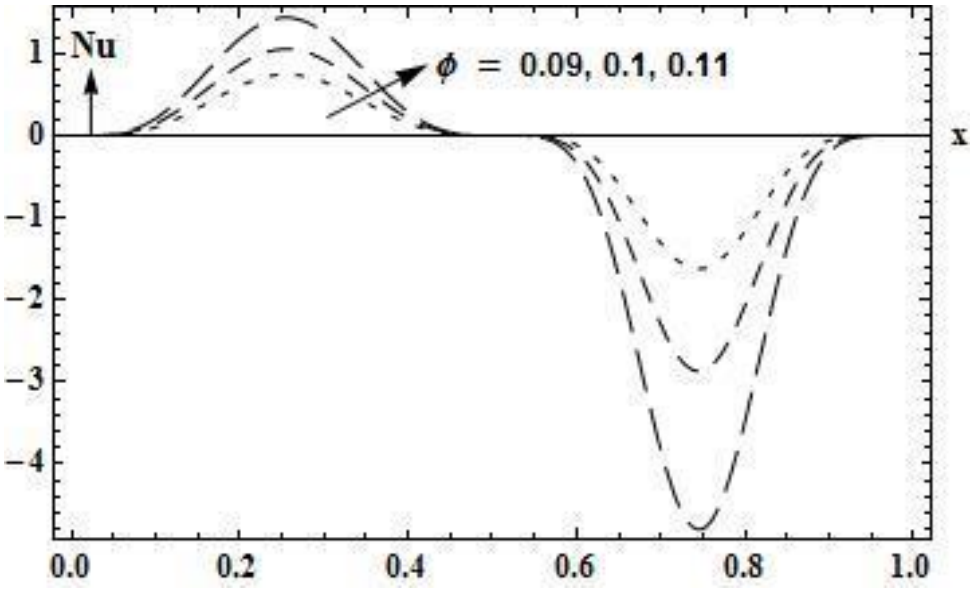

Fig. 5.13: Effect of ϕ on the Nusselt number with:

$n = 3;\ k = 0.02;\ a = 1;\ \bar{Q} = 0.3;\ \epsilon = 0.3;\ \tau = 0.1;\ \alpha = 0.3;\ Da = 0.3;\ Br = 2$

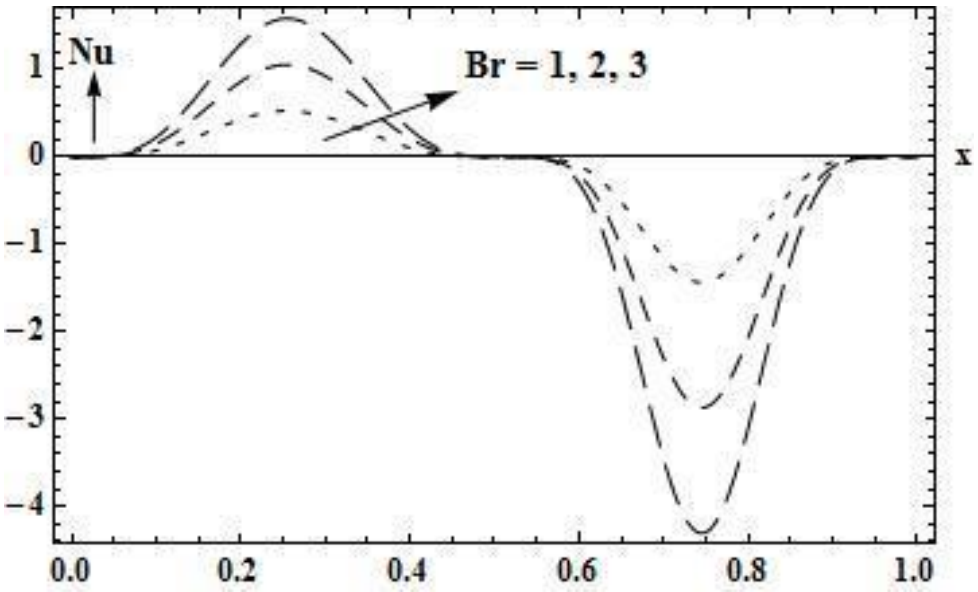

Fig. 5.14: Effect of Br on the Nusselt number with:

$n = 3;\ k = 0.02;\ a = 1;\ \phi = 0.1;\ \bar{Q} = 0.3;\ \epsilon = 0.3;\ \tau = 0.1;\ \alpha = 0.3;\ Da = 0.3;$

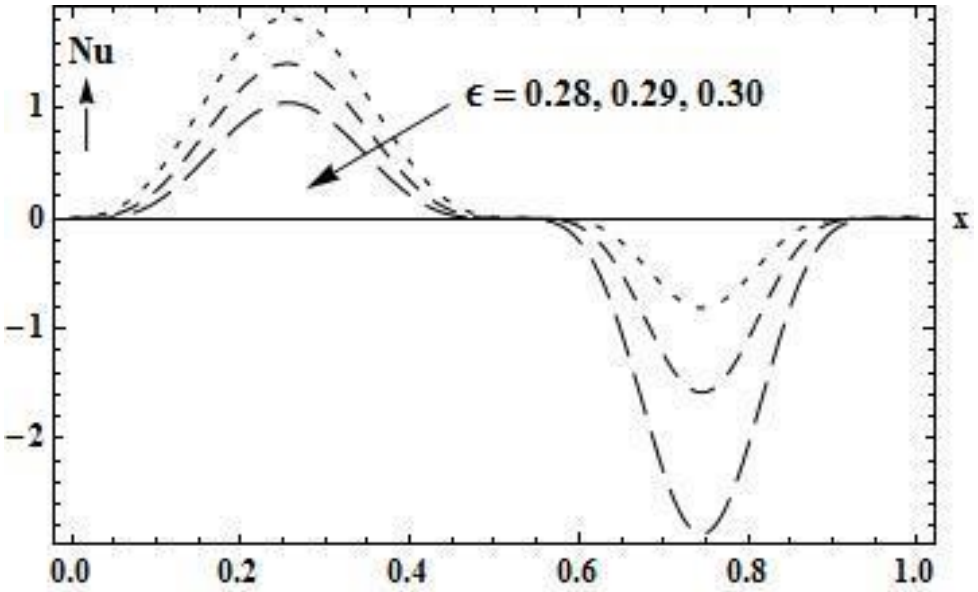

Fig. 5.15: Effect of ϵ on the Nusselt number with:

$n = 3;\ k = 0.02;\ a = 1;\ \phi = 0.1;\ \bar{Q} = 0.3;\ \tau = 0.1;\ \alpha = 0.3;\ Da = 0.3;\ Br = 2$

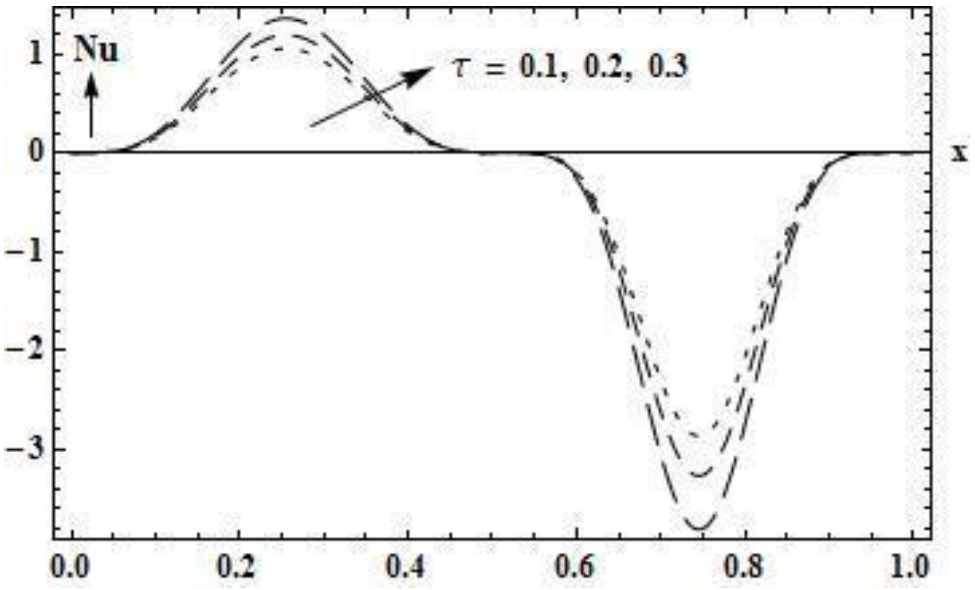

Fig. 5.16: Effect of τ on the Nusselt number with:

$n = 3;\ k = 0.02;\ a = 1;\ \phi = 0.1;\ \bar{Q} = 0.3;\ \epsilon = 0.3;\ \alpha = 0.3;\ Da = 0.3;\ Br = 2$

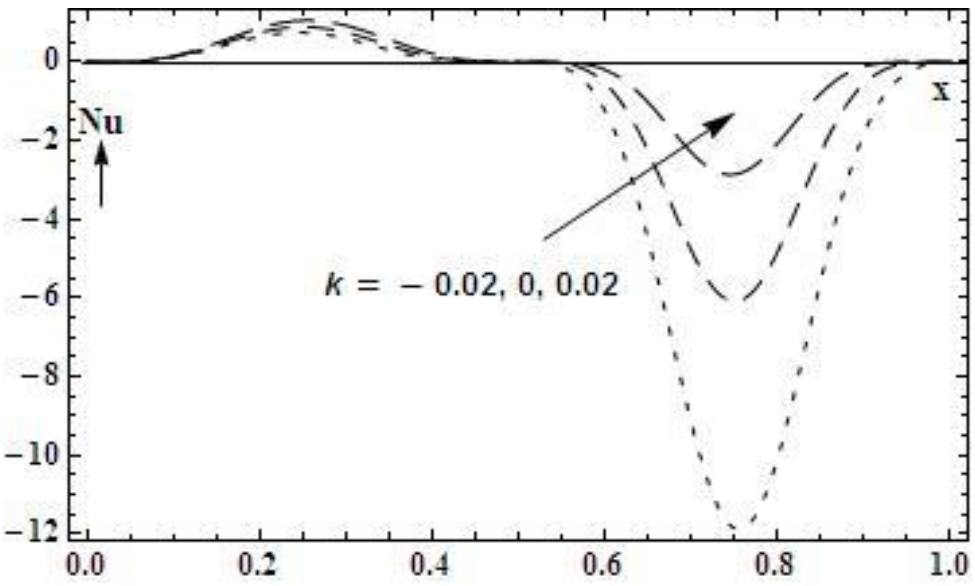

Fig. 5.17: Effect of k on the Nusselt number with:

$n = 3;\ a = 1;\ \phi = 0.1;\ \bar{Q} = 0.3;\ \epsilon = 0.3;\ \tau = 0.1;\ \alpha = 0.3;\ Da = 0.3;\ Br = 2$

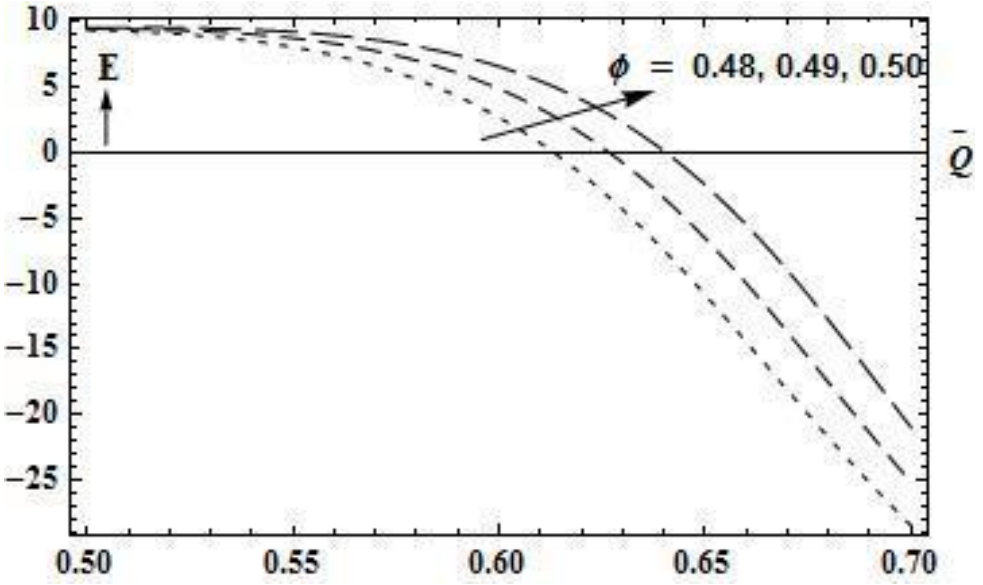

Fig. 5.18: Effect of ϕ on Mechanical efficiency with:

$n = 3$; $k = 0.02$; $a = 1$; $\epsilon = 0.3$; $\tau = 0.1$; $\alpha = 0.1$; $Da = 0.3$

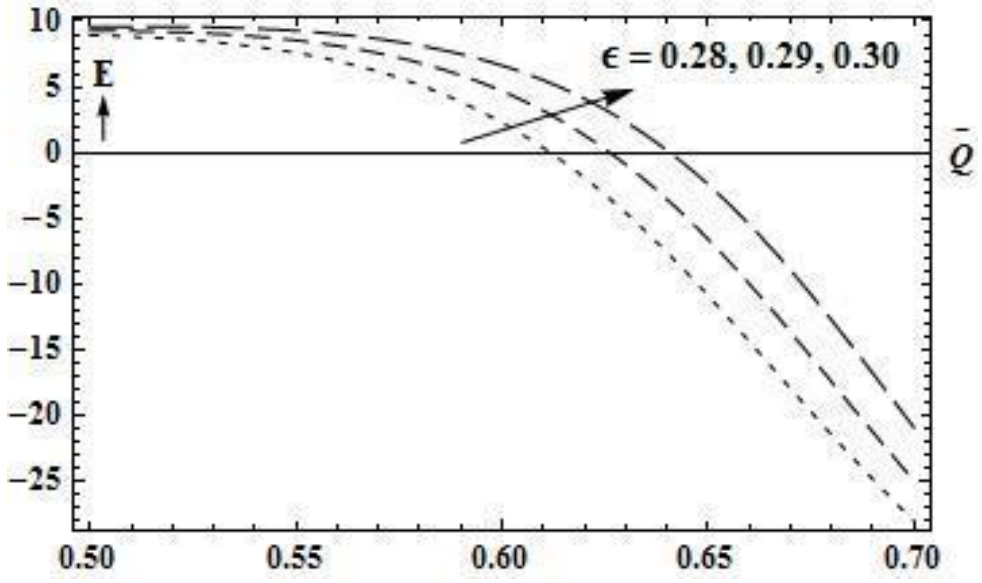

Fig. 5.19: Effect of ϵ on Mechanical efficiency with:

$n = 3$; $k = 0.02$; $a = 1$; $\phi = 0.5$; $\tau = 0.1$; $\alpha = 0.1$; $Da = 0.3$.

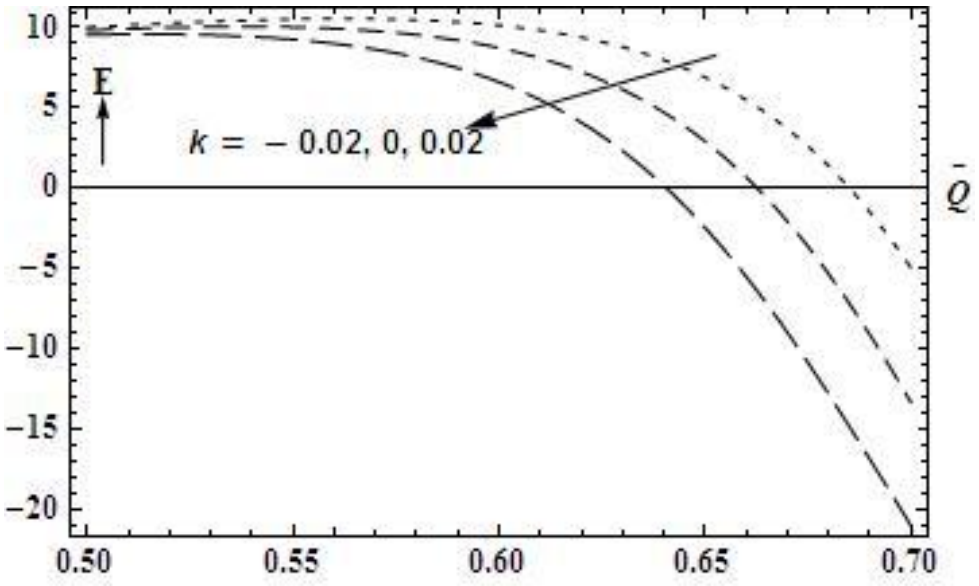

Fig. 5.20: Effect of k on Mechanical efficiency with:

$\boldsymbol{n = 3;\ a = 1;\ \phi = 0.5;\ \epsilon = 0.3;\ \tau = 0.1;\ \alpha = 0.1;\ Da = 0.3}$

CHAPTER-6

Non-Newtonian Fluid Flow in a Peristaltic Channel Lined with Porous Material under Low Intensity Magnetic Field

6.1 Introduction:

Peristaltic mechanism occurs broadly in many biological and biomedical systems that help in the transportation of fluids present in the body. The applications of this mechanism are also seen in industry.

Relating some of the problems on movement of conducting physiological fluids as in pump machinery and flow of blood in vessels, the study of peristaltic motion under magneto hydrodynamic effects is being expanded by researchers. In view of this, this chapter extends our study to explore the magneto hydro dynamic effects on the transport of Herschel Bulkley fluid through a uniform channel coated with permeable matter.

Several scholars have examined the peristalsis under the MHD effect in porous media (Dheia and Abdulhadi [105], Rathod and Laxmi [111], Hayat et al. [112]). The wall property as well as the MHD effect on the peristaltic motion under the heat transfer was explored by Kothandapani and Srinivas [113]. Hayat et al. [114], Sankad and Radhakrishnamacharya [115], Kumari and Radhakrishnamacharya [116], Nadeem and Akram [117], Mekheimer et al. [118] also have considered the magnetic field in their analysis.

Shear thickening or shear thinning fluids take in a significant role in biomedical science. As known, flows having a non linear strain stress connection, either with shear thickening or shear thinning fluids, is well elucidated by the Herschel Bulkley fluid model. After the report of Scott Blair [71] that, though blood comply with the Casson's model but it is the Herschel Bulkley fluid model that agrees more with the blood flow, a number of scholars have concentrated on the study of Herschel Bulkley fluid (Chaturani and Samy [119], Medhavi [77], Sreenadh et al. [78]. Maruthi Prasad and Radhakrishnamacharya [120]).

Considering the research work carried out, it is inferred that the transport of Herschel–Bulkley fluid under peristalsis with the low intensity magneto hydrodynamic effect has not yet been worked out. Therefore this model is solved in the current chapter under perturbation method for pressure rise and frictional force. The stream lines are also sketched to analyze the trapping phenomenon.

6.2 Mathematical formulation:

The motion of a non–Newtonian Herschel–Bulkley fluid is considered to flow in a peristaltic channel, whose walls are coated with porous material. A low intensity Magnetic field is considered vertical to the wall of the channel. The channel is supposed to have a plug flow region between $0 \leq y \leq y_0$, where $\tau_{xy} \leq \tau_0$ and $\tau_{xy} \geq \tau_0$ for $y_0 \leq y \leq H$.

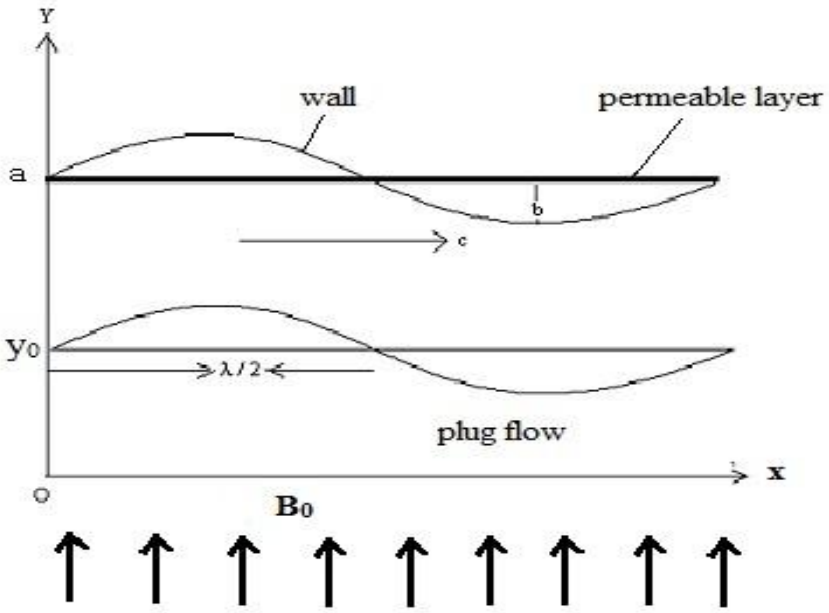

Fig. 6.1: Flow geometry

The channel wall is governed through,

$$Y = H(X,t) = a + b\, sin\frac{2\pi}{\lambda}(X - ct), \tag{6.1}$$

The flow geometry and the transformation from laboratory frame to wave frame is considered along with the necessary geometric conditions and the non-dimensional parameters, accordingly as mentioned in Chapter-2.

The governing equations after removing primes are as follows:

$$h(x) = 1 + \phi\, sin\, 2\pi x\,. \tag{6.2}$$

$$\frac{\partial}{\partial y}(\tau_{yx}) = -\frac{\partial p}{\partial x} - Mu, \quad where\ \tau_{yx} = \left(-\frac{\partial u}{\partial y}\right)^n + \tau_0. \tag{6.3}$$

and the dimensionless peripheral conditions are

$$at\ \ y = 0 :\ \ \psi = 0, \tag{6.4}$$

$$at\ \ y = 0\ ;\ \psi_{yy} = 0. \tag{6.5}$$

$$at\ \ y = 0\ ;\ \tau_{yx} = 0. \tag{6.6}$$

$$at\ \ y = h(x) - \epsilon\ ;\ u_0 = \psi_{0y} = -\frac{\sqrt{Da}}{\alpha}\frac{\partial u}{\partial y} - 1. \tag{6.7}$$

$$at\ \ y = h(x) - \epsilon\ ;\ u_1 = \psi_{1y} = 0\ . \tag{6.8}$$

$$at\ \ y = 0\ ;\ u_{0y} = u_{1y} = 0. \tag{6.9}$$

where u, α, Da, ϵ, τ, ψ are the parameters with their usual meanings as already discussed in Chapter-2.

6.3 Solution of the problem:

The perturbation solution in Magnetic parameter M is opted for the solution

$$u = u_0 + M\,u_1 + \cdots \ldots\ldots \tag{6.10}$$

$$\frac{\partial \mathrm{p}}{\partial \mathrm{x}} = \frac{\partial \mathrm{p}_0}{\partial \mathrm{x}} + \mathrm{M}\frac{\partial \mathrm{p}_1}{\partial \mathrm{x}} \ldots\ldots\ldots\ldots \tag{6.11}$$

$$\psi = \psi_0 + M\psi_1 + \cdots \ldots\ldots\ldots \tag{6.12}$$

Using (6.3) and (6.10) and collecting the various powers of M we get,

the zeroth order equation: $\frac{\partial}{\partial y}\left(\left(-\frac{\partial u}{\partial y}\right)^n + \tau_0\right) = -\frac{\partial p_0}{\partial x} = P_0,$ (6.13)

and the first order equation: $\frac{\partial}{\partial y}\left(n\left(-\frac{\partial u_1}{\partial y}\right)^n + \left(-\frac{\partial u_1}{\partial y}\right)\right) = -\frac{\partial p_1}{\partial x} - u_0 = P_1 - u_0.$ (6.14)

6.3.1 Zeroth order solution:

On solving equation (6.13) along with $u = \frac{\partial \psi}{\partial y}$ and $v = -\frac{\partial \psi}{\partial x}$, and the relevant boundary conditions, we obtain the velocity field as

$$u_0 = {P_0}^m \left[H^m T_1 - \frac{(y - y_o)^{m+1}}{m+1} \right] - 1, \tag{6.15}$$

where $H = h - \epsilon - y_o$ and $T_1 = \left(\frac{\sqrt{Da}}{\alpha} + \frac{H}{m+1} \right)$.

Velocity in the plug flow region is obtained by the substitution $y = y_0$ in (6.15), as:

$$u_{P_0} = {P_0}^m H^m T_1 - 1 . \tag{6.16}$$

Integrating equations (6.15) and (6.16) and using $at\ y = 0$, $\psi_p = 0$ and at $y = y_o$, $\psi = \psi_p$, we get the stream functions as:

$$\psi_0 = {P_0}^m \left[H^m T_1 y - \frac{(y - y_o)^{m+2}}{(m+1)(m+2)} \right] - y . \tag{6.17}$$

$$\psi_{P_0} = \int u_{P_0} dy = {P_0}^m H^m T_1 y - y . \tag{6.18}$$

The volume flow rate q_0 is then given by,

$$q_0 = \int_0^{y_0} u_{P_0} dy + \int_{y_0}^{h-\epsilon} u_0 \, dy ,$$

and therefore we obtain,

$$q_0 = {P_0}^m H^m \left[T_1 (h - \epsilon) - \frac{H^2}{(m+1)(m+2)} \right] - (h - \epsilon). \tag{6.19}$$

From equation (6.19) we get,

$$P_0 = -\frac{\partial p_0}{\partial x} = \left[\frac{(q + h - \epsilon)(m+1)(m+2)}{H^m \left\{ \frac{\sqrt{Da}}{\alpha} (m+1)(m+2)(h-\epsilon) + H(h-\epsilon)(m+1) + H y_o \right\}} \right]^{\frac{1}{m}} \tag{6.20}$$

6.3.2 First order solution:

For first order solution, considering equation (6.14) and the appropriate boundary conditions, we obtain the velocity field as,

$$u_1 = \frac{AP_0{}^{m-1}}{(m+1)}(T_2 - H^m T_3) + (T_4 - T_5). \tag{6.21}$$

where

$A = -P_1 + P_0{}^m H^m T_1 - 1$; $T_2 = (y - y_0)^m (my + y_0)$; $T_3 = m(h - \epsilon) + y_0$;

$T_4 = \frac{mP_0{}^{2m-1}}{(m+1)(m+2)(2m+2)}$; $T_5 = H^{2m+2} - (y - y_0)^{2m+2}$;

Velocity in the plug flow region is

$$u_{P_1} = \frac{AP_0{}^{m-1}}{(m+1)}(-H^m T_3) + T_4 H^{2m+2}. \tag{6.22}$$

The volume flow rate q_1 is given by,

$q_1 = \int_0^{y_0} u_{P_1} dy + \int_{y_0}^{h-\epsilon} u_1 \, dy$ and it yields,

$$q_1 = \frac{-AP_0{}^{m-1}H^m}{(m+1)^2}\left\{T_3{}^2 + \frac{mH^2}{(m+2)}\right\} + \frac{T_4 H^{2m+2}}{(2m+3)}\{(2m+2)(h-\epsilon) + y_0\}. \tag{6.23}$$

Equations (6.21) and (6.22) are respectively integrated to obtain the stream functions as,

$$\psi_1 = \frac{AP_0{}^{m-1}}{(m+1)}\left\{\frac{(y-y_o)^{m+1}(my+2y_0)}{(m+2)} - H^m T_3 y\right\} + T_4\left\{H^{2m+2}\, y - \frac{(y-y_o)^{2m+3}}{2m+3}\right\} \tag{6.24}$$

$$\psi_{p_1} = \frac{AP_0{}^{m-1}}{(m+1)}(-H^m T_3 y) + T_4\,(H^{2m+2}\, y). \tag{6.25}$$

The volume flow rate $Q(X,t)$ and the time-averaged volume flow rate $\bar{Q}$ are calculated using the formulas mentioned in previous chapter, given in equation no (2.16) and (2.17) respectively.

Integrating equation (6.11) w. r. t 'x' over one wavelength, we obtain the pressure rise as:

$$\Delta P = \int_0^1 \frac{\partial p}{\partial x}\, dx = -\int_0^1 (P_0 + MP_1) dx\,. \tag{6.26}$$

The Frictional force F at the wall is:

$$F = \int_0^1 h\left(-\frac{\partial p}{\partial x}\right) dx. \tag{6.27}$$

6.4. Results and discussion:

From equation (6.10), the pertinent parameters are varied to study their effects on the axial velocity through the graphical representations as shown in Figs. 6.2 to 6.5. The values of the parameters under consideration are: $n = 3;\ Da = 0.1;\ \alpha = 1;\ \tau = 0.1;\ \epsilon = 0.3;\ \phi = 0.1;\ z = 0.1;\ \bar{Q} = 0.1;\ M = 0.2;$

It is inferred from Fig. 6.2 that the Darcy number Da has little effect on the axial velocity. Strengthening the magnetic field M reduces the axial velocity upto $y = 0.75$ and further we observe increase in the velocity with M, as observed from Fig. 6.3. From Fig. 6.4 it can be said that thickening the porous lining of the wall ϵ increases the axial velocity. The yield stress τ has an oscillating behavior on the velocity with hardly any effect. Fig. 6.5 exposes that rise in the yield stress τ slightly increases the axial velocity upto $y = 0.75$ and further there is slight decrease in the velocity.

Using equation (6.26), the pumping action is analyzed through the graphs plotted with the help of Mathematica software, taking: $n = 3;\ Da = 0.1;\ \alpha = 1;\ \tau = 0.8;\ \epsilon = 0.8;\ \phi = 0.1;\ z = 0.1;\ M = 0.2.$

Figures 6.6 and 6.7 reveal that rise in the values of Darcy number Da and magnetic parameter M, increases the pumping. This infers that application of strong magnetic field to the flow field necessitates high pressure gradient to pass the flow, thus suggests that fluid pressure can be controlled by the application of suitable magnetic field strength. This phenomenon is helpful during surgery and critical operation to attenuate of loss of blood. From Fig. 6.8 and Fig. 6.9 it is clear that there is pressure drop for rise in the porous

thickening ϵ and yield stress τ. But the effect of ϵ is very much less on the pressure drop and is also oscillating in nature.

The impact of variation in the values of parameters of interest on the Frictional force against the time average velocity $\bar{Q}$ with: $n = 3;\ Da = 0.1;\ \alpha = 1;\ \tau = 0.8;\ \epsilon = 0.8;\ \phi = 0.1;\ z = 0.1;\ M = 0.2$, can be seen from the Fig. 6.10 – Fig. 6.13.

The frictional force declines with rise in the Darcy number Da as well the magnetic parameter M as observed in Fig. 6.10 and Fig. 6.11, where as there is enhancement in the Frictional force with increase in the porous thickening ϵ and the yield stress τ as depicted in Fig. 6.12 and Fig. 6.13. Again it is noted that the impact of ϵ on the Frictional force is very slight.

Also we see that pressure rise behaves exactly the opposite to that of Frictional force, when plotted against $\bar{Q}$.

The inside circulation of the stream lines form the bolus of the fluid, called trapping. The peristaltic wave drags this trapped bolus along with it. Stream lines are plotted to visualize the trapping phenomenon for the parameters of interest taking: $n = 3;\ Da = 0.1;\ \alpha = 1;\ \tau = 0.8;\ \epsilon = 0.8;\ \bar{Q} = 0.1;\ \phi = 0.1;\ M = 0.04$.

From Fig. 6.14 it is inferred that enhancing the Darcy number increases the bolus volume. Intensifying the magnetic field shrinks the bolus and is shown in Fig. 6.15. The results of Kalidas [109] also infer that bolus size decreases with increase in M. Increasing the porous thickening ϵ increases the size of the bolus as plotted in Fig. 6.16. This depicts the fact that trapping is supplemented in the non porous region. Again for more yield stress τ the bolus gains volume and is revealed from Fig. 6.17.

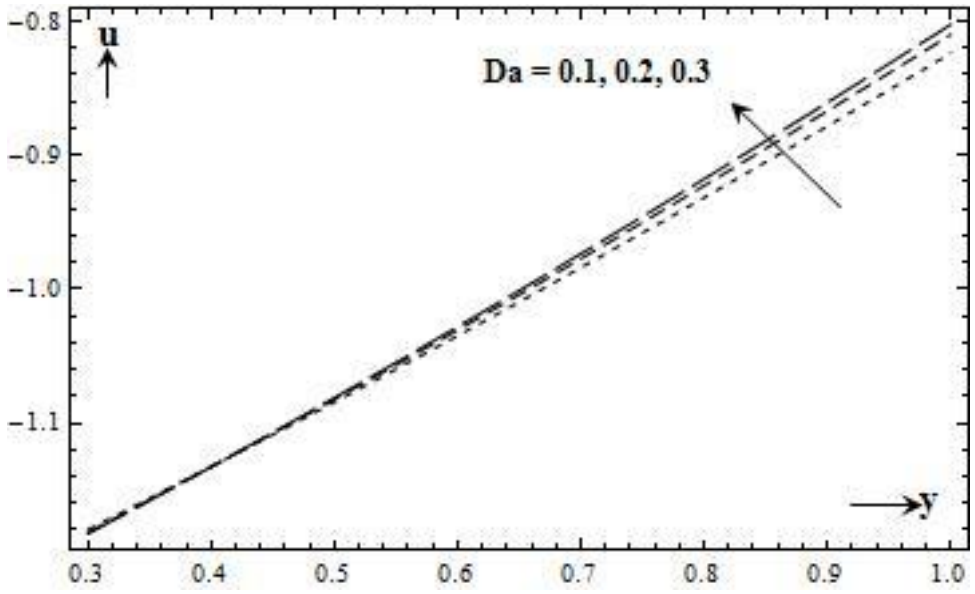

Fig. 6.2: Effect of Da on the axial velocity with :

$$n = 3;\ \alpha = 1;\ \tau = 0.1;\ \epsilon = 0.3;\ \phi = 0.1;\ z = 0.1;\ \bar{Q} = 0.1;\ M = 0.2$$

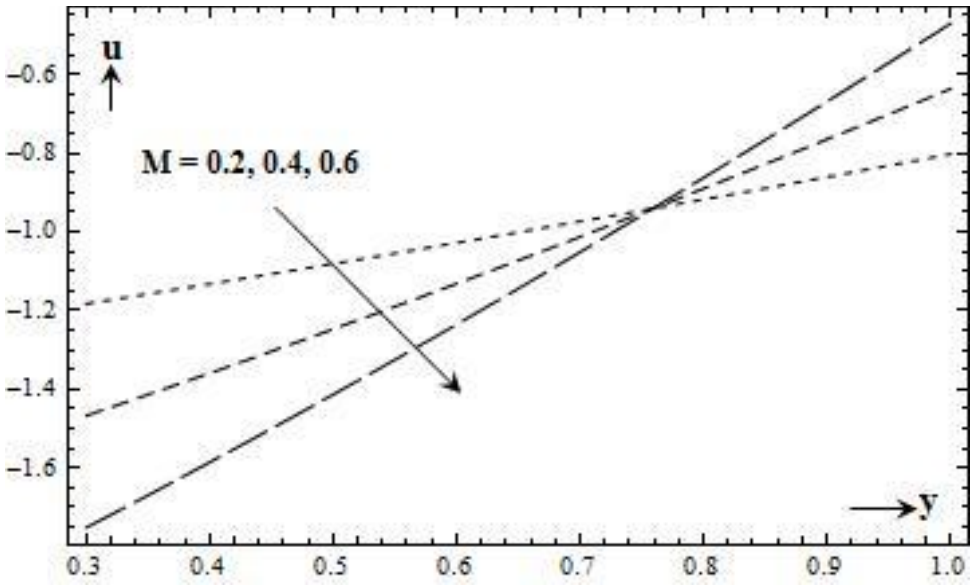

Fig. 6.3: Effect of M on the axial velocity with:

$$n = 3;\ Da = 0.1;\ \alpha = 1;\ \tau = 0.1;\ \epsilon = 0.3;\ \phi = 0.1;\ z = 0.1;\ \bar{Q} = 0.1$$

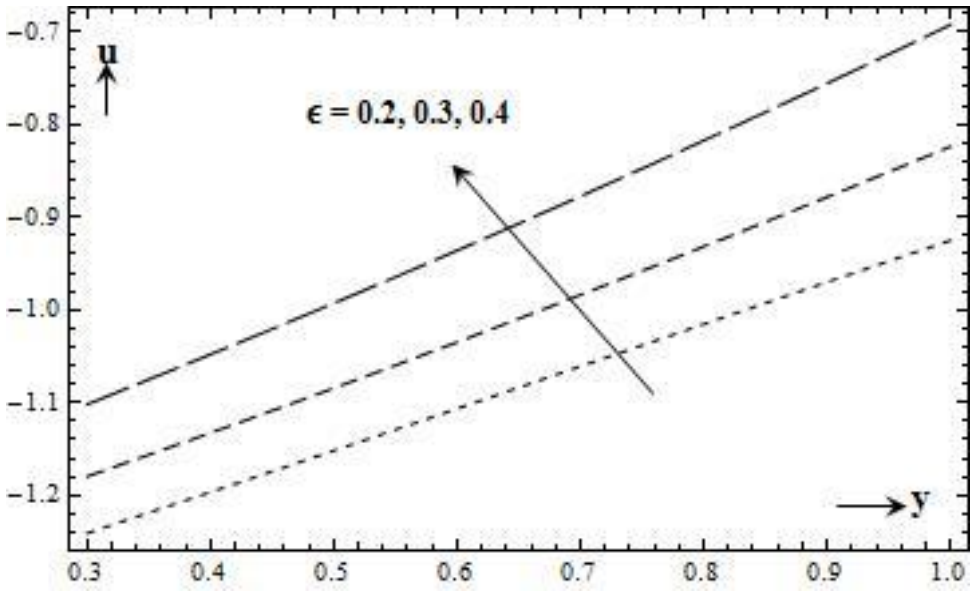

Fig. 6.4: Effect of ϵ on the axial velocity with:

$$n = 3;\ Da = 0.1;\ \alpha = 1;\ \tau = 0.1;\ \phi = 0.1;\ z = 0.1;\ \bar{Q} = 0.1;\ M = 0.2$$

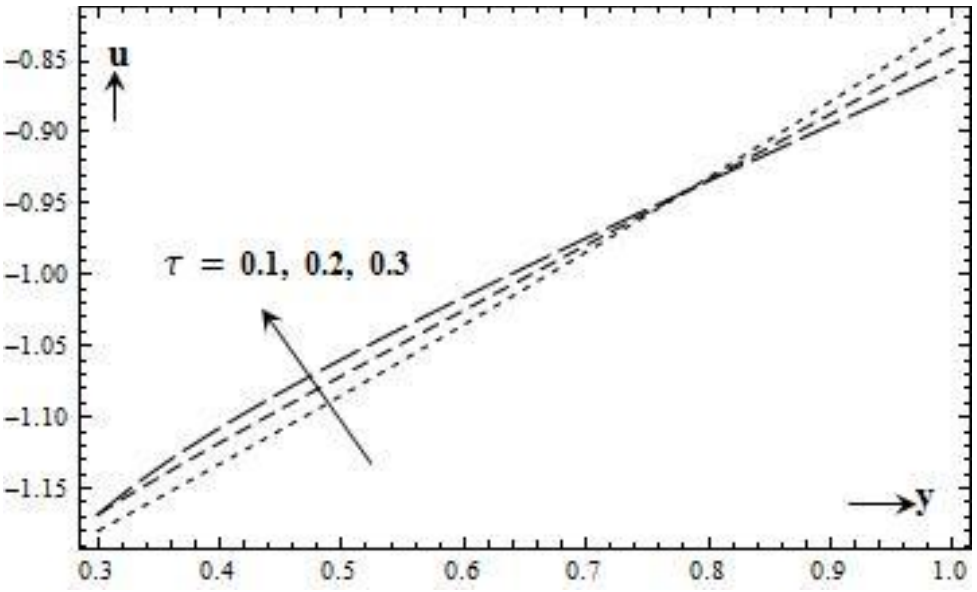

Fig. 6.5: Effect of τ on the axial velocity with:

$$n = 3;\ Da = 0.1;\ \alpha = 1;\ \epsilon = 0.3;\ \phi = 0.1;\ z = 0.1;\ \bar{Q} = 0.1;\ M = 0.2$$

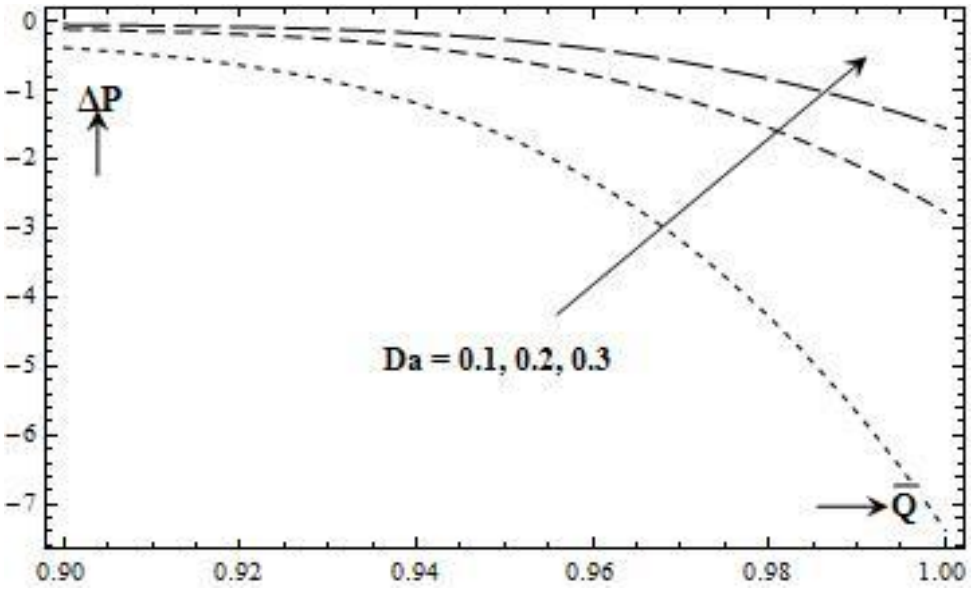

Fig. 6.6: Effect of Da on ΔP against $\bar{Q}$ with:

$n = 3;\ \alpha = 1;\ \tau = 0.8;\ \epsilon = 0.8;\ \phi = 0.1;\ z = 0.1;\ M = 0.2$

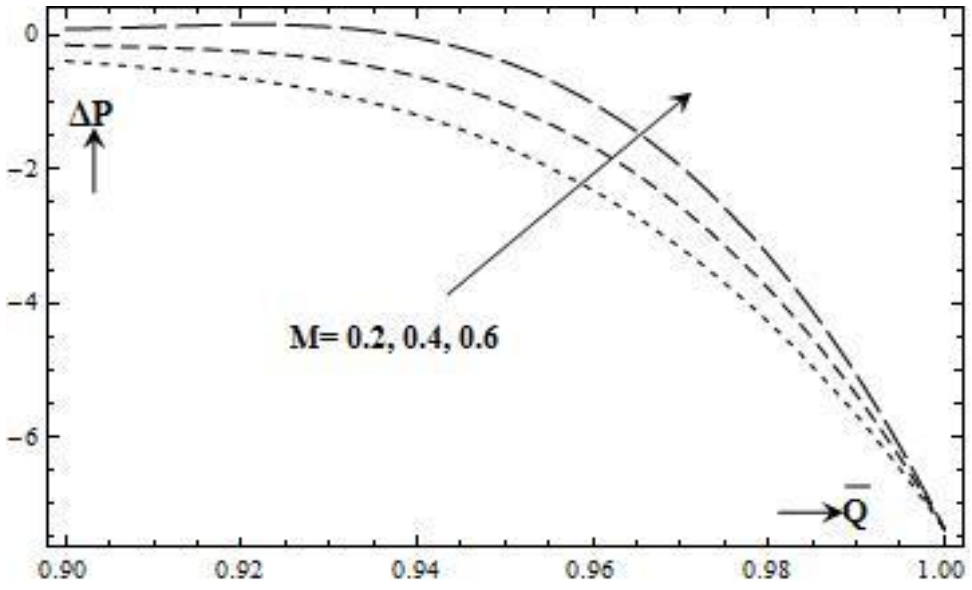

Fig. 6.7: Effect of M on ΔP against $\bar{Q}$ with:

$n = 3;\ Da = 0.1;\ \alpha = 1;\ \tau = 0.8;\ \epsilon = 0.8;\ \phi = 0.1;\ z = 0.1$

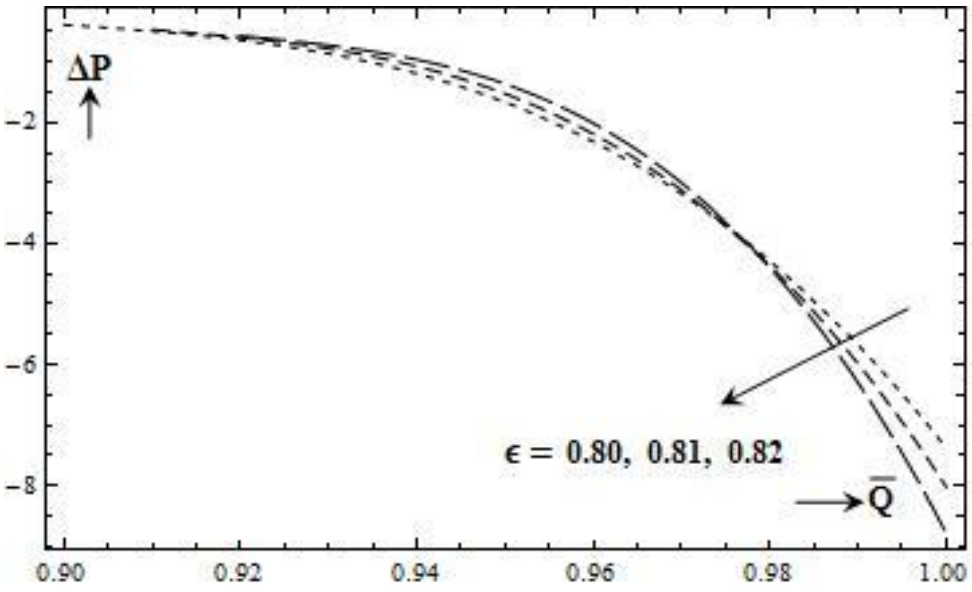

Fig. 6.8: Effect of ϵ on ΔP against $\overline{Q}$ with:

$n = 3;\ Da = 0.1;\ \alpha = 1;\ \tau = 0.8;\ \phi = 0.1;\ z = 0.1;\ M = 0.2$

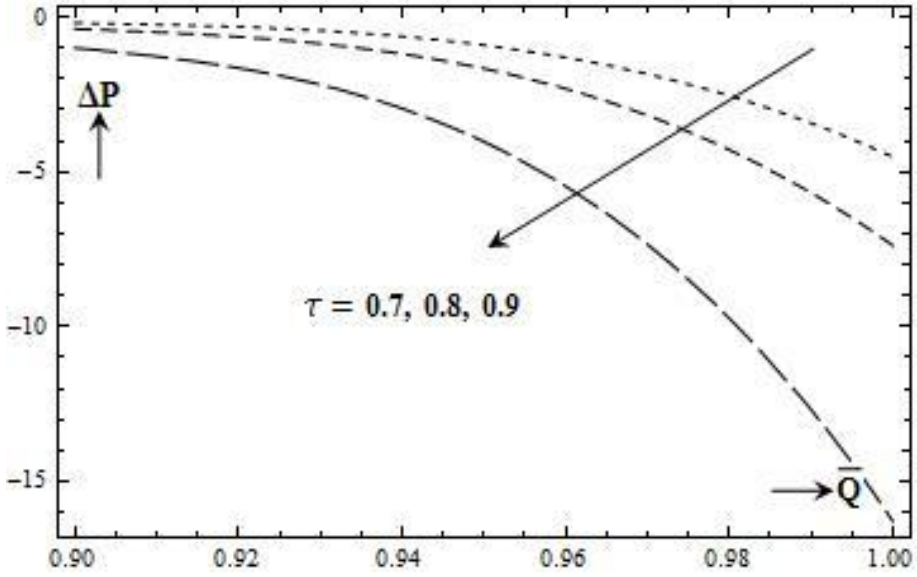

Fig. 6.9: Effect of τ on ΔP against $\overline{Q}$ with:

$n = 3;\ Da = 0.1;\ \alpha = 1;\ \epsilon = 0.8;\ \phi = 0.1;\ z = 0.1;\ M = 0.2$

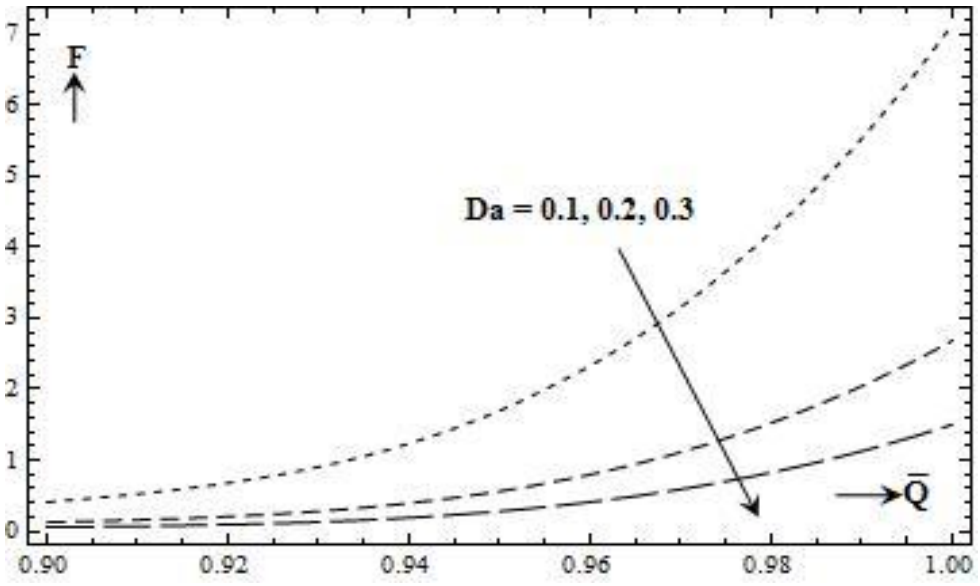

Fig. 6.10: Effect of Da on F against $\bar{Q}$ with:

$$n = 3;\ \alpha = 1;\ \tau = 0.8;\ \epsilon = 0.8;\ \phi = 0.1;\ z = 0.1;\ M = 0.2$$

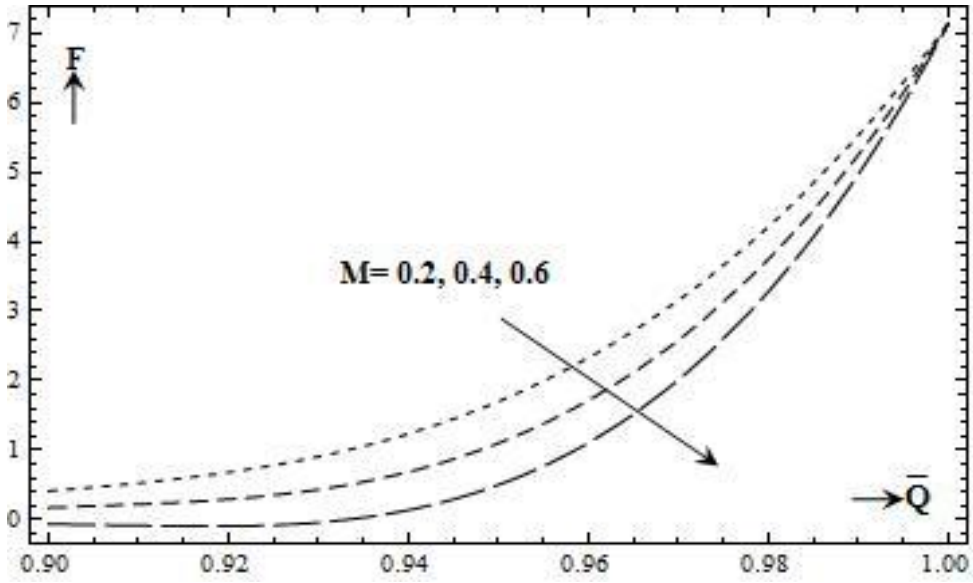

Fig. 6.11: Effect of M on F against $\bar{Q}$ with:

$$n = 3;\ Da = 0.1;\ \alpha = 1;\ \tau = 0.8;\ \epsilon = 0.8;\ \phi = 0.1;\ z = 0$$

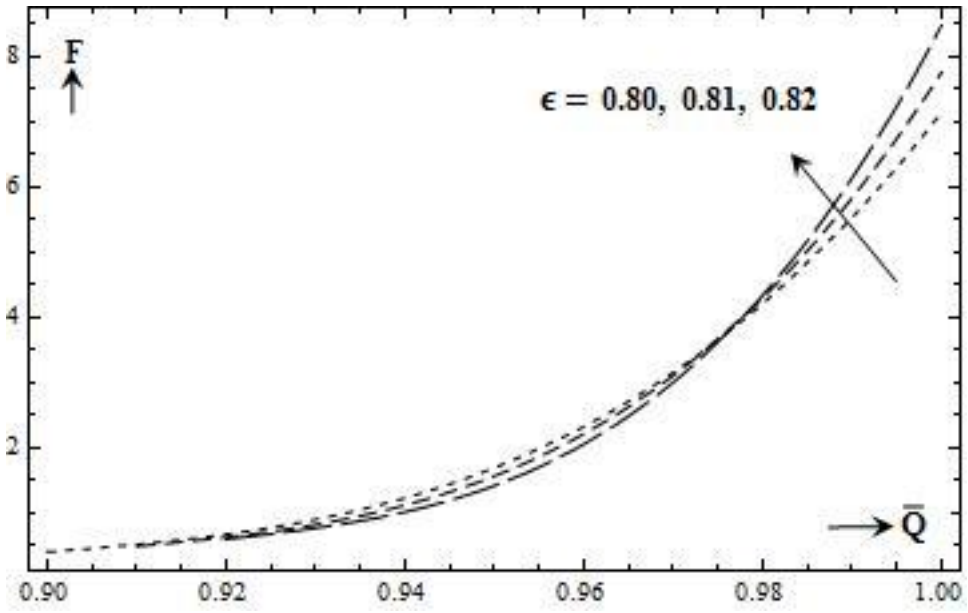

Fig. 6.12: Effect of ϵ on F against $\bar{Q}$ with:

$$n = 3;\ Da = 0.1;\ \alpha = 1;\ \tau = 0.8;\ \phi = 0.1;\ z = 0.1;\ M = 0.2$$

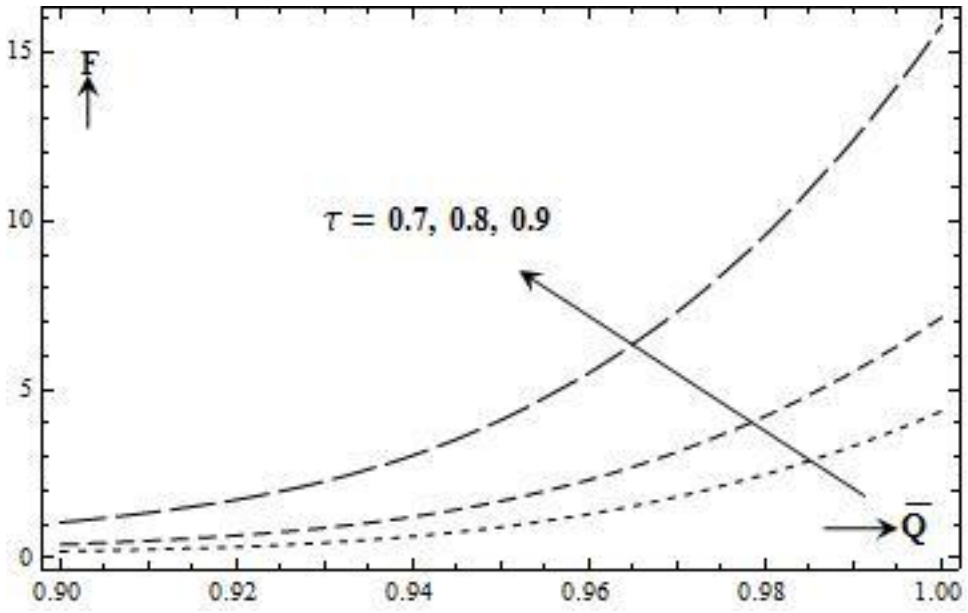

Fig. 6.13: Effect of τ on F against $\bar{Q}$ with:

$$n = 3;\ Da = 0.1;\ \alpha = 1;\ \epsilon = 0.8;\ \phi = 0.1;\ z = 0.1;\ M = 0.2$$

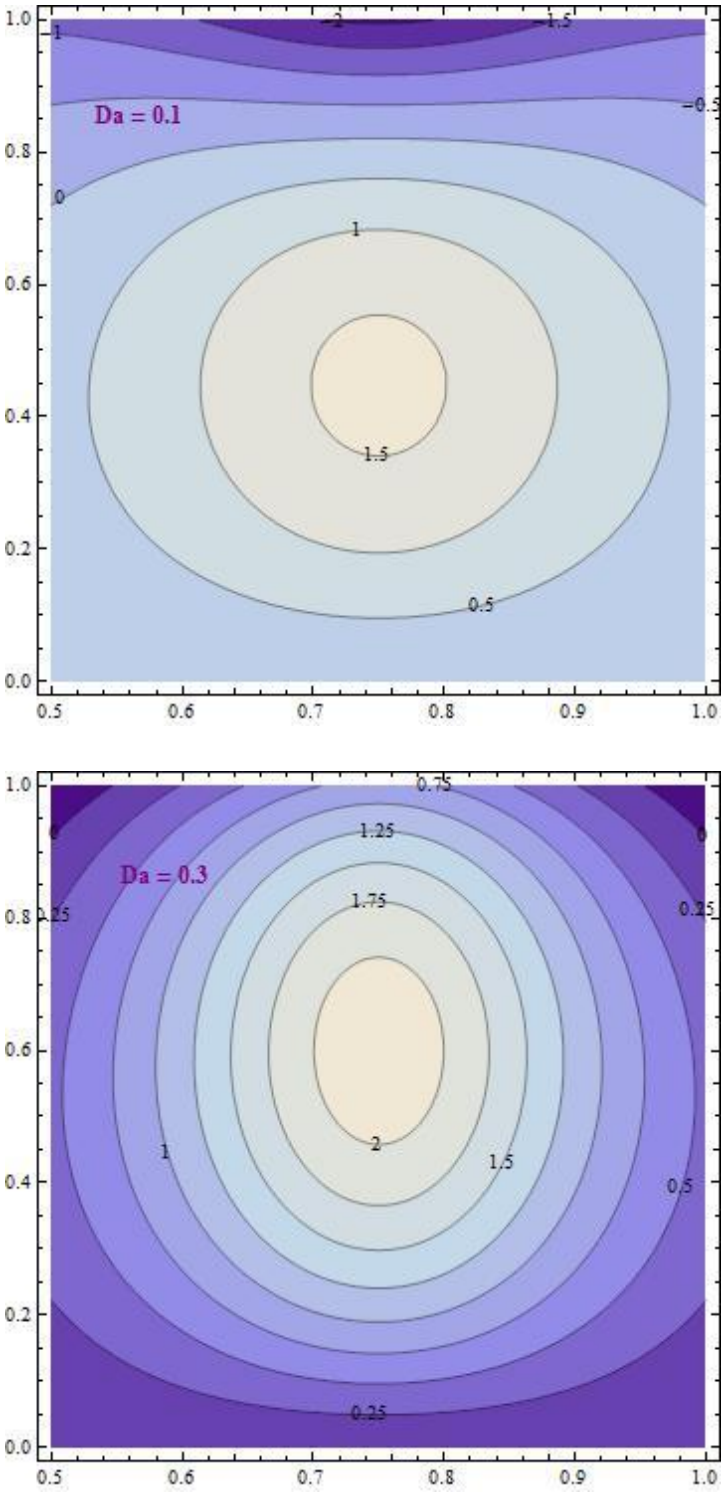

Fig. 6.14: Stream line plots for variation in Darcy number with:
$\boldsymbol{n = 3;\ \alpha = 1;\ \tau = 0.8;\ \epsilon = 0.8;\ \bar{Q} = 0.1;\ \phi = 0.1;\ M = 0.04}$

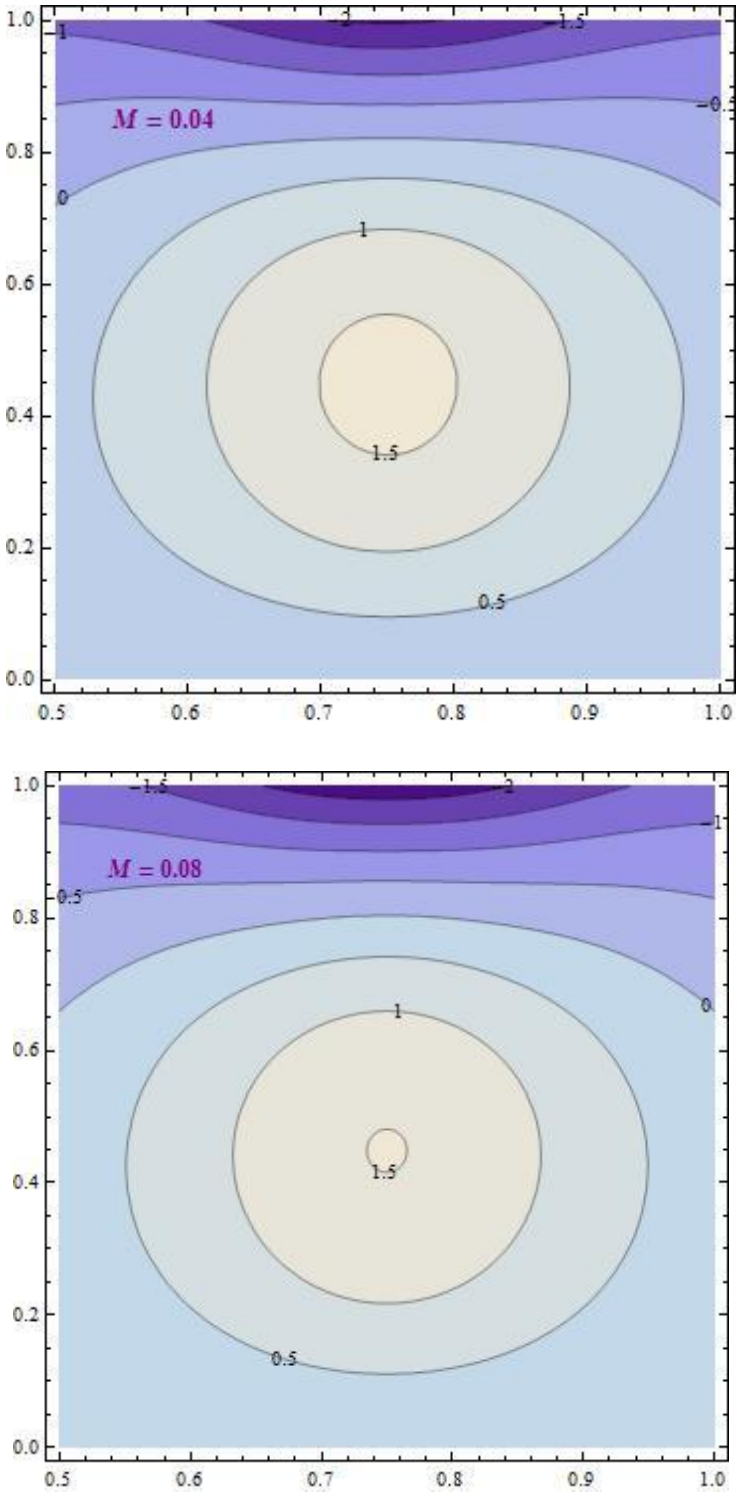

Fig. 6.15: Stream line plots for variation in Magnetic parameter with:

$$n = 3;\ \mathrm{Da} = 0.1;\ \alpha = 1;\ \tau = 0.8;\ \epsilon = 0.8;\ \bar{Q} = 0.1;\ \phi = 0.1$$

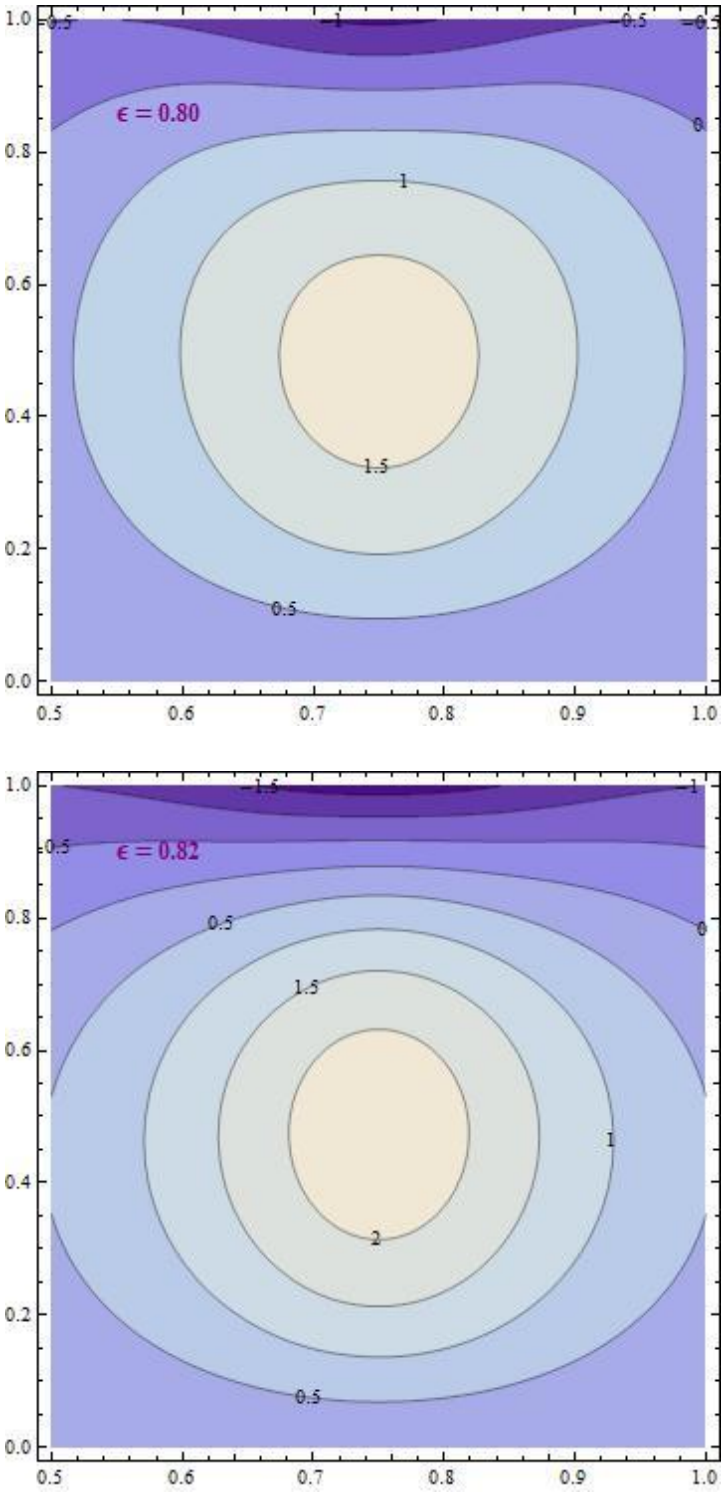

Fig. 6.16: Stream line plots for variation in porous thickening with:
$n = 3;\ \mathrm{Da} = 0.1\ ; \alpha = 1;\ \tau = 0.8;\ \bar{Q} = 0.1;\ \phi = 0.1;\ M = 0.04$

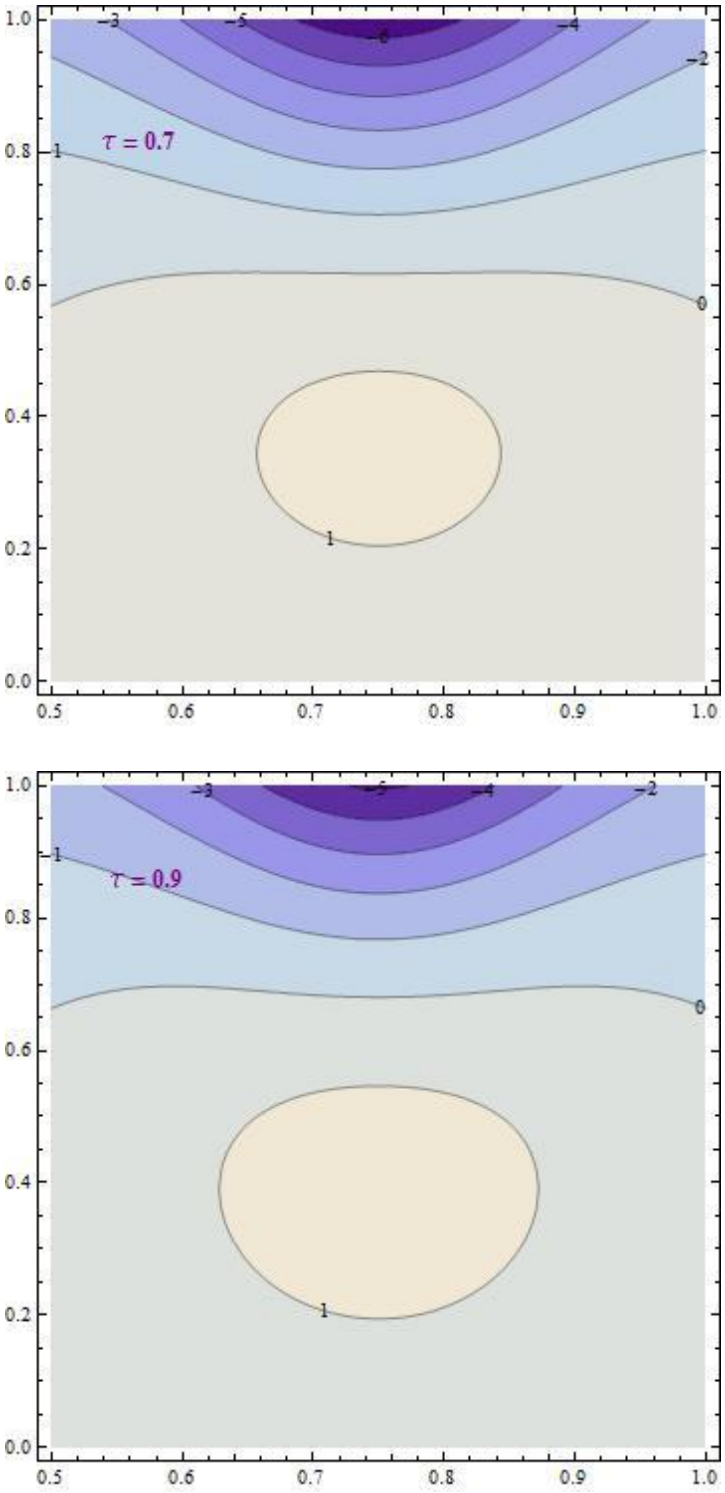

Fig. 6.17: Stream line plots for variation in yield stress with:

$n = 3;\ \mathrm{Da} = 0.1;\ \alpha = 1;\ \epsilon = 0.8;\ \bar{Q} = 0.1;\ \phi = 0.1;\ M = 0.04$

CHAPTER-7

Conclusion and scope for future work

7.1 Conclusion:

Peristaltic flow of a non-Newtonian fluid obeying Herschel–Bulkley fluid properties is investigated under lubrication approach in a channel lined with porous medium. Such a study probably explicate the pathological situations when a distribution of fatty cholesterol and artery clogging, blood clots are created in the lumen of the coronary artery, which can be well thought of as equivalent to a fictious porous media.

The expressions for pressure rise, frictional force, temperature profile, heat transfer coefficient, rate of heat transfer and the Mechanical efficiency are obtained analytically and are numerically analyzed through graphs, using the MATHEMATICA software. Assuming a magnetic field applied vertically to the channel length, the significance of the pertinent parameters is also analyzed.

Through the graphical results it is analyzed that increase in the porous thickening, yield stress, amplitude ratio and the angle of intersection increases the pumping. With rise in the values of yield stress and Brinkmann number the temperature profile also increases. The angle of inclination inclines the channel making the fluid to fall down rapidly which increases the pressure difference. Also with rise in the threshold yield stress, molecules are put together accounting to more deformation and in turn increase in the pressure difference as well as the temperature. With rise in the values of Brinkman number, there corresponds a strong viscous dissipation effect resulting in temperature rise.

Intensifying the magnetic field reduces the velocity but enhances pumping. This infers that application of strong magnetic field to the flow field necessitates high pressure gradient to pass the flow, thus suggests that fluid pressure can be controlled by the application of suitable magnetic field strength. This phenomenon is helpful during surgery and critical operation to attenuate of loss of blood.

Under all the situations considered in the thesis, it is observed that the trapped bolus increases in size with increase in the yield stress and the amplitude ratio, complying with the earlier results. Consequently, this helps in understanding the movement of food bolus in the gastrointestinal tract and the development of thrombus in blood.

7.2 Future work:

The present work in the thesis investigates the peristaltic transport of non-Newtonian Herschel-Bulkley fluid under different circumstances. The analysis has been carried out with the presumptions of long wavelength and low Reynolds number where the peristaltic wavelength is assumed to be very large in comparison with the mean half width of the channel.

This analysis may be undertaken using numerical methods or homotopy analysis. The study could also be investigated for small amplitude ratio instead of long wave length assumption. The study can be promoted under dispersion and wall effects.

Bibliography

1. H. Bergman, The Ureter, Springer-Verlag, 1981.

2. R. Krstic, Human Microscopic Anatomy, *Springer-Verlag*, 1991.

3. Ayukawa, K. and Takabatake, S., Numerical Analysis of Two-Dimensional Peristaltic Flow, *Bulletin of the JSME*, Vol. 25, 1982, pp: 1061–1069.

4. Bayliss, W. M. and Starling, E. H., The Movements and Innervations of the Small Intestine, *The Journal of Physiology*, Vol.24, 1899, pp: 99–143.

5. T. W. Latham, Fluid Motion in a Peristaltic Pump, *M.Sc. Thesis, MIT, Cambridge, MA*, 1966.

6. Shapiro, A. H., Pumping and Retrograde Diffusion in Peristaltic Waves, *Proc. Workshop in Uretral Revolume Flow Rate in Children, Nat. Acad. Sci., Washington, D.C.*, Vol.1, 1967, pp: 109–126.

7. Fung, Y. C. and Yih, C. S., Peristaltic Transport, *J. Appl. Mech.*, Vol. 35, 1968, pp: 669–675.

8. Shapiro, A. H., Jaffrin, M. Y. and Weinberg, S. L., Peristaltic Pumping with Long Wavelengths at Low Reynolds Number, *J. Fluid Mech*., Vol. 37, 1969, pp: 799–825.

9. Burns, J. C. and Parkes, J., Peristaltic Motion, *J. Fluid Mech*., Vol. 29, 1967, pp: 731–743.

10. Jaffrin, M. Y. and Shapiro, A. H., "Peristaltic Pumping", *Ann. Rev. Fluid Mech.*, Vol. 3, 1971, pp: 13–36.

11. Radhakrishnamacharya, G., Long Wavelength Approximation to Peristaltic Motion of Power Law Fluid, *Rheol. Acta.*, Vol. 21, 1982, pp: 30–35.

12. Yin, F. and Fung, Y. C., Peristaltic Waves in Circular Cylindrical Tubes, *Trans. ASME J. Appl. Mech.*, Vol. 36,1969, pp: 579–587.

13. Batra, S. K., Sperm Transport Through Vas Deferens, *Review of hypothesis and suggestions for a quantitative model, Fertility, Sterility*, Vol. 25,1974, pp: 186 – 202.

14. Guha, S. K., Kaur, H. and Ahmed, H., Mechanics of Fluid Transport in the Vasdeferns, *Med. Boil. Engg.*, Vol. 13, 1975, pp: 518–522.

15. Srivastava, L. M. and Srivastava, V. P and Sinha, S. N., Peristaltic Transport of a Physiological Fluid: Part I: Flow in non-Uniform Geometry, *Biorheology*, Vol. 20, 1983, pp: 153–166.

16. Lew, G. S., Fung, Y. C. and Owensein, C. B. L., Peristaltic Carrying and Mixing of Chime in Small Intestine. *J. Biomechanics*, Vol. 4, 1971, pp: 297–315.

17. Bohme, G. B. and Friedrich, R., Peristaltic Flow of Visco Elastic Liquids, *J. Fluid Mech.*, Vol. 138, 1983, pp:109–122.

18. Srivastava, L. M. and Srivastava, V. P., Peristaltic transport of blood: casson model II, *Journal of Biomechanics*, Vol. 17, 1984, pp: 821–829.

19. DeVries, K., Loyns, E. A., Ballard, J., Levi, C. S. and Lindsay, D. J., Contractions of the Inner Third of Myometrium, *Am. J. Obstetrics Gynecol.*, Vol. 162, 1990, pp: 679–682.

20. Eytan Osmat and Elad David, Analysis of Intrauterine Fluid Motion by Uterine Contraction, *Bull Math, Biol.*, Vol. 61, 1999, pp: 221–238.

21. Eytan Osmat, Jaffa Ariel and Elad David, Peristaltic Flow in a Tapered Channel: Applications to Embryo Transport within the Uterine Cavity, *Medical Engg. Phys.*, Vol. 23, 2001, pp: 473–482.

22. Misra, J. C. and Ghosh, S. K., A mathematical Model for the Study of Blood Flow Through a Channel with Permeable Walls, *Acta Mechanica*, Vol. 122, 1997, pp: 137–153.

23. Misra, J. C. and Pandey, S. K., Peristaltic Transport of a non Newtonian Fluid with a Peripheral Layer, *Int. J. Eng Sci.*, Vol. 37, 1999, pp: 1841–1858.

24. KrishnaKumari, S. V. H. N., RaviKumar, Y. V. K., RamanaMurthy, M. V. and Sreenadh, S., Peristaltic Pumping of a Jeffrey Fluid under the Effect of Magnetic Field in an Inclined Channel, *Applied Mathematical Sciences*, Vol. 5, 2011, pp: 447–458.

25. Tang, H. T. and Fung, Y. C., Fluid Movement in a Channel with Permeable Walls Covered by Porous Media: A Model of the Lung Alveolar Sheet, *ASME. J. Appl. Mech.*, Vol. 97, 1975, pp: 45–50.

26. Misery, A. M. El., Shehawey, A. El. and Hakeem, A. El., Peristaltic Motion of an Incompressible Generalized Newtonian Fluid in a Planar Channel, *J. Phys. Soc., Japan*, Vol. 65, 1996, pp: 3524–3529.

27. Shehawey, E. F. El., Sobh, A. M. F. and Elbarbary, E. M. E., Peristaltic Motion of a Generalized Newtonian Fluid Through a Porous Medium, *Phys. Soc. Jpn.*, Vol. 69, 2000, pp: 401–407.

28. Hakeem, A. El., Naby, A. El. and Misery, A. E. M. El., Effects of Endoscope and Generalized Newtonian Fluid on Peristaltic Motion, *Applied Mathematics and computation*, Vol. 128, 2002, pp: 19–35.

29. Mishra, M. and Rao, A. R., Peristaltic Transport of a Newtonian Fluid in an Asymmetric Channel, *Z Angew, Math. Phys.*, Vol. 54, 2003, pp: 532–550.

30. Ebaid, Effects of Magnetic Field and Wall Slip Condition on the Peristaltic Transport of a Newtonian Fluid in an Asymmetric Channel, *Phys. letters A.*, Vol. 372, 2008, pp: 4493–4499.

31. C. Bruce, *Ph.D. Thesis Stansford University, Stansford*, (1969).

32. Joseph, D. D., An Integral Invariant for Jets of Liquid into Air, *ARMA*, Vol. 79, 1980, pp: 389–393.

33. Majhi, S. N. and Nair, V. R., Pulsatile Flow of Third Grade Fluids under Body Acceleration- Modeling Blood Flow, *Int. J. Engg. Sci.*, Vol. 32, 1996, pp: 839–846.

34. Raju, K. K. and Devanathan, R., Peristaltic Motion of a non-Newtonian Fluid, *Rheol. Acta.,* Vol. 11, 1972, pp: 170–179.

35. J. N. Kapur, *Mathematical Models in Biology and Medicine,* Affiliated East–West Press Pvt. Ltd., New York, 1985.

36. Subba Reddy, M. V. Ramachandra Rao, A. and Sreenadh, S., Peristaltic Motion of a Power Law Fluid in an Asymmetric Channel, *Int. J. Non-Linear Mech.,* Vol. 42, 2007, pp: 1153–1161.

37. Akram, S. and Nadeem, S., Significance of Nanofluid and Partial Slip on the Peristaltic Transport of a Non-Newtonian Fluid with Different Wave Forms, *IEEE Transactions on Nano Technology*, Vol. 13, 2014, pp: 375–385.

38. Pozrikidis, C. A., *Journal of Fluid Mechanics,* Vol. 180, 1987, pp: 515–527.

39. Nagarani, P., Peristaltic Transport of a Casson Fluid in an Inclined Channel, *Korea-Australia Rheology Journal,* Vol. 22, 2010, pp: 105–111.

40. Beavers, G. S. and Joseph, D. D., Boundary Conditions at a Naturally Permeable Wall, *Journal of Fluid Mechanics*, Vol. 30, 1967, pp: 197–207.

41. Saffman, P. G., On the Boundary Conditions at the Surface of a Porous Medium, *Stud. Appl. Math.,* Vol. 1, 1971, pp: 93–101.

42. A. E. Scheidegger, The Physics of Flow Through Porous Media, 3rd Ed., *University of Toronto Press, Toronto, Canada,* 1974.

43. G. W. Reese, and H. J. Rath, A Model of a Combined Porous Peristaltic Pumping System, In L. S. Srinath and M. Singh (Eds), *Physiological Fluid Dynamics II, Proc. 2nd International Conference on Physiological Fluid Dynamics, IIT Madras, 1987, Tata Mcgraw-Hill, New Delhi,* 190–195.

44. Gopalan, N. P., Pulsatile Blood Flow in Rigid Pulmonary Alveolar Sheet with Porous Walls, *Bull Math Biol,* Vol. 43, 1981, pp: 563–577.

45. Chaturani, P. and Ranganathan, T. R., Solute Transfer in Fluid Flow in Permeable Tubes with Application to Flow in Glomerular Capillaries, *Acta Mechanica*, Vol. 96, 1993, pp:139–154.

46. Shehawey, E. F. El., Mekheimer, Kh. S., Kalidas, S. F., and Afifi, N. A. S., Peristaltic Transport Through a Porous Medium, *J. Biomath,* Vol. 14, 1999.

47. Shehawey, E. F. El., and Husseny, S. Z. A., Effects of Porous Boundaries on Peristaltic Transport through a Porous Medium, *Acta Mechanica,* Vol. 143, 2000, pp: 165–177.

48. Shehawey, E. F. El. and Sebaei, W. El., Peristaltic Transport in a Cylindrical Tube Through a Porous Medium, *Int. J. Math Sci.,* Vol. 24, 2000, pp: 217–230.

49. Shehawey, E. F. El., Eldabe, N. T., Elghazy, E. M. and Ebaid, A., Peristaltic Transport in an Asymmetric Channel Through a Porous Medium, *Applied Mathematics and Computation*, Vol. 182, 2006, pp: 140–150.

50. Vasudev, C., Rajeswara Rao, U., Prabhakara Rao, G. and Subba Reddy, M. V., Peristaltic Flow of a Newtonian Fluid Through a Porous Medium in a Vertical Tube Under the Effect of Magnetic Field, *International Journal Of Current Scientific Research*, Vol. 1, 2011, pp: 105–110.

51. Ravi Kumar, Y. V. K., Krishna Kumari, S. V. H. N., Ramana Murthy, M. V. and Sreenadh, S., Peristaltic Transport of a Power Law Fluid in an Asymmetric Channel Bounded by Permeable Walls., *Advances in Applied Science Research (Pelgia Research Library),* Vol. 2, 2011, pp: 396–406.

52. Rami Reddy, G. and Venkataramana, S., Peristaltic Transport of a Conducting Fluid Through a Porous Medium in an Asymmetric Vertical Channel, *Advances in Applied Science Research (Pelgia Research Library),* Vol. 2, 2011, pp: 240–248.

53. Raghunatha Rao, T. and Prasada Rao, D. R. V., Peristaltic Transport of a Couple Stress Fluid Through a Porous Medium in a Channel at Low Reynolds Number, *Int. J. of Appl. Math and Mech.,* Vol. 8, 2012, pp: 97–116.

54. Jyothi, B. and Koteswara Rao, P., Slip Effects on MHD Peristaltic Transport of a Williamson Fluid through a Porous Medium in a Symmetric Channel**,** *J. Math. Comput. Sci.,* Vol. 3, 2013, pp: 1306–1324.

55. Navaneeswara Reddy, S. and Vishwanatha Reddy, G., Slip Effects on the Peristaltic Pumping of a Jeffrey Fluid through a Porous Medium in an Inclined Asymmetric Channel, *Int. J. of Mathematical Archive,* Vol. 4(4), 2013, pp: 183–196.

56. Nagachandrakala, G., Leelarathnam, A. and Sreenadh, S., Influence of Slip Conditions on MHD Peristaltic Flow of a Hyperbolic Tangent Fluid in a non-Uniform Porous Channel with Wall Properties, *International Journal of Engineering Science & Technology,* Vol. 5, 2013, pp: 951–963.

57. Alsaedi, A., Ali, N., Tripathi, D. and Hayat, T., Peristaltic Flow of Couple Stress Fluid through Uniform Porous Medium, *Applied Mathematics and Mechanics,* Vol. 35, 2014, pp: 469 – 480.

58. Ellahi, R., Bhatti, M. M. and Arshad, Kiaz, Effects of Magneto Hydrodynamics on Peristaltic Flow of Jeffery Fluid in a Rectangular Duct through a Porous Media, *Journal of Porous Media,* Vol. 17, 2014, pp: 143–157.

59. Ali Abbas, M., Bai, Y. D., Bhatti, M. M. and Rashidi, M. M., Three Dimensional Peristaltic Flow of Hyperbolic Tangent Fluid in non-Uniform Channel having Flexible Walls, *Alexandria Engineering Journal*, Vol. 55, 2016, pp: 653–662.

60. Ramesh, K. and Devakar, M., Peristaltic Transport of MHD Williamson Fluid in an Inclined Asymmetric Channel through Porous Medium with Heat Transfer, *J. Cent. South Univ.*, Vol. 22, 2015, pp: 3189–3201.

61. Srivastava, L. M. and Srivastava, V. P., Peristaltic Transport of a Power Law Fluid: Application to the Ductus Efferntes of the Reproductive Tract, *Rheo. Acta.,* Vol. 27, 1988, pp: 428–433.

62. Mekheimer, Kh. S., Peristaltic Transport of a Couple Stress Fluid in Uniform and non-Uniform Channels, *Biorheology,* Vol. 39, 2002, pp: 755–765.

63. Sankad, G. C. Radhakrishnamacharya, G. and Ramanamurthy, J. V., Long Wave Length Approximation to Peristaltic Motion of Micropolar Fluid with Wall Effects, *Adv. Appl. Math. and Mech.*, Vol. 2, 2010, pp: 222–237.

64. Sankad, G. C. and Radhakrishnamacharya, G., Effect of Wall Properties on the Peristaltic Transport of Micropolar Fluid in a non-Uniform Channel, *Int. J. of Appl. Math. and Mech.,* Vol. 6(1), 2010, pp: 94–107.

65. Ali Abbas, M., Bai, Y. D., Rashidi, M. M. and Bhatti, M. M., Application of Drug Delivery in Magneto Hydrodynamics Peristaltic Flow of Hyperbolic Tangent Fluid in non-Uniform Channel Having Flexible Walls, *Journal of Mechanics in Medicine and Biology,* 16(4), 2015, pp: 1650052–1650067.

66. Mekheimer, Kh. S., Peristaltic Flow of Blood Under Effect of a Magnetic Field in a non Uniform Channel, *Appl. Math. Comput*., Vol. 153, 2004, pp: 763–777.

67. Sankad, G. C. and Radhakrishnamacharya, G., Effect of Magnetic Field on Peristaltic Motion of Micropolar Fluid with Wall Effects, *Journal of Applied Mathematics and Fluid Mechanics,* Vol. 1, 2009, pp: 37–50.

68. Ramana Kumari, A. V. and Radhakrishnamacharya, G., Effect of Slip on Heat Transfer to Peristaltic Transport in the Presence of Magnetic Field with Wall Effects, *ARPN Journal of Engineering and Applied Sciences,* Vol. 6, 2011, pp: 118–131.

69. Shit, G. C. and Roy, M., Hydro Magnetic Effect on Inclined Peristaltic Flow of a Couple Stress Fluid, *Alexandria Engineering Journal*, Vol. 53, 2014, pp: 949–958.

70. Bhatti, M. M. and Ali Abbas, M., Simultaneous Effects of Slip and MHD on Peristaltic Blood Flow of Jeffrey Fluid Model through a Porous Medium, *Alexandria Engineering Journal*, 2016, doi 10.1016/j.aej.2016.03.002.

71. Scott Blair, G. W., An Equation for the Flow of Blood, Plasma and Serum through Glass Capillaries, *Nature,* Vol. 183, 1959, pp: 613–614.

72. Tu, C and Deville, M., Pulsatile Flow Of non-Newtonian Fluids through Arterial Stenosis, *J. Biomech*, Vol. 29 (7), 1996, pp: 899–908.

73. G. W. S. Blair and D. C. Spanner, An Introduction to Biorheology, *Elsevier, Amsterdam*, 1974.

74. Vajravelu, K., Sreenadh, S. and Ramesh Babu, V., Peristaltic Transport of a Herschel-Bulkley Fluid in an Inclined Tube, *Int. J. Non-Linear Mechanics*, Vol. 40, 2005, pp: 83–90.

75. Vajravelu, K., Sreenadh, S. and Ramesh Babu, V., Peristaltic Pumping of a Herschel Bulkley Fluid in a Channel, *Applied Mathematics and Computation*, Vol. 169, 2005, pp: 726–735.

76. Maruthi Prasad, K. and Radhakrishnamacharya, G., Effect of Multiple Stenoses on Herschel Bulkley Fluid through a Tube with non-Uniform Cross-Section, *International e-Journal of Engineering Mathematics: Theory and Application*, Vol. 1, 2007, pp: 69–76.

77. Medhavi Amit, Peristaltic Pumping of a non-Newtonian Fluid, *AAM*, Vol. 3, 2008, pp: 137–148.

78. Sreenadh, S., Rajender, S., Krishna Kumari, S. V. H. N. and Ravi Kumar, Y. V. K., Flow of Herschel-Bulkley Fluid in an Inclined Flexible Channel Lined with Porous Material under Peristalsis, *IJITCE*, Vol. 1, 2011, pp: 24–31.

79. Vajravelu, K., Sreenadh, S., Devaki, P. and Prasad, K.V., Peristaltic Transport of a Herschel–Bulkley Fluid in an Elastic Tube, *Heat Transfer— Asian Research*, Vol. 44(7), 2015, pp: 585–598.

80. Maiti, S. and Misra. J. C., non-Newtonian Characteristic of Peristaltic Flow of Blood in Micro-Vessels, *Commun Nonlinear Sci. Numer. Simul.*, Vol. 18, 2013, pp: 1970–1988.

81. Hummady, L. Z. and Abdulhadi, A. M., Effect of Heat Transfer on the Peristaltic Transport of MHD with Couple-Stress Fluid through a Porous Medium with Slip Effect, *Mathematical Theory and Modeling, IISTE,* Vol. 4, 2014, pp: 1–18.

82. Akbar, N. S. and Butt, A. W., Heat Transfer Analysis for the Peristaltic Flow of Herschel Bulkley Fluid in a Non Uniform Inclined Channel, *Z. Naturforsch*, Vol. 70, 2015, pp: 23–32.

83. Srinivas, A. N. S., Hemadri Reddy, R., Srinivas, S. and Sreenadh, S., Peristaltic Transport of a Casson Fluid in a Channel with Permeable Walls, *International Journal of Pure and Applied Mathematics,* Vol. 90, 2014, pp: 11–24.

84. Santhosh Nallapu and Radhakrishnamacharya, G., Herschel-Bulkley Fluid Flow through Narrow Tubes, *Research Article Physics. Flu-Dyn., Cent. Eur. J. Phys.,* Vol. 30, 2014, pp: 1–12.

85. Sankad, G. C. and Radhakrishnamacharya, Influence of Wall Properties on the Peristaltic Motion of Herschel-Bulkley Fluid in a Channel, ARPN Journal of Engineering and Applied Sciences, Vol. 4 (10), 2009, pp: 27-35.

86. Gupta, B. B. and Sheshadri, V., Peristaltic Pumping in non-Uniform Tubes, *J. Bio. Mech.,* Vol. 9, 1976, pp: 105–109.

87. Haynes, H. R., Physical Bases of the Dependence of Blood Viscosity on Tube Radius, *Am. J. Physiol,* Vol. 198, 1960, pp: 1193–1200.

88. Lee, J. S. and Fung, Y. C., Flow in Non-Uniform Small Blood Vessels, *Microvase. Re.,* Vol. 3, 1971, pp: 272–279.

89. Sobh, A. M., Interactions of Couple Stresses and Slip Flow on Peristaltic Transport in Uniform and non-Uniform Channels, *Turkish Journal of Engineering Environmental Sciences,* Vol. 32, 2008, pp: 117–123.

90. Sobh, A. M. and Mady, H. H., Peristaltic Flow through a Porous Medium in a non-Uniform Channel, *Journal of Applied Sciences,* Vol. 8, 2008, pp: 1085–1090.

91. Hakeem, A. El., Naby. A. El. and Shamy. I. I. El., Slip Effects on Peristaltic Transport of Power-Law Fluid through an Inclined Tube, *Appl. Math. Sciences*, Vol. 1, 2007, pp: 2967–2980.

92. Riahi, D. N. and Ranadhir Roy, Mathematical Modeling of Peristaltic Flow of Chyme in Small Intestine, *Appl. Appl. Math.*, Vol. 6, 2011, pp: 428–444.

93. Sankad, G. C. and Radhakrishnamacharya, G., Influence of Wall Properties on the Peristaltic Transport of Micropolar Fluid in an Inclined Channel, Journal of New Results in Science, Vol. 6, 2014, pp: 62-75.

94. Krishna Kumari, S. V. H. N. P., Saroj D. Vernekar, and Ravi Kumar, Y. V. K., Peristaltic Motion of a Micropolar Fluid under the Effect of a Magnetic Field in an Inclined Channel, *The International Journal of Engineering and Science (IJES)*, Vol. 2, 2013, pp: 31–40.

95. Smita, Dey and Anamol Kumar Lal, Study of Peristaltic Flow of Blood in Artery, *International Journal of Sciences: Basic and Applied Research (IJSBAR)*, Vol. 12, 2013, pp: 220–228

96. Kothandapani, M. and Prakash, J., Influence of Heat Source, Thermal Radiation and Inclined Magnetic Field on Peristaltic Flow of a Hyperbolic Tangent Nanofluid in a Tapered Asymmetric Channel, *IEEE Transactions on Nano Bioscience*, Vol. 14, 2015, pp: 385–392.

97. Rathod,V. P. and Sridhar. N. G., Peristaltic Flow of a Couple Stress Fluids in an Inclined Channel, *International Journal of Allied Practice, Research and Review.* Vol. *II*, (2015) 27–38.

98. Govindaraja, A., Siva, E. P. and Vidhya, M., Combined Effect of Heat and Mass Transfer on MHD Peristaltic Transport of a Couple Stress Fluid in an Inclined Asymmetric Channel through a Porous Medium, *International Journal of Pure and Applied Mathematics*, Vol. 105, 2015, pp: 685–707.

99. Fung, Y. C. and Yin, F. C. P., Comparison of Theory and Experiment in Peristaltic Transport, *J. Fluid Mech.*, Vol. 47, 1971, pp: 93–112.

100. Victor, S. A. and Shah, V. L., Steady State Heat Transfer to Blood Flowing in the Entrance Region of a Tube, *Int. J. of Heat and Mass Transfer*, Vol. 19, 1976, pp: 777–783.

101. Radhakrishnamacharya, G. and Srinivasalu, Ch., Influence of Wall Properties on Peristaltic Transport with Heat Transfer, *Comptes Rendus Mechanique*, Vol. 335, 2007, pp: 369–373.

102. Mekheimer, Kh. S. and Abd. Elmaboud, Y., The Influence of Heat Transfer and Magnetic Field on Peristaltic Transport of a Newtonian Fluid in a Vertical Annulus: Application of an Endoscope, *Phys. Lett. A.*, Vol. 372, 2008, pp: 1657–1665.

103. Srinivas, A. N. S. and Gayathri, R., Peristaltic Transport of a Newtonian Fluid in a Vertical Asymmetric Channel with Heat Transfer and Porous Medium, *Applied Mathematics and Computation*, Vol. 215, 2009, pp: 185–196.

104. Akbar, N. S., Hayat, T., Nadeem, S. and Obaidat, S., Peristaltic Flow of Williamson Fluid in an Asymmetric Channel with Partial Slip and Heat Transfer, *Int. J. of Heat and Mass Transfer*, Vol. 55, 2012, pp: 18855–18862.

105. Dheia, G. and Abdulhadi, A. M., Effects of Wall Properties and Heat Transfer on the Peristaltic Transport of a Jeffery Fluid through Porous Medium Channel, *Mathematical Theory and Modelling*, Vol. 4, 2014, pp: 86–99.

106. Hayat, T., Hina, S. and Hendi, A. A., Peristaltic Motion of Power-Law Fliuid with Heat and Mass Transfer, *Chin. Phys. Lett.*, Vol.28, 2011, pp: 084707(1 - 4)

107. Hina, S., Hayat, T., Asghar, S. and Hendi, A. A., Influence of Compliant Walls on Peristaltic Motion with Heat/Mass Transfer and Chemical Reaction, *Int. J. Heat and Mass Transfer*, Vol. 55, 2012, pp: 3386–3394.

108. Lakshminarayana, P., Sreenadh, S. and Sucharita, G., The Influence of Slip Wall Properties on the Peristaltic Pumping of a Conducting Bingham Fluid with Heat Transfer, *Proceedia Engineering, Int. Conference on Computational Heat and Mass Transfer-2015*, Vol. 127, 2015, pp: 1087–1094.

109. Kalidas Das, Simultaneous Effects of Slip Conditions and Wall Properties on MHD Peristaltic Flow of a Maxwell Fluid with Heat Transfer, *Journal of Siberian Federal University, Mathematics and Physics,* Vol. 5, 2012, pp: 303–315

110. Dhananjaya, S., Arunachalam, Sreenadh and Lakshminarayana, The Influence of Slip Condition, Wall Properties and Heat Transfer on Peristaltic Pumping of a Bingham Fluid, *Internet source*.

111. Rathod, V. P. and Laxmi, D., Effects Of Heat Transfer on the Peristaltic MHD Flow of a Bingham Fluid through a Porous Medium in a Channel, *Int. J. Biomath*, Vol. 7, 2014, pp: 1450060–1450080.

112. Hayat, T., Javed, M. and Ali, N., MHD Peristaltic Transport of a Jeffery Fluid in a Channel with Compliant Walls and Porous Space, *Transport in Porous Media*, Vol. 74, 2008, pp: 259–274.

113. Kothandapani, M. and Srinivas, S., On the Influence of Wall Properties in the MHD Peristaltic Transport with Heat Transfer and Porous Medium, *Phys. Lett. A.*, Vol. 372, 2008, pp: 4586–4591.

114. Hayat, T., Saleem, N. and Ali, N., Effect of Induced Magnetic Field on Peristaltic Transport of a Carreau Fluid, *Communications in Non Linear Science and Numerical Simulation*, Vol. 15, 2010, pp: 2407–2423.

115. Sankad, G. C. and Radhakrishnamacharya, G., Effect of Magnetic Field on the Peristaltic Transport of Couple Stress Fluid in a Channel with Wall Properties, *Int. J. of Biomathematics,* Vol. 4, 2011, pp: 365–378.

116. Kumari, A. V. R. and Radhakrishnamacharya, G., Effect of Slip and Magnetic Field on Peristaltic Flow in an Inclined Channel with Wall Effects. *Int. J. of Biomathematics*, Vol. 5, 2012, pp: 1250015–1250032.

117. Nadeem, S. and Akram, S., Heat Transfer in a Peristaltic Flow of MHD Fluid with Partial Slip, *Communications In Nonlinear Science and Numerical Simulation*, Vol. 15, 2010, pp: 312–321.

118. Mekheimer, Kh. S., Najma, S. and Hayat, T., Simultaneous Effects of Induced Magnetic Field and Heat and Mass Transfer on the Peristaltic Motion of Second-Order Fluid in a Channel, *International Journal For Numerical Methods in Fluids,* Vol. 70, 2012, pp: 342–358.

119. Chaturani, P. and Ponnalagar Samy, R., A Study of non-Newtonian Aspects of Blood Flow through Stenosed Arteries and its Applications in Arterial Diseases, *Biorheol.,* Vol. 22, 1985, pp: 521–531.

120. Maruthi Prasad, K. and Radhakrishnamacharya, G., Peristaltic Transport of a Herschel Bulkley Fluid in a Channel in the Presence of Magnetic Field of Low Intensity, *International Journal of Computational Intelligence Research and Applications,* Vol. 1(1), 2007, pp: 17–81.

List of papers published/communicated

List of published papers:

1. Sankad, G. C., Nagathan, P. S., **Asha Patil** and Dhange**,** M. Y., **Peristaltic Transport of a Herschel–Bulkley Fluid in a Non-Uniform Channel with Wall Effects**, *International Journal of Engineering Science and Innovative Technology (IJESIT),* Vol. 3, 2014, pp: 669 – 678.

2. Sankad, G. C. and **Asha Patil, Effect of Porosity on the Peristaltic Pumping of a Non-Newtonian Fluid in a Channel**, *Journal of New Results in Science*, Vol.10, 2016, pp: 01– 09.

3. Sankad, G. C. and **Asha Patil**, **Peristaltic Flow of Herschel Bulkley Fluid in a Non–Uniform Channel with Porous Lining**, *Proceedia Engineering, Int. Conference on computational heat and mass transfer-2015*, Vol. 127, 2015, pp: 686 – 693.

4. Sankad, G. C. and **Asha Patil**, **Impact of Permeable Lining of the Wall on the Peristaltic Flow of Herschel Bulkley Fluid**, *Applications and Applied Mathematics* (AAM), Vol. 11(2), 2016, pp: 663−669.

5. Sankad, G. C. and **Asha Patil**, **Non-Newtonian Fluid Flow in a Peristaltic Channel Lined with Porous Material under Low Intensity Magnetic Field**, *International Journal of Pure and Applied Mathematics* (IJPAM), Vol. 113(6), 2017, pp: 422−431.

List of communicated papers:

1. Sankad, G. C. and **Asha Patil**, **Heat Transfer Inferences on the Herschel Bulkley Fluid Flow under Peristalsis**, communicated to *Frontiers in Heat and Mass Transfer*.